COOLANT VOID EFFECTS IN NEUTRON MULTIPLYING MEDIA

by

WILLIAM J. GARLAND, B.Eng., M.Eng.

A Thesis

Submitted to the Faculty of Graduate Studies

in Partial Fulfilment of the Requirements

for the Degree

Doctor of Philosophy

McMaster University

Hamilton, Ontario, Canada.

September, 1975

© WILLIAM J. GARLAND 1976

COOLANT VOID EFFECTS IN NEUTRON MULTIPLYING MEDIA

DOCTOR OF PHILOSOPHY (1975)
Department of Chemical Engineering

MCMASTER UNIVERSITY
Hamilton, Ontario.

TITLE: Coolant Void Effects in Neutron Multiplying Media

AUTHOR: William J. Garland, B.Eng. (McMaster), M.Eng. (McMaster)

SUPERVISORS: Dr. A.A. Harms, Department of Engineering Physics.
Dr. J. Vlachopoulos, Department of Chemical Engineering.

NO. OF PAGES: xv, 260

ABSTRACT

Various models of the nuclear reactor system are developed and evaluated in order to provide insight on the fundamental phenomena involved in the coolant void effect as a guide to future simulation studies and experimental design.

The mathematical description of the fundamental phenomena and consideration of the macroscopic physical characteristics define models for the neutron flux density and the coolant void fraction for the case of boiling-light-water nuclear reactors. Experimental comparisons are made whenever possible to evaluate the effectiveness of these models. The two-group neutron diffusion model and Hancox's void model were found necessary to describe the steady state behaviour of the nuclear reactor cell. The errors and limitations of present day models and techniques are delineated; the directions for improvement are also indicated. In general, it was found that independent experimental estimates of the fundamental parameters are needed to replace the current reliance on extensive experimental-model correlations. In this way the need for expensive prototypes can be eliminated.

A temporal transformation of the general space-time neutron equations is developed to facilitate their solution by standard numerical techniques. It was found that the computation time can be reduced over threefold for transient control problems.

The coupling of the fluid model and the neutron flux model proves

most interesting and shows that coolant voiding can have a profound effect on both the steady state and the transient behaviour of nuclear reactors. It is also shown that errors in present day techniques for investigating the coupling effect can lead to errors in reactivity estimates of more than the prompt critical limitation.

ACKNOWLEDGEMENTS

I would like to express my sincere thanks to my research supervisors, Dr. A.A. Harms and Dr. J. Vlachopoulos for their guidance and openmindedness throughout this study and to the supervisory committee, consisting of the above plus Dr. T.W. Hoffman and Dr. J.E. Robinson, for their suggestions. Thanks are due to those members of McMaster University who have shown interest and have provided stimulating discussions. I am indebted to the staff of Atomic Energy of Canada Limited, especially J.W. Griffiths, for accommodating my many requests concerning the computer code, LATREP. Credit is due to Canadian Westinghouse Company Limited, in particular Dr. W.T. Hancox, for help with the fluid models.

Special thanks to my wife, Elsie, for her undaunted confidence in my abilities, her moral and physical support, and for making the development of both our careers enjoyable and meaningful. Further thanks are due to friends and relatives, especially my parents, for their encouragement, understanding, and acceptance throughout the years.

Sandi Evans and Lillian Mogensen deserve special mention for their perseverance in typing and retyping.

Finally, I am grateful to McMaster University and to the National Research Council of Canada for financial support.

TABLE OF CONTENTS

LIST OF FIGURES

LIST OF TABLES

PAGE

CHAPTER 1

INTRODUCTION

Nuclear reactors consist of composites of discrete geometric regions having various material properties. One form of such spatial inhomogeneity is coolant voiding. Coolant voiding can arise as an expected phenomenon, as in boiling-light-water nuclear reactors, or as an accidental phenomenon, as in the case of loss of coolant due to pipe failure. Whether the voiding is expected or accidental, its effect on the reactor system can be described symbolically by the feedback scheme shown in figure 1.1.

This feedback can be of two basic forms. The first type includes all reversible effects, such as, changes in coolant density due to a rise in power or a reduction in flow rate. The second type includes all irreversible effects, such as, changes in coolant density due to local temperature peaks which lead to fuel failure and subsequent system degradation. The scope of this dissertation is limited to the first type, reversible coolant density feedback.

Present day experience in operating boiling-water reactors on a commercial basis have shown that the lack of knowledge of the coolant-void effect can lead to instabilities and loss of control (1,2). These problems lead to overdesign and higher cost, preventing the inherently better heat transport characteristics of boiling-water nuclear reactors from being appropriately exploited (2). This lack of knowledge imposes

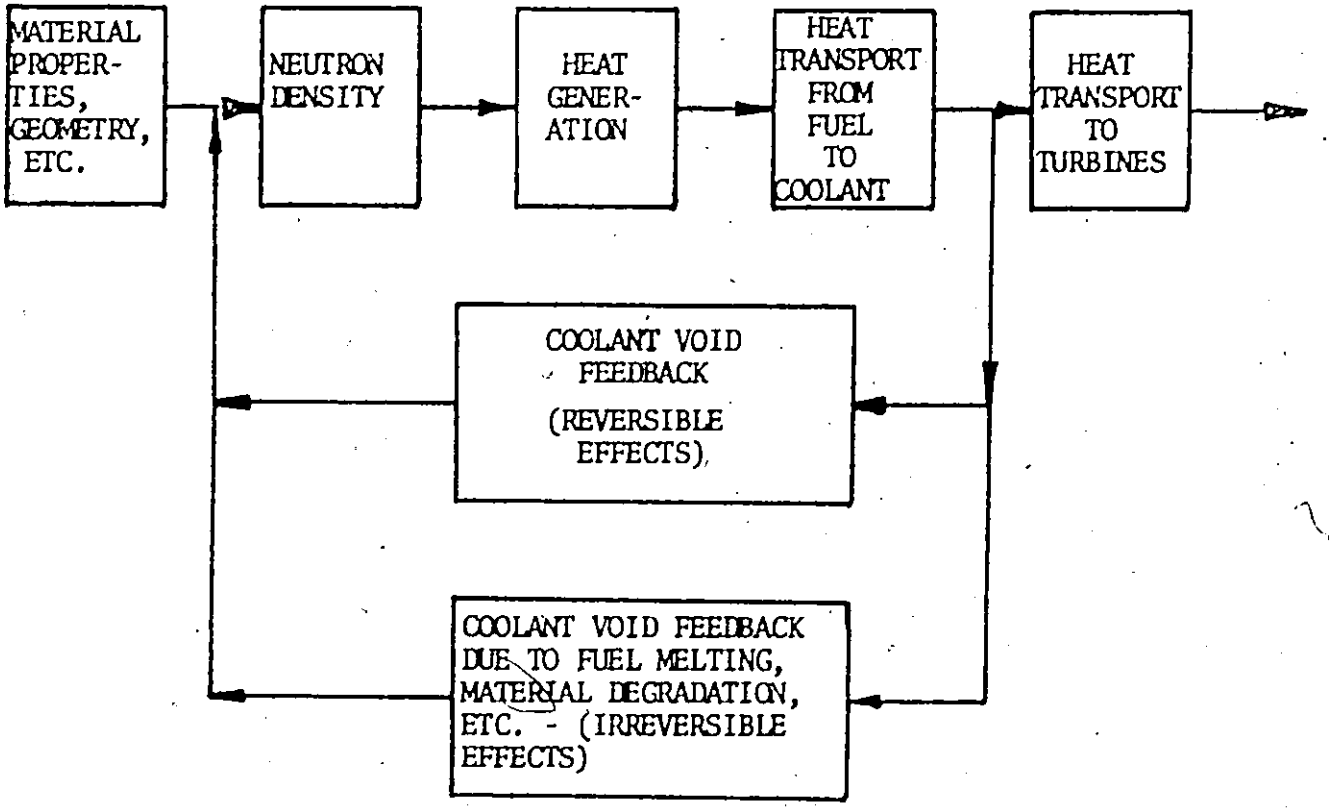

FIGURE 1.1: Feedback schematic for a nuclear reactor illustrating the effect of voiding.

a reliance on accurate prototype scale-up and on the use of empirical relationships outside the conditions under which they were developed. This works well if the design is not too far removed from past experience, but this is not the case for boiling-water reactors.

A recent review (3) describes the scope of the Canadian work being carried out on reactor coolants and their effects on reactors. The intensity of this work indicates the importance of the problem from an economic and a safety standpoint. However, the emphasis has been placed on fluid model development with little consideration of the coupling between coolant voiding and neutron flux. To fully appreciate the important characteristics of coolant voiding and to direct future research in this area, consideration must be given to the coupling effect.

The direction of research in this area is, then, clear. Reliable models of the interaction of the coolant with the neutron flux in a nuclear reactor are required to provide the needed knowledge, and these models should be based on fundamental phenomena as much as possible. Consequently, the objective of this dissertation is to develop, present and evaluate various models of the boiling-light-water nuclear reactor system which will provide insight on and understanding of the fundamental phenomena for future simulation studies and experimental design.

CHAPTER 2

OVERVIEW OF THE LITERATURE

A survey of the literature dealing with boiling channels in nuclear reactors shows that the previous research can be grouped into three major areas: neutron flux models; fluid models; and coupled neutron flux-fluid models. Accordingly, these areas represent the main modes in which researchers have worked.

Some researchers have chosen to use extremely simple fluid models and heat transfer mechanisms coupled with simple neutronics to simulate boiling-light-water reactors (4-7). Hold (4), assuming lumped parameter models for the fluid and the neutrons, incorporates a functional form of the power transients to investigate the frequency response of the nuclear reactor model. Some agreement with experimental data is achieved. Nahavandi (5-7) simulated the space-dependent dynamics of boiling-light-water reactors using one-dimensional forms of the semi-two-group neutron equations and the homogenized two-phase mass, momentum and energy equations. No experimental comparison is attempted. The rather restrictive assumptions employed and the lack of experimental and theoretical comparisons limit the usefulness of the predictions of these models. Further, this approach gives no information about local conditions in a given channel - just the overall effect. This is insufficient since investigation of possible local hot-spots, dryout and other heat transfer crises are essential to proper nuclear reactor design.

To circumvent this, other researchers have established channel modelling with no feedback from the reactor neutronics. Such detail is essential in determining the properties and behaviour of boiling-water channels. Kjaerheim (8) gives a good review of the basic concepts of boiling channels, while Tong (9) reviews the various empirical and theoretical correlations derived over the past years. Early attempts, surveyed in references (10-14), at model formulation were characterized by restrictive assumptions. The lack of detailed information on mass, momentum and energy interchange across vapour-liquid interfaces necessitated the use of mixture conservation equations plus correlation relationships in place of the individual phase conservation equations. The complexity of the flow profiles led to a cross sectional average approach and, hence, one-dimensional equations. Because of the errors introduced by the above approach, copious quantities of empirical correlations were required. Such investigations seem to have come close to their logical culmination in the work of Ahmad (10). The next step needed was the formulation of models that were more inherently capable of incorporating fundamental phenomena. Only in this way could one hope to arrive at a forced convective boiling channel model capable of general applicability.

Zuber (11,12) formulated a void propagation equation from the two-phase flow equations, i.e., mass balances for each phase, using the concept of distribution parameters to account for the variations in the void over the channel cross section. This work represents the first successful attempt to account for the inhomogeneities associated with forced convective boiling and to account for each phase by its

appropriate continuity equation rather than a corrected mixture equation. Empirical correlations provide information on energy transfer and void generation. Zuber's formulation, however, assumes fully developed flow and thermal equilibrium between the phases which severely limit the applicability of the void propagation equation.

In more recent works (13,14), Hancox and Nicoll remove the restrictive assumptions of thermal equilibrium and fully developed flow inherent in Zuber's work. Up-to-date experimental correlations are included and additional distribution parameters are introduced. Extensive comparisons with experimental data, covering a wide parametric range, are moderately successful in predicting forced convective boiling for spatially uniform, steady and transient heat inputs.

All of the above fluid models are limited by a reliance on experimental correlations. Until such correlations are eliminated, the ability of any of the present fluid models to predict results outside of the present experimental range is questionable. Consequently, a need exists to extend the work to include more general heat input shapes, to account explicitly for the flashing effect due to channel pressure drops, to extend the work to subchannel flow, and to remove the assumptions inherent in the models. The latter is presently being studied by Younis (15). Also, a need exists to relate these models to the overall characteristics of a neutron multiplying system in a consistent, comprehensive manner, as considered herein. In this dissertation, then, the fluid models are taken as given. Subsequent use of these models will reveal where improvements are needed in simulation models for boiling-light-water reactors,

and will provide insight not obtainable from studies of the fluid and neutron flux models as separate entities.

Detailed modelling of the neutron distribution has also received considerable attention in the past (16-20). Various levels of approximation have been applied to a variety of practical problems. The neutron density is, in general, a function of space and time. However, further complications arise because the neutron density is also characterized by energy and direction of motion. In this general case, neutron transport theory (16,18,19) is needed to describe the neutron motion. Integration over the direction of motion leads to neutron diffusion theory (18-20). The continuous energy dependence can be approximated as a discrete dependence (16,17) leading to equations similar to multi-component mass diffusion with sources and sinks. This represents the highest level of approximation that practical solutions to real problems employ. Further simplifications are achieved in a manner analogous to mass diffusion in multi-component systems by, for instance, reduction of energy groups, reduction of the number of spatial dimensions, reduction to steady state, or homogenization of a heterogeneous system (16). It remains, therefore, to choose the models appropriate to the system in question.

Theoretical and experimental correlations, in the area of coolant voiding have been researched mainly by industrial and national laboratories, such as, Atomic Energy of Canada Limited, those of the United States Atomic Energy Commission and, to a lesser degree, various concerns abroad.

Very frequently, the findings of these investigators are classified, leading to a lack of available experimental data in the published literature. Some results have appeared (21-26) which will allow a partial correlation, at least, between theoretical models and experimental data. These results are discussed in later sections as needed.

CHAPTER 3

SOME CHARACTERISTICS OF NUCLEAR REACTORS

3.0 INTRODUCTION

Before engaging in the details of the void-reactivity effect, we consider a summary-review of the basic elements in and processes of nuclear reactor theory (27) and forced convective boiling(8). Subsequently, some simple cases, representing extremes of the real reactor system, are examined. In this manner, a few dominant trends and characteristics become evident and the nature of the interaction between the neutron density and the coolant voiding is illustrated.

3.1 THE FISSION PROCESS

A nuclear reactor is a device designed to release fission energy in a controlled and usable manner. 'Fission' denotes the process in which a free neutron is absorbed by a fissile nucleus inducing it to split into smaller fragments. This splitting of the nucleus is accompanied by the release of neutrons and gamma photons. In total, some 212 Mev (million electronvolts) appears per fission; about 81% of this energy is contained in the kinetic energy of the fission fragments. As these fission fragments slow down upon collision with atoms in the material, their kinetic energy is transformed into heat. Since 1 Mev is equivalent to 1.6×10^{-13} watt-s, the fission of one U-235 nucleus releases 3.4×10^{-11} watt-s of energy. Thus,

3.0×10^{10} fissions per second are required to produce one watt of power.

Pure uranium contains 2.5×10^{21} atoms per gram. Complete fissioning of one gram of uranium thus releases 8.5×10^{10} watt-s or 3.1×10^{4} kw-hr which is more than one megawatt day. If 1 kg of U-235 fissioned completely in a one-day period, this would be equivalent to more than 1000 Mw of thermal energy. If this were converted to electricity with an efficiency of 30%, it would be equivalent to the electrical production of a large conventional power plant consuming about 2500 tons of coal per day. Complete fissioning of a gram of uranium yields approximately one million times as much energy as is released by the same mass of uranium undergoing a chemical reaction such as oxidation. This comparison between nuclear energy and chemical energy illustrates a major feature unique to nuclear reactors.

We might note that there is only one naturally occurring isotope which fissions readily. This is the isotope of uranium having an atomic weight of 235 (U-235) constituting 0.72% of natural uranium; U-238 constitutes the remaining 99.28%. There are two other fissionable isotopes of practical interest, Pu-239 and U-233, which can be produced by the nuclear transmutation of U-238 and Th-232 respectively.

3.2 THE CHAIN REACTION

A fissioning uranium atom releases from 0 to 5 neutrons; the average number depends upon the fissile nuclei and the energy of the incident neutron but is of the order of 2 to 3. The achievement of a chain reaction, which is required in a nuclear reactor, depends on the result of competition for these neutrons among four processes:

1. fission of fissile nuclei, with the emission of additional neutrons;
2. nonfission capture of neutrons by fissile nuclei;
3. nonfission capture of neutrons by other materials;
4. leakage, i.e., escape of neutrons from the reactor.

If the loss of neutrons by the last three processes is less than or equal to the surplus produced by the first, then the chain reaction occurs; otherwise, it does not. Thus, a chain reaction is possible only if at least one neutron released by fission successfully causes fission in another fissile nucleus. Obviously, the conservation of neutrons is of prime importance in reactor design.

3.3 CRITICAL SIZE

The necessity for a favorable neutron economy imposes certain conditions on a chain-reacting system. One such condition is size. If a fissile material is distributed in some regular fashion in an assembly, production of neutrons depends on the volume while the probability of escape depends on the surface area. In a very small system the surface-to-volume ratio is large so that many neutrons escape, preventing a chain reaction. But, as the size of the system increases, the escape of neutrons and their nonfission absorption are less likely to outweigh their production. For any given geometry there is a certain minimum size, called the 'critical size', for which the production of neutrons by fission just balances their loss by nonfission capture and escape; hence, a chain reaction is possible. The requirement of a critical size

to maintain a fission chain reaction contrasts sharply with chemical reactions, which may proceed regardless of system size.

3.4 THE NEUTRON CYCLE IN A THERMAL REACTOR

Neutrons released at fission are highly energetic, with kinetic energies up to several Mev, although the average is about 2 Mev. These neutrons are known as fast neutrons, with kinetic energies corresponding to speeds of the order of 2×10^7 meters per second. If these fast neutrons collide with uranium atoms, there is a high probability that they will lose some of their energy without being absorbed or inducing fission. These slower neutrons cannot produce fission in U-238 but can do so in U-235. These slower neutrons may also continue to slow down, be captured or absorbed by the various materials present, or escape from the system. When the neutron energy has been decreased to about 100 ev, a resonance region is encountered in uranium as shown in figure 3.4.1. This essentially means that U-238 has a particularly large affinity for neutrons whose energies are in the vicinity of 100 ev. Neutron absorption by U-238 occurs so readily at these energies that too few neutrons are left to sustain a chain reaction in natural uranium regardless of the size of the system. The neutrons that have their energies below the resonance region will behave in the same manner as those above the resonance region, that is, they will fission U-235, be captured, continue to slow down, or leak from the system. Neutrons of any energy can cause fission in U-235 as shown in figure 3.4.1 and a chain reaction can be achieved with a relatively small mass of this isotope.

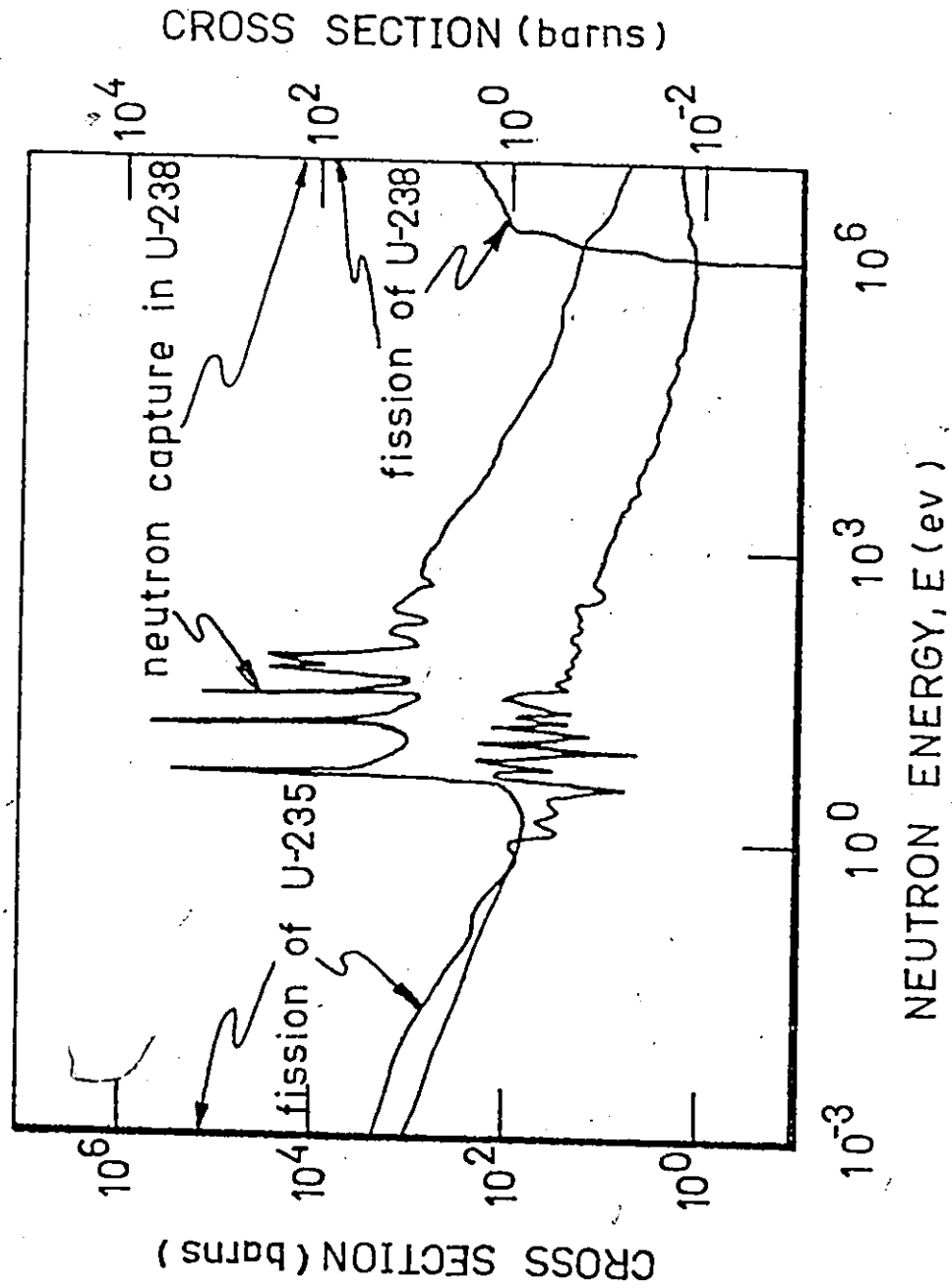

FIGURE 3.4.1: Absorption and fission cross sections for uranium as a function of the energy of the incident neutron.

A chain reaction can also be achieved in natural uranium if the uranium is arranged in a regular pattern of small lumps, so that many of the fast neutrons diffuse out of the uranium into the surrounding material where most of them are slowed down to energies below the resonance region before diffusing back into the uranium. Thus, a greater portion of neutrons is preserved for fission of U-235 by making them less likely to be captured by U-238. Material which enhances the neutron energy loss is known as a moderator. It is obvious that the moderator must not absorb too many neutrons or the reaction will stop. In effect, fast neutrons released by fission are not as likely to be absorbed as slower neutrons, hence it is desirable to provide conditions which will allow the neutrons to reduce their energy to that corresponding to the medium temperature. They are then in thermal equilibrium with the atoms or molecules of the moderator. Such neutrons are called thermal and have kinetic energies in the order of 0.025 ev, implying a speed of about 2×10^3 meters per second. The probability that a U-235 nucleus will fission is over 300 times greater with a thermal neutron than with a fast neutron, which provides the incentive for utilizing thermal neutrons. Suitable moderators are light and heavy water, carbon, beryllium and beryllium compounds.

The neutron balance in a thermal reactor may be illustrated in terms of a cycle. In figure 3.4.2 we start with the fission of a U-235 nucleus by a single thermal neutron. Due to fission, ν fast neutrons are emitted. Some of these high energy neutrons may cause fission of U-238 nuclei. For this to occur, the fast neutrons must collide with

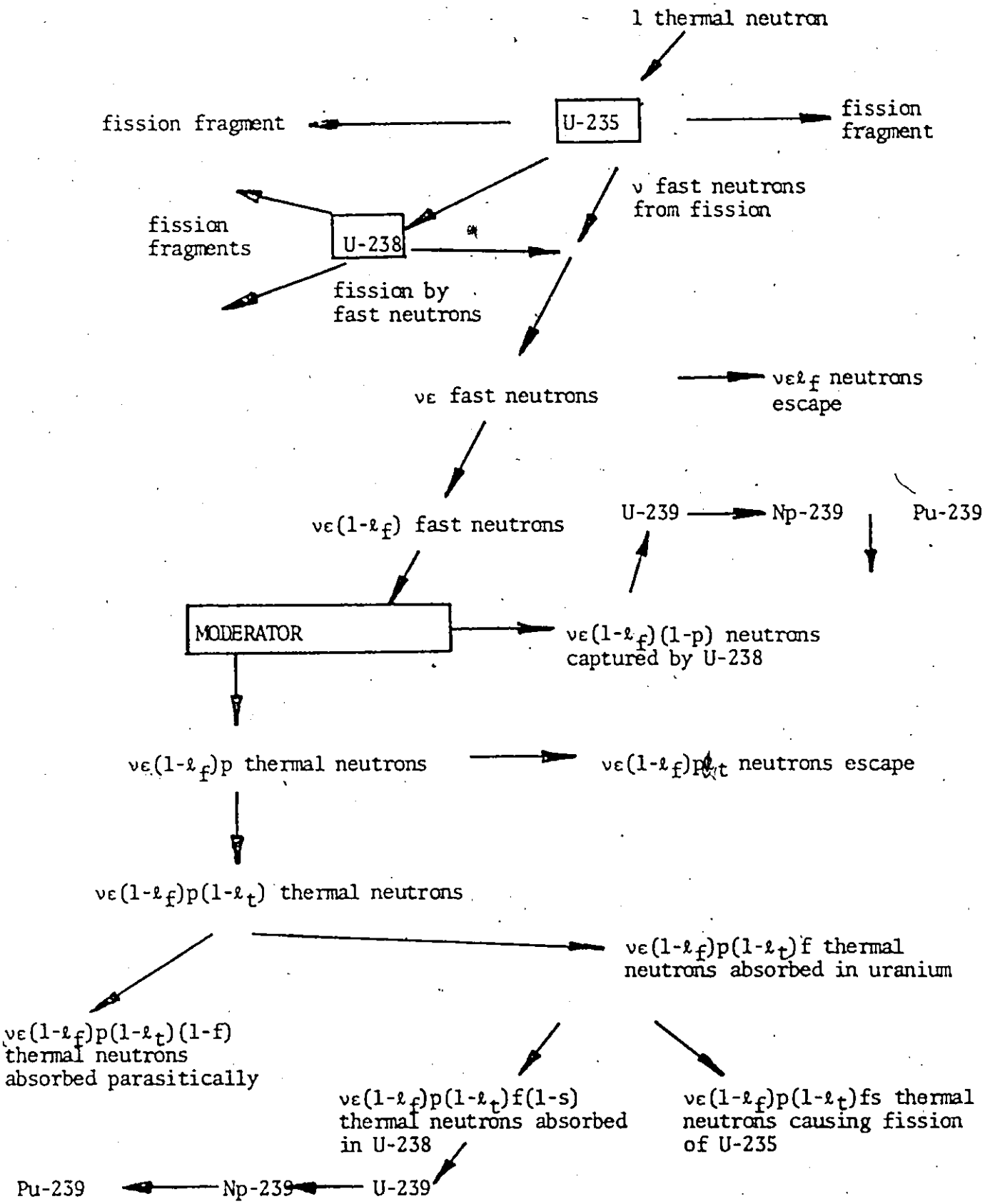

FIGURE 3.4.2: Schematic representation of the neutron cycle in the chain reaction of uranium fission.

U-238 nuclei before colliding with moderator nuclei. The small fraction of neutrons causing fission in U-238 produces additional fast neutrons. Thus the total number of fast neutrons is increased from ν to $\nu\varepsilon$, where ε, the fast fission factor, is equal to or greater than unity.

The $\nu\varepsilon$ neutrons move randomly through the uranium-moderator system. Many are slowed down, although a fraction, ℓ_f, the fast leakage probability, escapes before reaching thermal energies, hence $\nu\varepsilon\ell_f$ neutrons are lost to the chain reaction. The remaining $\nu\varepsilon(1-\ell_f)$ neutrons are slowed to thermal energies by the moderator atoms. During this process, however, $\nu\varepsilon(1-\ell_f)(1-p)$ neutrons are captured by U-238 to form U-239 which subsequently decays to Np-239 and then to Pu-239. The remaining $\nu\varepsilon(1-\ell_f)p$ neutrons escape capture. The quantity, p, is called the resonance escape probability. Although the neutrons captured by U-238 are lost in the sense that they will cause no further fission of U-235, they contribute to the ultimate production of Pu-239, which is fissile.

The $\nu\varepsilon(1-\ell_f)p$ neutrons are slowed to thermal energies. Some of these neutrons migrate in the system and escape. If the fraction escaping is ℓ_t, the thermal leakage, there are $\nu\varepsilon(1-\ell_f)p(1-\ell_t)$ neutrons left. Of these, a fraction, f, the thermal utilization factor, will be absorbed in the uranium and the remaining fraction, (1-f), will be absorbed in other materials, such as, the moderator, structural materials, and coolant. Of the $\nu\varepsilon(1-\ell_f)p(1-\ell_t)f$ neutrons absorbed by uranium, a fraction s will cause fission and the remaining (1-s) will be absorbed

to form U-239, where s is the ratio of the fission probability to the absorption probability. The number of neutrons that cause fission and thereby start a second cycle is $\nu\varepsilon(1-\ell_f)p(1-\ell_t)fs$.

This number of second-generation fission neutrons, obtained as a result of each fission of U-235 by a first-generation neutron, is called the effective reproduction factor or effective multiplication factor, and is denoted by k_{eff} for systems of finite size. It follows that

$$k_{eff} = \nu\varepsilon(1-\ell_f)p(1-\ell_t)fs \quad . \tag{3.4.1}$$

The product νs is the number of fission neutrons produced for each thermal neutron absorbed in the uranium and is called η. We rewrite the equation as

$$k_{eff} = \varepsilon\eta fp(1-\ell_f)(1-\ell_t) \quad . \tag{3.4.2}$$

To have a chain-reacting system in a steady state, k_{eff} must be unity, i.e., the system must be exactly critical. If k_{eff} is less than unity, no chain reaction is possible and the system is subcritical; if k_{eff} is greater than unity, the number of free neutrons and fissions increases from cycle to cycle, the chain reaction is said to be divergent and the system is supercritical. Another classically defined parameter, reactivity $\rho = (k_{eff}-1)/k_{eff}$, is more amenable to everyday use since $k_{eff} \approx 1$. A positive ρ indicates supercriticality while a negative

ρ indicates subcriticality.

The value of k_{eff} for an infinitely large system is especially useful in the theory and preliminary design of nuclear reactors. Since there can be no leakage from an infinite system, ℓ_f and ℓ_t are both zero and the multiplication factor becomes

$$k_\infty = \varepsilon \eta f p \quad , \tag{3.4.3}$$

which is known as the four-factor formula. Of these four factors, η depends only on the nuclear parameters of the fuel, while ε depends on the size and shape of the fuel as well as its nuclear properties. The other two quantities, p and f, depend on the nuclear properties of the fuel, moderator and all other materials present, and on the manner in which these materials are arranged.

3.5 CONTROL OF A REACTOR

If a reactor were built to exactly critical size, it would become subcritical after a few fissions since U-235 atoms are removed from the systems. Consequently, a reactor is constructed with some excess fissionable material. Thus, k_{eff} is greater than unity and the number of neutrons present increases exponentially since the reaction feeds on itself. If k_{eff} were very large, so that a great multiplication took place in a fraction of a second, an explosion due to the sudden heat release may result. Even if the reaction took place slowly, the

reactor would be destroyed by melting if multiplication continued long enough.

One effective way in which control can be exercised is by passing special rods through the core by means of channels provided for that purpose. These rods contain elements, for example, cadmium, boron, and certain rare earth elements, that readily absorb neutrons. If the rods are fully inserted into the fissioning system, they absorb so many neutrons that the chain reaction stops. If they are slowly withdrawn, a point is reached at which the chain reaction just maintains itself. If they are withdrawn further, the neutrons multiply and the reactor operates with increasing power. To reduce the multiplication rate, the rods are inserted. Thus to raise the power output, the rods are withdrawn until the desired power level is reached and then returned to the operating point while the reactor continues operating at the increased level. This contrasts with conventional power plants controls; to increase the power of an oil-fired boiler, fuel and air flows are increased.

The preceding discussion implies that the time factor is slow enough to allow an operator to maintain control by manual operation or by some mechanism that is relatively slow acting. This can be done, but only because of what are known as delayed neutrons. Depending on fuel type, geometry and other factors governing the neutron energy spectrum, about 99.3% of the neutrons are released by the fissioning nucleus in about 10^{-17} seconds after fission occurs. The neutrons are called prompt neutrons. The fission fragments are in a highly unstable

condition, and some of them release the remaining neutrons over a period averaging about 20 seconds. In order to ensure controllability, the multiplication factor for the prompt neutrons must be less than unity. If the factor is greater than unity, then the neutron level will grow exponentially in a time interval too short for control, irrespective of the delayed neutrons. For this reason, then, for a controllable reactor,

$$(1-0.007)\ k_{eff} \lesssim 1 \ . \qquad (3.5.1)$$

The limiting value of k_{eff} is, thus, given by

$$0.993\ k_{eff} = 1 \ , \qquad (3.5.2)$$

that is, $k_{eff} \lesssim 1.007$ or $\rho \lesssim .007$ depending on the fissile material involved. As long as this limitation is observed, the prompt neutron multiplication effect is bounded and presents no control problem. Normal operating conditions, then, respect this limit and no excess reactivity insertions greater than 7 mk ($\rho = .007$) are permitted. The condition of $\rho \geq .007$ is generally designated 'prompt critical'. When less than prompt critical, the control of the reactor does not present unmanagable problems since the time constant involved is determined by the weighted average time constant for both prompt and delayed neutrons and is of the order of tens of seconds. A pictorial display of these concepts is given by figure 3.5.1.

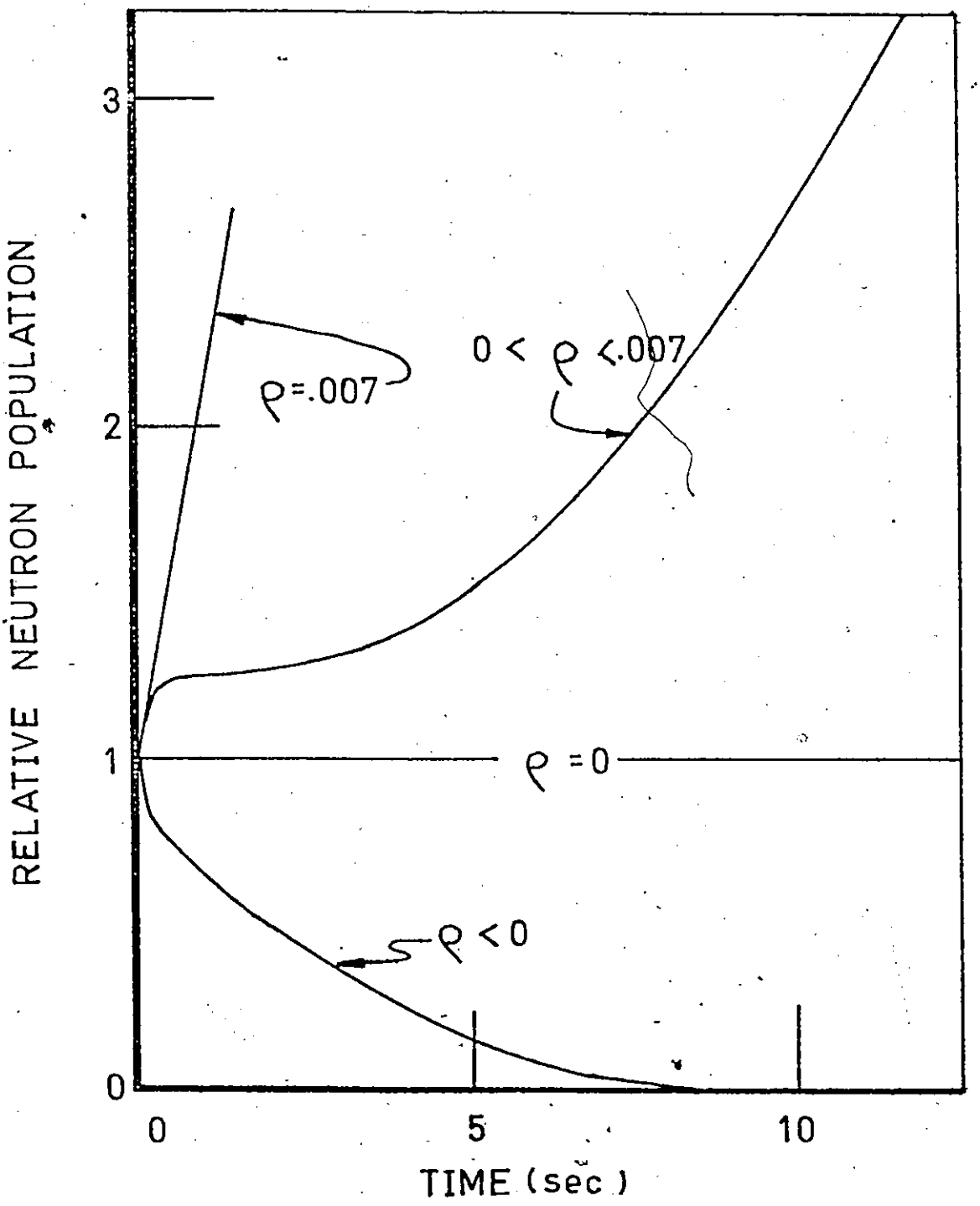

FIGURE 3.5.1: Dependence of neutron level on excess reactivity, ρ.

We will refer to this 7 mk limit again since coolant voiding can, under many conditions, easily insert more than 7 mk excess reactivity.

3.6 BASIC COMPONENTS OF A REACTOR

The preceding discussion of the neutron cycle was expressed in terms of a thermal reactor, one in which most of the fissions are caused by thermal neutrons. The basic components of a simple thermal reactor are shown in figure 3.6.1. Here, the fuel is physically located in fuel elements in the form of pure metal, a metallic alloy or a ceramic encased in another metal or alloy. This casing serves as a mechanical support and a container to keep the fission products inside the element and protects the fuel from corrosion by the coolant. The fuel elements are arranged in a regular pattern with the moderator. This arrangement of fuel and moderator, which the neutrons see as a non-homogeneous medium, classifies the reactor as heterogeneous.

The fuel-moderator core is surrounded by a reflector, a material which can also serve as a moderator. The purpose of the reflector is to act as a mirror and reflect neutrons back into the core so that the escape of neutrons will be minimized and the neutron economy thereby improved. On the exterior, completely enclosing the entire reactor, is biological shielding. This shielding absorbs the leakage neutrons and gamma rays, reducing their intensity to an acceptable level. The control rod exercises control and maintains a steady state of operation.

One important component not illustrated in figure 3.6.1 is the coolant. We recall that each fission is accompanied by release of

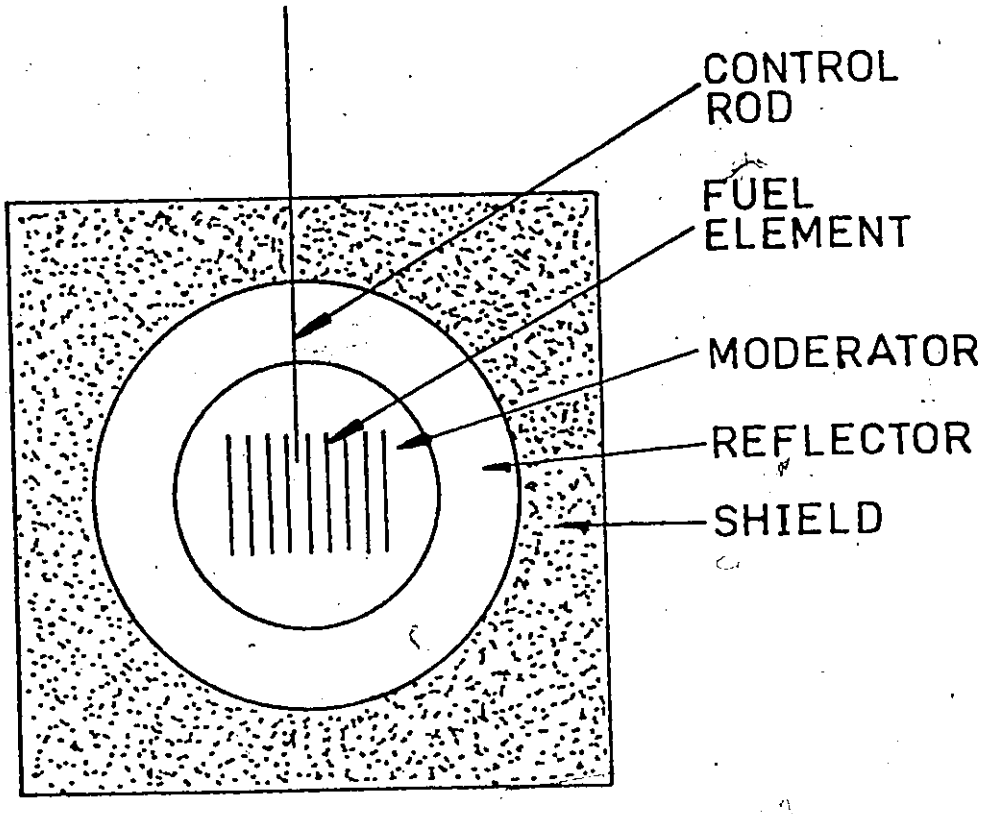

FIGURE 3.6.1: Simplified representation of a heterogeneous thermal reactor.

about 212 Mev of energy. Of this energy, some 172 Mev appears in the form of kinetic energy of the fission fragments while the remaining 40 Mev is associated with neutrons, beta rays, gamma rays, and neutrinos. Since the fission fragments rarely travel further than about 0.01 mm from the point of fission, most of the fission energy is transformed into heat close to the point of fission. For steady state operation, the heat must be removed. This is normally done by circulating a coolant through the reactor. The coolant can be a gas, such as, helium, air and carbon dioxide, or a liquid, such as, light or heavy water, organic liquids, liquid metals and molten salts. The choice of coolant depends on the design of the reactor and is limited by nuclear and engineering considerations. The coolant usually adds to nonfission capture of neutrons, and the decrease in neutron economy must be balanced against the efficiency of heat removal.

3.7 HEAT TRANSFER IN BOILING-WATER COOLED NUCLEAR REACTORS

An appreciation of the phenomena occurring in a coolant channel of a nuclear reactor can be obtained by considering the simple geometry of a long, vertical, uniformally heated tube and introducing subcooled water at the inlet. Several distinct flow regimes, as in figure 3.7.1, can be identified.

At the inlet the heat produced is being used to heat the water by forced convection (zone A) and no steam bubbles are being formed. When the surface temperature exceeds the saturation temperature by a few degrees, the liquid in contact with the heated surface is super-

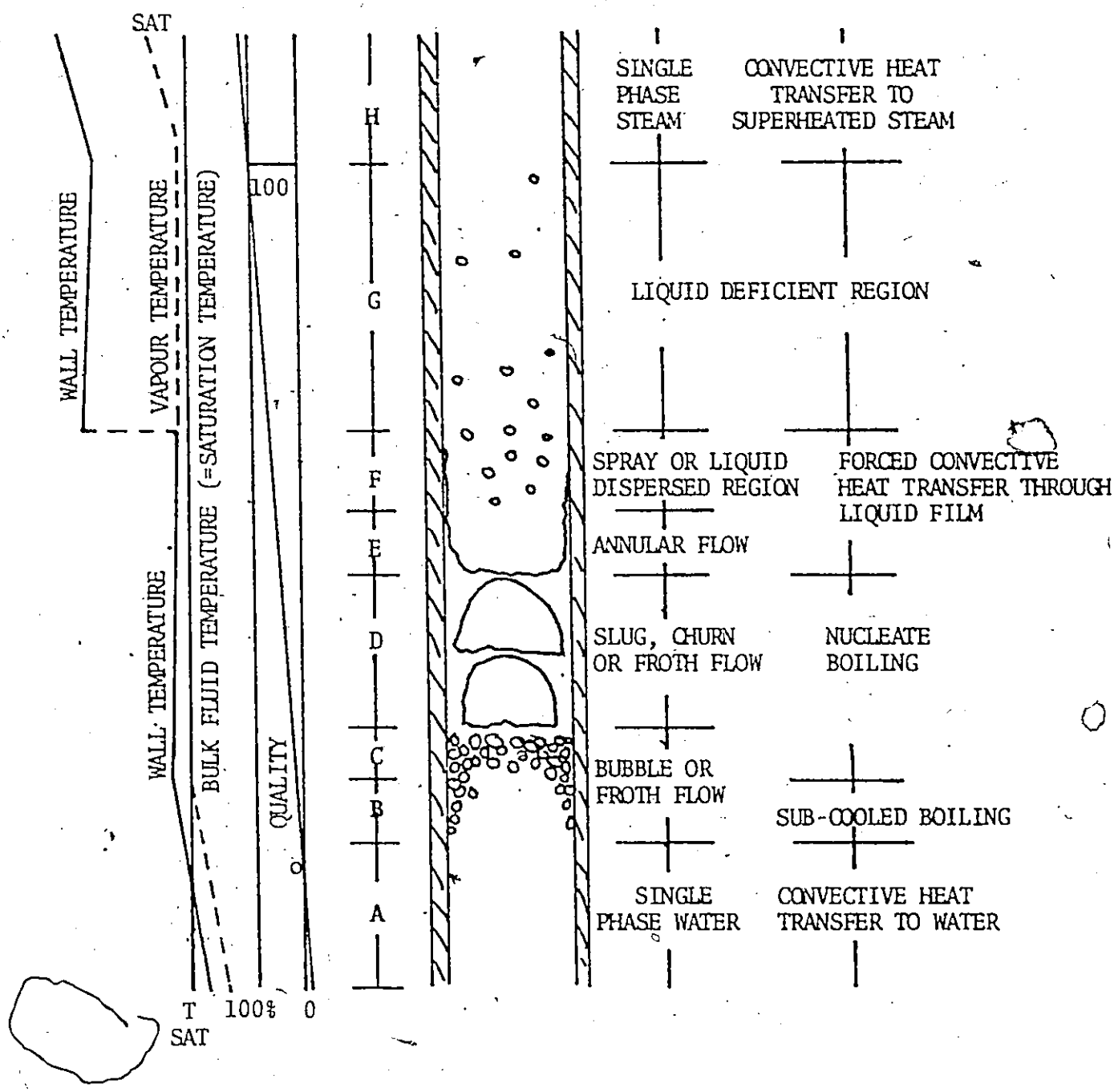

FIGURE 3.7.1: Regimes of two-phase flow.

heated a sufficient amount to allow bubble formation. As the average coolant temperature increases up the channel, the maximum bubble size increases. The bubbles may either collapse on the wall or detach and travel into the colder liquid where they condense. This is the subcooled boiling region (zone B).

When the average coolant temperature has reached saturation temperature, the bubbles no longer condense, but become entrained by the flow. This is the nucleate boiling heat transfer region with bubble flow. Up to and including the flow nucleate boiling stage, heat is transferred from the heated surface to the liquid through several mechanisms (9):

1. heat transfer by single-phase forced convection on the wetted bare surface;
2. heat transport by continuous evaporation from a liquid microlayer at the root of the bubble and the corresponding condensation at the top of the bubble while the bubble is still attached to the wall;
3. heat transfer by liquid-vapor exchange during bubble detachment from the wall;
4. heat transport by the latent heat carried by detached bubbles.

Mechanisms (1) and (2) are the modes of heat transfer until the early stages of nucleate boiling. As the heat flux continues, the heat transfer mechanism gradually shifts to mechanisms (3) and (4).

Further up the heated channel the bubbles will increase in

number and will finally coalesce to form larger bubbles or slugs which are fairly flat at the bottom end and dome-shaped at the top end. The water between the slugs may contain small diameter bubbles. This 'slug flow regime' (zone D) represents the transition from continuous-phase water to continuous-phase steam.

Further up the channel the bubbles merge to form a continuous steam column, with the water displaced to the walls. The central core of steam flows at a higher rate than the superheated liquid film on the walls. The steam core may contain entrained droplets. The interface between the liquid film and the steam core is covered by a complex pattern of waves, a necessary condition for droplet entrainment in annular flow. Heat transfer in this flow regime takes place by conduction across the liquid film and evaporation on the interface, and by nucleation on the heated wall causing entrainment of superheated water droplets into the steam core. Liquid may also be entrained into the steam flow from the top of the large waves in the liquid film. The thickness of the liquid layer is governed by the rate of droplet deposition on the film, which tends to increase the thickness, and by evaporation and entrainment of droplets, both of which tend to decrease the thickness.

Moving further up the channel, there is a continous reduction in the ratio between the deposition rate and the entrainment and evaporation rates until the liquid film at one position, determined by the heat flux and the shear stress, disappears completely and water exists only as dispersed droplets in the steam core. The water droplets hitting the heated wall can no longer wet the wall, the 'dryout point' has been

reached and the wall temperature rises. This is the 'liquid deficient' region with film boiling. Finally all liquid will have evaporated and there is convective heat transfer to the dry saturated steam.

Different combinations of the flow regimes described above may appear, particularly in the transition between slug flow and annular flow where the slug flow regime begins to break down and the gas bubbles are unstable. Here a flow structure termed semi-annular or churn flow can exist. In large diameter tubes, this unstable regime leads to an oscillation or churning flow. A wispy annular flow regime may sometimes appear, having relatively slow-moving, fairly thick liquid film containing dispersed gas bubbles. The entrained phase in the core of the channel flows in large agglomerates. Modelling of such flows is complicated by the fact that the flow regimes are influenced by many factors including geometry, water and steam velocities, and fluid properties.

The coolant temperature remains essentially constant in the boiling region and the efficient heat transfer caused by the nucleate boiling mechanism keeps the fuel cladding temperature at relatively modest values, 20-40°C above coolant temperature.

3.8 THE FEEDBACK EFFECT

Typically, hydraulic response to a power perturbation occurs in a time of the order of 10 seconds and greater. The feedback from the coolant voiding to the neutron level by changes in the moderation and absorption processes, then, is controllable by on-line controllers

monitoring the neutron level provided the reactivity insertions are less than prompt critical. However, the flow oscillations which can occur in forced convective boiling channels have time constants of the order of 0.1 seconds to 1 second. These oscillations and the resulting perturbations on reactivity may prove too much for the simple feedback control employed in today's generation reactors.

In both these cases, the reactivity insertion can be prompt critical and, hence, adequate modelling of the fluid and neutronic phenomena are essential in counteracting this feedback by either preventing the perturbation through design or by feedforward control. As we shall see, the errors in the predictions of the present day techniques can lead to very consequential results.

With the preceeding introduction to the basic concepts, we now consider some simple examples to illustrate some dominant characteristics of voiding in a neutron multiplying system.

3.9 EXAMPLE 1 - THE INFINITE HOMOGENEOUS SYSTEM

The infinite homogeneous reactor is a simple example but is one which still allows coolant-neutron flux interaction. The neutron flux density is, for this example, subject to the following constraints:

1. spatial independence;
2. one neutron energy group;
3. the effect of the delayed neutrons is incorporated by adjusting the effective neutron velocity;

4. the reactor is comprised of a homogeneous mixture of fuel, moderator and a flowing coolant.

The neutron conservation equation, analogous to the mass conservation equation, is

$$\begin{pmatrix}\text{net rate of change}\\ \text{of neutron density}\end{pmatrix} = \begin{pmatrix}\text{rate of production}\\ \text{by fission}\end{pmatrix} - \begin{pmatrix}\text{rate of loss}\\ \text{by absorption}\end{pmatrix} . \tag{3.9.1}$$

Symbolically,

$$\frac{dn(t)}{dt} = k_\infty \Sigma_{aF} v n(t) - \Sigma_{aT} v n(t) \tag{3.9.2}$$

or

$$\frac{1}{v}\frac{d\phi(t)}{dt} = (k_\infty \Sigma_{aF} - \Sigma_{aT})\,\phi(t) , \tag{3.9.3}$$

where $t \equiv$ time [s] ,

$n(t) \equiv$ scalar neutron density [neutrons/cm^3] ,

$k_\infty \equiv$ infinite multiplication constant of the fuel [dimensionless],

$\Sigma_{aF}, \Sigma_{aT} \equiv$ macroscopic absorption cross sections of the fuel and of the total reactor, respectively [cm^{-1}],

$v \equiv$ neutron speed, a constant [cm/s],

$\phi(t)=n(t)v \equiv$ scalar neutron flux, [neutrons/cm^2 s]

As a neutron passes through an assemblage of atoms, the probability of it colliding and reacting in a particular fashion with an atom depends on the effective size of the microscopic cross section of the nucleus

of the atom. This cross section is usually expressed in units of 10^{-24} cm^2 called barns. This effective size bears no direct relationship to atomic sizes as normally determined and varies greatly from one isotope to another and to some extent with the energy or speed of the neutron. The fission cross section is a measure of the probability of collision followed by fission of the nucleus in question. Likewise, the absorption cross section is a measure of the probability of collision followed by absorption of the neutron by the nucleus. A more useful unit for many purposes is the macroscopic cross section, Σ, expressed in units of inverse length. It is obtained by multiplying the microscopic cross section by the atomic density of the medium. The macroscopic cross section represents the interaction probability in a medium per unit length travelled by the neutron. Multiplying the macroscopic cross section by the scalar neutron flux, ϕ, gives the total interaction rate per unit volume. Interaction rates of 10^{13} neutrons/cm^3s are typical of nuclear reactors. Since typical atom densities are of the order of 10^{21} atoms/cm^3 the interactions of the neutrons with the nuclei can be considered independent events. Consequently, cross sections are additive; superposition applies. Tables of cross sectional data for Σ are given for pure materials. Cross sectional data for mixtures are obtained by a number weighted average of the cross sections of the individual nuclei. If the densities of the individual materials in the mixture are unchanged from that given by the pure material data, then the volume fraction can be used in the weighting procedure.

The parameters, Σ_{aF} and k_∞, are properties of the nuclear fuel and can thus be considered independent of time and the void fraction in the coolant. The total macroscopic absorption coefficient, Σ_{aT}, is a function of the fuel, moderator and coolant properties. Hence, the effect of voiding on Σ_{aT} must be considered.

Defining V_F, V_C and V_M as the volume fraction of fuel, coolant and moderator respectively, the total cross section is simply the sum of the individual cross sections weighted by their respective volume fractions. Thus,

$$\Sigma_{aT} = V_F \Sigma_{aF} + V_C \Sigma_{aC} (1 - \alpha(t)) + V_M \Sigma_{aM} , \qquad (3.9.4)$$

where Σ_{aC} is weighted by the density factor, $(1 - \alpha(t))$, to account for coolant voiding. Here, $\alpha(t)$ represents the void fraction of the coolant. Equations (3.9.3) and (3.9.4) constitute our neutron model.

Turning now to the void model, we postulate that the heat generated is proportional to the neutron density. We also postulate a space and time independent heat removal rate, Q [cal /cm^{3}s], due to an inlet and outlet coolant temperature difference. A heat balance gives

$$\begin{pmatrix}\text{rate of heat}\\ \text{production}\end{pmatrix} = \begin{pmatrix}\text{rate of heat removal by}\\ \text{coolant temperature}\\ \text{difference}\end{pmatrix} + \begin{pmatrix}\text{rate of heat removal}\\ \text{by vaporization of}\\ \text{coolant}\end{pmatrix} \qquad (3.9.5)$$

or

$$g_\alpha''' \phi(t) = Q + \lambda \rho_c \frac{d\alpha(t)}{dt} , \qquad (3.9.6)$$

where λ is the latent heat of vaporization in units of cal /gm , g_o''' [cal /neutron cm] is a proportionality constant relating the scalar neutron flux to the heat generation and ρ_c [gm/cm^3] is the coolant density. Rearranging yields,

$$\frac{d\alpha(t)}{dt} = \frac{g_o''' \phi(t) - Q}{\lambda \rho_c} \quad , \tag{3.9.7}$$

subject to the constraint,

$$0 \leq \alpha(t) \leq 1. \tag{3.9.8}$$

For illustration, we consider the following calculational case. Suppose that at t = 0, $\phi(0) = Q/g_o'''$ and $\alpha(0)$ is taken to ensure that $k_\infty \Sigma_{aF} = \Sigma_{aT}$. That is,

$$\alpha(o) = \frac{-k_\infty \Sigma_{aF} + V_F \Sigma_{aF} + V_M \Sigma_{aM} + V_C \Sigma_{aC}}{V_C \Sigma_{aC}} \quad . \tag{3.9.9}$$

Thus, from equations (3.9.3) and (3.9.7) if the system remains unperturbed, the steady state condition will persist for all time. However, we introduce a small increase in the neutron multiplication constant for a finite length of time, which results in a small increase in ϕ. This increase in ϕ results in a small increase in α via equation (3.9.7). From equation (3.9.4), Σ_{aT} is reduced and hence the factor, $k_\infty \Sigma_{aF} - \Sigma_{aT}$ is increased, resulting in a further increase in ϕ.

By a similar argument, an initial decrease in k_∞ results in a decrease in the void fraction, α, which leads to a decreased ϕ, and so on. Thus, the system in this approximation is unstable for any void perturbation of the system. This is illustrated in figures 3.9.1 and 3.9.2. The equations were solved by a straightforward Euler integration using typical parameters.

The foregoing reactor system exhibits what is generally termed a positive void coefficient, implying that an increase in void results in a positive power transient. This type of behavior characterizes the Canadian reactor design as we shall see in subsequent chapters.

3.10 EXAMPLE 2 - THE FINITE HOMOGENEOUS SYSTEM

As a second and more realistic example we consider a semi-infinite slab reactor. Again, we assume a homogeneous mixture of coolant, moderator and fuel. Maintaining the same notation as in section 3.9 we write

$$\frac{1}{v}\,\frac{\partial\phi(x,t)}{\partial t} = (k_\infty\Sigma_{aF} - \Sigma_{aT})\;\phi(x,t) + \frac{D\partial^2\phi(x,t)}{\partial x^2}\;, \qquad (3.10.1)$$

where the last term represents an additional loss of neutrons by diffusion and where D [cm] is the diffusion coefficient. This coefficient, when multiplied by the velocity, v, is analogous to that of mass and heat diffusion, having units of cm^2/s. The diffusion coefficient can be evaluated from fundamental scattering and absorption cross section data. In general, $D\alpha\Sigma^{-1}$ and, thus, the diffusion coefficient for a mixture can be obtained by the weighted average of the inverses as follows:

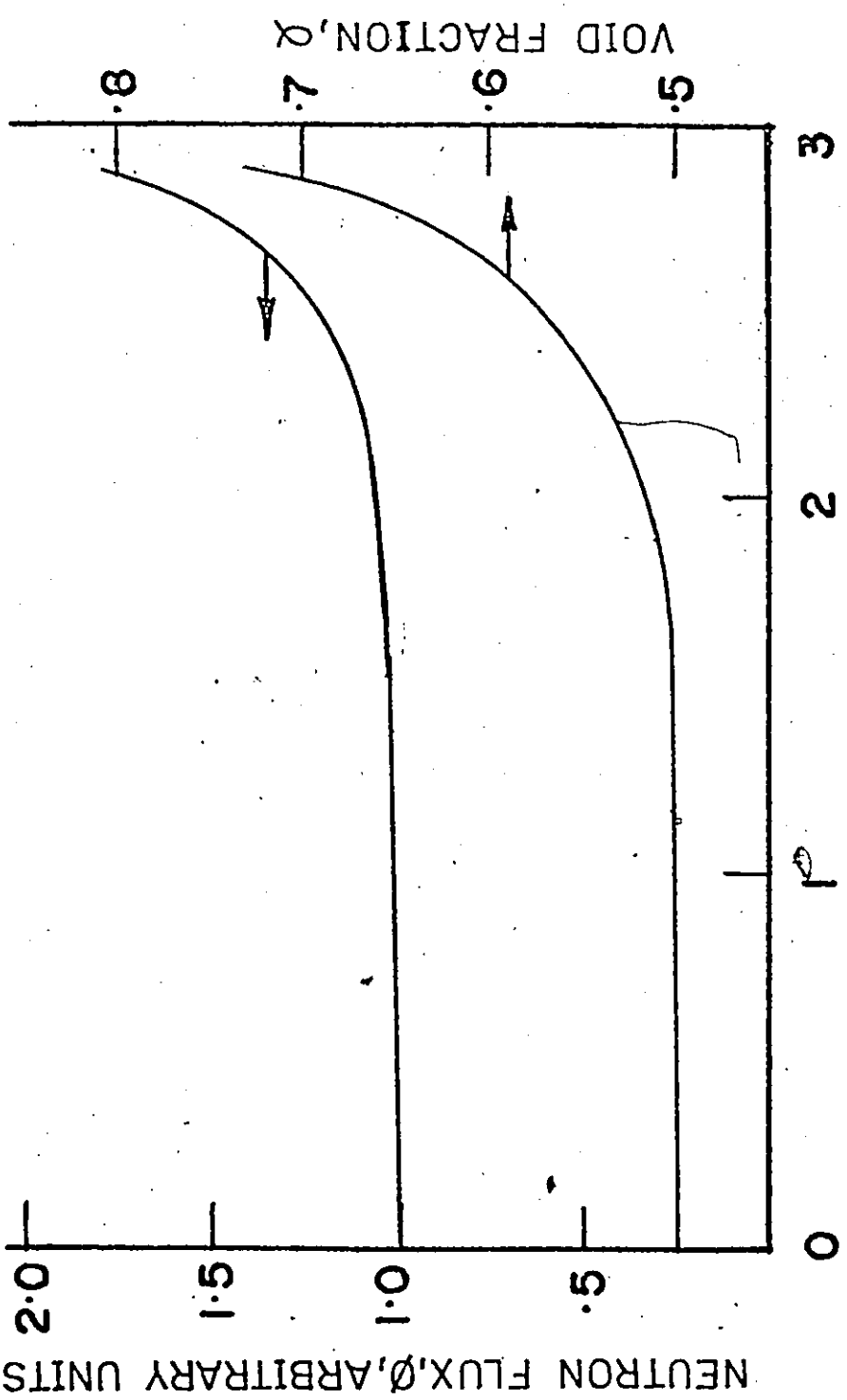

FIGURE 3.9.1: Transient response of the scalar neutron flux, ϕ, and the void function, α, for a positive reactivity insertion in an infinite nuclear reactor.

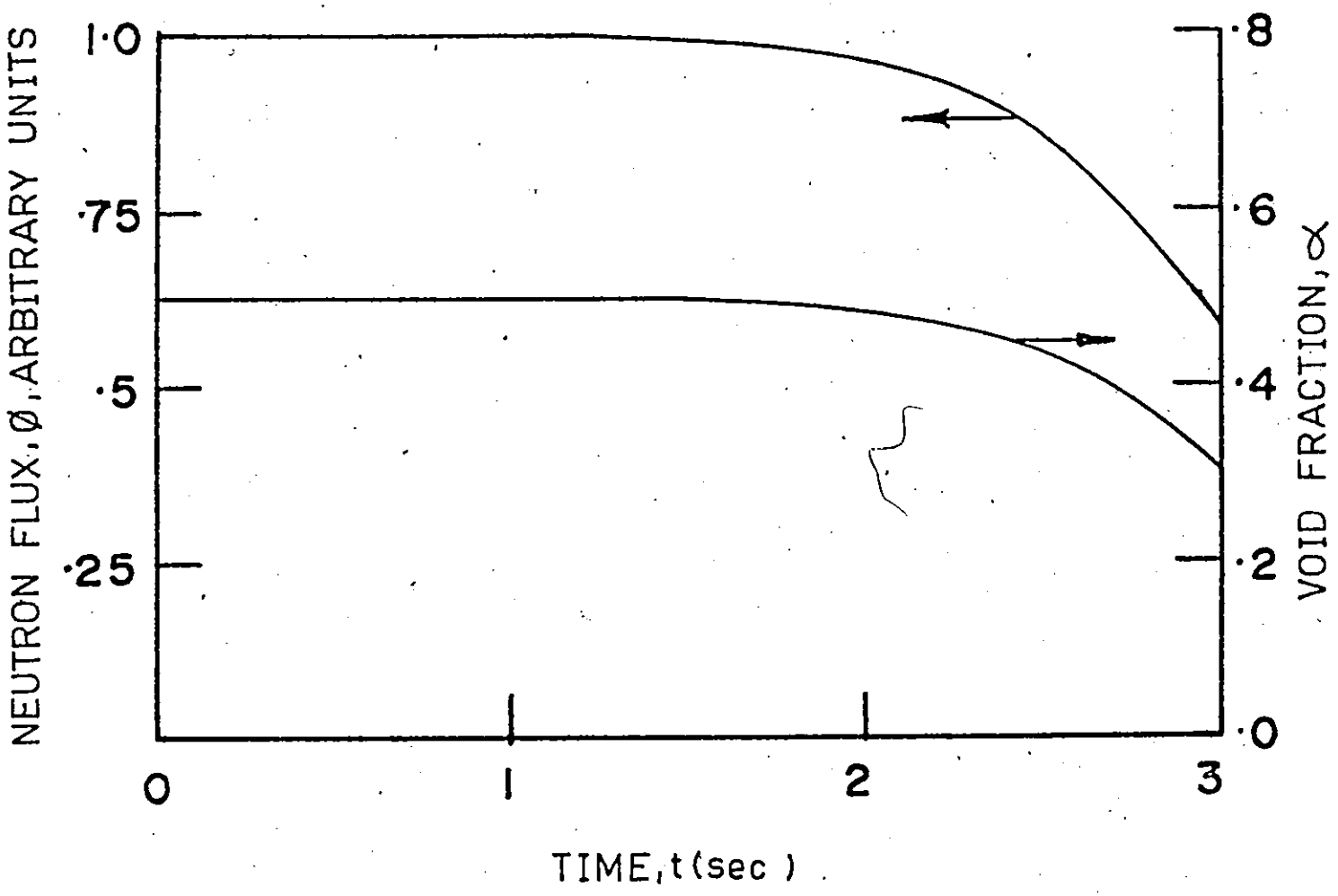

FIGURE 3.9.2: Transient response of the scalar neutron flux, ϕ, and the void fraction, α, for a negative reactivity insertion in an infinite nuclear reactor.

$$\frac{1}{D} \equiv \frac{V_F}{D_F} + \frac{V_C\,[1 - \alpha(x,t)]}{D_C} + \frac{V_M}{D_M} \,. \qquad (3.10.2)$$

Here, we notice that, although the coolant, fuel and moderator are homogeneously mixed, the properties are a function of space and time since the void is a function of space and time. To simplify the present analysis, we specify that the void is a function of time only, that is, we assume the heat generation results in homogeneous void. This implies that the spatial distribution of the scalar neutron flux is the steady state cosine distribution which satisfies the boundary conditions of symmetry about the centerline, $x = 0$, and zero scalar neutron flux at the slab boundaries, $\pm a$. Incorporating this gives

$$\frac{1}{v}\,\frac{d\phi(t)}{dt} = [k_\infty \Sigma_{aF} - \Sigma_{aT} - D(\pi/2a)^2]\,\phi(t) \qquad (3.10.3)$$

and

$$\frac{d\alpha(t)}{dt} = [2/\pi\; g_o'''\;\phi(t) - Q]/\lambda\,\rho_c \,. \qquad (3.10.4)$$

These equations are analogous to those of section 3.9 and herein are solved by Euler integration.

If the system is assumed at steady state at $t = 0$ and then perturbed, as was done in the previous case, the result of this perturbation is not as obvious as that of the infinite nuclear reactor case.

If upon application of a positive change in void, the factor, $(k_\infty \Sigma_{aF} - \Sigma_{aT} - D(\pi/2a))^2$ increases, then the reactor is said to have a positive void coefficient and the result is unchanged from that of the infinite reactor; a positive change in void results in a positive change in power. If the above factor decreases, then the reactor has a negative void coefficient and the perturbation results in a stable oscillation about the steady state conditions. Figure 3.10.1 shows such a sustained oscillation.

Similar fluctuations can occur with a reduced amplitude in real reactors (3). Thus, the direct coupling of coolant voids with neutronics, as opposed to more indirect coupling, such as, neutron energy spectrum hardening effects, system pressure oscillations and coolant pump fluctuations, is of considerable importance. With this background, we now consider the formulation and testing of models describing in detail both the neutron density and the fluid behaviour. Chapter 4 deals with the neutron density formulation while chapter 5 considers the fluid formulation.

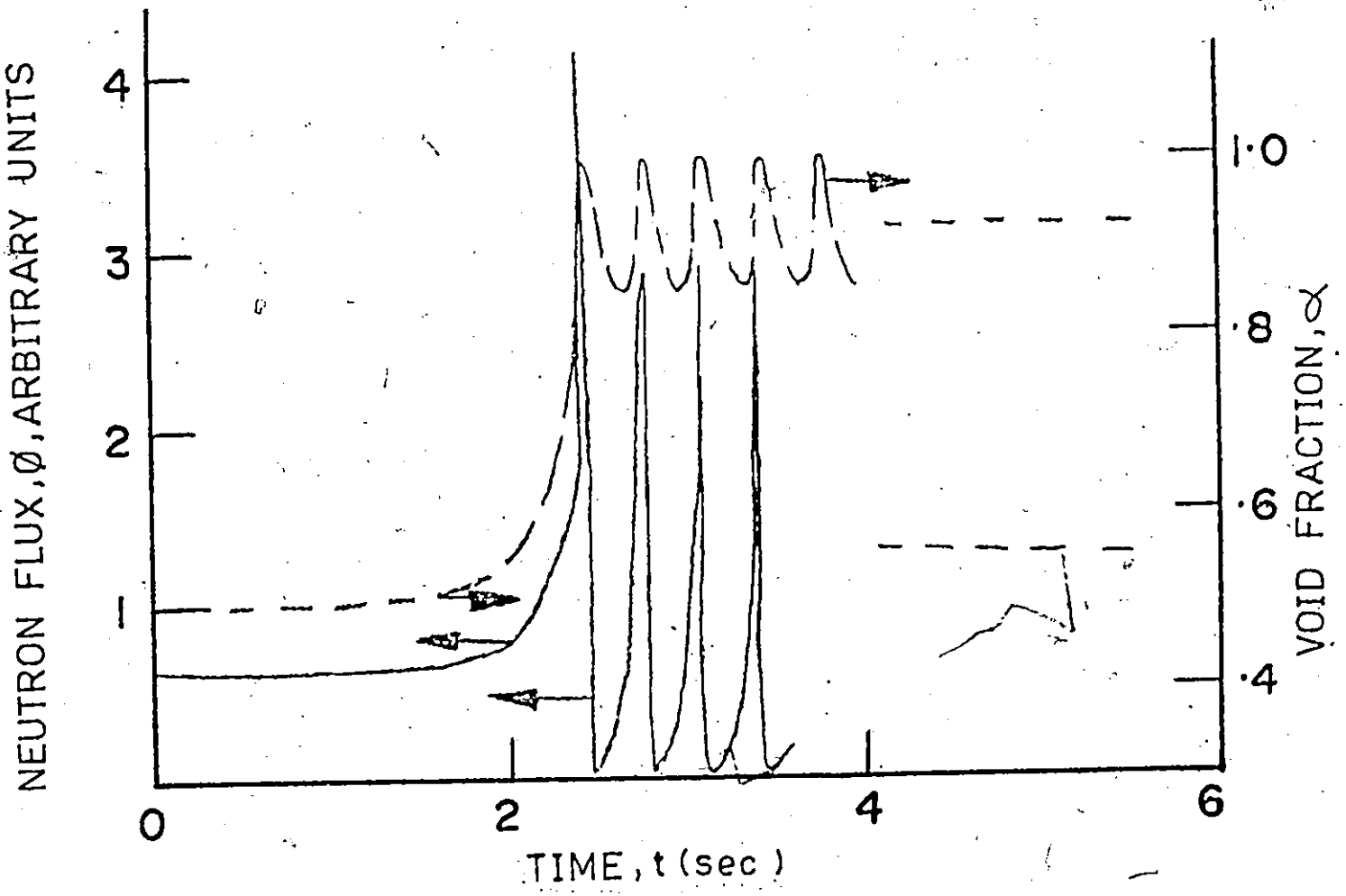

FIGURE 3.10.1: Sustained oscillations of the scalar neutron flux, ϕ, and the void fraction, α, for a positive reactivity insertion in a finite nuclear reactor.

CHAPTER 4

NEUTRON FLUX MODELLING

4.0 INTRODUCTION

In order to provide a common basis for the development of the neutron model, a generalized treatment of the neutron transport equations and the assumptions inherent in transforming these equations to a workable form is given in appendix 1. Assuming this common basis, then, we proceed to the formulation and testing of the neutron models.

This task is eased somewhat by the fact that the published experiments incorporated spatially uniform void insertions in the coolant region. This allows analytical solutions to the neutron equations, as we shall see in the first section of this chapter.

However, since the final simulation goal is to investigate the effect induced by boiling channels which are characterized by spatially non-uniform voiding, it is necessary to also investigate and formulate a neutron model capable of handling general spatial distributions of voids. This, then, is the subject of subsequent sections.

4.1 MODEL FORMULATION AND TESTING FOR UNIFORM VOIDING

To test the neutronic models accurately, it is essential that the tests be performed within the bounds of real boiling water-reactors. That is, the models should be comprised of components of comparable size and

physical properties with respect to the final simulation goal and the experiments should be chosen accordingly. The CANDU, Canadian-Deuterium-Uranium, test lattice reactors of Atomic Energy of Canada Limited fulfill these requirements.

Recent experiments (26) on the ZED-2 reactor at Chalk River have yielded results on the effect of simulated boiling on reactor reactivity by uniform air-bubble injection. The reactor consisted of a lattice of fuel bundles immersed in a heavy water (D_2O) moderator. The fuel bundles, as shown in figure 4.1.1, were comprised of uranium dioxide (UO_2) fuel pencils cooled by light water (H_2O) flowing between pencils. In these experiments the reactivity effect of the simulated voids was measured by noting the change in moderator height, H, necessary to maintain steady state. The geometric axial buckling is herein defined as $(\pi/H)^2$. An increase in buckling arising from an increase in voiding indicates that the increase in void has added reactivity to the system. A more detailed account of the experimental procedure is given in appendix 2.

To reconstruct the experimental results by a theoretical analysis, a simplified physical model is chosen and three steady-state neutron flux model formalisms are investigated: one-group diffusion theory, semi-two-group diffusion theory and two-group diffusion theory. These three models represent, respectively, increasingly detailed approximations to the neutron energy distribution.

The semi-two-group approximation incorporates a correction to one-group diffusion theory to partially account for the existence of a second group of neutrons. Two-group theory gives a full account of the second

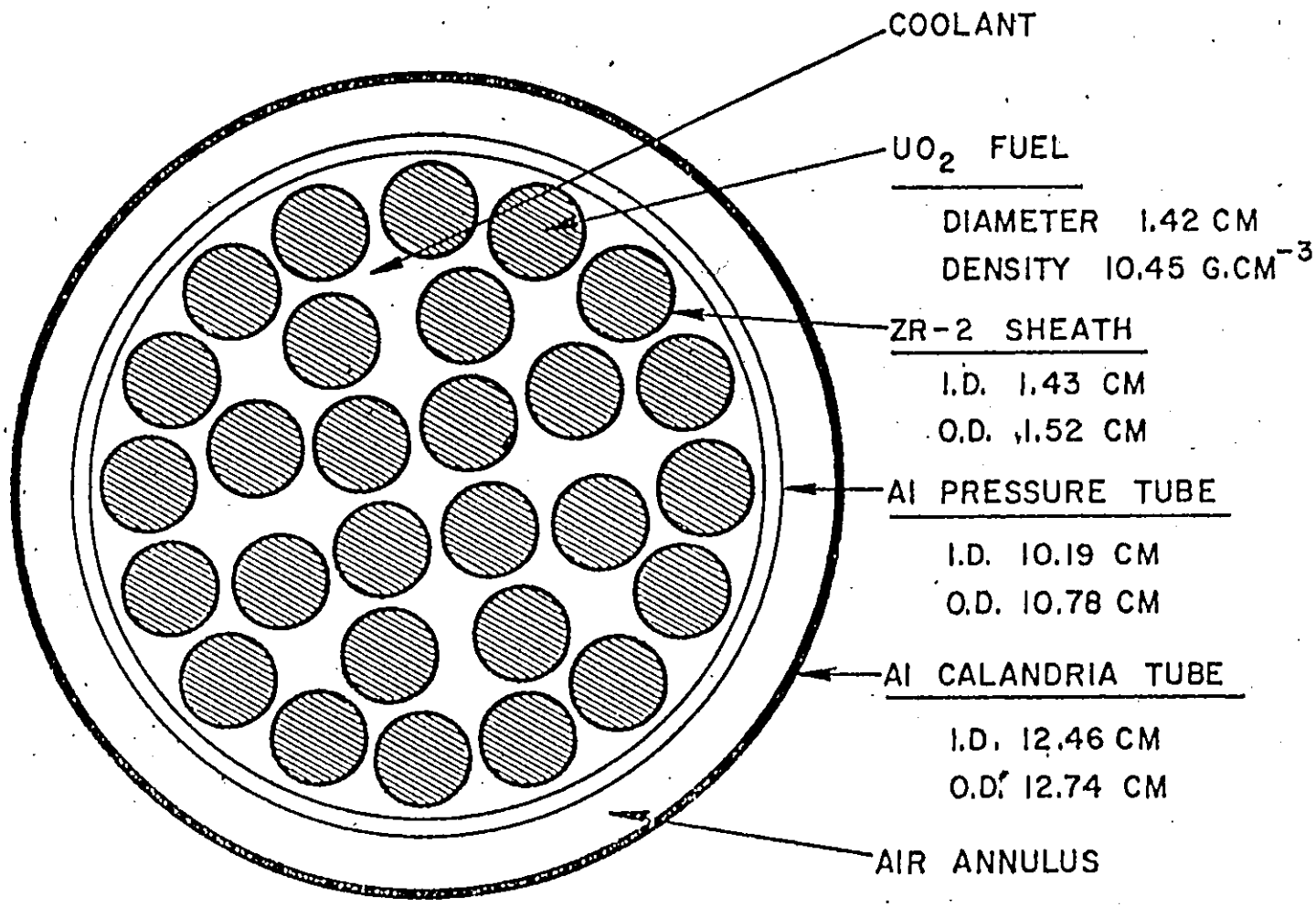

FIGURE 4.1.1: Cross section of 28-element natural UO_2 fuel assembly.

energy group. Of course, further improvements of both the neutron flux model and the physical model of the reactor are possible. It will be shown, however, that these models represent the actual reactor sufficiently well to extract useful information.

4.1.1 THE REACTOR MODEL

Figure 4.1.2 shows the physical model chosen, a simplification of the actual cell but sufficiently detailed to permit extracting information which could be compared to the experimental results. The fuel-coolant region is assumed homogeneous. This assumption is necessary in view of the complex geometry of a fuel bundle and is justified by the fact that the mean free path of a neutron is larger than the spatial inhomogeneity dimensions. Thus the model consists of two regions, the fuel-coolant region and a surrounding moderator region. This two region cell is repeated many times to form the reactor lattice. The experiments were performed on the innermost cells and by the substitution procedure, detailed in appendix 2, the radial boundary effects of the finite experimental reactor were negated. For this reason, as pointed out in reference (26), the reactor lattice can be considered to consist of an infinite number of identical cells for the purposes of experimental-model comparisons.

4.1.2 ONE-GROUP DIFFUSION THEORY

The basic theories for the three neutron flux models considered herein can be found in most texts on nuclear engineering. Lamarsh (28), for instance, describes the basic representations of diffusion theory.

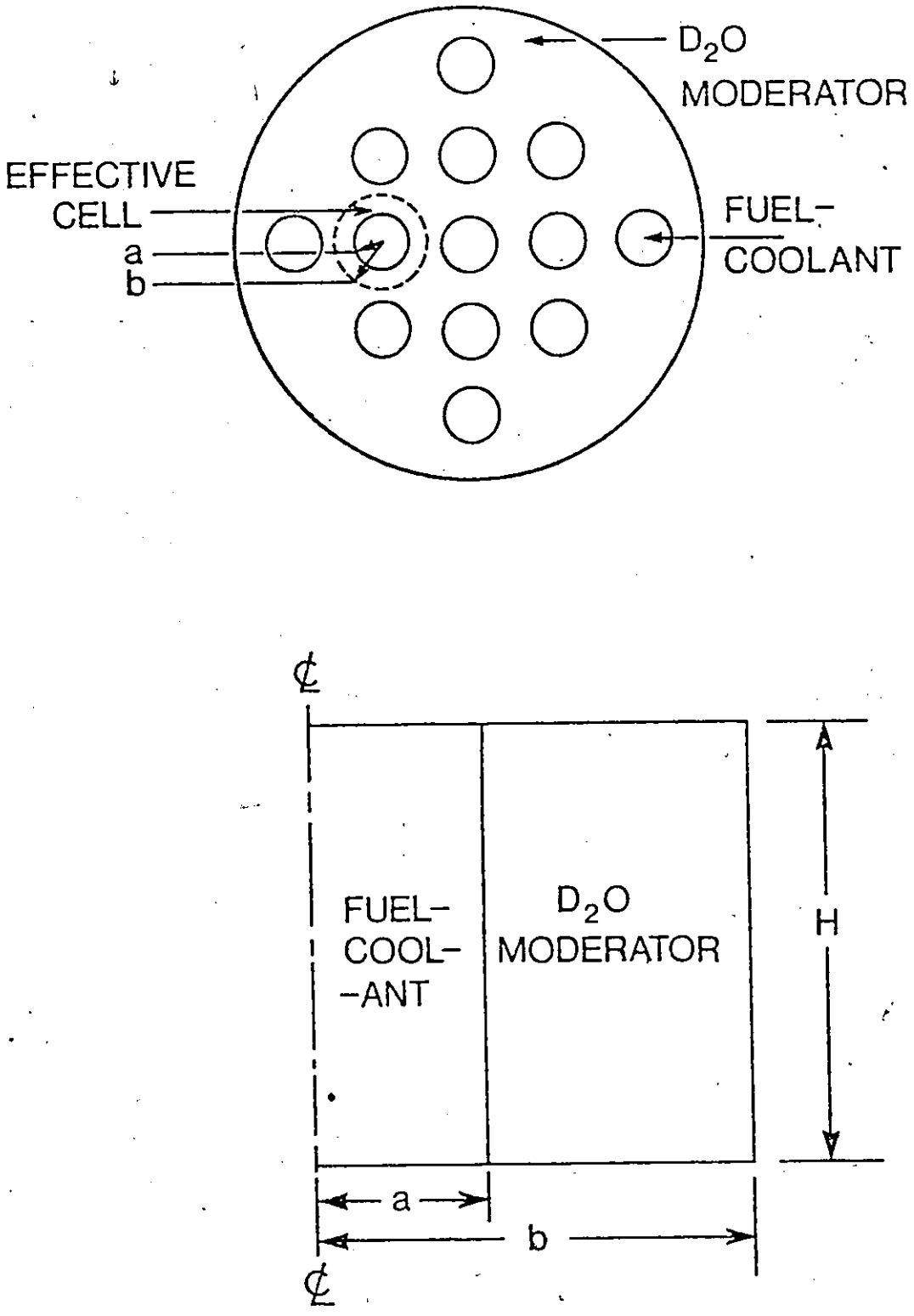

FIGURE 4.1.2 Schematic of the nuclear reactor model showing the top view of the lattice structure of fuel bundles and a side view of the two region cell . The values of a and b are 6.37 and 15.75 cm respectively.

The application of these representations to the system considered here requires extension to cylindrical geometry, extension to two dimensions and a redefinition of some fundamental parameters. Alternatively, these representations can be obtained from the general neutron transport equation as in appendix 1.

The one-group neutron diffusion equations for this system are written as

$$D_{FC}\left(\frac{1}{r}\frac{\partial}{\partial r}\left(r\frac{\partial\phi_{FC}(r,z)}{\partial r}\right)+\frac{\partial^2\phi_{FC}(r,z)}{\partial z^2}\right) + (k\Sigma_F - \Sigma_{FC})\,\phi_{FC}(r,z) = 0 \quad (4.1.1)$$

and

$$D_M\left(\frac{1}{r}\frac{\partial}{\partial r}\left(\frac{r\partial\phi_M(r,z)}{\partial r}\right) + \frac{\partial^2\phi_M(r,z)}{\partial z^2}\right) - \Sigma_M\,\phi_M(r,z) = 0 \quad , \quad (4.1.2)$$

where the subscripts FC, F, and M refer to the fuel-coolant, fuel, and moderator respectively. Also,

$\phi(r,z)$ = scalar neutron flux [neutrons/cm^2 s] ,

D = diffusion coefficient [cm] ,

Σ = macroscopic absorption cross-section [cm^{-1}] ,

k = infinite multiplication constant of the fuel[dimensionless],

r = radial coordinate [cm] ,

and z = axial coordinate [cm] .

Based on separation of variables (29), the solutions to these equations are

$$\phi_{FC}(r,z) = \phi_{OFC}\,J_o(\xi_{FC}r)\cos(\nu_{FC}z) \quad (4.1.3)$$

$$\phi_M(r,z) = \phi_{OM}\left[I_o(\xi_M r) + \mu_M\,K_o(\xi_M r)\right]\cos(\nu_M z) \quad , \quad (4.1.4)$$

subject to the constraints

$$\xi_{FC}^2 + \nu_{FC}^2 = (k\Sigma_F - \Sigma_{FC})/D_{FC} \tag{4.1.5}$$

and

$$\xi_M^2 - \nu_M^2 = \Sigma_M/D_M \quad . \tag{4.1.6}$$

Here, J_o is the zero order Bessel function of the first kind, and I_o and K_o are the zero order modified Bessel functions of the first and second kind respectively.

Evaluation of the constants, ϕ_{OFC}, ϕ_{OM}, ξ_{FC}, ν_{FC}, ξ_M, μ_M, and ν_M is possible by the application of the boundary conditions: (1) zero scalar neutron flux at $z = \pm H/2$; (2) continuity of scalar neutron flux and current at the radial interface; and (3) zero neutron current at the cell boundary. This is consistent with the identical cell approximation already mentioned. Symmetry has been applied to equations (4.1.3) and (4.1.4). Application of these conditions to equations (4.1.3) and (4.1.4) gives

$$\nu_{FC} = \nu_M = \pi/H \tag{4.1.7}$$

and

$$\mu_M = I_1(\xi_M b)/K_1(\xi_M b) \quad , \tag{4.1.8}$$

where b is the cell radius, and I_1 and K_1 are the first order modified Bessel functions of the first and second kind respectively. Also, we find

$$- D_{FC} J_1(\xi_{FC}a)\xi_{FC}[I_o(\xi_M a)K_1(\xi_M b) + I_1(\xi_M b)K_o(\xi_M a)]$$

$$= D_M J_o(\xi_{FC}a)\xi_M[I_1(\xi_M a)K_1(\xi_M b) - I_1(\xi_M b)K_1(\xi_M a)] , \qquad (4.1.9)$$

which is known as the 'criticality equation' because it relates geometry and material parameters for a critical assembly. Given all but one parameter (geometric or material), equations (4.1.5) to (4.1.9) define the remaining parameter required for criticality.

The effect of voiding is realized through the void dependence of Σ and D (1,28) as discussed previously:

$$\Sigma = \sum_i V_i \Sigma_i , \qquad (4.1.10)$$

$$1/D = \sum_i V_i/D_i , \qquad (4.1.11)$$

where the subscript, i, refers to a particular atomic species, V_i refers to the volume fraction of that species and the summation is performed over all species present in the medium under consideration. Equations (4.1.10) and (4.1.11) are, of course, approximations of the true effect of voiding. For a more detailed account, transport theory considerations are needed. For the present, the neutron flux models will be evaluated using the equations (4.1.10) and (4.1.11). Transport corrections will be introduced as required. A model-experiment comparison will be given after the presentation of semi-two-group and two-group models and the discussion of parameter sensitivity since the discussion applies to all three models and is essential to the experimental comparison.

4.1.3 SEMI-TWO-GROUP DIFFUSION THEORY

In a nuclear reactor, neutrons are born at high energy by the fission process in the fuel region. These fast neutrons subsequently slow down by elastic and inelastic collisions with nuclei in the system. Low atomic weight elements give more efficient slowing down and hence most of the slowing down occurs in the moderator rather than in the heavy elements of the fuel region. The slow neutrons then diffuse back to the fuel region and the cycle continues. Herein, a correction is applied to one-group theory to account for the slowing down of neutrons; we assume that the neutrons are born in the fuel, are subsequently transported without loss to the moderator, become thermalized and finally allowed to diffuse back to the fuel. We further assume that the slowing down and the thermalization in the moderator is not dependent on the radial position within the moderator. We note that this is not a two-group, two-region approximation since all slowing down and thermalization occurs only in the moderator. In the two-group, two-region approximation each region contributes to slowing down, thermalization and absorption.

The basic equations for this approximation are

$$D_{FC}\left(\frac{1}{r}\frac{\partial}{\partial r}\left(r\frac{\partial\phi_{FC}(r,z)}{\partial r}\right)+\frac{\partial^2\phi_{FC}(r,z)}{\partial z^2}\right) - \Sigma_{FC}\,\phi_{FC}(r,z) = 0 \qquad (4.1.12)$$

and

$$D_M\left(\frac{1}{r}\frac{\partial}{\partial r}\left(r\frac{\partial\phi_M(r,z)}{\partial r}\right)+\frac{\partial^2\phi_M(r,z)}{\partial z^2}\right) - \Sigma_M\,\phi_M(r,z) + q(\cos(\nu_M z)), \qquad (4.1.13)$$

where the previously defined notation is maintained and where q is the

slowing down density. Lamarsh (28) gives the solution for the one-dimensional case. Extension to two dimensions is straightforward and leads to

$$\phi_{FC}(r,z) = AI_o(\xi_{FC}r)\cos(\nu_{FC}z) \tag{4.1.14}$$

and

$$\phi_M(r,z) = \{[A'I_o(\xi_M r) + CK_o(\xi_M r)] + q/\Sigma_M\}\cos(\nu_M a) \ . \tag{4.1.15}$$

Applying the same boundary conditions as before gives

$$\nu_{FC} = \nu_M = \pi/H \tag{4.1.16}$$

and

$$q/A = I_o(\xi_{FC}a)\Sigma_M \{1 - \frac{D_{FC}\,\xi_{FC}\,I_1(\xi_{FC}a)}{D_M\,\xi_M\,I_o(\xi_{FC}a)} \times [\frac{I_o(\xi_M a)K_1(\xi_M b) + K_o(\xi_M a)\,I_1(\xi_M b)}{I_1(\xi_M a)\,K_1(\xi_M b) - K_1(\xi_M a)\,I_1(\xi_M b)}]\} \tag{4.1.17}$$

where

$$\xi^2_{FC} = \Sigma_{FC}/D_{FC} + \nu^2_{FC} \tag{4.1.18}$$

and

$$\xi^2_M = \Sigma_M/D_M + \nu^2_M \ . \tag{4.1.19}$$

We can easily relate q, the slowing down density, to the effective multiplication constant, k, from a balance of the neutron production in the fuel to the slowing down density in the moderator, giving

$$k = q/A\,\frac{(b^2 - a^2)\,\xi_{FC}}{aI_1(\xi_{FC}a)\,\Sigma_{FC}} \ . \tag{4.1.20}$$

Specifying all but one parameter in the material and geometric parameter set and using equations (4.1.16) to (4.1.20) allows the determination of the value of the remaining parameter necessary for criticality.

4.1.4 TWO-GROUP DIFFUSION THEORY

Although the neutron energy spectrum is continuous, it is characterized by two peaks, the thermal peak and the fission peak plus a 1/E region, as discussed in appendix 1. Two-group theory, as the name implies, assumes the existence of: (1) the thermal group; and (2) the 1/E plus the fast group. The basic equations are thus,

$$D_{1FC}\left(1/r\,\frac{\partial}{\partial r}\left(r\,\frac{\partial\phi_{1FC}(r,z)}{\partial r}\right)+\frac{\partial^2\phi_{1FC}(r,z)}{\partial z^2}\right)-\Sigma_{1FC}\,\phi_{1FC}(r,z)+\epsilon nf\,\Sigma_{2FC}\,\phi_{2FC}(r,z)=0\,, \tag{4.1.21}$$

$$D_{2FC}\left(1/r\,\frac{\partial}{\partial r}\left(r\,\frac{\partial\phi_{2FC}(r,z)}{\partial r}\right)+\frac{\partial^2\phi_{2FC}(r,z)}{\partial z^2}\right)-\Sigma_{2FC}\,\phi_{2FC}(r,z)+p\Sigma_{1FC}\,\phi_{1FC}(r,z)=0\,, \tag{4.1.22}$$

$$D_{1M}\left(1/r\,\frac{\partial}{\partial r}\left(r\,\frac{\partial\phi_{1M}(r,z)}{\partial r}\right)+\frac{\partial^2\phi_{1M}(r,z)}{\partial z^2}\right)-\Sigma_{1M}\,\phi_{1M}(r,z)=0, \tag{4.1.23}$$

and

$$D_{2M}\left(1/r\,\frac{\partial}{\partial r}\left(r\,\frac{\partial\phi_{2M}(r,z)}{\partial r}\right)+\frac{\partial^2\phi_{2M}(r,z)}{\partial z^2}\right)-\Sigma_{2M}\,\phi_{1M}(r,z)+\Sigma_{1M}\,\phi_{1M}(r,z)=0\,, \tag{4.1.24}$$

where subscripts 1 and 2 refer to the fast and slow groups respectively and

p = resonance escape probability,

η = number of fission neutrons emitted per thermal neutron absorbed by fuel,

ε = number of fission neutrons emitted by all fissions per number emitted by thermal fissions,

and

f = fraction of thermal neutrons absorbed by fuel in fuel-coolant region.

A factorization and rearrangment (28) transforms the starting differential equations to the well-known wave or Helmholtz equations which can be solved by separation of variables. Thus,

$$\phi_{1FC}(r,z) = [AJ_o(\xi_{FC}r) + CI_o(\sigma_{FC}r)] \cos(\nu_{FC}z) , \tag{4.1.25}$$

$$\phi_{2FC}(r,z) = [AS_I J_o(\xi_{FC}r) + CS_2 I_o(\sigma_{FC}r)] \cos(\nu_{FC}z) , \tag{4.1.26}$$

$$\phi_{1M}(r,z) = F[I_o(\xi_{1M}r) K_1(\xi_{1M}b) + I_1(\xi_{1M}b) K_o(\xi_{1M}r)] \cos(\nu_M z) , \tag{4.1.27}$$

and

$$\phi_{2m}(r,z) = S_3\phi_{1M}(r,z) + G[I_o(\xi_{2M}r) K_1(\xi_{2M}b) + I_1(\xi_{2M}b) \cdot K_o(\xi_{2M}r)] \cos(\nu_M z) . \tag{4.1.28}$$

where

$$\xi_{FC}^2 = \nu_{FC}^2 - \gamma^2 \tag{4.1.29}$$

$$\sigma_{FC}^2 = \nu_{FC}^2 + \kappa^2 , \tag{4.1.30}$$

$$\gamma^2\kappa^2 = \frac{k - 1}{\tau_{FC}L_{FC}^2} = \frac{\varepsilon nfp - 1}{\tau_{FC}L_{FC}^2} , \tag{4.1.31}$$

$$\kappa^2 - \gamma^2 = \frac{1}{\tau_{FC}} + \frac{1}{L_{FC}^2} , \tag{4.1.32}$$

$$\tau_{FC} = D_{1FC}/\Sigma_{1FC} , \tag{4.1.33}$$

$$L_{FC}^2 = D_{2FC}/\Sigma_{2FC} , \tag{4.1.34}$$

$$S_1 = \frac{p\ \Sigma_{1FC}/\Sigma_{2FC}}{1 + \gamma^2 L_{FC}^2} , \tag{4.1.35}$$

$$S_2 = \frac{p\ \Sigma_{1FC}/\Sigma_{2FC}}{1 - \kappa^2 L_{FC}^2} , \tag{4.1.36}$$

$$\xi_{1M}^2 = \Sigma_{1M}/D_{1M} + \nu_M^2 , \tag{4.1.37}$$

$$\xi_{2M}^2 = \Sigma_{2M}/D_{2M} + \nu_M^2 , \tag{4.1.38}$$

and

$$S_3 = \frac{\Sigma_{1M}/D_{2M}}{\xi_{2M}^2 - \xi_{1M}^2} . \tag{4.1.39}$$

Equations (4.1.25) to (4.1.28) incorporate the boundary conditions of radial symmetry at the cell center, r = o, and zero neutron flux current at the cell boundary, r = b. Using the boundary conditions of symmetry in the z direction and zero neutron flux at the extrapolated endpoints, z = ± H/2, we find that

$$\nu_{FC} = \nu_M = \pi/H . \tag{4.1.40}$$

Equations (4.1.29) to (4.1.40), then, relate all the unknowns except A, C,

F and G. These four unknowns can be related by the application of the boundary conditions of continuity of flux and current for both neutron groups at the interface, r = a. Algebraic manipulation yields a set of four simultaneous linear equations in the unknowns A, C, F and G. This set is satisfied by

$$\begin{vmatrix} 1 & 1 & 1 & 0 \\ D_{1FC}X'/X & D_{1FC}Y'/Y & D_{1M}Z'/Z & 0 \\ S_1 & S_2 & S_3 & 1 \\ D_{2FC}S_1X'/X & D_{2FC}S_2Y'/Y & D_{2M}S_3Z_1'/Z_1 & D_{2M}Z_2'/Z_2 \end{vmatrix} = 0 \quad , \quad (4.1.41)$$

where

$$X = J_o(\xi_{FC}r) \quad , \quad (4.1.42)$$

$$Y = I_o(\sigma_{FC}r) \quad , \quad (4.1.43)$$

$$Z_1 = I_o(\xi_{1M}r)\, K_1(\xi_{1M}b) + I_1(\xi_{1M}b)\, K_o(\xi_{1M}r) \quad , \quad (4.1.44)$$

$$Z_2 = I_o(\xi_{2M}r)\, K_1(\xi_{2M}b) + I_1(\xi_{2M}b)\, K_o(\xi_{2M}r) \quad , \quad (4.1.45)$$

and the prime indicates the radial derivative. The criticality determinant, equation (4.1.41), can be satisfied by any consistent set of the material parameters appearing in equations (4.1.21) to (4.1.24) and the geometric parameters, a, b and H. Herein, we specify all but H, the height of the reactor. Equation (4.1.41) gives this height for criticality through the use of equations (4.1.29) to (4.1.40).

Before comparing the experimental data with the predictions of the three models presented here, the effects of errors in the parameters need to be discussed.

4.1.5 PARAMETER SENSITIVITY CONSIDERATIONS

We illustrate the effect of parametric error on model prediction by considering one-group theory applied to a one-dimensional slab, homogeneous, critical reactor. The neutron balance equation in the steady state is

$$\frac{\partial^2 \phi(x)}{\partial x^2} + \frac{\Sigma}{D}(k - 1)\phi(x) = 0 \quad , \qquad -a \leq x \leq a \quad , \tag{4.1.46}$$

where the previously defined symbolism applies. The solution is of the form

$$\phi(x) = \phi_o \cos(B_n x) \tag{4.1.47}$$

and, since $\phi = 0$ at the slab boundaries ($\pm a$),

$$B_n = n\pi/a, \qquad n = 1, 3, 5 \ldots\ldots\ldots \quad . \tag{4.1.48}$$

Of the full set of eigenvalues, B_n, and eigenfunctions, $\cos(B_n x)$, only one value of n has physical significance in the steady state other than the trivial solution, $n = 0$. This one value is $n = 1$, corresponding to the fundamental mode. Equations (4.1.46) and (4.1.47) give, by substitution,

$$- B_1^2 \phi(x) + \frac{\Sigma}{D}(k - 1)\phi(x) = 0 \quad , \tag{4.1.49}$$

or

$$B_1^2 = \frac{\Sigma}{D}(k - 1) \quad . \tag{4.1.50}$$

The term B_1^2 is often denoted the geometric buckling and the term $\Sigma(k - 1)/D$

is denoted the material buckling. In order for steady state conditions to hold, the two must be equal. Equation (4.1.50) is the criticality equation, corresponding to that developed for the models in the previous sections.

An error in Σ or D of, say, 10% (typically) will introduce an error in B^2 of approximately 10%. This is tolerable. However, since k - 1.1 in most cases, an error of 10% in k will introduce a huge error in (k - 1) and, consequently, in B^2. In order to predict the size or material properties needed to build a critical reactor, the value of k has to be accurately known. This is presently accomplished by building prototypes and by experimental-theoretical correlations.

No accurate a priori predictions based solely on fundamental parameters are available. The theoretical models are effectively curve fitted for the particular situation under consideration. One is never sure, then, that the theory is adequate since there are usually enough free parameters to ensure agreement between model and data. Indeed, recent experience at C.R.N.L. has shown that when extrapolating the models beyond present day fuels to the next generation fuels, thorium or plutonium, completely erroneous predictions result (30).

The above discussion is based on a simple neutron model. The effect is similar for the more detailed neutron models, as presented in previous sections, though not as easily visualized as in the above case.

Because of the large errors in present predictions of (k - 1), as, for instance given by the code LATREP, described below, it is necessary to use one piece of experimental data to obtain a better estimate of this

parameter. Equally well any void fraction, α, could be used as the fitted point, but to provide maximum sensitivity to the void effect either $\alpha = 0.0$ or $\alpha = 1.0$ should be used. Herein, $\alpha = 0.0$ is chosen.

4.1.6 CALCULATIONS AND RESULTS

The calculations of the model predictions are easily done by a computer and require only a few seconds of computation time. Appendices 3 to 5 detail the codes for the one-group, semi-two-group and two-group models, respectively. In these calculations, one value of the experimental axial buckling data at $\alpha = 0.0$ is used. This allows the calculation of k, the infinite multiplication constant. We are able, now, to predict the buckling vs. void fraction relationship for the experimental-model comparison.

The parametric data for all three models is that of the ZED-2 nuclear reactor. A literature search (26,31) reveals approximate values for cross sections, diffusion coefficients and the terms of the four factor formula. These are listed in table 4.1.1. The effect of the parametric uncertainty is depicted by the spread of the curves in figure 4.1.3.

Figure 4.1.3 compares the three models: one-group, semi-two-group and two-group using parametric data from table 4.1.1. We see that successive models, representing successive improvements in treating the energy spectrum, experience successively better agreement with the experimental data. This indicates that the discrepancies of the first two models can be accounted for by a better representation of the energy groups. We also note that the semi-two-group model of Nahavandi (5-7),

MATERIAL	$\Sigma_1(cm^{-1})$	$D_1(cm)$	$\Sigma_2(cm^{-1})$	$D_2(cm)$	$\epsilon\eta$	p	f
H_2O	0.05	1.55	0.0197	0.16	--	--	--
D_2O(99.66%)	9.96×10^{-3}	1.29	9.6×10^{-5}	0.869	--	--	--
UO_2	$.01\leq\Sigma_1\leq.2$	1.25	$.05\leq\Sigma_1\leq.17$	$.1\leq D_2\leq2.0$	1.36	0.9	calculated

Table 4.1.1 Approximate parametric values for the diffusion models. The parameter, f, is calculated as the volume weighted ratio of thermal neutron absorption by fuel to thermal neutron absorption by fuel plus coolant. The thermal parameters are used for the one-group and semi-two-group models, as well as the two-group model.

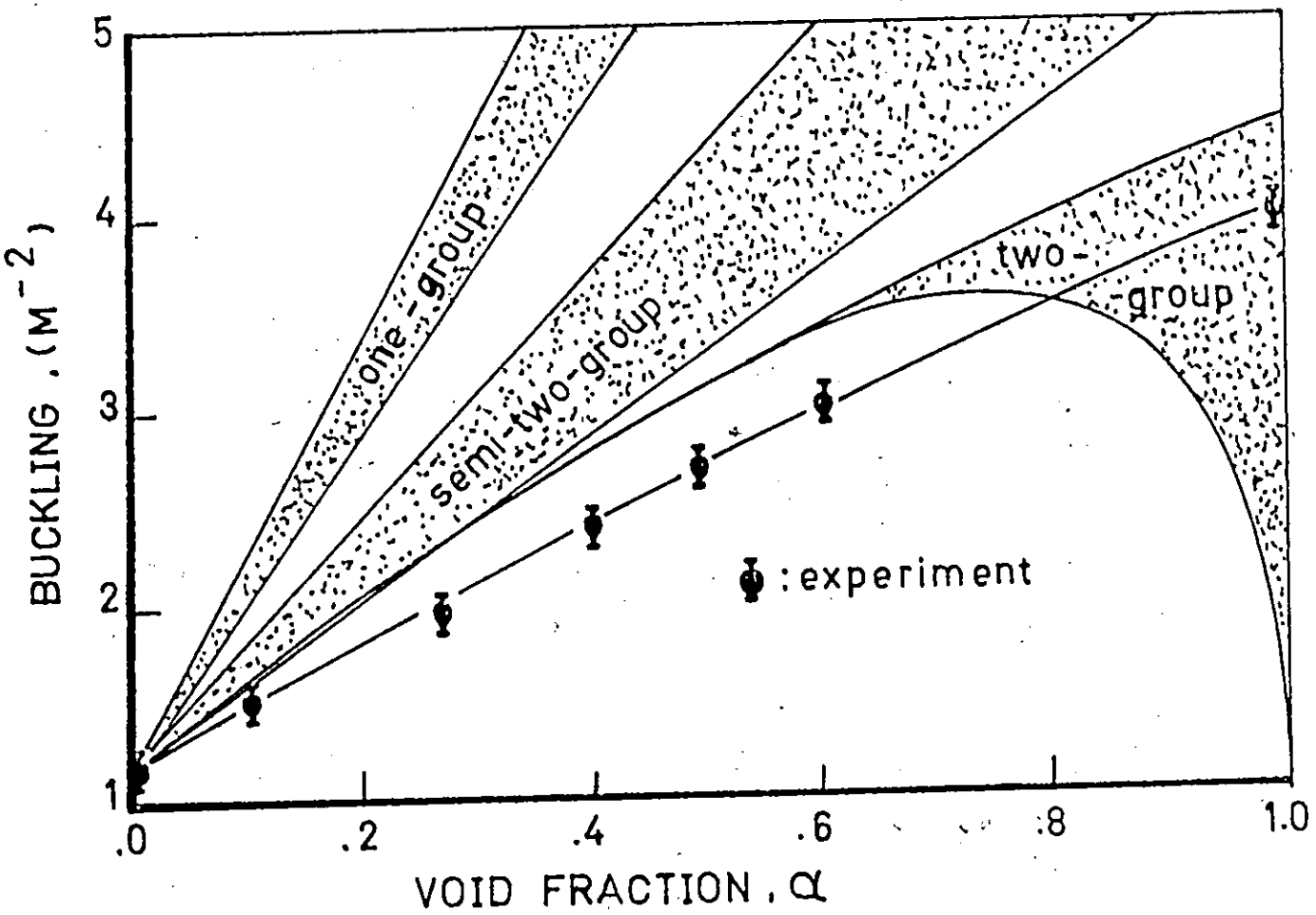

FIGURE 4.1.3: Comparison between experimentally observed and calculated buckling for the simulated boiling H_2O-cooled and D_2O-moderated cylindrical assembly.

mentioned earlier, would not be adequate and, hence, such previous attempts at modelling the coupling effect are inadequate. In addition, we shall see that a two-dimensional formalism is essential since considerable radial effects occur. This area, too, has been neglected by past researchers.

For the two-group theory, however, the discrepency is of the order of that caused by errors in the parameters. In an effort to reduce the uncertainty in the two-group parameters and in particular, to account more correctly for the variation of the four factor parameters with void fraction so as to test the validity of the two-group theory, the lattice representation code (32-33), LATREP, of Chalk River Nuclear Laboratories, was used.

Briefly, given a lattice configuration, an estimate of the neutron spatial and energy distribution and a reference library of cross sections, LATREP employs probability analysis to estimate the group parameters of the cell and the neutron spatial and energy distribution. This procedure is repeated several times giving a consistent set of parameters and neutron distributions. A more detailed account of LATREP is given in appendix 6.

The major sources of error lie in the experimental cross sections in its library (errors approaching 10%) and in the energy spectra used to calculate the cell average parameters. Consequently, it is of little avail to attempt to obtain more accurate answers by a more sophisticated model until the errors in the parameters are reduced.

Table 4.1.2 shows the parameters given by LATREP for various void fractions of the coolant. It has been found necessary, within LATREP, to

VOID FRACTION	0.0	0.2	0.4	0.6	0.8	1.0
D_{2FC}	0.8631	0.9180	0.9906	1.093	1.259	1.578
Σ_{2FC}	0.04296	0.04190	0.04123	0.04070	0.04038	0.04031
D_{1FC}	1.463	1.534	1.611	1.697	1.793	1.899
Σ_{1FC}	0.01635	0.01366	0.01097	0.008277	0.005586	0.002914
D_{2M}	0.8485	0.8500	0.8509	0.8519	0.8533	0.8551
Σ_{2M}	1.013×10^{-4}	9.699×10^{-5}	9.671×10^{-5}	9.635×10^{-5}	9.590×10^{-5}	9.530×10^{-5}
D_{1M}	1.294	1.294	1.294	1.294	1.294	1.294
Σ_{1M}	0.01137	0.01136	0.01136	0.01136	0.01136	0.01136
ϵ_{nf}	1.18057	1.2068	1.23096	1.2567	1.2853	1.3175
p	0.90548	0.904091	0.903438	0.903837	0.905968	0.911814

Table 4.1.2 Parametric data as calculated by LATREP

artificially adjust one of the factors of the four factor formula in order to get agreement with the experimental critical sizes. The amount of adjustment necessary was found to depend mainly on the type of fuel used. This adjustment accounts for all the shortcomings inherent in the LATREP formalism due to geometry simplifications, spectrum approximations, library data errors, etc. The adjustment can be as much as 10% (33). This gives us an estimate of the probable error associated with the four factor formula. Figure 4.1.4 compares the predictions of the two-group model using the LATREP parameters. Using the nominal parameters except for εf, and allowing εf to vary within the specified 10% about the nominal value, we find that the experimental data can be matched to within the buckling error bounds of ± 0.1 m, except for a slight overshot at $\alpha = 1.0$ as given by curve 1. Even this overshot can be eliminated by allowing the other parameters to vary within their error bounds as seen by curve 2. Thus it is possible to reproduce the experimental results exactly by varying the parameters within their error bounds. We can conclude, then, that until better estimates of the lattice parameters can be obtained, it seems it is not necessary to represent the neutron energy spectrum by more than two groups for the purposes of coolant void-reactivity studies.

The effect of parametric error in the two-group model can easily be seen by calculating the response in the i^{th} parameter necessary to restore criticality when the j^{th} parameter is perturbed. Table 4.1.3 shows the results for a void fraction of 0.0. Similar results are obtained at other void fractions. The responses required in, say, p to

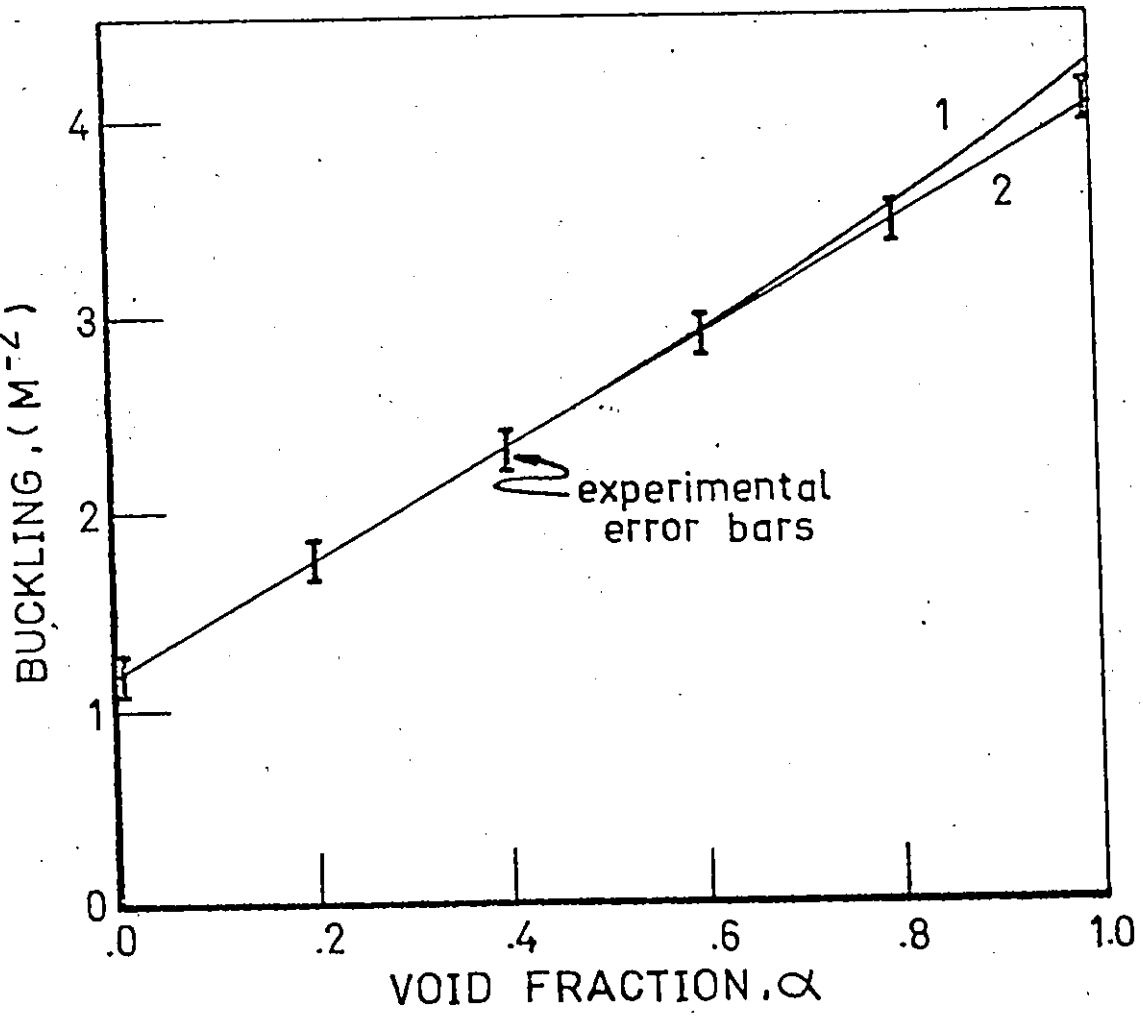

FIGURE 4.1.4: Comparison of experimentally observed buckling and predictions of the two-group model using adjusted LATREP parameters.

PERTURBED PARAMETER	RESPONSE PARAMETER												
	D_{2FC}	Σ_{2FC}	D_{1FC}	Σ_{1FC}	$\epsilon\eta f$	D_{2M}	Σ_{2M}	D_{1M}	Σ_{1M}	p	Fuel Radius	Cell Area	$B_z^2 = (\pi/H)^2$
D_{2FC}	-1.0	-.033	1.18	.043	-.0008	.088	-.028	0.20	-.035	-.0030	-.031	.027	-.028
Σ_{2FC}	-8.1	-1.0	16.	1.3	-.024	2.6	1.40	4.8	-.98	-.087	-.085	0.79	0.69
D_{1FC}	-0.80	.027	-1.0	-.037	.0007	-.073	-.028	-.17	.029	.0025	.026	-.022	-.028
Σ_{1FC}	----	0.77	----	-1.0	.019	-2.1	-1.22	----	0.82	.065	-0.86	0.63	-.51
$\epsilon\eta f$	----	----	----	----	-1.0	80.	59.08	----	----	-3.4	-8.6	23.	31.
D_{2M}	----	0.38	----	-0.50	.0099	-1.0	-5.06	-3.1	0.41	.035	0.37	-0.31	-0.27
Σ_{2M}	----	0.67	----	-0.87	.017	-1.9	-1.0	----	0.73	.060	0.66	-.53	-0.51
D_{1M}	----	0.17	----	-0.23	.0043	-0.45	-.27	-1.0	0.18	.015	0.16	-.14	-0.03
Σ_{1M}	-7.9	-0.86	16.	1.2	-.023	2.3	1.4	4.9	-1.0	-.084	-0.73	0.71	-.69
p	----	-7.15	----	54.	-0.28	24.	16.8	34.	-9.8	-1.0	-4.0	6.9	9.2
Fuel Radius	-8.3	-0.92	14.	1.1	-.022	2.5	1.4	4.6	-.87	-.074	-1.0	0.82	0.69
Cell Area	----	1.3	----	-1.7	.033	-3.5	-.17	----	1.5	0.12	1.2	-1.0	-0.98
$B_z^2=(\pi/H)^2$	----	1.3	----	-1.6	.032	-3.3	-1.9	----	1.3	0.11	1.4	-.99	-1.0

Table 4.1.3 Listing of the response required to maintain criticality for parametric perturbations. The response shown is the ratio of the fractional change in the responding parameter to the fractional change of the perturbed parameter.

restore criticality caused by perturbations in other parameters are given by the column under the heading p. The response is given as the fractional change in p per fractional change in the perturbed parameter. The larger the number, the larger the response needs to be to counteract the perturbation. For example, a change in p of 0.06% is required for a change in Σ_{ZM} of 1% about the nominal parametric value.

Responses which were very large are merely designated by a dash. This indicates a parameter which is not important enough to exert much influence on the criticality. The diffusion coefficients fall into this category. One can conclude that large variations in the diffusion coefficients would be necessary if they were used as a means of reactor control. The absorption cross sections fare somewhat better in this respect. System criticality, however, is governed strongly by the values of ϵnf and p as indicated by the small responses necessary to maintain criticality. We also note that the value of p is of lesser importance than the product, ϵnf.

The reasons behind the different responses or sensitivities are imbedded in the criticality determinant of equation (4.1.41). But, we can gain considerable insight by referring to the differential equations for the fuel-coolant region, equations (4.1.21) and (4.1.22):

$$(- D_{1FC} B_1^2 + \Sigma_{1FC}) \phi_{1FC}(r,z) + \epsilon nf \ \Sigma_{2FC} \phi_{2FC}(r,z) = 0 \quad , \qquad (4.1.51)$$

and

$$(- D_{2FC} B_2^2 + \Sigma_{2FC}) \phi_{2FC}(r,z) + p\Sigma_{1FC} \phi_{1FC}(r,z) = 0 \quad , \qquad (4.1.52)$$

where the local buckling is given by

$$B_r^2 \equiv \left[\frac{1}{r}\frac{\partial}{\partial r}\left(r\,\frac{\partial\phi(r,z)}{\partial r}\right)\right]/\phi(r,z) \quad , \tag{4.1.53}$$

$$B_z^2 \equiv \frac{\partial^2\phi(r,z)}{\partial z^2}/\phi(r,z) \quad , \tag{4.1.54}$$

and

$$B^2 \equiv B_r^2 + B_z^2 \quad . \tag{4.1.55}$$

The definitions apply to both the fast and the slow flux. We will recall that, for our reactor cell model, $B_{1z}^2 = B_{2z}^2$. The buckling represents the normalized curvature of the neutron flux and is a point value, a function of position. The values of B_1^2 and B_2^2 depend upon the solution to the neutron flux equations, subject to the boundary conditions. Substitution of equation (4.1.52) into equation (4.1.51) yields

$$\frac{\epsilon\eta f p}{(1 + L_1^2 B_1^2)(1 + L_2^2 B_2^2)} \equiv \frac{k_\infty}{(1 + L_1^2 B_1^2)(1 + L_2^2 B_2^2)}$$

$$\equiv k_{eff} \equiv 1 \quad , \tag{4.1.56}$$

where the definition of diffusion area, $L^2 = D/\Sigma$, has been used. Equation (4.1.56) is the local criticality condition and depends on the parameters of the fuel-coolant region, k_∞, L_1^2 and L_2^2. The criticality condition also depends upon the moderator properties and boundary conditions through the dependence upon the local bucklings. A perturbation in the input parameters is felt as a perturbation in any or all of the parametric groups, k_∞, $L_1^2 B_1^2$ and $L_2^2 B_2^2$. The parameter, L^2, has been defined as D/Σ and thus the perturbations, as felt by L_1^2 and L_2^2, are obvious.

Perturbations in B^2 are introduced by spatial changes in the flux distributions and as such are implicit changes. Usually, the flux distribution changes so as to dampen out the effect of a perturbation. For instance, changing p by 5%, if nothing else changes, would require a change in ϵ_{nf} of 5%. The response as shown in table 4.1.3 was dampened by the fact that an increase in p, the fraction of neutrons escaping resonance capture, leads to an increased number of neutrons moderating in the fuel rather than the moderator. This alters the interchange of neutrons between moderator and re-shuffles the flux distributions accordingly. Hence the denominator, specifically B_{1r}^2 and B_{2r}^2, of equation (4.1.56) is altered.

This leads to an interesting disclosure. In the past, the calculation of the resonance escape probability, p, has received considerable attention. Most models used to date, for instance, LATREP of appendix 6 and MICRETE3 of appendix 2, lump the fuel cell together and treat it as a whole, that is, the p used is a cell-averaged term. The criticality condition given by equation (4.1.56) would be altered accordingly and reflect a 5% change in ϵ_{nf} for a 5% change in p. Since an accurate value of p is difficult to calculate, it has been the major unknown in criticality estimations. By a reformulation of the model, as done herein, with separate moderator and fuel-coolant regions, the importance of its errors are reduced. The LATREP formalism relies on this sensitivity of p as a means of compensating for hidden errors and shortcomings (26, 33). This cannot be done herein. This is not to suggest that this model is inherently superior because it is not as sensitive to p. It matters

little in the final analysis whether ε_{nfp} or ε_{nf} is the adjustable parameter. What is important, however, is the recognization of the fact that errors in p are not as important as depicted by a cell-averaged model formalism. This suggests, to future investigations, the need to place more weight on areas other than the resonance escape probability, such as independent estimates of the parameter ε_{nf}.

We turn now, to a discussion of the buckling terms. Since the axial dimension is large compared to the radial dimension, cell radius b, and since the buckling goes as the square of the inverse dimension, that is, $(1/H)^2$ or $(1/b)^2$, it follows that the axial portion of the total buckling is small compared to the radial portion. The axial portion, in effect, provides small corrections to the total buckling. This accounts for the insensitivity of the system to the parameter, B_z^2. This also illustrates the fallacy in previous experimental techniques for criticality determinations. Past work emphasized model fitting rather than model delineation or testing. In these experiments the critical height, or some other measurement of an insensitive parameter such as B_z^2, is made and the model is fitted by model-experimental data correlation. However, because of the insensitivity of the system to B_z^2, it is difficult to reverse the procedure and accurately estimate the critical value of B_z^2 from the model given independent experimental estimates of all other parameters. Any small error in the model would be amplified in the model's prediction of the value of B_z^2.

The curve fitting approach is adequate provided one does not extrapolate outside the experimental range. This has been the case in

the past since most nuclear reactor design work has been based on extensive prototype correlation and gradual range extrapolation. The trend is, however, moving away from the philosophy of expensive prototype building. This, plus the fact that spatial control becomes more of a problem as the size of plants increases, necessitates that model testing, rather than fitting, be adopted for large nuclear reactors. This requires that accurate parametric estimates, independent of the buckling data already presented, be obtained.

Finally, while on the subject of the systems sensitivity to LATREP predictions, we note that the code, LATREP, was used in the determination of the experimental data and again in the parameter estimation for the model. One would expect some correlation between model and data to exist; the two are not completely independent. The correlation is not significant, however, when one considers the experimental technique as described in appendix 3. First, the cell-averaged model of the system used in the experimental investigation is different than that of the two-region model presented herein. This reduces the correlation by providing an independent physical basis. Second, and most important, is the fact that LATREP contains an adjustable parameter used to obtain agreement between its predictions and experimental data. As pointed out, the sensitivity of the system to the adjusted parameter, ϵ_{nfp}, is sufficiently strong to dominate the error in the response to void insertions. The subsequent use of LATREP herein entails an independent adjustment of ϵ_{nf} at $\alpha = 0.0$. This reduces the correlation since most of the correlation has been removed from the dominant term.

Third, an independent check on the full voiding case confirmed the validity of the use of LATREP. This confirms that most of the error in predicting the system response to coolant voiding is contained in the adjustable parameter. This again shows that the presence of the adjustable parameter removes any important correlation present in the analysis technique. Here, once more, we have found motivation for obtaining an independent estimate of the dominant parameter, εnf.

4.2 SPACE-TIME FLUX MODELS FOR APPLICATION TO NON-UNIFORM VOIDING

Although much insight can be gained from the uniform voiding models presented in the previous section, consideration must be given to the fact that coolant voiding in nuclear reactors is not uniform. Rather, it is, in general, a function of axial and radial position. The mathematical effect of non-uniform voiding, $\alpha = \alpha(r,z)$, on the basic neutron flux equations is to induce variability in the coefficients, thereby introducing non-linearities. The magnitude and complexity of the non-linearities necessitates that numerical techniques be employed. Furthermore, the multidimensional, multigroup aspect of the neutron flux equations dictates long computation times (34).

Reactor transient analysis can be divided into two broad classes (35). The first, flux synthesis (36), involves approximating a spatial, spectral, angular or temporal portion of the flux distribution to yield a smaller set of equations to be solved. As has been pointed out (35), this technique suffers from a lack of definitive error bounds and the need for intuitive guessing of the spatial, spectral, angular or temporal

portion. The second class, the direct solution technique, involves finite difference approximations to the differential equations. In this technique, the disadvantages of the flux synthesis technique are overcome at the expense of computation time.

Because of the disadvantages of the flux synthesis technique and because a detailed account of spatial distributions is necessary for this non-linear problem, the flux synthesis technique was deemed unsatisfactory. Consequently, we now turn to finite difference techniques.

Carnahan et al (37) indicate that the best available technique for numerically solving this type of partial differential equation is the alternating direction implicit (ADI) technique. Furthermore, they show that the transient solution can be solved as readily as the steady-state solution. This being so, the transient formulation is considered herein. Additionally, it is desirable to consider transient formalisms since the long term goal is that of simulating transient behaviour.

The ADI technique was applied to the two-group neutron equations as will be discussed in section 4.3. Excessively long computation times were encountered, however, for accurate simulations. This can be attributed to the differences in axial and radial diffusion times. Since the length of the cell is some 10 times the radius, the neutron distribution in the radial direction develops much more quickly than in the axial direction. This dictates small time step increments to follow the radial behaviour. Many interations are required, therefore, to follow the slow axial transients, leading to long computation times. Non-linearities are such that, a priori, no representative radial distribution could be

assigned for a quasi-steady state approach. This rules out that technique as a possible means of reducing the computation time. Consequently, another technique was explored in search of a means of reducing the computation time.

Herein, we consider the direct solution approach and introduce a technique for reducing the computation time needed to investigate a certain class of nuclear reactor systems. Specifically, we consider those systems for which the time scale for spatial changes is much larger than the time scale for overall amplitude changes. Most nuclear reactor systems exhibit this characteristic since neutron slowing down and thermalization is usually a much quicker process than neutron diffusion and since these processes are much quicker than the delayed precursor response time.

A method of analysis has recently been developed (35, 38, 39) whereby the dominant time dependence is extracted from the general space-time multigroup neutron diffusion equations, leaving equations which vary much more slowly in time. The result is a reduction in computation time due to the admission of larger time steps in the calculation. The underlying principle is a transformation of the time variable. Though this is not a new approach (29, 36, 40, 41), the success of the application is in the appropriate choice of transformation.

A related example of the utilization of the dominant trend concept is given by Orbach and Crowe (42) in their work on chemical plant simulation. They use the dominant eigenvalue to accelerate convergence of a complex system.

In these examples, the transient solution is developed by suitable numerical techniques until a trend can be established. One drawback associated with these approaches is their inability to adjust immediately to perturbations in system parameters (35). Here, we extend this formalism by removing this restriction and thus admit computation time reductions even in the region where the dominant time growth has not been attained. This leads to a significant saving in computation time for those situations in which system parameters are constantly changing. The following analysis has recently appeared in published form(43).

4.2.1 THEORY

We consider the general multigroup neutron diffusion equation in its well known form,

$$\frac{1}{v_g}\frac{\partial \phi_g(\underline{r},t)}{\partial t} = \nabla.D_g(\underline{r},t)\,\nabla\phi_g(\underline{r},t) + \sum_{g'=1}^{G} \Sigma_{gg'}(\underline{r},t)\,\phi_{g'}(\underline{r},t) \quad , \qquad (4.2.1)$$

where the usual symbolism holds. In particular, we define

$v_g \equiv$ velocity of group g [cm/s],

$\phi_g(\underline{r},t) \equiv$ neutron flux density of group g [neutrons/cm^2 s] ,

$D_g(\underline{r},t) \equiv$ diffusion coefficient of group g [cm],

$\Sigma_{gg'}(\underline{r},t) \equiv$ cross section for a neutron in group g' transferring to group g [cm^{-1}],

$\underline{r} \equiv$ space vector [cm],

$t \equiv$ time [s],

$g \equiv$ group number, g = 1,2, ... G.

It is interesting to note that extension of this system to include delayed precursors is straightforward since the delayed precursor equations are of the same form as equation (4.2.1). We need only redefine G to include the delayed precursor groups and to appropriately define the diffusion coefficients and cross sections for these new groups. We omit these groups in the following formalism since no generality is lost and since the delayed precursors are not needed for the purposes of this dissertation, as noted in appendix 1.

In solving these equations, Reed et al (38), as well as Wight et al (39), used the transformation

$$\phi_g(\underline{r},t) = \psi_g(\underline{r},t)\ e^{\omega_g(\underline{r})t} \quad , \tag{4.2.2}$$

while Ferguson and Hansen (35) considered the special case of equation (4.2.2),

$$\phi_g(\underline{r},t) = \psi_g(\underline{r},t)\ e^{\omega(\underline{r})t} \quad . \tag{4.2.3}$$

In equations (4.2.2) and (4.2.3), it is understood that the functions $\omega_g(\underline{r})$ and $\omega(\underline{r})$ are evaluated at each spatial mesh point of the numerical solution and are considered constant over the time interval in question.

Herein, we consider an extension of the above and choose to use a transformation based on all the exponential time components as follows:

$$\phi_g(\underline{r},t) = \sum_{\ell=1}^{G} \psi_{g\ell}(\underline{r},t)\ e^{\omega_\ell(\underline{r})t} \equiv \phi_g(\underline{r},t) \sum_{\ell=1}^{G} \beta_{g\ell}(\underline{r})\ e^{\omega_\ell(\underline{r})t}, \tag{4.2.4}$$

where we have defined

$$\psi_{g\ell}(\underline{r},t) \equiv \phi_g(\underline{r},t)\ \beta_{g\ell}(\underline{r}) \quad . \tag{4.2.5}$$

Here, again, the functions, $\omega_\ell(\underline{r})$, and the coefficients, $\beta_{g\ell}(\underline{r})$ are evaluated at each spatial mesh point and are considered constant over the time interval in question. As will become clear, this provides algebraic consistency throughout and permits enough flexibility to ensure that the boundary and initial conditions are satisfied. From equation (4.2.4), we note that each neutron group is composed of a weighted sum of G exponentials. This is in contrast to equations (4.2.2) and (4.2.3) which contain only one exponential for each group. This choice of ansatz was not arbitrary, rather, it was motivated by the solution to a simplified form of equation (4.2.1). Consider, for example, the case in which the spatially dependent leakage term, $\nabla.D_g\nabla\phi_g$, is known. Equation (4.2.1) is then of the space independent form with the solution given by

$$\phi_g(t) = \sum_{\ell=1}^{G} \beta_{g\ell}\, e^{\omega_\ell t} \quad . \tag{4.2.6}$$

The problem, then, is to find $\beta_{g\ell}(\underline{r})$ and $\omega_\ell(\underline{r})$ of equation (4.2.4) at each spatial mesh point for a given approximation of $\phi_g(\underline{r},t)$, leaving a finite difference equation in $\phi_g(\underline{r},t)$ which can be solved by conventional means. The solution to this differential equation varies, in general, much more slowly in time since the dominant time dependence of the system has been extracted by the exponential transformation. We perform this transformation by substituting equation (4.2.4) into

equation (4.2.1) and obtain

$$\frac{1}{v_g}\sum_{\ell=1}^{G}\beta_{g\ell}(\underline{r})\,e^{\omega_\ell(\underline{r})t}\left[\omega_\ell(\underline{r})\,\phi_g(\underline{r},t)+\frac{\partial\phi_g(\underline{r},t)}{\partial t}\right]$$

$$=\sum_{\ell=1}^{G}\beta_{g\ell}(\underline{r})\,e^{\omega_\ell(\underline{r})t}\,\nabla.D_g(\underline{r})\,\nabla\phi_g(\underline{r},t)$$

$$+\,\phi_g(\underline{r},t)\,\nabla.D_g(\underline{r})\,\nabla\sum_{\ell=1}^{G}\beta_{g\ell}(\underline{r})\,e^{\omega_\ell(\underline{r})t}$$

$$+\sum_{g'=1}^{G}\Sigma_{gg'}(\underline{r})\left(\sum_{\ell=1}^{G}\beta_{g'\ell}(\underline{r})\,e^{\omega_\ell(\underline{r})t}\right)\phi_{g'}(\underline{r},t)\quad , \tag{4.2.7}$$

where the coefficients, $\Sigma_{gg'}$, and D_g, are assumed constant over the time interval, Δt. We define our initial time, $t = o$, as the beginning of the time interval under consideration. Thus, we have, at $t = o$, $\phi_g(\underline{r},o)$ from either the initial condition or the results of the previous iteration. Hence,

$$\phi_g(\underline{r},o) = \phi(\underline{r},o)\sum_{\ell=1}^{G}\beta_{g\ell}(\underline{r})\quad . \tag{4.2.8}$$

If we assign a normalization to $\beta_{g\ell}(\underline{r})$ of the type

$$\sum_{\ell=1}^{G}\beta_{g\ell}(\underline{r}) \equiv 1\quad , \text{ for all } \underline{r}, \tag{4.2.9}$$

then

$$\phi_g(\underline{r},o) = \phi(\underline{r},o)\quad . \tag{4.2.10}$$

Equation (4.2.7) can be simplified by recognizing that we are

evaluating $\beta_{g\ell}$ and ω_ℓ at the start of each iteration. The best evaluation, then, of the second term of the right-hand-side of equation (4.2.7) is accomplished at t = o. But using equation (4.2.9) we note that

$$\phi_g(\underline{r},t)\ \nabla\cdot D_g(\underline{r})\ \nabla \sum_{\ell=1}^{G} \beta_{g\ell}(\underline{r})\ e^{\omega_\ell(\underline{r})t}\Big|_{t=o} = \phi_g(r,t)\ \nabla.D_g(\underline{r})\ \nabla(1) \equiv 0. \quad (4.2.11)$$

Thus, equation (4.2.7) reduces to

$$\frac{1}{v_g} \sum_{\ell=1}^{G} \beta_{g\ell}(\underline{r})\ e^{\omega_\ell(\underline{r})t} \left[\omega_\ell(\underline{r},t)\ \phi_g(\underline{r},t) + \frac{\partial\phi_g(\underline{r},t)}{\partial t}\right]$$

$$= \sum_{\ell=1}^{G} \beta_{g\ell}(\underline{r})\ e^{\omega_\ell(\underline{r})t}\ \nabla.D_g(\underline{r})\ \nabla\phi_g(\underline{r},t)$$

$$+ \sum_{g'=1}^{G} \Sigma_{gg'}(\underline{r}) \left(\sum_{\ell=1}^{G} \beta_{g'\ell}(\underline{r})\ e^{\omega_\ell(\underline{r})t}\right) \phi_{g'}(\underline{r},t)\ . \quad (4.2.12)$$

Since this is valid for all time t we may write

$$\frac{1}{v_g} \beta_{g\ell}(\underline{r}) \frac{\partial\phi_g(\underline{r},t)}{\partial t} = -\frac{1}{v_g} \beta_{g\ell}(\underline{r})\ \omega_\ell(\underline{r})\ \phi_g(\underline{r},t)$$

$$+ \beta_{g\ell}(\underline{r})\ \nabla\cdot D_g(\underline{r})\ \nabla\phi_g(\underline{r},t) + \sum_{g'=1}^{G} \Sigma_{gg'}(\underline{r})\ \beta_{g'\ell}(\underline{r})\ \phi_{g'}(\underline{r},t) \quad (4.2.13)$$

Further, we assume that for the time interval, Δt, $\phi_g(\underline{r},t)$ does not change significantly compared to the exponential variation. Equation (4.2.13) now becomes

$$0 = -\frac{1}{v_g}\,\beta_{g\ell}(\underline{r})\,\omega_\ell(\underline{r})\,\phi_g(\underline{r},o) + E_g(\underline{r})\,\phi_g(\underline{r},o)\,\beta_{g\ell}(\underline{r}) + \sum_{g'=1}^{G}\Sigma_{gg'}(\underline{r})\,\beta_{g'\ell}(\underline{r})\,\phi_{g'}(\underline{r},o)\ , \tag{4.2.14}$$

where we have defined

$$E_g(\underline{r}) \equiv [\nabla\cdot D_g(\underline{r})\,\nabla\phi_g(\underline{r},o)]/\phi_g(\underline{r},o)\ . \tag{4.2.15}$$

Equation (4.2.14) can be reduced to

$$-\frac{1}{v_g}\psi_{g\ell}(\underline{r})\,\omega_\ell(\underline{r}) + E_g(\underline{r})\,\psi_{g\ell}(\underline{r}) + \sum_{g'=1}^{G}\Sigma_{gg'}(\underline{r})\,\psi_{g'\ell}(\underline{r}) = 0\ . \tag{4.2.16}$$

From this equation, then, it is possible to evaluate $\psi_{g\ell}(\underline{r})$ and $\omega_\ell(\underline{r})$ for all $\underline{r}$ at each time interval based on the most recent value of $E_g(\underline{r})$ and $\Sigma_{gg'}(\underline{r})$; these terms, thus, are updated at the beginning of each iteration.

At this point, we drop the explicit notation of the spatial dependence for algebraic convenience. Equation (4.2.16) can be conveniently written in matrix notation as

$$\underline{\underline{A}}_\ell\underline{\psi}_\ell = 0\ , \tag{4.2.17}$$

where

$$\underline{\psi}_\ell \equiv \begin{bmatrix} \psi_{1\ell} \\ \psi_{2\ell} \\ \vdots \\ \psi_{G\ell} \end{bmatrix} \tag{4.2.18}$$

and

$$\underline{\underline{A}}_\ell \equiv \begin{bmatrix} -\omega_\ell + \nu_1(E_1 + \Sigma_{11}) & \nu_1\Sigma_{12} \cdots\cdots\cdots\cdots \nu_1\Sigma_{1G} \\ \nu_2\Sigma_{21} & -\omega_\ell + \nu_2(E_2 + \Sigma_{22}) \cdots\cdots \nu_2\Sigma_{2G} \\ \vdots & \vdots \\ \nu_G\Sigma_{G1} & \nu_G\Sigma_{G2} \cdots\cdots -\omega_\ell + \nu_G(E_G + \Sigma_{GG}) \end{bmatrix} \quad (4.2.19)$$

The eigenvalues, ω_ℓ, of this system of equations are given by the condition,

$$\left|\underline{\underline{A}}_\ell\right| = 0 \quad , \quad (4.2.20)$$

and the eigenvectors, $\underline{\psi}_\ell$, are given by any non-zero column of the adjoint of $\underline{\underline{A}}_\ell$, $\mathrm{ADJ}[\underline{\underline{A}}_\ell]$, to within arbitrary constants (44). These constants can be determined from the initial conditions,

$$\sum_{\ell=1}^{G} \psi_{g\ell}(\underline{r}) = \phi_g(\underline{r},o) \quad . \quad (4.2.21)$$

Thus, in principle, we have found ω_ℓ and $\psi_{g\ell}$ for all $\underline{r}$. Since $\phi_g(\underline{r},o)$ is known, we readily calculate $\beta_{g\ell}$ from equation (4.2.5) for all $\underline{r}$. These values of ω_ℓ and $\beta_{g\ell}$ are substituted into equation (4.2.12) leaving an equation in ϕ_g which can be solved by standard numerical techniques to yield $\phi_g(\underline{r},\Delta t)$. For this purpose we have chosen the ADI method based on the Crank-Nicholson formalism (37). Using the updated values of ϕ_g, from equation (4.2.4) we obtain the flux $\phi_g(\underline{r},\Delta t)$ at the end of the time step. Repeating this process propagates the system in time. It should be noted

that the calculation of the eigenvectors and eigenvalues at each spatial point is straightforward since the elements of $\underline{\underline{A}}_\ell$ are block diagonal, that is, each element can be evaluated explicitly based upon the local spatial values of the system.

4.2.2 PROPERTIES OF THE TRANSFORMED EQUATIONS

It is convenient to rewrite the basic neutron equations in matrix notation

$$\frac{d\underline{\phi}(r,t)}{dt} = \underline{\underline{A}}\ \underline{\phi}(\underline{r},t) \quad , \tag{4.2.22}$$

where the square matrix, $\underline{\underline{A}}$, is defined similarly to that of $\underline{\underline{A}}_\ell$ in equation (4.2.19),

$$\underline{\underline{A}} \equiv \begin{bmatrix} \nu_1(T_1 + \Sigma_{11}) & \nu_1 \Sigma_{12} \cdots \nu_1 \Sigma_{1G} \\ \nu_2\Sigma_{21} & \nu_2(T_2 + \Sigma_{22}) \cdots \nu_2 \Sigma_{2G} \\ \vdots & \vdots \\ \nu_G \Sigma_{G1} & \nu_G \Sigma_{G2} \cdots \nu_G(T_G + \Sigma_{GG}) \end{bmatrix} . \tag{4.2.23}$$

The elements, T_i, consist of the elements of $\underline{\underline{A}}$ which represent the spatial differencing terms. These elements, then, constitute a block matrix spanning the spatial mesh. The remaining elements are block diagonal. The flux vector, $\underline{\phi}$, has G subvectors, each subvector spanning the spatial nodes of the finite differencing.

The matrix, $\underline{\underline{A}}_\ell$, is similar, except that it includes the temporal transformation and that the elements, T_i, are replaced by the block diagonal elements E_i.

In the previous section we employed a transformation on ϕ. In matrix notation, we have

$$\underline{\phi} = \underline{\underline{\Omega}}\,\underline{\Phi} \quad , \tag{4.2.24}$$

where

$$\underline{\underline{\Omega}} \equiv \begin{bmatrix} \sum_{\ell=1}^{G} \beta_{1\ell} e^{\omega_\ell t} & & & 0 \\ & \sum_{\ell=1}^{G} \beta_{2\ell} e^{\omega_\ell t} & & \\ & & \ddots & \\ 0 & & & \sum_{\ell=1}^{G} \beta_{G\ell} e^{\omega_\ell t} \end{bmatrix} \tag{4.2.25}$$

and each element, $\sum_{\ell=1}^{G} \beta_{i\ell} e^{\omega_\ell t}$, is block diagonal spanning the spatial mesh. The vector, $\underline{\Phi}$, is similar to the vector, $\underline{\phi}$. Substituting equation (4.2.24) into equation (4.2.22) yields

$$\frac{d\underline{\Phi}}{dt} = \underline{\underline{\Omega}}^{-1}(\underline{\underline{A}} - \dot{\underline{\underline{\Omega}}}\underline{\underline{\Omega}}^{-1})\,\underline{\underline{\Omega}}\,\underline{\Phi} \quad , \tag{4.2.26}$$

where $\dot{\underline{\underline{\Omega}}}$ is the time derivative of $\underline{\underline{\Omega}}$. The stability and convergence properties of this equation, when solved by alternating direction implicit (ADI) and explicit (ADE) techniques, are guaranteed if $(\underline{\underline{A}} - \dot{\underline{\underline{\Omega}}}\underline{\underline{\Omega}}^{-1})$ is constant and negative definite (38). A sufficient condition for negative

definiteness is that the diagonals be negative and the off-diagonals be positive. The choice of $\underline{\Omega}$, then, is of utmost importance for stability, and, hence, convergence.

Following the transformation employed by Reed et al (38) and several subsequent investigations (35, 39) we write

$$\underline{\Omega} \equiv \begin{bmatrix} e^{\omega_1 t} & & & 0 \\ & e^{\omega_2 t} & & \\ & & \ddots & \\ 0 & & & e^{\omega_G t} \end{bmatrix} . \qquad (4.2.27)$$

For this transformation, it was found (38) that stability and convergence could be guaranteed for the case when $\underline{A}$ and ω_i are constant, provided that

$$(\Sigma_{ii} - \omega_i) < 0 \quad . \qquad (4.2.28)$$

This condition is satisfied in most reactor analyses. However, ω_i does, in general, change at each iteration because either the material properties or the spatial distributions of flux may be changing. To test for stability in these cases, recourse to numerical experiments had to be taken.

For this analysis, $\underline{\Omega}$ is given by equation (4.2.25) and the eigenvectors, ψ_ℓ, and eigenvalues, ω_ℓ, are defined by equation (4.2.14) or, equivalently, equation (4.2.16). In matrix notation, equation (4.2.16) becomes

$$\underline{\underline{A}}_\ell \underline{\underline{\Delta}}_\ell \underline{\Phi} = \underline{\underline{\Delta}}_\ell \underline{\Psi}_\ell = (\underline{\underline{A}}' - \omega_\ell \underline{\underline{I}})\ \underline{\underline{\Delta}}_\ell \underline{\Phi} = 0 \quad , \tag{4.2.29}$$

where $\underline{\underline{A}}'$ is simply $\underline{\underline{A}}_\ell$ without the frequency terms and where $\underline{\underline{\Delta}}_\ell$ is defined as

$$\underline{\underline{\Delta}}_\ell \equiv \begin{bmatrix} \beta_{1\ell} & & 0 \\ & \beta_{2\ell} & \\ & & \ddots \\ 0 & & \beta_{G\ell} \end{bmatrix} \quad . \tag{4.2.30}$$

Multiplying equation (4.2.29) by $e^{\omega_\ell t}$ and summing on ℓ gives

$$\sum_{\ell=1}^{G} (\underline{\underline{A}}' - \omega_\ell \underline{\underline{I}})\ \underline{\underline{\Delta}}_\ell \underline{\Phi}\ e^{\omega_\ell t} = (\underline{\underline{A}}' \underline{\underline{\Omega}} - \dot{\underline{\underline{\Omega}}})\ \underline{\Phi} = (\underline{\underline{A}}' - \dot{\underline{\underline{\Omega}}} \underline{\underline{\Omega}}^{-1})\ \underline{\underline{\Omega}} \underline{\Phi} = 0 \quad . \tag{4.2.31}$$

Thus,

$$\underline{\underline{\Omega}}^{-1} (\underline{\underline{A}}' - \dot{\underline{\underline{\Omega}}} \underline{\underline{\Omega}}^{-1})\ \underline{\underline{\Omega}} \underline{\Phi} = 0 \quad . \tag{4.2.32}$$

Subtracting equation (4.2.32) from (4.2.26) gives

$$\frac{d\underline{\Phi}}{dt} = \underline{\underline{\Omega}}^{-1} (\underline{\underline{A}} - \underline{\underline{A}}')\ \underline{\underline{\Omega}} \underline{\Phi} \quad . \tag{4.2.33}$$

The properties of $(\underline{\underline{A}} - \underline{\underline{A}}')$, then, define the stability properties of the system. As noted previously, the only difference between $\underline{\underline{A}}$ and $\underline{\underline{A}}'$ is the treatment of the spatial differencing terms. Consequently,

$$\underline{\underline{A}} - \underline{\underline{A}}' = \begin{bmatrix} \nu_1(T_1 - E_1) & & & 0 \\ & \nu_2(T_2 - E_2) & & \\ & & \ddots & \\ 0 & & & \nu_G(T_G - E_G) \end{bmatrix} . \tag{4.2.34}$$

Recalling that the spatial differencing is of the form

$$D\nabla^2\phi \sim \frac{D}{\Delta x^2}(\phi_{n+1} - 2\phi_n + \phi_{n-1}) , \tag{4.2.35}$$

where n is a spatial mesh point, it follows that the off-diagonals of T_i, as well as $(T_i - E_i)$ since E_i is diagonal, are positive. Since the diagonal of E_i is given by

$$D\nabla^2\phi/\phi \approx D\nabla^2\phi/\phi , \tag{4.2.36}$$

and, according to equation (4.2.35), noting that $\phi \geq 0$:

$$|D\nabla^2\phi| \leq \left|\frac{2D\phi}{\Delta x^2}\right| , \tag{4.2.37}$$

we conclude that

$$T_1 - E_1 \approx -\frac{2D}{\Delta x^2} - D\frac{\nabla^2\phi}{\phi} \leq 0 \tag{4.2.38}$$

and the diagonals of $\underline{\underline{A}} - \underline{\underline{A}}'$ are negative. This matrix, then, is negative

definite. Thus, stability and convergence are guaranteed for constant $\underline{A} - \underline{A}'$.

Instabilities can arise due to the coefficients of $\underline{A} - \underline{A}'$ being non-constant, as in the method employed by Reed et al (38). However, an important difference between the previous work and this work exists. While both methods are subject to instabilities caused by non-constant values for the temporal transformation, the stability of the transformed system, presented here, is not directly affected by non-constant off-diagonal terms. This is an important distinction from the method of Reed et al (38). It is realized, of course, that non-constant off-diagonals in $\underline{A}'$ can introduce instabilities by their influence on the value of $\underline{\Omega}$. However, the system is guaranteed stable for constant $\underline{A} - \underline{A}'$ irrespective of the value of $(\Sigma_{ii} - \omega_i)$ of equation (4.2.28).

This transformation is, therefore, inherently more stable than that previously presented. It is recognized, that a price is paid due to extra computations. This price can be worth paying, as shown by the following examples, particularly in those cases in which perturbations are constantly introduced and the flux trends have not developed.

In the following examples, as for most systems, we find accuracy proves to be the more demanding criteria, not stability. The time step sizes required for accurate answers insured stabilitity.

4.2.3 TWO-GROUP ANALYSIS

For a calculational analysis we consider the case of two-group diffusion. In this case we have $G = 2$ and $\ell = 1, 2$. The matrix becomes

$$\underline{A}_\ell = \begin{bmatrix} -\omega_\ell + v_1(\Sigma_1 + \Sigma_{11}) & v_2\,\Sigma_{12} \\ v_2\,\Sigma_{21} & -\omega_\ell + v_2(\Sigma_2 + \Sigma_{22}) \end{bmatrix} . \qquad (4.2.39)$$

Recalling that the elements of $\underline{A}_\ell$ are block diagonal, we can consider each spatial point separately. The elements, then, are no longer block diagonals but merely scalars. We introduce the following two group notation, consistent with that of section 4.1:

1 ≡ subscript identifying the fast group;

2 ≡ subscript identifying the thermal group;

$\Sigma_{11} \equiv -\Sigma_1$;

$\Sigma_{22} \equiv -\Sigma_2$;

$\Sigma_{12} \equiv \epsilon\eta f\Sigma_2$;

$\Sigma_{21} \equiv p\Sigma_1$.

Thus, we have

$$\underline{A}_\ell = \begin{bmatrix} -\omega_\ell + v_1(\Sigma_1 - \Sigma_1) & v_1\,\epsilon\eta f\Sigma_2 \\ v_2 p\Sigma_1 & -\omega_\ell + v_2(\Sigma_2 - \Sigma_2) \end{bmatrix} . \qquad (4.2.40)$$

The eigenvalues, ω_ℓ, are given by the condition

$$|\underline{A}_\ell| = 0 \quad , \qquad (4.2.41)$$

which may be expanded to yield

$$[-\omega_\ell + \nu_1(E_1 - \Sigma_1)][-\omega_\ell + \nu_2(E_2 - \Sigma_2)] - \nu_1\nu_2\,\mathrm{cnf}p\Sigma_1\Sigma_2 = 0 \quad . \tag{4.2.42}$$

Solving the quadratic equation yields two values of ω, ω_1 and ω_2, at each r.

The eigenvectors, Ψ_ℓ, are given by any non-zero column of $\mathrm{ADJ}(\underline{\Delta}_\ell)$.

Now,

$$\mathrm{ADJ}(\underline{\Delta}_\ell) = \begin{bmatrix} -\omega_\ell + \nu_2(E_2 - \Sigma_2) & -\nu_1\,\mathrm{cnf}\Sigma_2 \\ -\nu_2 p\Sigma_1 & -\omega_\ell + \nu_1(E_1 - \Sigma_1) \end{bmatrix} , \tag{4.2.43}$$

and

$$\Psi_\ell = \begin{bmatrix} \psi_{1\ell} \\ \psi_{2\ell} \end{bmatrix} \alpha \begin{bmatrix} -\omega_\ell + \nu_2(E_2 - \Sigma_2) \\ -\nu_2 p\Sigma_1 \end{bmatrix} \alpha \begin{bmatrix} -\nu_1\,\mathrm{cnf}\Sigma_2 \\ -\omega_\ell + \nu_1(E_1 - \Sigma_1) \end{bmatrix} . \tag{4.2.44}$$

The initial conditions give

$$\sum_{\ell=1}^{G} \psi_{g\ell} = \phi_g(o) \quad , \tag{4.2.45}$$

that is,

$$\psi_{11} + \psi_{12} = \phi_1(o) \quad , \tag{4.2.46}$$

and

$$\psi_{21} + \psi_{22} = \phi_2(o) \quad . \tag{4.2.47}$$

Equation (4.2.44) yields

$$\frac{\psi_{1\ell}}{\psi_{2\ell}} = \frac{\nu_1 \, \epsilon n f \Sigma_2}{\omega_\ell - \nu_1(E_1 + \Sigma_1)} = \frac{\omega_\ell - \nu_2(E_2 - \Sigma_2)}{\nu_2 p \Sigma_1} \equiv C_\ell . \tag{4.2.48}$$

Equation (4.2.42) ensures that the above equality holds. After some algebraic manipulation we find

$$\psi_{22} = \frac{C_1 \, \phi_2(o) - \phi_1(o)}{C_1 - C_2} \quad ,$$

$$\psi_{12} = C_2 \psi_{22} \quad ,$$

$$\psi_{11} = \phi_1(o) - \psi_{12} \quad , \tag{4.2.49}$$

and

$$\psi_{21} = \phi_2(o) - \psi_{22} \quad .$$

Thus, we have the eigenvalues and eigenvectors at each $\underline{r}$ as required. These values are used in the procedure mentioned previously.

The two differential equations to be solved are given by

$$\frac{1}{\nu_1}\left[\beta_{11} e^{\omega_1 t}\left(\omega_1 \phi_1 + \frac{\partial \phi_1}{\partial t}\right) + \beta_{12} e^{\omega_2 t}\left(\omega_2 \phi_1 + \frac{\partial \phi_1}{\partial t}\right)\right]$$

$$= \left[\beta_{11} e^{\omega_1 t} + \beta_{12} e^{\omega_2 t}\right] \left[\nabla . D_1 \nabla \phi_1 - \Sigma_1 \phi_1\right]$$

$$+ \epsilon n f \Sigma_2 \phi_2 \left[\beta_{21} e^{\omega_1 t} + \beta_{22} e^{\omega_2 t}\right] \quad , \tag{4.2.50}$$

and

$$\frac{1}{v_2}\left[\beta_{21}\, e^{\omega_1 t}\left(\omega_1\phi_2 + \frac{\partial\phi_2}{\partial t}\right) + \beta_{22}\, e^{\omega_2 t}\left(\omega_2\phi_2 + \frac{\partial\phi_2}{\partial t}\right)\right]$$

$$= \left[\beta_{21}\, e^{\omega_1 t} + \beta_{22}\, e^{\omega_2 t}\right] \left[\nabla . D_2\nabla\phi_2 - \Sigma_2\phi_2\right]$$

$$+ p\Sigma_1\phi_1\left[\beta_{11}\, e^{\omega_1 t} + \beta_{12}\, e^{\omega_2 t}\right] . \qquad (4.2.51)$$

These can easily be rewritten in finite difference form in the unknowns ϕ_1 and ϕ_2 as described in detail in section 4.3.

For illustrative purposes we consider a CANDU-BLW lattice cell (26). Figure 4.1.2 shows a graphical representation of this system; table 4.2.1 lists the various lattice parameters. The reactor height, H, is 290 cm. For algebraic convenience we take the neutron speed v_1 and v_2 to be equal to that of thermal neutrons. Although this does change the time scale of the power transients it does not detract from the general characteristics of this solution procedure.

The boundary conditions are: (1) zero net neutron current in the radial direction at the cell center and at the cell boundary; and (2) zero neutron flux at the axial end points. The initial flux distributions were assumed to be flat. An 11 x 11 spatial mesh was chosen.

The standard two group equations and the transformed two group equations were solved by the alternating direction implicit (ADI) method previously mentioned. In figures 4.2.1 and 4.2.2 we show a comparison between methods. We note that in this case, ϕ_1 and ϕ_2 have totally different time dependences; ϕ_1 is increasing with time while ϕ_2 is decreasing with

$v_1 = 2 \times 10^5$ cm/s	$\Sigma_{1FC} = .002914\ cm^{-1}$	$D_{1FC} = 1.899$ cm
$v_2 = 2 \times 10^5$ cm/s	$\Sigma_{2FC} = .04031\ cm^{-1}$	$D_{2FC} = 1.578$ cm
$\epsilon\eta f = 2.0$	$\Sigma_{1M} = .01136\ cm^{-1}$	$D_{1M} = 1.294$ cm
$p = .911814$	$\Sigma_{2M} = .0000953\ cm^{-1}$	$D_{1M} = .8551$ cm

Table 4.2.1 System parameters for the CANDU-BLW reactor used in the calculations. The value of $\epsilon\eta f$ is imposed to induce a transient.

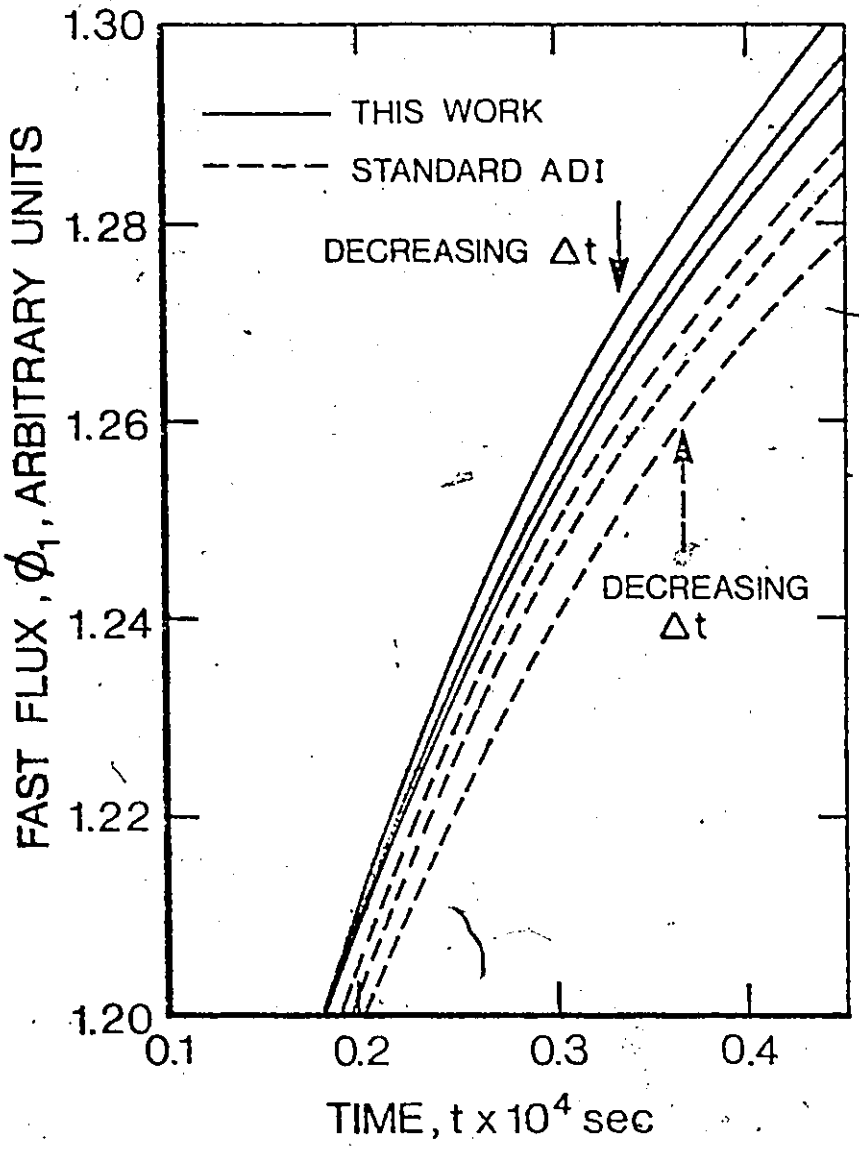

FIGURE 4.2.1 Fast flux vs. time at the cell center for various time steps, $\Delta t = 1.0 \times 10^{-6}$, 0.5×10^{-6} and 0.25×10^{-6} sec. Case study: Initial Perturbation.

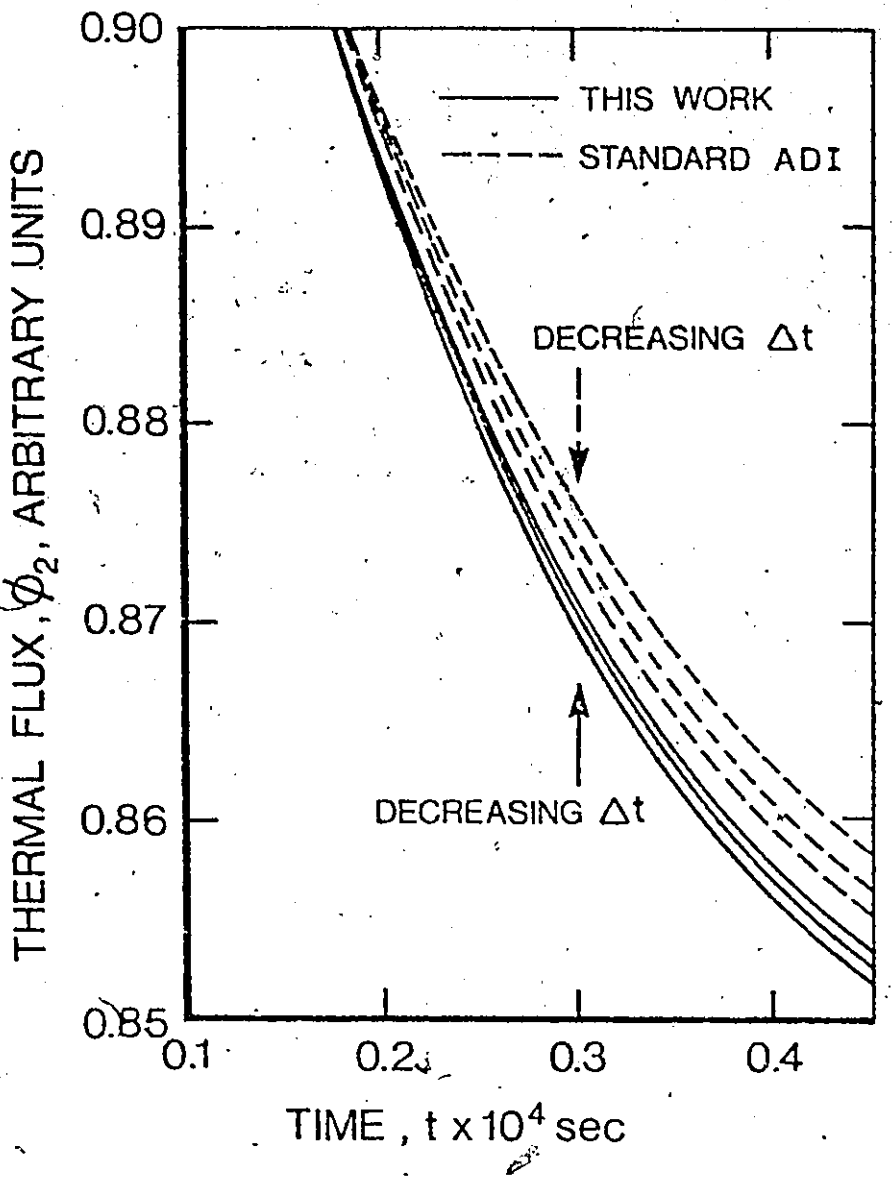

FIGURE 4.2.2 Thermal flux vs. time at the cell center for various time steps, $\Delta t = 1.0 \times 10^{-6}$, 0.5×10^{-6} and 0.25×10^{-6} sec. Case study: Initial Perturbation.

time. The method of Ferguson and Hansen (35) would fail to give a time reduction in this case since this method relies on all energy groups having the same time dependence. The method of Wight et al (39) would give a time reduction similar to this work only after the neutron groups develop their dominant trend.

Table 4.2.2 shows the relative accuracy of this work compared to the standard solution, which does not incorporate a transformation, at various times for the fast flux. Row 1 is the ratio of errors, (standard-exact)/(transformed-exact), obtained for the test case. The exact solution was obtained by extrapolating both numerical solutions to zero Δt. Both solutions gave, in general, the same exact solution. A ratio of 2 means that, for the same time step, the transformed equations experience only 1/2 the error of the standard equations. For this example, however, the transformed equations require 60% more computer time per iteration. Hence, for the same accuracy, the standard technique requires 2/1.6 times the time of the transformation technique as shown in row 2.

We note that the ratios vary as time proceeds. This can be attributed to the changing stiffness of the equations or, more specifically, to the changing importance of the generation and diffusion processes at different points in time, that is, the generation process possesses a short characteristic time compared to the diffusion process. At the start of the simulation, adjustment to the spatial distribution occurs as well as changes in the relative magnitudes of ϕ_1 and ϕ_2. If a steady state distribution had been used as the initial condition, only the generation term would have been significant and immediate savings would have resulted.

Time $(x10^4)s$	0.07	0.1	0.15	0.2	0.25	0.3	0.45	0.7
Error Ratio (Standard/ Transform)	0.7	1.67	2.6	2.9	2.9	2.9	1.8	1.4
Time Requirement Ratio (Standard/ Transform)	0.4	1.0	1.6	1.8	1.8	1.8	1.0	0.9

Table 4.2.2 Error ratio and time requirement ratio for same accuracy for the fast flux at the cell center point. Case study: Initial Perturbation.

Hence, we find no savings by the transformation method until the spatial distribution corrections become smaller. At $t = 1 \times 10^{-3}$ s, the computer time savings due to increased accuracy just surpasses the computer time losses due to increased computational complexity. The saving peaks at approximately 2.5×10^{-3} s and drops off at later times as the transients die away. At approximately 5×10^{-3}s, the diffusion terms again approach the generation term in magnitude. An analysis of the thermal flux yields similar results and hence is not quoted here. At much later times the transients of both fluxes approach the dominant trend of exponential growth or decay. In this time region, the eigenvalues approach that of Ferguson and Hansen (35) and the two methods become equivalent.

A more explicit example of the time saving available is that of a control situation in which the parameter product, εnf, is adjusted to maintain constant productivity. We consider the control problem which requires

$$\int_{\text{fuel}} \varepsilon nf(t)\ \phi_2(\underline{r},t)d\underline{r} = \text{CONSTANT} \quad . \tag{4.5.52}$$

Figures (4.2.3), (4.2.4) and (4.2.5) show the temporal variation of ϕ_1, ϕ_2 and εnf at the cell centre point. Tables 4.2.3 and 4.2.4 give the error ratios and time requirement ratios for the fast flux and for εnf. Again we note that, following the initial spatial adjustment, significant computer time savings result. In this example, the savings continue as time proceeds since the parameter, εnf, introduces perturbations in the

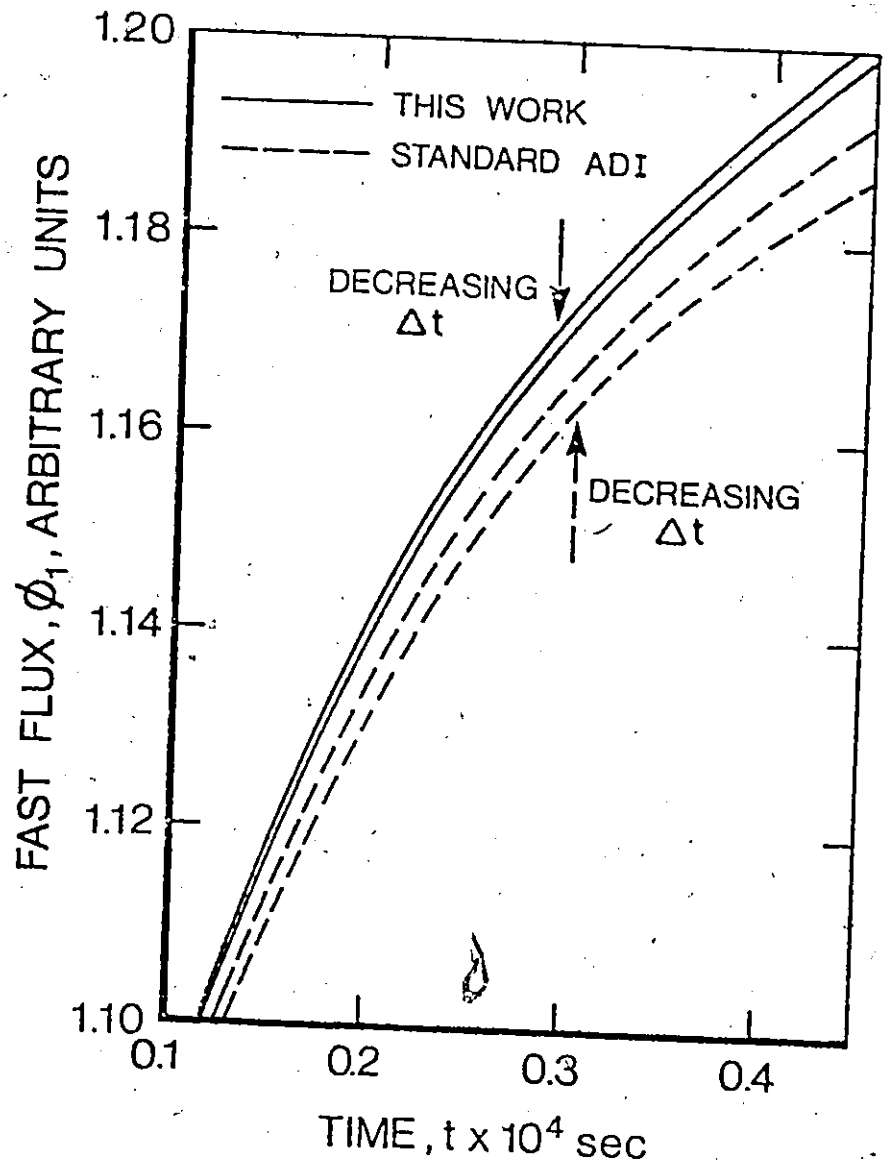

FIGURE 4.2.3 Fast flux vs. time at the cell center for various time steps, $\Delta t=1.0\times10^{-6}$, and 0.5×10^{-6} sec. Case study: Constant Productivity Simulation.

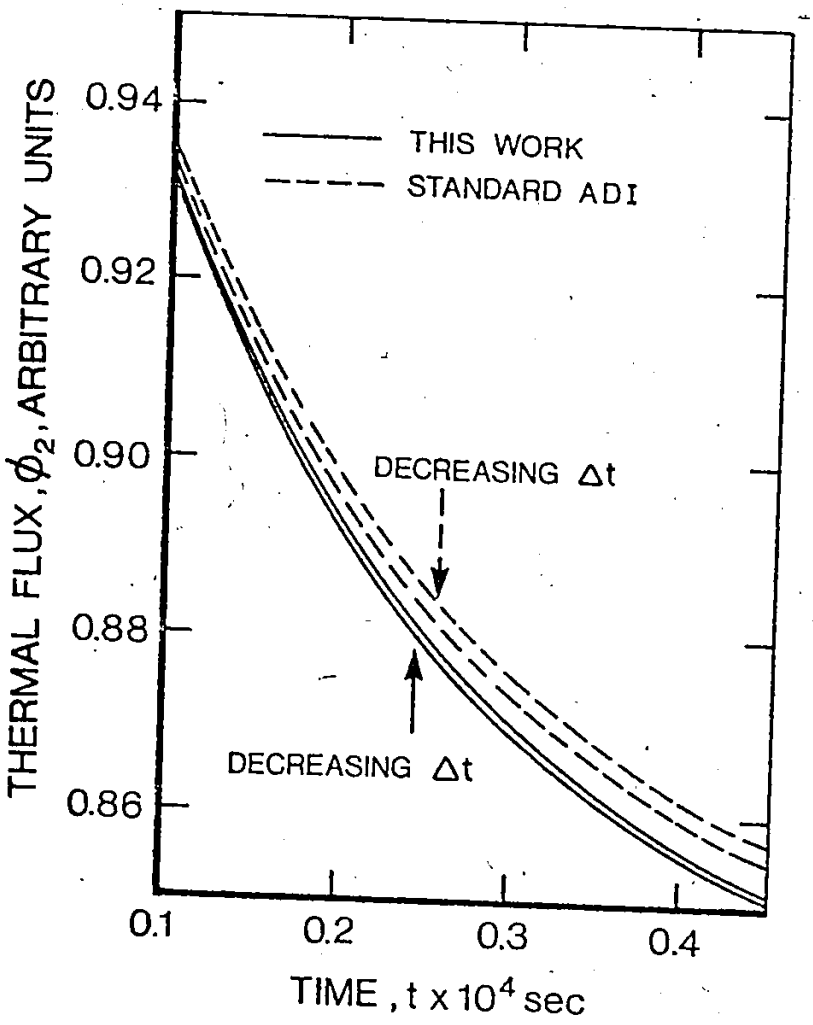

FIGURE 4.2.4 Thermal flux vs. time at the cell center for various time steps, $\Delta t = 1.0 \times 10^{-6}$ and 0.5×10^{-6} sec. Case study: Constant Productivity Simulation.

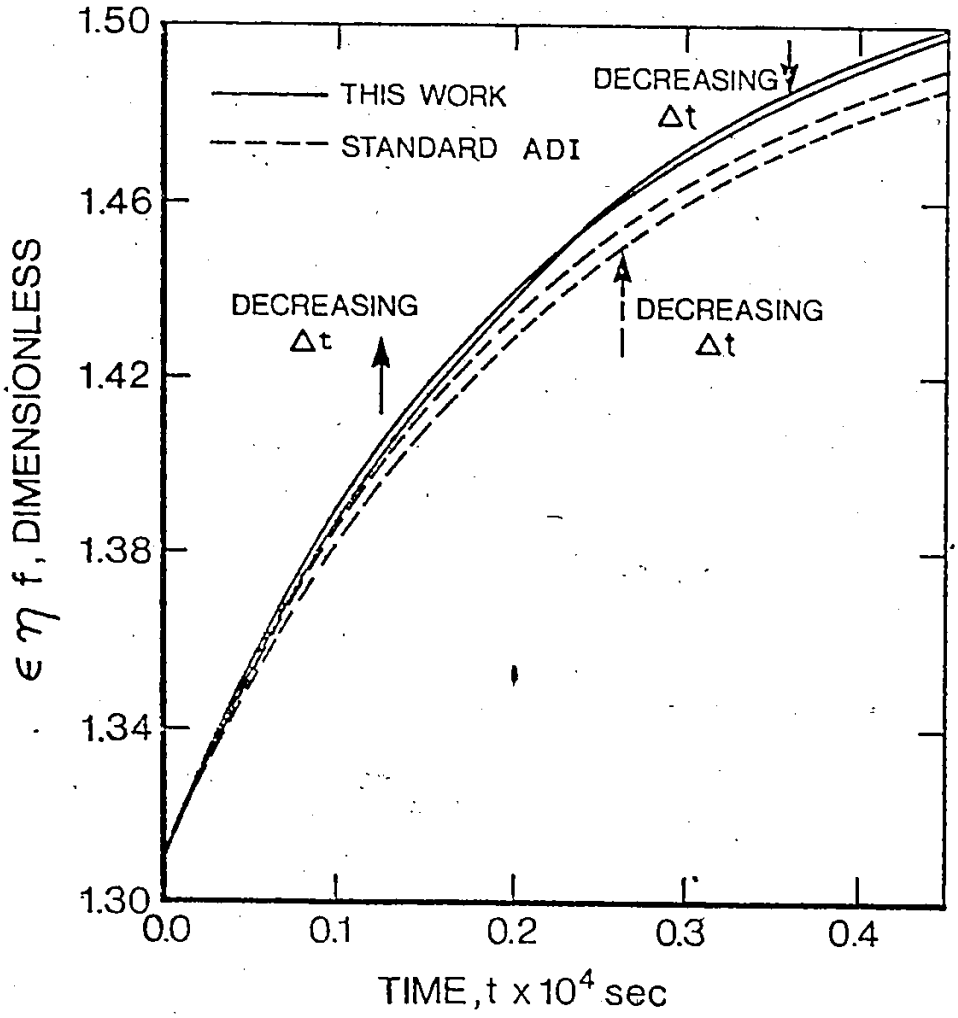

FIGURE 4.2.5 Parameter, ϵnf, vs. time for various time steps, $\Delta t = 1.0 \times 10^{-6}$ and 0.5×10^{-6} sec. Case study: Constant Productivity Simulation.

Time ($x10^4$) s	0.1	0.2	0.3	0.4	0.45
Error Ratio (Standard/Transform)	1.0	2.6	4.5	2.5	2.5
Time Requirement Ratio (Standard/Transform)	0.63	1.6	2.8	1.5	1.5

Table 4.2.3 Error ratio and time requirement ratio for same accuracy for the fast flux at the cell center point. Case study: Constant Productivity Simulation.

Time ($x10^4$) s	0.1	0.2	0.3	0.4	0.45
Error Ratio (Standard/Transform)	6.0	5.5	5.5	5.5	5.5
Time Requirement Ratio (Standard/Transform)	3.7	3.4	3.4	3.4	3.4

Table 4.2.4 Error ratio and time requirement ratio for same accuracy for the parameter, ε_{nf}, at the cell center point. Case Study: Constant Productivity Simulation.

generation term at each iteration.

We note that if one were only interested in the reactivity insertion necessary to maintain constant productivity or criticality, then, according to the results listed in table 4.2.4 the computational time ratio is approximately 3.4. Similar results were obtained at other spatial points.

It is informative to point out an important difference between the method explored here and the methods of Reed et al (38), Wight et al (39) and of Ferguson et al (35). These methods are not able to make intrinsically good guesses at the future flux trends when the parameters of the system are varying at each iteration.

4.2.4 CRITERIA FOR APPLICABILITY

It is conceivable that even within a given calculation there will be regions which will benefit from this transformation and regions which will not. It is, therefore, useful to have a criteria to determine when to use this method of analysis.

From the foregoing analysis we note that the deciding factor is the ratio of diffusion to generation.

$$R_g = |\nabla . D_g \nabla \phi_g / \sum_{g'=1}^{G} |\Sigma_{gg'} \phi_{g'}|| \quad , \quad g = 1,2,.....G \quad . \qquad (4.2.53)$$

If the ratio is less than unity, one can expect increased accuracy with the transformed equations. But, since the transformed equations require more computer time per iteration than the original equations, a cutoff ratio of about 0.5 might be more appropriate. This ratio depends upon

the relative values of the fluxes; it is not readily calculable before the actual simulation unless approximate values can be assigned. In any case, this ratio can be calculated on-line and the simulation can then switch to the appropriate method as dictated by the value of the ratio.

It should be noted that even if one energy group has a ratio above the cutoff while another has a ratio below the cutoff, there is nothing to restrict one from using different techniques for different groups.

4.2.5 CONCLUSIONS

The merits of the method of temporal transformation as explored here are clear. The relative computational time saving depends almost solely on the mathematical stiffness of the system of equations to be solved. A very stiff set, for instance, one approaching a homogeneous reactor or point reactor, can be quickly solved with large computational time savings since the spatial corrections are relatively unimportant. On the other hand, for systems in which the spatial variations occur in approximately the same time scale as temporal variations, there would probably be no computational time saving.

It is worthwhile noting here that this approach is not limited to the applications employed here. The overall scheme is to solve the approximate equations analytically and calculate only the corrections numerically. This scheme can thus be adapted to other kinds of space-time problems. The advantage of this approach over the dominant eigenvalue approach is its ability to give accurate results immediately after

a system perturbation where the dominant temporal trend has not been established. It is just such a system which is of interest to us since the final simulation model will entail a controller to maintain constant power in the reactor. This controller and the fluctuating voids will give the system a perturbation at each time iteration.

4.3 NUMERICAL SOLUTION OF THE DIFFERENTIAL EQUATIONS

In this section we look closely at the numerical procedure used in solving the differential equations of the previous section. First, the algorithm is detailed and, subsequently, it is evaluated in terms of its accuracy in approximating the solution to the differential equations.

4.3.1 THE ALGORITHM

The general space-time neutron flux equations have been given as

$$\frac{d\underline{\phi}(\underline{r},t)}{dt} = \underline{\underline{A}}(\underline{r},t)\ \underline{\phi}(\underline{r},t) \quad , \tag{4.3.1}$$

subject to initial condition, $\underline{\phi}(\underline{r},o)$, and the boundary conditions,

$$\underline{\phi}(\underline{r},t)\Big|_{z=\pm H/2} = 0 \quad , \tag{4.3.2}$$

$$\frac{\partial \underline{\phi}(\underline{r},t)}{\partial r}\Big|_{r=o} = 0 \quad , \tag{4.3.3}$$

and

$$\left.\frac{\partial \underline{\phi}(\underline{r},t)}{\partial r}\right|_{r=b} = 0 \qquad (4.3.4)$$

The elements of $\underline{\underline{A}}$, as given by equation (4.2.23), are functions of space and time with the diagonal containing spatial derivatives. Hence, equation (4.3.1) constitutes a set of non-linear, simultaneous, partial differential equations.

The numerical techniques used to solve such a set may take on many forms. However, a feature common to all methods used for such systems is a discretization in time and space. Shown in figure 4.3.1 is the two-dimensional form used herein. Each element of $\underline{\underline{A}}$, is, in itself, a matrix spanning the spatial and temporal mesh points. The flux vector, $\underline{\phi}$, is also discretized into subvectors. We denote the matrix elements as $a_{\ell m}^{ijk}$ and the flux elements as ϕ_{ℓ}^{ijk}, where

i = radial mesh point index, i = 1,2,...M,

j = axial mesh point index, j = 1,2,...N,

k = temporial mesh point index, k = 1,2,...,

ℓ = neutron flux equation index, ℓ = 1,2...G,

and

m = coefficient index for the equations, m = 1,2,...G.

Equation (4.3.1) becomes

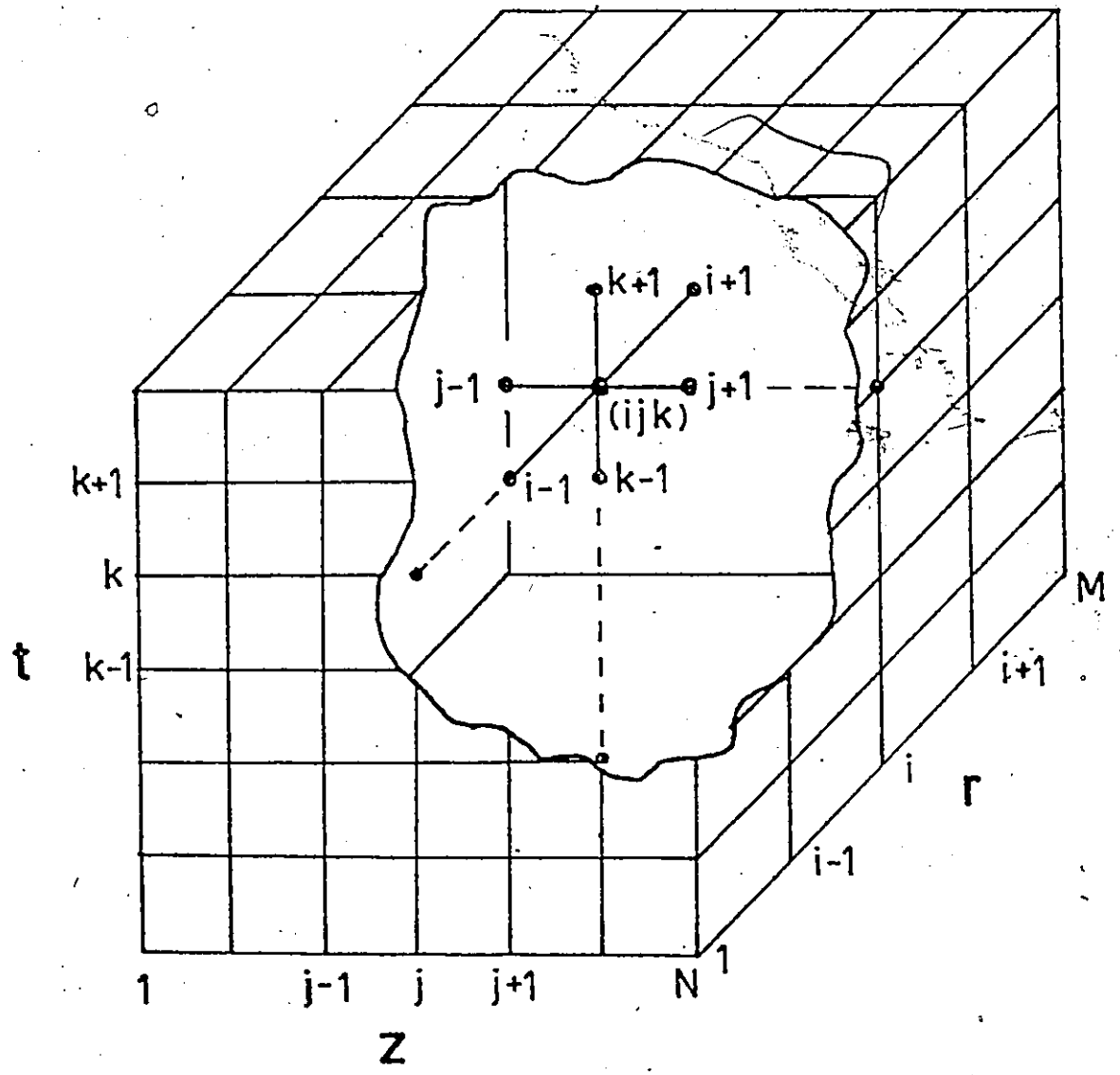

FIGURE 4.3.1: Discretized space and time.

$$\begin{bmatrix} \frac{d\phi_1^{ijk}}{dt} \\ \vdots \\ \frac{d\phi_\ell^{ijk}}{dt} \\ \vdots \\ \frac{d\phi_G^{ijk}}{dt} \end{bmatrix} = \begin{bmatrix} a_{11}^{ijk} & \cdots & a_{1m}^{ijk} & \cdots & a_{1G}^{ijk} \\ \vdots & & \vdots & & \\ a_{\ell 1}^{ijk} & \cdots & a_{\ell m}^{ijk} & \cdots & a_{\ell G}^{ijk} \\ \vdots & & \vdots & & \\ a_{G1}^{ijk} & \cdots & a_{Gm}^{ijk} & \cdots & a_{GG}^{ijk} \end{bmatrix} \begin{bmatrix} \phi_1^{ijk} \\ \vdots \\ \phi_\ell^{ijk} \\ \vdots \\ \phi_G^{ijk} \end{bmatrix} , \qquad (4.3.5)$$

where each term spans the spatial and temporal mesh, ijk. The derivatives are approximated by a Taylor's series expansion about the nodal point in question. The resulting expressions appropriate to our systems are

$$\frac{\partial \phi_\ell^{ijk}}{\partial t} = \frac{\phi_\ell^{ij,k+1} - \phi_\ell^{ijk}}{\Delta t} \equiv \Delta_t \, \phi_\ell^{ijk} , \qquad (4.3.6)$$

$$\frac{\partial \phi_\ell^{ijk}}{\partial r} = \frac{\phi_\ell^{i+1,jk} - \phi_\ell^{i-1,jk}}{2\Delta r} \equiv \Delta_r \, \phi_\ell^{ijk} , \qquad (4.3.7)$$

and

$$\frac{\partial^2 \phi_\ell^{ijk}}{\partial r^2} \quad \frac{\phi_\ell^{i+1,jk} - 2\phi_\ell^{ijk} + \phi_\ell^{i-1,jk}}{(\Delta r)^2} \equiv \Delta^2_r \, \phi_\ell^{ijk} , \qquad (4.3.8)$$

with similar notation for the axial derivatives. The boundary conditions are also discretized and are imposed upon equation (4.3.5) in the usual manner. We rewrite equation (4.3.5) using equation (4.3.6) to give

$$\begin{bmatrix} \phi_1^{ij,k+1} \\ \vdots \\ \phi_\ell^{ij,k+1} \\ \vdots \\ \phi_G^{ij,k+1} \end{bmatrix} = \begin{bmatrix} (1 + \Delta ta_{11}^{ijk}) & \cdots & \Delta ta_{1m}^{ijk} & \cdots & \Delta ta_{1G}^{ijk} \\ \vdots & & \vdots & & \vdots \\ \Delta ta_{\ell 1}^{ijk} & \cdots & (\delta_{\ell m} + \Delta ta_{\ell m}^{ijk}) & \cdots & \Delta ta_{\ell G}^{ijk} \\ \vdots & & \vdots & & \vdots \\ \Delta ta_{G1}^{ijk} & \cdots & \Delta ta_{Gm}^{ijk} & \cdots & (1 + \Delta ta_{GG}^{ijk}) \end{bmatrix} \begin{bmatrix} \phi_1^{ijk} \\ \vdots \\ \phi_\ell^{ijk} \\ \vdots \\ \phi_G^{ijk} \end{bmatrix} , \quad (4.3.9)$$

where $\delta_{\ell m}$ is the delta function defined by:

$$\delta_{\ell m} = 0, \ \ell \neq m$$
$$= 1, \ \ell = m \ . \quad (4.3.10)$$

In matrix notation, equation (4.3.9) becomes

$$\underline{\phi}^{k+1} = (\underline{I} + \Delta t \ \underline{A}) \ \underline{\phi}^{k} \ , \quad (4.3.11)$$

where $\underline{I}$ is the identity matrix.

Thus, based on the known flux distribution at time k, we can easily calculate the flux distribution at time k+1. This method, known as Explicit Finite Differencing, suffers from stability problems and an inability to properly simulate the propagation of flux perturbations. Both of these problems arise from the explicit nature of the technique; the calculation of $\phi_\ell^{ij,k+1}$ is based solely on the values of a_ℓ^{ijk} and ϕ_ℓ^{ijk} at time k. These problems can be removed by using an average value of ϕ_ℓ over the time interval, Δt. This value is not known a priori but,

by taking a weighted average of the values of time k and k+1, we find that

$$\underline{\phi}^{k+1} = \theta\Delta t\underline{A}^{k+1} + (\underline{I} + (1-\theta)\ \Delta t\ \underline{A})\ \underline{\phi}^{k} \quad , \tag{4.3.12}$$

where $o \leq \theta \leq 1$. This can be rewritten to give

$$(\underline{I} - \theta\Delta t\ \underline{A})\ \underline{\phi}^{k+1} = (\underline{I} + (1-\theta)\ \Delta t\ \underline{A})\ \underline{\phi}^{k} \quad . \tag{4.3.13}$$

Multiplying both sides of equation (4.3.13) by $(\underline{I} - \theta\Delta t\ \underline{A})^{-1}$ gives the solution,

$$\underline{\phi}^{k+1} = (\underline{I} - \theta\Delta t\ \underline{A})^{-1}(\underline{I} + (1-\theta)\ \Delta t\ \underline{A})\ \phi^{k} \quad . \tag{4.3.14}$$

We maintain the evaluation of $\underline{A}$ at time k in order to permit the solution of equation (4.3.13) by direct matrix inversion. These values can be updated on an iterative basis if necessary. The value of $\underline{A}$, however, remains essentially constant compared to the flux variation over the time interval, Δt, normally used to accurately simulate the flux variations. Hence, the iterations on $\underline{A}$ are not necessary.

We have now eliminated the problems of the explicit finite difference technique. However, the inversion of the general matrix, $(\underline{I} - \theta\Delta t\ \underline{A})$, is subject to round off errors and excessive time requirements. If the matrix is tridiagonal or triangular, these problems are significantly reduced. It was because of this that the Alternating Direction Implicit scheme evolved. The ADI scheme is defined by the following algorithm (39):

The matrix $\underline{A}$, or $\Omega^{-1}(\underline{A}-\underline{A}')\ \Omega$ of the transformed equations, is split

into the sum of two parts,

$$\underline{\underline{A}} = \underline{\underline{A}}_1 + \underline{\underline{A}}_2 = \underline{\underline{A}}_3 + \underline{\underline{A}}_4 \tag{4.3.15}$$

where $\underline{\underline{A}}_1 = \underline{\underline{R}} + \underline{\underline{L}}_1$, $\underline{\underline{A}}_2 = \underline{\underline{Z}} + \underline{\underline{L}}_2$, $\underline{\underline{A}}_3 = \underline{\underline{Z}} + \underline{\underline{L}}_3$, $\underline{\underline{A}}_4 = \underline{\underline{R}} + \underline{\underline{L}}_4$.

Here, $\underline{\underline{R}}$ is a symmetric tridiagonal matrix associated with diffusion in the radial direction, and $\underline{\underline{Z}}$ is a similar, symmetric three stripe matrix associated with diffusion in the axial direction. We write, using $h = \Delta t/2$,

$$(\underline{\underline{I}} - h\underline{\underline{A}}_1)\ \phi^{k+1/2} = (\underline{\underline{I}} + h\underline{\underline{A}}_2)\ \phi^{k} \tag{4.3.16}$$

and

$$(\underline{\underline{I}} - h\underline{\underline{A}}_3)\ \phi^{k+1} = (\underline{\underline{I}} + h\underline{\underline{A}}_4)\ \phi^{k+1/2} \quad , \tag{4.3.17}$$

where $\phi^{k+1/2}$ is an intermediate vector computed on the first half-step.

Such a scheme has been investigated (39) and evaluated for various choices of L_i, $i = 1,2,\ldots4$, which lead to tridiagonal or triangular matrices for the inversion. It was concluded that most choices give satisfactory results for the systems of interest herein. Upon application of this algorithm to the transformed equations given by equation (4.2.33), we find that the time consuming exponential evaluations had to be performed twice, once for each half step. These calculations can be combined into a single evaluation by using the following modification to equations (4.3.16) and (4.3.17):

$$\phi^{k+1} = \frac{1}{2}\left[(\underline{\underline{I}} - \Delta t\, \underline{\underline{A}}_1)^{-1}(\underline{\underline{I}} + \Delta t\, \underline{\underline{A}}_2)\right.$$

$$\left. + (\underline{\underline{I}} - \Delta t\, \underline{\underline{A}}_3)^{-1}(\underline{\underline{I}} + \Delta t\, \underline{\underline{A}}_4)\right] \phi^{k} \quad , \qquad (4.3.18)$$

with no apparent loss in truncation error or stability for the two-group cell model of this dissertation. Hence this modified algorithm was used in the numerical solution of the neutron flux equations. By numerical experimentation, the choice of L_i was not found to be critical and, hence, for convenience, the L_i are chosen to ensure that the matrices to be inverted A_1 and A_3, are tridiagonal. The computer codes for the standard equations and the transformed equations are given in appendices 8 and 9.

Having detailed the algorithm, we now discuss its utility when applied to the cell model.

4.3.2 MESH SIZE CONSIDERATIONS

Numerical experiments, using the nominal parametric values for the no void condition given by table 4.1.2, were carried out to estimate the error associated with the number of spatial mesh points chosen and to confirm that the computer code results do, for increasing number of mesh points, tend toward the analytical predictions. The analytical results could be obtained only for uniform voiding, hence the reason for these numerical experiments being restricted to uniform voiding. For these experiments, the initial flux distributions and the steady-state or critical value of the parameter, $\varepsilon\eta f$, were that given by the analytical steady-state solution. Then, for a given time step, $\Delta t = 2 \times 10^{-6}$ seconds,

the system was allowed to propagate in time. The divergence of the flux distributions at some later time indicated the effect of a finite mesh size. Table 4.3.1 shows the results.

We note that the numerical results approach the analytic results as the spatial mesh is refined, that is, as M and N increase. The importance of an adequate radial mesh refinement is illustrated and we conclude that the errors are dominated by the radial mesh errors. Thus, to provide reasonable answers, $M \geq 11$ is required. The axial mesh refinement is not nearly as critical as for the radial mesh. However, in subsequent studies, sufficient axial refinement will be necessary in order to pick up the structure of the axial void distribution. Consequently, we can conclude that an 11 x 11 mesh is necessary in general. Further refinements are limited by computational cost considerations.

The cause of the difference in sensitivity of the numerical code to variations in N and M can be seen by considering equation (4.2.42) in the steady state or equivalently equation (4.1.56):

$$(E_1 - \Sigma_1)(E_2 - \Sigma_2) - \varepsilon\eta f p \, \Sigma_1 \, \Sigma_2 = 0 \quad , \tag{4.3.19}$$

i.e.,

$$\frac{k_\infty}{(1 - E_1/\Sigma_1)(1 - E_2/\Sigma_2)} = 1 = k_{eff} \quad . \tag{4.3.20}$$

Now,

M	N	$\phi_1\|_{t=2\times10^{-6}s}$	$\phi_2\|_{t=2\times10^{-6}s}$	$\phi_1\|_{t=1\times10^{-4}s}$	$\phi_2\|_{t=1\times10^{-4}s}$
5	5	0.7733	0.6891	0.8359	0.6334
5	11	0.7733	0.6891	0.8358	0.6344
8	5	0.7734	0.6890	0.7730	0.6895
11	5	0.7735	0.6889	0.7731	0.6896
11	11	0.7735	0.6889	0.7730	0.6896
∞	∞	0.7735	0.6888	0.7735	0.6888

Table 4.3.1 Numerical simulation results showing the convergence to analytical results as $N,M \to \infty$. The time step, Δt, is held at 2×10^{-6} s for this study.

$$E_1/\Sigma_1 = - L_1^2 B_1^2 = - L_1^2 (B_{1z}^2 + B_{1r}^2) \qquad (4.3.21)$$

and

$$E_2/\Sigma_2 = - L_2^2 B_2^2 = - L_2^2 (B_{1z}^2 + B_{1r}^2) \quad , \qquad (4.3.22)$$

as previously defined. We also recall that $B_z^2 << B_r^2$. From the above discussion and from equation (4.3.20) we see that numerical errors in axial mesh approximations are less important than those in the radial case. For studies of the effect of radial void distributions, then, we can afford to reduce N, the number of axial mesh points, to a minimum. For axial void distributions, however, both N and M must be increased in order to adequately represent the system by the numerical approximation.

4.3.3 NUMERICAL CONTROL

Since the neutron models are not self-limiting but entail inherently uncontrolled neutron multiplication, it follows that, in the numerical simulation in which the reactor is brought to steady state, a controller is necessary. This controller provides feedback to either the reactor size or material properties, simulating the effort to bring the reactor back to steady state after a perturbation. In this work the reactivity ρ or equivalently the parameter ϵnf, which is a function of void fraction, is altered by a multiplicative gain factor g. Thus a perturbation in the system is felt as a variation in g necessary to bring the system back to steady state operation and as implicit, simultaneous flux perturbations.

Various proportional and integral-proportional controllers were

employed in the search for the controller which brings the system back to steady state in the shortest simulation time. It was found that a simple proportional controller,

$$g = 1 + g_o(\phi_1 \Big|_{\substack{z=+H/2 \\ r=\bar{o} \\ t=t}} - \phi_1 \Big|_{\substack{z=+H/2 \\ r=\bar{o} \\ t=o}}) \quad , \tag{4.3.33}$$

with the appropriate gain g_o, provides the necessary action and is sufficient for the desired purpose. The value of genf does not contain any offset, that is, any error at steady state conditions, but the controlled variable, $\phi_1 \Big|_{\substack{z=+H/2 \\ r=\bar{o} \\ t=t}}$ does. This is of little concern since the absolute flux value is arbitrary; the satisfaction of the steady state condition suffices. If offset in the flux value is to be suppressed, the addition of an integral term adequately provides the necessary action. This proportional-integral or PI controller is given by

$$g = 1 + g_o(\phi_1|_{t=t} - \phi_1|_{t=o}) + g_1 v_1 \int_o^t (\phi_1|_{t=t} - \phi_1|_{t=o})dt) \quad . \tag{4.3.24}$$

Table 4.3.2 shows the optimal controllers found for this system. For the proportional controller, $g_1 = 0$. These values are approximate only and vary with the nominal operating conditions. We interject here that the thermal flux, ϕ_2, could have equally well been controlled since the two energy groups are tightly coupled.

As the eigenvalues and eigenvectors of the system are known at all

M	N	g_o	g_1
5	5	- 0.05	- .001
5	11	- 0.05	- .001
11	5	-10.	-1.
11	11	-10.	-1.

Table 4.3.2 Approximate values for g_o and g_1 for the PI controller at various mesh sizes.

points in time and space, it is tempting to try and devise a controller based on the long-term predictions made possible by this knowledge. Recalling that

$$\phi_i - \psi_{i1} e^{\omega_1 t} + \psi_{i2} e^{\omega_2 t}, \quad i=1,2, \tag{4.3.25}$$

long term steady state operation requires that $\omega_1 = 0$ and $\omega_2 = 0$, giving

$$\phi_i \Big|_{t=\infty} = \psi_{i1} + \psi_{i2} = \text{CONSTANT} \quad . \tag{4.3.26}$$

Hence equation (4.2.42) is transformed into equation (4.3.19),

$$(E_1 - \Sigma_1)(E_2 - \Sigma_2) - g \; \epsilon\eta f p \; \Sigma_1 \Sigma_2 = 0 \quad , \tag{4.3.27}$$

and we thus have the predicted value of g necessary for steady state operation based on the flux distributions at time t. This predicted value can then be used until an updated value is available at the next iteration. It was found that this method did not give convergence any quicker than the simple controller previously described and, henceforth, the simple controller will be used. We conclude, then, that the diffusion controlled time constant of the system is sufficiently long as to make the control of the simulation an easy task.

Although the transformation technique discussed in section 4.2 provides computational savings in transient studies, numerical experiments have shown that as the system approaches steady state, no computational gain occurs since all methods dampen out to the same answer. This occurs for the system under consideration since the time step size, Δt, is

limited by stability considerations. The problem is inherently non-linear and subject to instability due to feedback of the controller and system parameters. This stability limit was reached at a small Δt since the radius of the reactor cell is small; $v_1 \Delta t/\Delta r^2 \lesssim \frac{1}{2}$ for numerical stability for this example. For the more general case truncation error, not stability, is the major limitation to a Δt increase (35). Thus, in general, the transformation method will give a cost saving even as the perturbations dampen out because it will have provided a more accurate solution throughout the transient and hence will have accumulated less error at any time during the transient. For these general systems, in which the stability criteria imposed on Δt by the small radial dimension is not present, large Δt's can be used and the control situation should be re-evaluated.

While on the subject of numerical details, we must consider the cost of the simulation study. Numerical experimentation has led to the following rule of thumb for typical case problems on the CDC 6400:

$$\text{TIME/ITERATION} \approx 12 + N \times M/120 \text{ seconds (standard ADI, Ferguson et al (35), etc.)}$$

$$\approx 12 + N \times M/75 \text{ seconds (transformed ADI).} \quad (4.3.28)$$

From given initial conditions approximately 2.5×10^{-3} seconds of reactor time are required to bring the system to steady state. Stability limitations dictate that $\Delta t \times M^2 \lesssim 2.5 \times 10^{-4}$ seconds and so

$$\text{TIME TO STEADY STATE} \approx 12 + N \times M^3/12 \text{ seconds (standard ADI, Ferguson et al (35), etc.)}$$

$$\approx 12 + N \times M^3/7.5 \text{ seconds (transformed ADI).} \quad (4.3.29)$$

Typical running times required to converge upon steady state are 95 seconds for N=5 and M=5 and 2000 seconds for N=11 and M=11. These are approximate times and will generally give the absolute steady state criticality condition to 0.1% or 1 mk. Axial perturbations may require additional time since the large axial dimension of this system increases the time constant for the propagation of axial perturbations.

4.3.4 NUMERICAL DETERMINATION OF REACTIVITY INSERTIONS

As pointed out in section 4.2, the motivation for resorting to numerical simulation rather than flux synthesis techniques, for determining reactivity insertions caused by a system perturbation, is that the detailed flux distribution perturbations must be accounted for. The procedure is to compare the two cases, perturbed and nominal; the difference in the gain, g, defines the magnitude of the perturbation. In order to ensure that the small difference between the two numerical solutions is meaningful, a test is carried out in which the solution can be compared to an analytical solution. Thus, the case of uniform voiding is taken using the nominal LATREP Predicted parameters fitted at a void fraction, α, = 0.0. Table 4.3.3 compares the numerical predictions with the analytical solutions. We see that it is possible to obtain an accurate estimate of reactivity perturbations by numerical means.

	ANALYTICAL	NUMERICAL	
		N=5, M=5	N=5, M=11
$\alpha = 0.0$	1.00000	.997668	1.00034
$\alpha = 0.1$	.98676	.992274	.98617
Δg	0.01324	.005394	0.01417

Table 4.3.3 Comparison of reactivity insertion determinations by numerical and analytical means.

CHAPTER 5

FLUID MODELLING

5.0 INTRODUCTION

The generalized mass, momentum and energy equations for multi-phase flow systems, as presented in appendix 9, are well known. However, their practical utility in describing the fundamental phenomena of forced convective channel boiling is prevented by the geometric complexities and the lack of information on the interphase mass, momentum and energy transport involved. Consequently, the bulk of the research has been directed towards experimental correlation development (9) to provide the data necessary for the engineering design of heat transfer systems. This plan of attack for design is still appropriate today but to a lesser degree. It is becoming increasingly evident that, in the design of nuclear reactors, an understanding of the basic phenomena is needed in order to provide an accurate a priori design. In this way, as the size and capacity of the systems grow, the dependence on expensive prototypes is reduced. The economic savings both at the design stage and at the startup stage can be considerable.

Early attempts (45-57) at modelling two-phase flow were little more than extensions of single-phase pipe flow analysis with a heavy reliance on experimental correlation and simplified flow equations characteristic of single-phase flow. It was soon recognized, however, that the flow patterns of the void, velocity and enthalpy distributions

played a major role. Attempts were made to account for this effect by empirically delineating the flow regimes (48-51), by using separate equations for each phase (52-55), and by formulating solutions appropriate to a particular flow regime (56,57).

Levy (48) developed approximate solutions for the annular flow region and later (52) formulated a momentum exchange model using separate momentum equations for each phase. Based on this momentum model, a turbulent mixing length theory (58) was also proposed to describe the flow. At about the same time, Griffith et al (49) developed a slug flow model based on the mixture momentum equation and Bankoff (50) investigated a variable density single-phase model using the usual pipe flow analysis for single-phase fluids. Separate mass conservation equations for the two phases were used by Houghton (53) assuming equal velocities for each phase. He found evidence to suggest that thermal equilibrium conditions do not generally exist in practical forced convective boiling systems. Quandt (59), Meyer et al (60) and Hudson et al (61) made a significant contribution by considering the mixture equations for all three mass, momentum and energy equations. Recently, Larsen (55) used separate two-phase mass and energy equations to study subcooled boiling and Ahmad (10) used separate energy equations to describe the flow over the total heated length.

These investigations, among many others, vary greatly in the details of the approach taken but they all have major restrictions in common. They are characterized by the use of only a few of the six conservation equations, the state equation and the boundary conditions

necessary to fully describe the system. The equations or conditions not used are replaced by empirical expressions which have limited applicability. For instance, the energy equations are often replaced by assuming thermal equilibrium and the mass balance equations are often replaced by a postulated vapour growth correlation.

These works are also characterized by an improper cross sectional homogenization procedure. In this procedure, the values of the dependent variables, void fraction, velocity and enthalpy, are assumed constant over the flow cross section. The radial dependence of the integral equations can then be directly integrated out. However, the integral equations are non-linear in the dependent variables; this leads to errors in the above procedure. The proper averaging procedure is to radially integrate the terms of the integral equations rather than the dependent variables.

Zuber et al (11,12) have made significant progress by recognizing this error. This led to the use of distribution parameters, as discussed herein. Additionally, this was the first successful treatment of separate mass equations. The effect of velocity slip between the two phases is empirically accounted for but thermal equilibrium and fully developed flow profiles are assumed. The thermal equilibrium assumption was removed by crude empiricism in a recent extension of this work (62). In a more successful extension of Zuber's model, Hancox et al (13,14) removed the thermal equilibrium assumption by the use of the mixture energy equation. Fully developed flow profiles were not assumed but slip was neglected to facilitate the solution procedure.

These latest works represent the state of the art. Although experimental correlation has been reduced, it is still required to compensate for the assumptions made. The trend seems to be towards the full utilization of the fundamental equations with an associated broadening in the range of applicability.

5.1 THE PHYSICAL MODEL

Before investigating the void formalisms, we consider the physical model appropriate for this study. The discussion of the reactor model in section 4.1.1 defines the geometry of the coolant channel. The coolant water, then, is confined to flow upwards between the fuel pencils in subchannel flow at the nominal operating pressure and flow rate. The present methods of subchannel flow analysis (63-69) do not allow us to be able to adequately describe inter-subchannel mixing; present models compensate for this by assigning an equivalent heated and wetted perimeter. As we shall see, the neutronic behaviour of the reactor system is not sensitive to the detailed subchannel radial void distribution. But the subchannel details are important in the determination of the radial average void fraction. This radial average void fraction can have a profound effect upon reactivity, as noted in section 5.6 and in chapter 6.

5.2 SIMPLE VOID FORMALISM

Herein, we consider a simple model for illustrative purposes and to assure ourselves that, indeed, a more sophisticated model is necessary to describe forced convective boiling in nuclear reactors.

The following assumptions are imposed:

1) thermal equilibrium exists between the liquid and vapour phases;

2) the fluid properties, such as phase density and latent heat, are constant;

3) there is no slip between the two phases;

4) homogenization of the liquid and vapour phases in the radial direction is valid.

The configuration appropriate is one-dimensional, cylindrical geometry. The flow is axial only, with $z = 0$ at the coolant inlet.

The equations of continuity in the steady state are known to be (70,71)

$$\frac{d}{dz}(\alpha\delta_g v) = \Gamma \qquad (5.2.1)$$

and

$$\frac{d}{dz}((1-\alpha)\delta_f v) = -\Gamma \,, \qquad (5.2.2)$$

where the subscripts g and f refer to the vapour and liquid phases respectively and where

α = void fraction = $\alpha(z)$ [dimensionless] ,

δ = fluid density [gm/cm^3] ,

z = axial coordinate [cm] ,

v = velocity ($v_g = v_f = v$) = $v(z)$ [cm/s]

and

Γ = vapour generation rate = $\Gamma(z)$ [gm/cm^3 s] .

Rearranging these equations and integrating gives

$$\nu(z) - \nu(o) = \frac{\Delta\delta}{\delta_f \delta_g} \int_o^z \Gamma \, dz \quad , \tag{5.2.3}$$

where $\Delta\delta \equiv \delta_f - \delta_g$.

But for thermal equilibrium, we require

$$\Gamma = g''/\lambda \quad , \tag{5.2.4}$$

where g'' [cal/cm^3 s] is the heat flux through the fluid surface into the fluid volume and λ [cal/gm] is the latent heat of vaporization. But, g'' is proportional to the radially averaged thermal neutron flux, $\bar{\phi}$. Hence

$$g'' \equiv g_o''' \; \bar{\phi} \quad , \tag{5.2.5}$$

where g_o''' [cal/neutron cm] depends upon the neutronic properties of the fuel, and

$$\nu(z) - \nu(o) = \frac{\Delta\delta g_o'''}{\delta_f \delta_g \lambda} \int_o^z \bar{\phi}(z) dz \quad . \tag{5.2.6}$$

Employing the definition of average density ($\delta_f \, \nu(o) \equiv \nu\alpha\delta_g + \nu(1-\alpha) \, \delta_f$) to equation (5.2.6) we obtain, after rearrangement,

$$\alpha(z) = \frac{1}{(1 - \frac{\delta_g}{\delta_f})} \left(1 - \frac{\nu(o)}{\nu(o) + \frac{\Delta\delta g_o'''}{\delta_f \delta_g \lambda} \int_o^z \bar{\phi}(z) dz} \right) \quad . \tag{5.2.7}$$

The above derivation represents a special case of the more general derivation of Hancox, which includes the effect of radial inhomogeneities and incorporates an experimentally correlated vapour generation function.

Figure 5.1 shows a comparison of this theory with experimental data based on an uniformly heated channel as cited by Hancox and defined by table 5.1. The example chosen for comparison was one of low inlet subcooling, not fully realistic in view of current reactors. A comparison with a higher sub-cooled case, that is, higher departure from thermal equilibrium, will result in a much larger discrepancy between models and experimental data. There are at least two deficiencies in the foregoing model: (1) failure to account for inlet subcooling; and (2) failure to account for radial inhomogeneities. The necessity of a more sophisticated model is indicated.

5.3 ZUBER'S MODEL

As mentioned previously, the work of Zuber incorporates a better void generation model to reduce the error due to subcooling effects and uses distribution parameters to account for the radial inhomogeneities. From Zuber et al (11,12) we adopt the following definitions:

j ≡ axial velocity of the center of volume [cm/s];

V_{gj} ≡ drift velocity of the vapour w.r.t. j[cm/s];

V_{fj} ≡ drift velocity of the liquid w.r.t. j[cm/s];

v_g ≡ local velocity of the vapour [cm/s];

v_f ≡ local velocity of the liquid [cm/s];

α ≡ local volumetric concentration of the vaopur [dimensionless];

j_f ≡ volumetric flux density of the liquid [cm/s];

j_g ≡ volumetric flux density of the vaopur [cm/s];

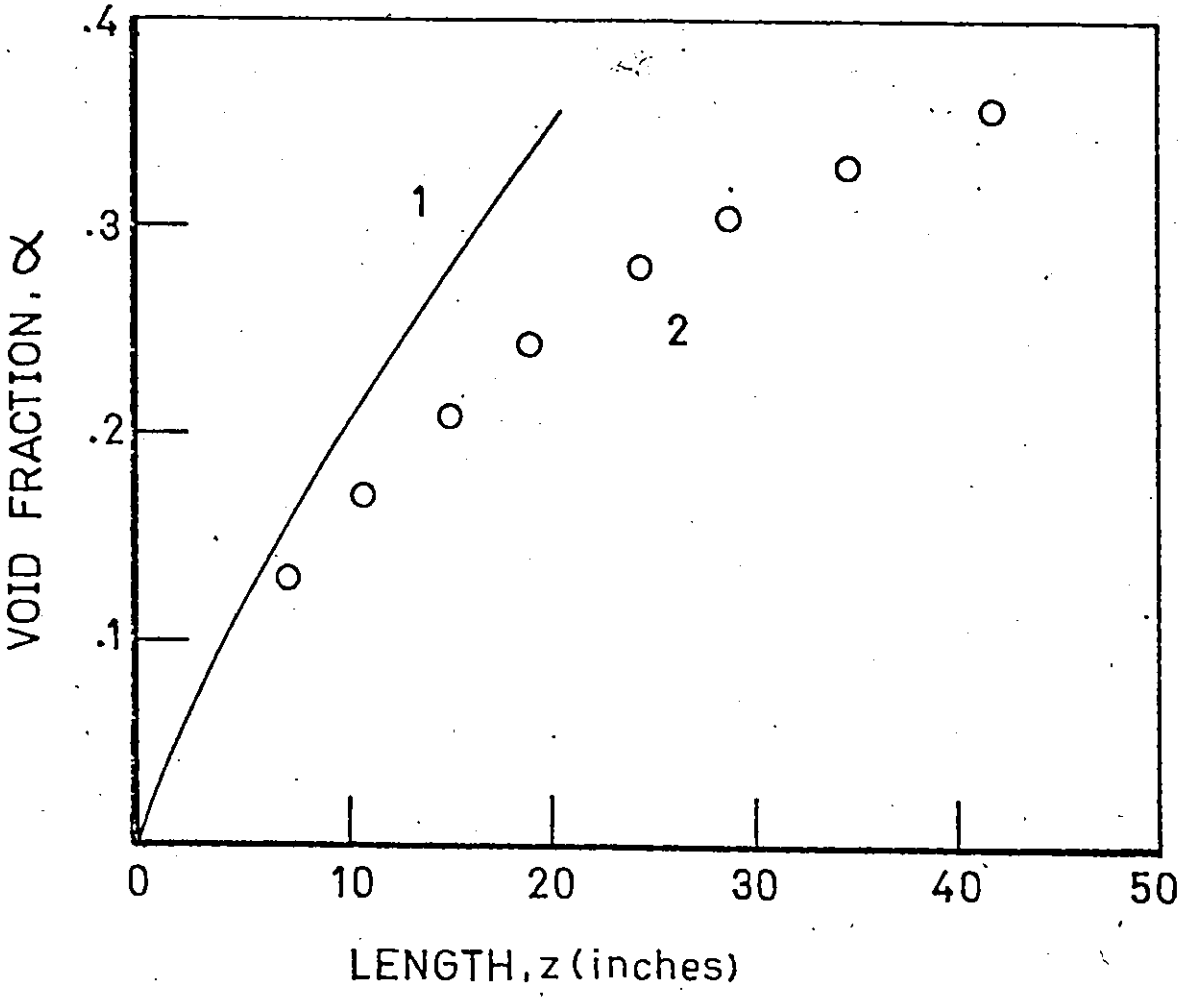

FIGURE 5.1: Comparison of void fraction, α, as a function of heated channel length, z , as predicted by: 1 - simple model; 2 - experimental data.

PARAMETER	VALUE
HEATED PERIMETER	12.5 cm
WETTED PERIMETER	12.5 cm
FLOW AREA (RECTANGULAR)	4.89 cm^2
PRESSURE	1.38 MN/m^2
SUBCOOLING	.3° C
FLOW RATE	1158 $Kgm/m^2/s$
HEAT FLUX	71.5 KW/m^2
LENGTH	1.27 m

Table 5.1 Parameters for model comparison.

and

$v_r \equiv$ relative velocity between the liquid and vapour phases [cm/s]. From physical considerations the relationships between these velocities and void fraction, α, immediately follow:

$$j_f = (1-\alpha)\, v_f \; ; \tag{5.3.1}$$

$$j_g = \alpha\, v_g ; \tag{5.3.2}$$

$$j = j_f + j_g = (1-\alpha)\, v_f + \alpha\, v_g ; \tag{5.3.3}$$

$$V_{fj} = v_f - j ; \tag{5.3.4}$$

$$V_{gj} = v_g - j ; \tag{5.3.5}$$

$$v_r = v_g - v_f ; \tag{5.3.6}$$

$$V_{fj} = -\alpha\, v_r ; \tag{5.3.7}$$

$$V_{gj} = (1-\alpha)\, v_r ; \tag{5.3.8}$$

and

$$V_{gj} - V_{fj} = v_r . \tag{5.3.9}$$

It has been shown that the form of the drift velocity, V_{gj}, is

$$V_{gj} = v_\infty (1-\alpha)^m \quad , \tag{5.3.10}$$

where v_∞ is the terminal velocity of a single gas bubble and m is an exponent varying with the flow regime. The explicit dependence on α is evident.

The differential mass balances for the two phases are

$$\frac{\partial(1-\alpha)\delta_f}{\partial t} + \nabla \cdot ((1-\alpha)\ \delta_f\ v_f) = -\ \Gamma \qquad (5.3.11)$$

and

$$\frac{\partial(\alpha\delta_g)}{\partial t} + \nabla \cdot (\alpha\delta_g\ v_g) = \Gamma \quad , \qquad (5.3.12)$$

where the densities of the two phases are denoted by δ_f and δ_g and the vapour generation is Γ. Rearranging these two equations and employing the previous definitions lead to

$$\frac{\partial}{\partial z}\left[(1-\alpha)\ v_f + \alpha v_g\right] = \frac{\partial f}{\partial z}$$

$$= \frac{\Gamma}{\delta_g}\frac{(\delta_f - \delta_g)}{\delta_f} - \frac{(1-\alpha)}{\delta_f}\left(\frac{\partial\delta_f}{\partial t} + v_f\frac{\partial\delta_f}{\partial z}\right)$$

$$- \frac{\alpha}{\delta_g}\left(\frac{\partial\delta_g}{\partial t} + v_g\frac{\partial\delta_g}{\partial z}\right) \cdot \qquad (5.3.13)$$

Integrating with respect to z gives the volumetric flux density along the channel length.

In general, the vapour generation term, Γ, is specified by the constitutive equation for the process in conjunction with the energy equations. For the special case of thermodynamic equilibrium, the energy equations alone can be used to specify Γ. Additionally, since a detailed knowledge of the energy interchange between the two phases is not available, only the mixture energy equation is considered. This equation is given by

$$(1-\alpha)\ \delta_f\frac{D_f E_f}{Dt} + \alpha\ \delta_g\frac{D_g E_g}{Dt} + \Gamma(E_g - E_f)$$

$$= h_o\ \Delta T\ \frac{\xi_h}{A} + g_d\frac{\partial P}{\partial t} + \delta_m\frac{\partial\Phi_p}{\partial t} \quad , \qquad (5.3.14)$$

where

$$\frac{D_f}{D_t} \equiv \frac{\partial}{\partial t} + \nu_f \frac{\partial}{\partial z} \quad ,$$

$$\frac{D_g}{D_t} \equiv \frac{\partial}{\partial t} + \nu_g \frac{\partial}{\partial z} \quad ,$$

$$\delta_m \equiv (1-\alpha)\ \delta_f + \alpha\delta_g \quad ,$$

$$E_f \equiv i_f + \frac{\nu_f^2}{2g_c} + \Phi_p \quad ,$$

$$E_g \equiv i_g + \frac{\nu_g^2}{2g_c} + \Phi_p \quad ,$$

$i_f \equiv$ liquid enthalpy [cal/gm] ,

$i_g \equiv$ vapour enthalpy [cal/gm] ,

$\Phi_p \equiv$ potential energy (normally independent of t) [cal/gm] ,

$h_o \equiv$ heat transfer coefficient [cal/cm^2 s °K] ,

$\Delta T \equiv$ subcooling [°K] ,

$A \equiv$ flow area [cm^2] ,

$\xi_h \equiv$ heated perimeter [cm] ,

$g_c \equiv$ proportionality constant [gm cm^2/cal s^2] ,

$g_d \equiv$ proportionality constant [cal/cm s-dynes]

and

$P \equiv$ pressure [dynes/cm^2] .

For thermodynamic equilibrium, the left hand side of equation (5.3.14) can be determined from the equilibrium enthalpies. Hence Γ is easily determined directly. For non-equilibrium conditions, however, a constitutive equation is required. In addition, the momentum equation

would be required to specify the system pressure variation. For Zuber's model, however, equilibrium is assumed and hence only the mixture energy equation is needed.

The foregoing equations, then, plus the appropriate boundary and initial conditions specify the void propagation of the system. Zuber continues, at this point, to develop equation (5.3.12) into the 'void propagation equation',

$$\frac{\partial \alpha}{\partial t} + U \frac{\partial \alpha}{\partial z} = N \quad , \tag{5.3.15}$$

in analogy with kinematic waves. Here U, the velocity of the kinematic wave, and N, the characteristic reaction frequency, are defined as

$$U \equiv j + V_{gj} + \alpha \frac{\partial V_{gj}}{\partial \alpha} \tag{5.3.16}$$

and

$$N = \frac{\delta_m}{\delta_f} \frac{\Gamma}{\delta_g} + \alpha(1-\alpha) \left[\frac{1}{\delta_f} \left(\frac{\partial \delta_f}{\partial t} + v_f \frac{\partial \delta_f}{\partial z}\right) - \frac{1}{\delta_g} \left(\frac{\partial \delta_g}{\partial t} + v_g \frac{\partial \delta_g}{\partial z}\right)\right] \quad . \tag{5.3.17}$$

Finally, in order to avoid having to deal with the detailed interfacial properties of the two phase system, the integral formalism should be used rather than the differential formalism presented above. We use the zeroth and first moments of the quantity W over the cross sectional area, A, that is,

$$\langle W \rangle = A^{-1} \int_A W \, dA \tag{5.3.18}$$

and

$$\bar{W} = \langle\alpha\rangle^{-1} A^{-1} \int_A \alpha W \, dA \quad . \tag{5.3.19}$$

Introducing the distribution parameter, C_o,

$$C_o \equiv \frac{\langle\alpha j\rangle}{\langle\alpha\rangle\langle j\rangle} \quad , \tag{5.3.20}$$

we obtain

$$\frac{\partial\langle\alpha\rangle}{\partial t} + \left(C_o V_{fj} + \bar{V}_{gj} + \langle\alpha\rangle \frac{\partial \bar{V}_{gj}}{\partial\langle\alpha\rangle} + \frac{C_o \Delta\delta}{\delta_f} \int_{z_o}^{z} \frac{\langle\Gamma\rangle dz}{\delta_g}\right) \frac{d\langle\alpha\rangle}{dz}$$

$$= \left(1 - \frac{C_o \, \Delta\delta\langle\alpha\rangle}{\delta_f}\right) \frac{\langle\Gamma\rangle}{\delta_g} \quad , \tag{5.3.21}$$

where $\Delta\delta = \delta_f - \delta_g$, and z_o is the point at which vapour generation begins. Zuber has shown that C_o varies between 1.0 and 1.5 for developed flows and can be less than 1.0 for the subcooled boiling region. Also, both C_o and $\bar{V}_{gj}$ remain essentially constant for a given flow regime. Adequate experimental agreement has been found by Zuber provided the limiting assumptions of equilibrium and fully developed flow are not violated. Experimental correlation was necessary in order to evaluate the distribution parameters and places added restrictions on the general applicability of Zuber's model.

5.4 HANCOX'S MODEL

Hancox's work is based on the foregoing model of Zuber. There are two major distinctions in Hancox's model: (1) thermodynamic

equilibrium and fully developed flow are not assumed; and (2) the relative velocities of the two phases is set to zero. The first distinction is a necessary upgrading of the past work, allows the extension to subcooled flow and permits the effect of undeveloped flow profiles to be taken into account empirically. The second distinction is a step backwards and was taken in order to permit a more tractable system of equations. This is an undesirable approximation but in practice most situations are at a high enough velocity for the effects of this assumption to be small. Also, the distribution parameters were still obtained by experimental correlation, rather than by independent experimental analysis. The equations of Hancox, then, are similar to those previously presented except that now the vapour generating function, Γ, requires the addition of constitutive relationships.

Based on postulated physical events, Hancox et al found that the position of significant void formation, z_o^+, occurred at

$$z_o^+ = 1 - \frac{0.624\,(Re)^{0.338}}{z_1'} \quad , \tag{5.4.1}$$

where

R_e = Reynolds number = $\delta_f \nu_i D_e/\mu_f$ [dimensionless] ,

ν_i = inlet velocity [cm/s] ,

D_e = equivalent diameter [cm] ,

μ_f = liquid viscosity [gm/cm s] ,

z_1 = $\dot{m}\,\Delta E_1/\dot{q}''\,\xi_h$ [cm] ,

ΔE_i = inlet subcooling [cal/gm] ,

$\dot{m}$ = mass flux [gm/s] ,

and

$\dot{q}''$ = heat flux [cal/cm^2 s] .

The subscripts, + and ', are defined by:

+ ≡ dimensionless w.r.t. z_1;

and

' ≡ dimensionless w.r.t. D_e.

The heat transfer coefficient was found to be

$$h_o = 0.40 \frac{k_f}{D_e} (Re)^{0.662} Pr^{1/3} , \qquad (5.4.2)$$

where k_f = liquid thermal conductivity [cal/cm^2 s °K]

and

Pr = liquid Prandtl number [dimensionless] .

It was further postulated that the vapour generation led to a vapour layer growth at saturation temperature. Describing this by conservation of mass and energy leads to

$$\langle \Gamma \rangle = \Gamma_m [1 - (1-\alpha)^{1/2} E^*/E_o^*] , \quad E^* \leq E_o^* ,$$

$$= 0 \qquad\qquad E^* > E_o^* , \qquad (5.4.3)$$

where

$E_o^* \equiv c_p \dot{q}_\omega''/h_o \Delta E$ [dimensionless] ,

$\Gamma_m \equiv 4 \dot{q}_\omega''/D_e \Delta E$ [gm/cm^3 s] ,

$c_p \equiv$ liquid specific heat [cal/gm °K] ,

$E^* \equiv (E_\ell - \langle E_f \rangle)/\Delta E$ [dimensionless] ,

$\Delta E \equiv E_v - E_\ell$ [cal/gm] ,

$E_f \equiv$ liquid enthalpy [cal/gm] ,

$E_\ell \equiv$ saturated liquid enthalpy [cal/gm] ,

$E_v \equiv$ saturated vapour enthalpy [cal/gm]

and

$\dot{q}''_\omega \equiv$ wall heat flux [cal/cm^2 s] .

Inherent in this formulation are the many assumptions required by the empirical analogies used.

By assuming that the vapour is at saturation and that the drift velocity is zero, equations (5.3.15) and (5.3.14) are transformed into

$$\frac{\partial \langle\alpha\rangle}{\partial t} + U_\alpha \frac{\partial \langle\alpha\rangle}{\partial z} = N_\alpha \qquad (5.4.4)$$

and

$$\frac{\partial E^*}{\partial t} + U_E \frac{\partial E^*}{\partial z} = N_E \ , \qquad (5.4.5)$$

where

$$U_\alpha = \left[C_o + \frac{\partial C_o}{\partial \langle\alpha\rangle} \langle\alpha\rangle\right] \langle v \rangle \ , \qquad (5.4.6)$$

$$N_\alpha = \left[1 - C_o \langle\alpha\rangle \Delta\delta/\delta_f\right] \frac{\langle\Gamma\rangle}{\delta_g} \ , \qquad (5.4.7)$$

$$U_E = \frac{C_2(1-C_o \langle\alpha\rangle) \langle v \rangle}{C_1 \langle 1-\alpha \rangle} \qquad (5.4.8)$$

and

$$N_E = \frac{-\Gamma_m - (1+E^*)\langle\Gamma\rangle}{C_1\,\delta_f\,\langle 1-\alpha\rangle} + \left[\left(\frac{C_2}{C_1} - 1\right)(1 - C_o\,\langle\alpha\rangle)\,\Delta\delta/\delta_g + \frac{1 - C_1}{C_1}\right]\frac{\langle E_f\rangle\langle\Gamma\rangle}{\delta_f\,\Delta E\,\langle 1-\alpha\rangle}$$

$$+ \left[\frac{U_E}{C_2}\,\frac{\partial C_2}{\partial\langle\alpha\rangle} + \left(\frac{C_2}{C_1} - 1\right)\frac{U_\alpha}{\langle 1-\alpha\rangle}\right]\frac{\langle E_f\rangle}{\delta_f\Delta E}\,\frac{\partial\langle\alpha\rangle}{\partial z} \quad . \qquad (5.4.9)$$

The above expressions employ the definitions,

$$C_1 \equiv \frac{\langle(1-\alpha)E_f\rangle}{\langle 1-\alpha\rangle\langle E_f\rangle}$$

and

$$C_2 \equiv \frac{\langle(1-\alpha)\,v_f E_f\rangle}{\langle(1-\alpha)\,v_f\rangle\langle E_f\rangle} \quad .$$

The lack of experimental data on enthalpy distributions dictate that these two parameters be set to unity, as would be the case if the value of either $(1-\alpha)\,v_f$ or E_f was independent of radial position. Empirical correlation gives the functional form of C_o as

$$C_o = \frac{1-\exp(-C_{o1}\alpha)}{1-\exp(-C_{o1})}\,(1 + C_{o2}) - C_{02}\,\alpha \quad , \qquad (5.4.10)$$

where

$$C_{o1} = 19 \quad ,$$

$$C_{02} = 1.164 - 1.14 \times 10^{-3}\,P + 0.357 \times 10^{-6}\,P^2$$

and

$P \equiv$ pressure [psia] .

Some discrepencies in model-experiment comparisons arose and it appears that geometry is the cause. This indicates that one should exercise care when extrapolating the model beyond the range of present

experiments. Hancox's model includes the momentum equation, analogous to that of appendix 9, with constitutive relationships for wall stress, velocity profiles, etc., to provide the pressure drop of the channel. He also considers two forms of pressure boundary conditions: open ended and fixed pressure drop. The fixed pressure drop condition dictates the simultaneous solution of the momentum equation with the mass and energy equations on an iterative basis. With the open ended pressure condition, the momentum equation becomes uncoupled and a march procedure is applicable since the equations become parabolic. The fixed pressure drop is realistic of reactor systems and can lead to sustained flow oscillations of significant magnitude. For this reason, the consideration of this system is important and is presently being investigated on many fronts as summarized by reference (72). But, for the steady state models of interest to this dissertation, the open ended pressure drop boundary condition is sufficient.

5.5 MODEL COMPARISON

We are now in a position to test the models derived in the previous sections. Maintaining the same channel conditions as in the comparison of the simple void model, figure 5.2 shows the predictions of the models. We note that it is necessary to use Hancox's model for good data fitting. The difference between Hancox's model in the homogeneous approximation and the above simple model is due to the better void generation model used by Hancox. The difference between the data and Zuber's model can be attributed to the assumptions of

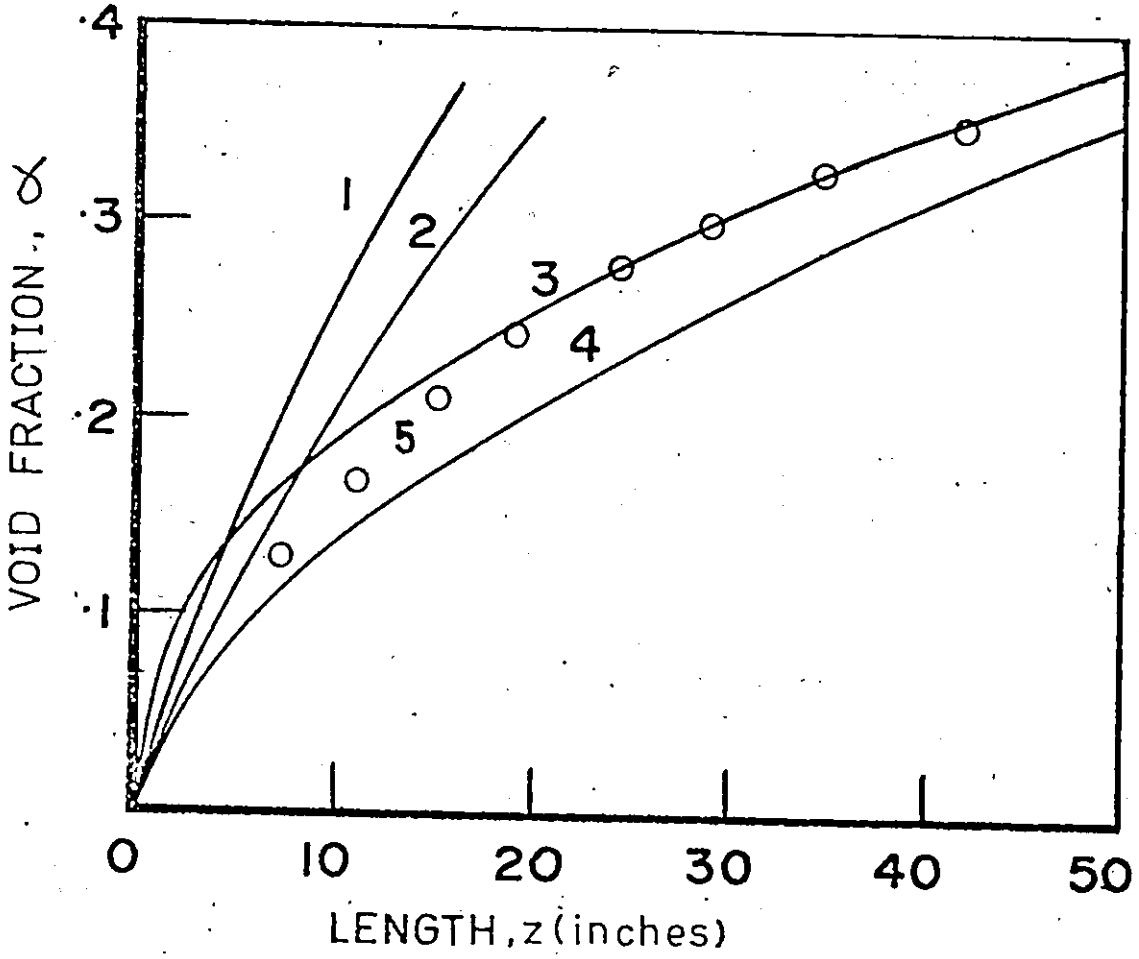

FIGURE 5.2: Comparison of void fraction, α, as a function of heated channel length, z, as predicted by: 1 - Hancox's model in the homogeneous approximation; 2 - simple model; 3 - Hancox's model; 4 - Zuber's model; 5 - experimental data.

thermal equilibrium and fully developed flow made by Zuber. As Hancox shows, his model is sufficient to adequately represent the boiling process in channel flow for a wide range of parameters. We conclude that Hancox's model adequately represents the fluid boiling, based on the experimental data available to date.

Although the best available model has been identified it is important to realize the rather severe limitations when applying it to boiling-light-water nuclear reactors. The experimental data used by Hancox et al and Zuber et al is restricted to simple geometric channel cross sections and channel lengths less than 1.5 meters. The geometric cross sections are, in reality, not simple and lengths are of the order of several meters. No void fraction measurements of in-core coolant channels have been made for the CANDU-BLW and, hence, the predictions of the void models will be taken with some reservation.

The directions for improvements on these models are clear. First, the distribution parameters must be correlated to the flow regime. Second, the best features of both models should be brought together by removing the zero slip assumption in Hancox's model. This will be necessary especially for such regimes as annular flow. Alternatively Zuber's model could be extended by employing constitutive relationships to arrive at the same end. These two areas are being investigated by Younis (15) at present. Thirdly, extension of the experiments to that of typical nuclear reactors is necessary as noted above and in the following section.

5.6 EFFECT OF ERRORS IN HANCOX'S VOID MODEL

We now investigate the effect of parametric error on the predictions of Hancox's void model in order to provide direction for future research. The input parameters of the void model are given in table 5.2. The associated errors given are approximate errors, assigned as reasonable. The void fraction errors as introduced by these error perturbations are given by table 5.3. In addition, the sensitivity of the predicted void fraction to variations in the parameter C_o and the subparameters C_{o1} and C_{o2} of equation (5.4.10) are shown. We see that the errors caused by the input parameters are not important compared to the inherent errors in the model itself, which could easily lead to errors in the nominal void fraction of more than 10% as estimated from previously published experimental-theoretical comparisons (13,14).

As was the case for the neutron model, in which the parameter ε_{nf} encompassed the shortcomings of the model, the void model contains the distribution parameter, C_o, to which the system is sensitive. This parameter can be estimated consistently to within small error bounds by experimental correlation, but conversely, a small error in C_o leads to significant errors in void fraction predictions. Consequently, the model should not be used beyond the range of the experimental data. This indicates some directions for future invesitgations. First, the implicit dependences inherent in the formulation of C_o should be removed to reduce the systems sensitivity to the experimental correlation errors in C_o. Second, the range of experimental data should be extended to the actual conditions of boiling-light-water reactors in order to

PARAMETER	VALUE
HEATED PERIMETER	1.335 m ± 1/2%
WETTED PERIMETER	1.665 m ± 1/2%
FLOW AREA	30.674 cm^2 ± 1/2%
PRESSURE	6.39 MN/m^2 ± 5%
SUBCOOLING	12° C ± 5%
FLOW RATE	4140 Kgm/m^2 s ± 5%
CELL RADIUS	15.75 cm
BUNDLE RADIUS	6.37 cm
CORE HEIGHT	290 cm
AXIAL MESH	21
OUTLET QUALITY	90%

Table 5.2 Parameters for sensitivity analysis.

PERTURBED PARAMETER	VOID FRACTION RESPONSE (%) AS A FUNCTION OF DIMENSIONLESS AXIAL POSITION, z*				
	z* = .2	z* = .4	z* = .6	z* = .8	z* = 1.0
FLOW AREA (+0.5%)	-0.25%	-0.097%	-0.053%	-0.038%	-0.034%
HEATED PERIMETER (+0.5%)	+0.31%	+0.11%	+0.058%	+0.041%	+0.037%
WETTED PERIMETER (+0.5%)	-0.05%	-0.004%	-0.001%	0	0
PRESSURE (+5%)	-0.92%	-0.22%	+0.01%	+0.078%	+0.093%
SUBCOOLING (+5%)	-1.8%	-0.19%	-0.052%	-0.025%	-0.021%
FLOW RATE (+5%)	-4.0%	-1.2%	-0.64%	-0.45%	-0.041%
C_{o1} (+5%)	+0.06%	+0.005%	+0.001%	+0.001%	0
C_{o2} (+5%)	+1.05%	+0.46%	+0.17%	+0.054%	+0.023%
C_o (+5%)	5.7%	7.0%	7.6%	7.8%	7.8%
NOMINAL VOID FRACTION AT Z*	0.46475	0.82804	0.94407	0.98346	.99290

Table 5.3 Effect of parameter perturbation on void fraction prediction.

evaluate the model error more accurately and to provide insight into future model formulation.

To appreciate the effect of the void model errors on the total system, a simulation run was carried out in which the void fraction, as predicted by Hancox's model, was reduced everywhere by 5%. This perturbation on the nominal case of 90% outlet quality inserted 10 mk negative reactivity into the system. It is important, then, to be able to predict the void fraction by better than 1% if an accurate knowledge of the system behaviour is to be determined. As we shall show in chapter 6, the average void fraction is of prime importance, but also, the axial distribution of the void fraction can have a considerable effect on reactivity and power distribution, affecting both the steady state case and the transient case.

5.7 NUMERICAL SOLUTION OF THE DIFFERENTIAL EQUATIONS

The mass, momentum and energy equations as developed by Zuber (11,12) and by Hancox (13,14) are non-linear, first order differential equations in the steady state. Since only the inlet conditions are specified, the numerical solutions to these parabolic equations are easily obtained compared to the neutron equations. The computer code, see appendix 10, as developed by Hancox, solves the one-dimensional equations by fourth order Runge-Kutta numerical integration (37). Computation time was small compared to that for the neutron equations and hence, no development work was necessary.

By numerical experimentation, it was found that less than 1%

error in void fraction determination could be obtained with 21 axial mesh points. Further refinements are not necessary since, at 21 mesh points points, the errors due to finite differencing are much less than those due to parametric and modelling errors. Furthermore, 21 mesh points are more than sufficient to describe the axial void distribution for use in the neutron model since, at most, 11 axial mesh points are used for the neutron model due to simulation cost considerations.

CHAPTER 6

COMBINED MODEL - INTERACTION EFFECTS

6.0 INTRODUCTION

Having defined the best available models for the system in the previous chapters as the two-group neutron diffusion approximation and Hancox's void model, the next step is to combine the models to determine the effect of void distributions on reactivity and the effect of neutron flux distributions on void distributions. This will enable a more realistic experimental design by indicating problem areas and will also provide the theoretical predictions for future comparisons with experiments.

The next three sections are devoted to the direct effect of various given void distributions while the remaining section discusses the steady state perturbed neutron flux and void distributions due to the interaction between power and coolant voiding.

6.1 EFFECT OF UNIFORM VOID DISTURBANCES

As discussed in chapter 4, criticality in a nuclear reactor system can be maintained after a reactivity disturbance by the adjustment of a material or geometric parameter. In section 4.1, the axial buckling, $(\pi/H)^2$, a geometric parameter, was used to maintain criticality in simulating the air-injection experiments since this was the method used in the experiments. This allows the models to be compared directly to the experimental results. An alternative method is to adjust the

multiplication constant or reactivity, as in section 4.3. This simulates the action of control rods, the method of control for conventional nuclear reactors. In this manner, a direct comparison can be made between the reactivity inserted and the prompt critical limitation of approximately 7 mk.

The analytical two-group model of section 4.1 is used herein to find the value of the gain, g, necessary to maintain criticality as the void fraction is varied from 0.0 to 1.0. The system parameters are as given previously by LATREP and are implicit functions of the void fraction. The buckling is held fixed at 1.17 m^{-2}, the critical value for $\alpha = 0.0$. The critical value of g, a function of α, gives the reactivity insertion necessary to counteract that due to voiding via

$$\rho(\alpha) = \frac{\epsilon\eta f p\big|_{\alpha} - \epsilon\eta f p\big|_{\alpha} \cdot g(\alpha)}{\epsilon\eta f p\big|_{\alpha}} \quad . \qquad (6.1.1)$$

The reactivity insertion due to voiding is, then, from equation (6.1.1),

$$\rho(\alpha) = 1 - g(\alpha) \quad , \qquad (6.1.2)$$

and is given by figure 6.1. We notice that the reactivity insertions due to changes in the average void fraction can exceed the prompt critical limitation.

Figures 6.2 and 6.3 show the radial flux distributions with the characteristic flux flattening under voiding conditions due to increased diffusion lengths. The axial distributions need not be given since they remain unchanged at the fundamental mode for uniform voiding.

The effects of $\bar{\alpha}$ variations represent the first order effects of

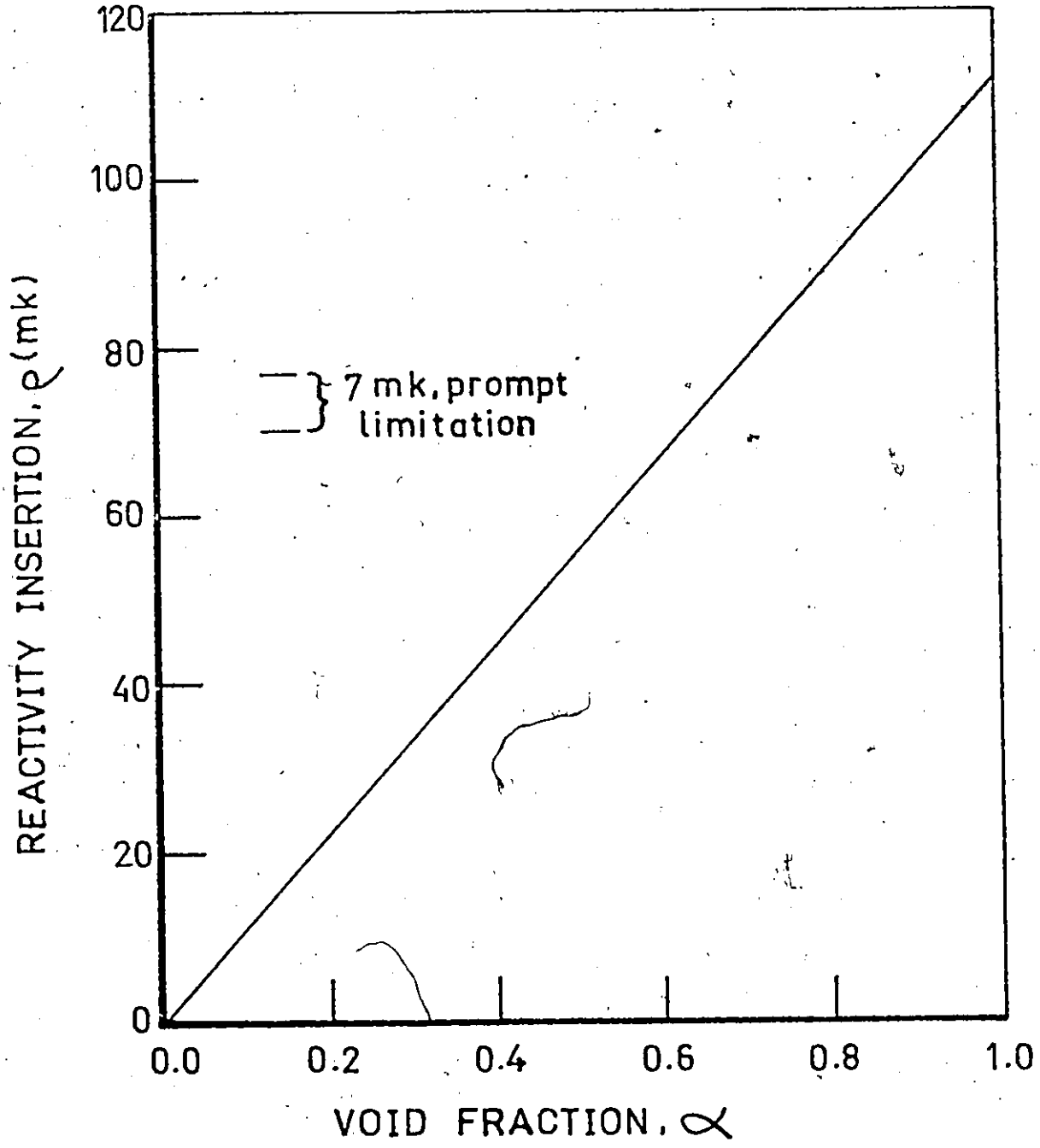

FIGURE 6.1: Reactivity insertion due to uniform voiding.

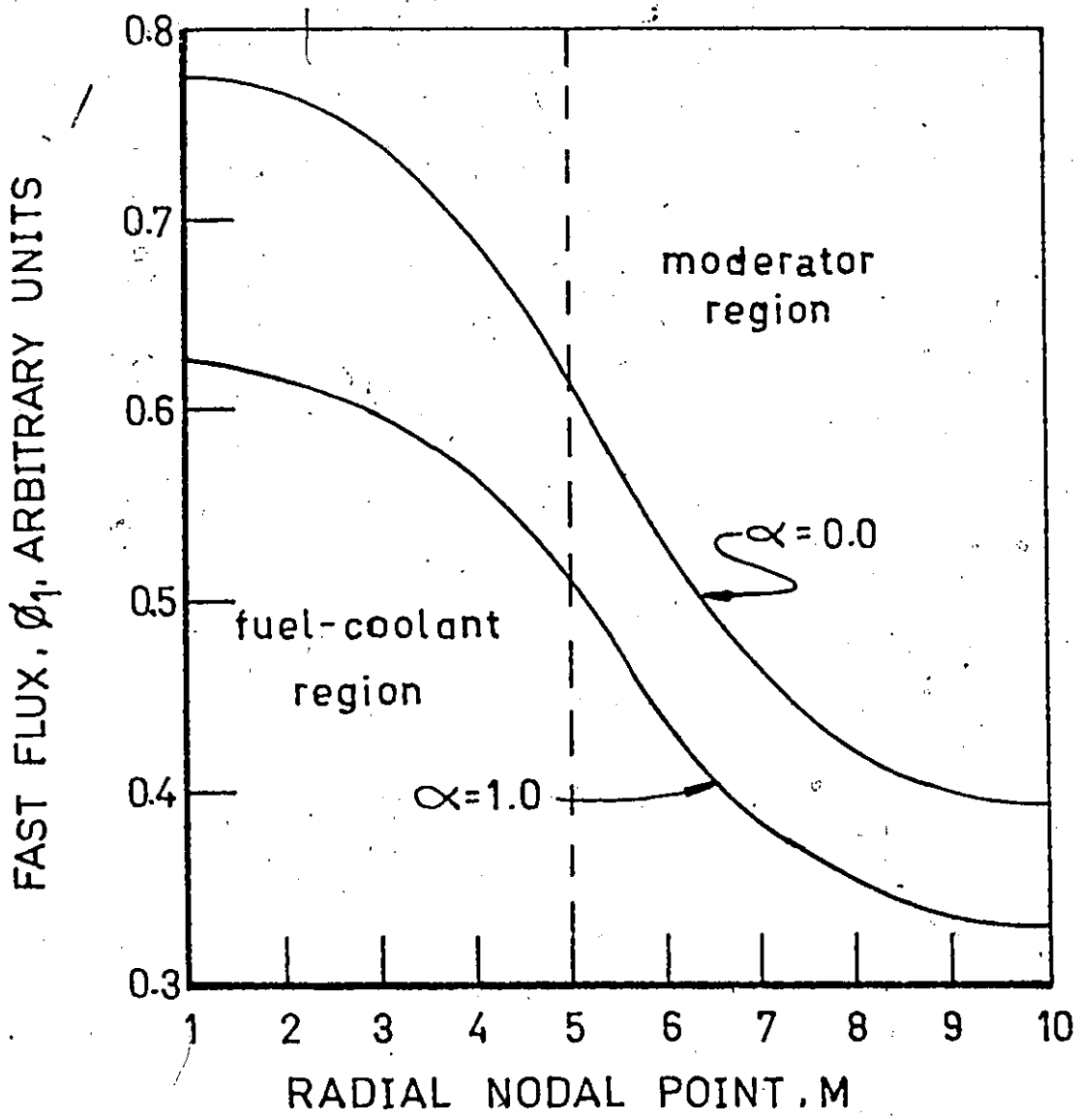

FIGURE 6.2: Radial fast flux distribution at zero and full voiding.

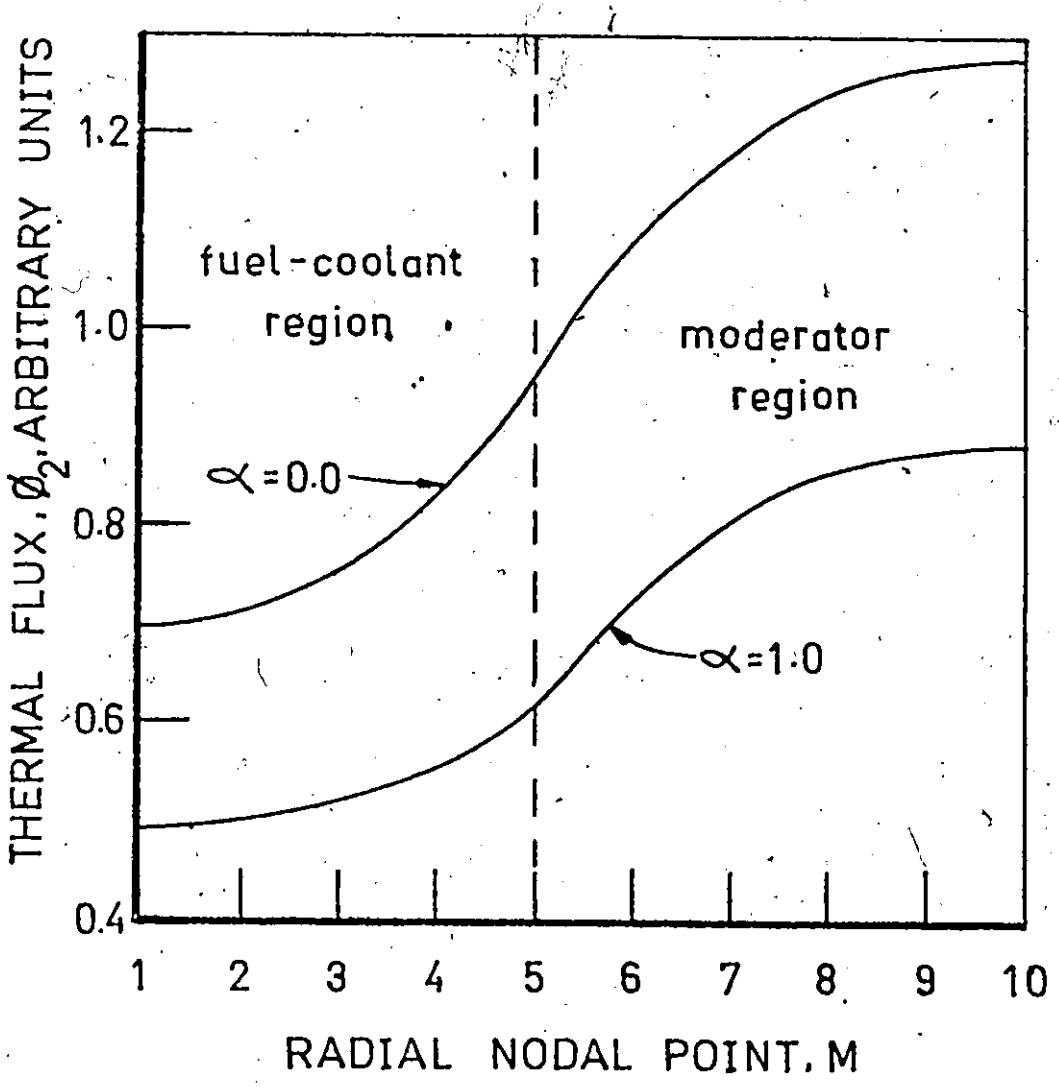

FIGURE 6.3: Radial thermal flux distribution at zero and full voiding.

coolant voiding. Second order effects due to spatially non-uniform voiding are given in the subsequent sections.

6.2 EFFECT OF RADIAL VOID DISTRIBUTIONS

As we have indicated, the present void models are not capable of giving the radial void distribution for the fuel bundle flow of our system. We must resort, then, to using radial void distributions considered reasonable for this system. Considering the fuel-coolant homogenization necessary in the neutron model, there is no need to postulate the detailed sub-channel void distributions. Rather, it suffices to describe the overall radial trend. Since inter-subchannel mixing is a vigorous process in forced convective flow in bundle geometry, we might expect this effect to dampen out any radial void variations. The main cause of any gross radial void distribution would be the radial power distribution, proportional to the thermal flux distribution. Since the thermal flux is depressed in the fuel region and rises as the radius is increased, one would expect the void distribution to follow the thermal flux distribution. The thermal flux varies no more than 50% across the fuel-coolant region, less as the void fraction increases. This plus the inter-subchannel mixing suggest only a modest variation in the gross characteristics of the radial void distribution. To evaluate the magnitude of the reactivity insertions due to radial void distributions, two extremes were taken. The first case studied was for a central void ($o \leq r < a/2$), where a = radius of fuel-coolant region, surrounded by an annulus of a non-voided coolant ($a/2 < r \leq a$) with $\alpha = .5$ at $r = a/2$.

The simulation was undertaken to calculate the critical values of g for this case and for the case of uniform voiding with the same average void fraction. As before, the difference in the critical values of g gives the reactivity perturbation introduced. The second case studied was with the void in the outer annulus of the coolant region, representing the mirror image of the first case.

Table 6.1 shows the perturbation due to the radial void distributions and figures 6.4 and 6.5 show the perturbation in the corresponding radial flux distributions. As in section 6.1, the axial flux is not perturbed. Considering the magnitude of the perturbation, very little effect is seen. We thus conclude that radial void distributions have little direct effect on flux distributions and reactivity and that one can simulate the void-reactivity effect using a flat radial void distribution with little error provided the local average radial void is correct.

This does not mean, however, that we can subsequently ignore the radial void distribution. This prediction should be verified by experiments. Further, the radial void distribution is conceivably quite important in determining the void generation in a voiding channel and consequently will affect the average void fractions. Subchannel experiments are needed to give some insight into this effect.

For the purposes of the numerical simulations of the neutron model, it is tempting to conclude from the above discussions that the system becomes one-dimensional in the axial direction and that the radial dimension need not be treated numerically when uniform radial voiding suffices. A two-dimensional model is still required because the void

RADIAL DISTRIBUTION	GAIN, g	
	CASE 1 CENTRAL VOID	CASE 2 ANNULUS VOID
$\alpha \neq \alpha(r)$	0.9385	0.8842
$\alpha = \alpha(r)$	0.9366	0.8785
Δg	0.0019 ($\sim$2mk)	0.0057 ($\sim$6mk)

Table 6.1 Reactivity insertions caused by radial void distributions.

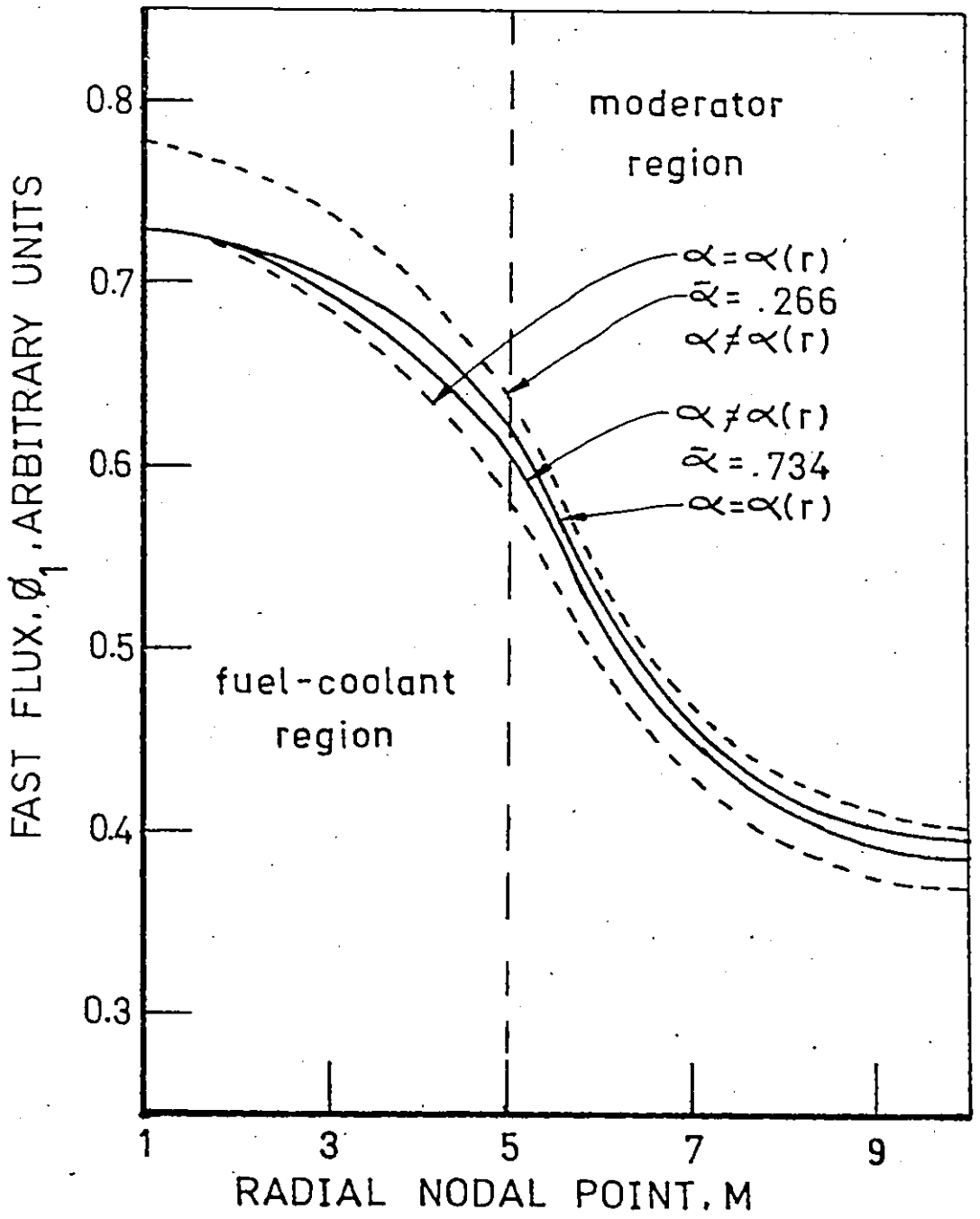

Figure 6.4 Fast flux vs. radial position, effect of radial void distributions.

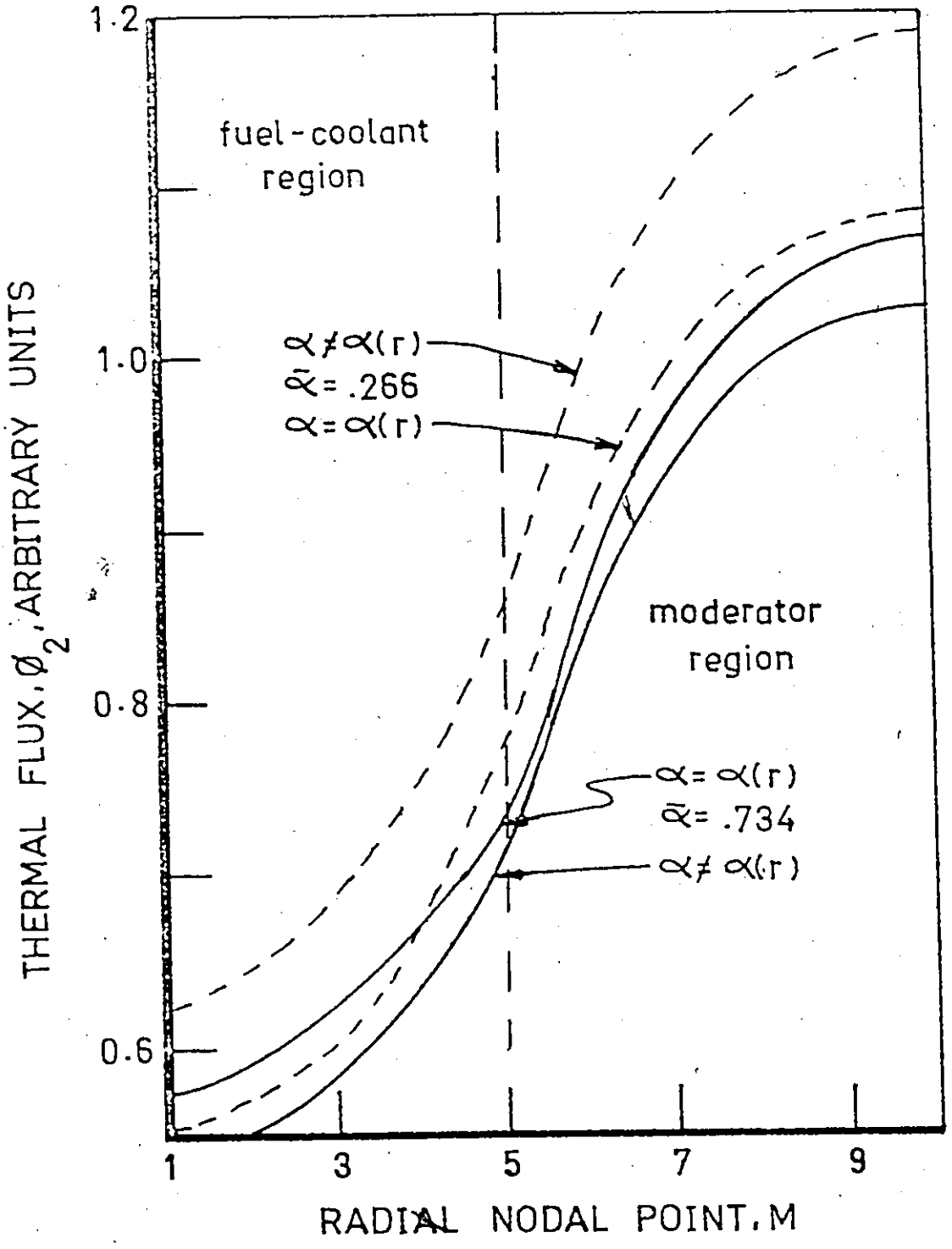

FIGURE 6.5: Thermal flux vs. radial position, effect of radial void distributions.

fraction remains a function of axial position, z, causing the radial flux distributions to change as a function of axial position. The mismatches which would occur at the axially discretized region boundaries. of a one-dimensional numerical approach prevents the adoption of such a scheme.

6.3 EFFECT OF AXIAL VOID DISTRIBUTIONS

To investigate the effect of axial voiding, three distributions, all having the same average void fraction, were used. The full range of average void fraction was covered. First, for reference purposes, a uniform void was introduced and the simulation was run to steady state noting the steady state value of g, the reactivity parameter. Second, a step change in the axial void distribution was introduced and third, the void distribution as predicted by Hancox's model was used. In each case the average void fraction was the same. Figure 6.6 shows the typical profiles used. This was repeated for various average void fractions to obtain figure 6.7. Plotted, as a function of average void fraction, is the difference in the criticality gain parameter,

$$\Delta g \equiv \left(g\Big|_{\text{void profile 1}} - g\Big|_{\text{void profile i}}\right), \qquad (6.3.1)$$

giving the reactivity insertion due to the change in axial void profile from the flat profile.

For the step profile, negligible reactivity insertion occurs. For this particular void profile, the change in reactivity induced by the upper half of the cell cancels the change in reactivity induced by

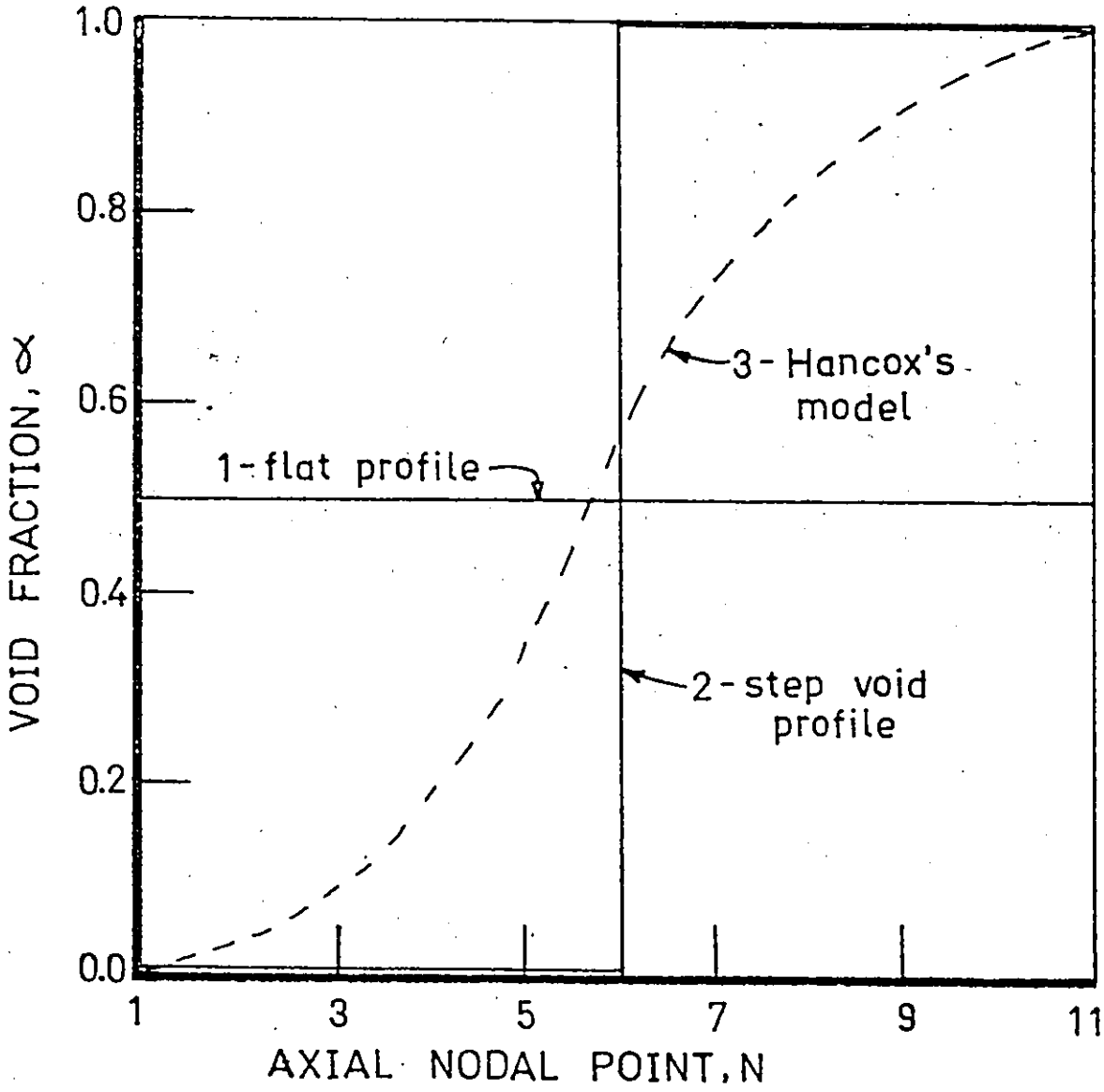

Figure 6.6 Axial void distributions used to determine the effect on reactivity insertions.

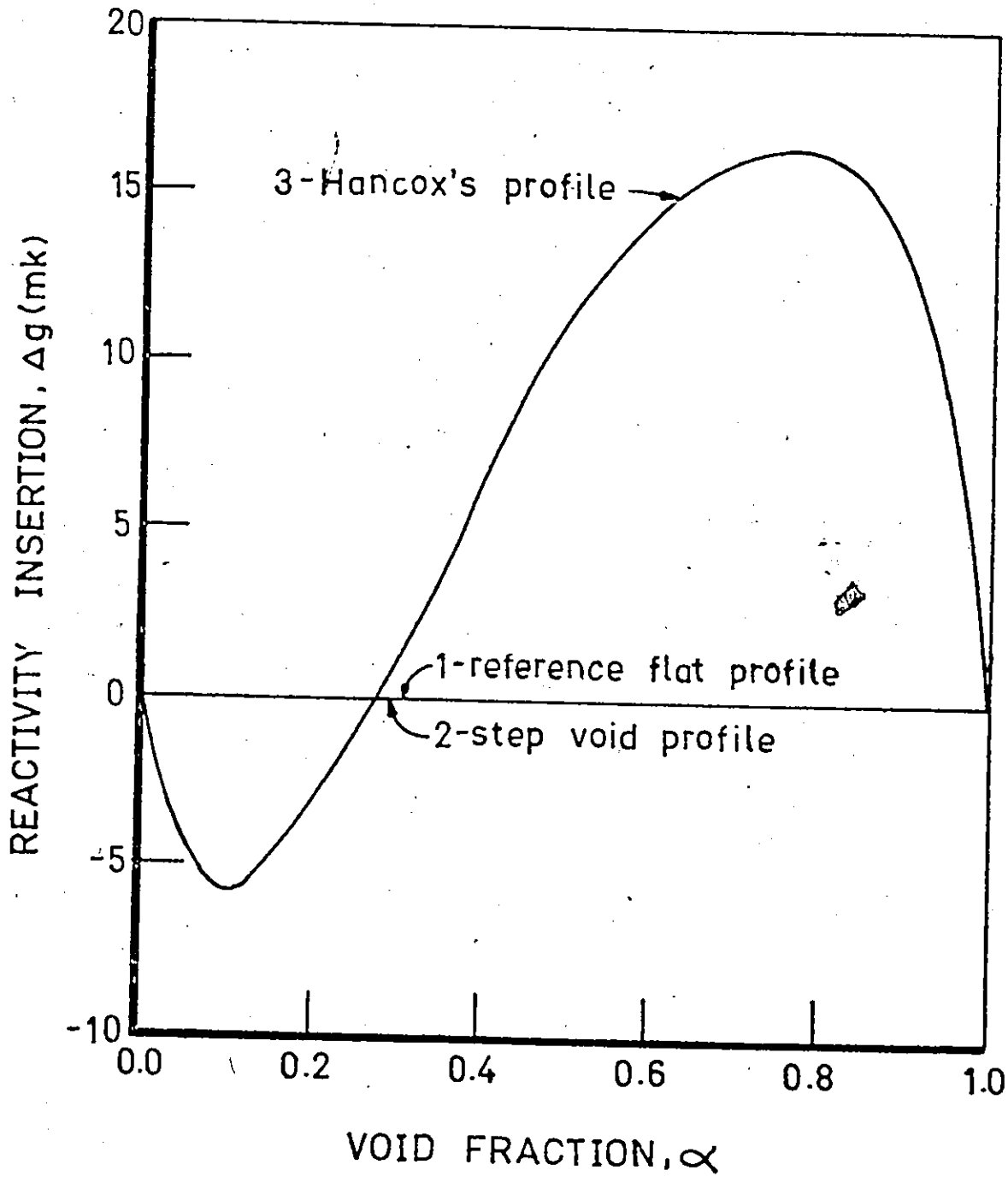

Figure 6.7 Reactivity insertions at various void fractions due to axially non-uniform voiding.

the lower half. Using the void profile predicted by Hancox's model we see inherently different results. For low voiding, negative reactivity feedback is introduced, whereas, for high-void fractions, positive feedback is introduced when changing from a uniform distribution to the non-uniform distribution. The important conclusion to be drawn is that the effect of the axial void distribution should be considered in the design of the nuclear reactor, consequently reducing the need for post-startup control systems. Considering the errors inherent in the present parametric data, one might expect difficulty in designing a stable reactor. However, subsequent modelling, based on more reliable parametric data would provide the tools needed to complete such a design.

In general, the design criteria for minimizing the feedback due to system fluctuations would be

$$\min_{\underline{\beta}_i} \sum_i \omega_i \sigma_i (\underline{\beta}) \frac{\partial \rho(\underline{\beta})}{\partial \beta_i} , \qquad (6.3.2)$$

where ρ, the reactivity, is a function of all the parameters, β_i, in the set, $\underline{\beta}$. The coefficient, σ_i, is the standard deviation of the parameter, β_i, and in general may be a function of the operating condition, $\underline{\beta}$. The coefficient, ω_i, is the weighting factor assigned to each effect and would, presumably, by unity unless emphasis on a selection of effects were required. As the function, $\rho(\underline{\beta})$, cannot be written explicitly for the models presented here, recourse to numerical optimization will have to be taken when the design is attempted.

We have shown here the danger of not including the effect of non-uniform void distributions. In terms of the criticality condition

a typical axial void distribution is significantly different from that of a uniformly voided system and reactivity differences greater than prompt critical can result. In addition, the criticality condition is sensitive to the details of the void distribution.

It has been pointed out (73) that the general practice in reactor design is to account for non-uniform voiding by using perturbation theory (28). In brief, perturbation theory assumes the neutron flux is not altered and calculates the reactivity insertion due to perturbations in the system parameters. The total perturbation introduced into the system is, then, made up of a direct perturbation due to the change in system parameters and an indirect perturbation due to the subsequent flux distribution changes. The non-linear model of chapter 4 gives the total effect, whereas perturbation theory accounts for the direct effect only.

It can easily be shown (28) that the direct component of the perturbation caused by system parameter perturbations is given by

$$\Delta g = \left\{ \int\int\int_V (\delta D_1 \nabla\phi_1 \cdot \nabla\psi_1 + \delta\Sigma_1 \phi_1 \psi_1 - g\delta(\epsilon\eta f \Sigma_2) \right.$$

$$\left. - \delta(p\Sigma_1) \phi_1 \psi_2 + \delta D_2 \nabla\phi_2 \nabla\psi_1 + \delta\Sigma_2 \phi_2 \psi_1) dV \right\} \Big/$$

$$\int\int\int_V \epsilon\eta f \Sigma_2 \phi_2 \psi_1 \, dV \quad . \qquad (6.3.3)$$

The total reactor cell volume is denoted by V and δD, $\delta\Sigma$, etc. are the perturbations introduced into the parameters by their implicit dependence

on the void fraction. The terms of the integrations are, in general, functions of r and z.

The neutron fluxes, ϕ_1 and ϕ_2, can be calculated from the criticality equation for the unperturbed system at uniform void,

$$\underline{A}\ \underline{\phi} = \underline{0}\ , \tag{6.3.4}$$

as in chapter 4. For our two-group model, equation (6.3.2) for the fuel-coolant region becomes

$$\begin{bmatrix} \nabla \cdot D_1\nabla - \Sigma_1 & \text{genf}\ \Sigma_2 \\ p\Sigma_1 & \nabla \cdot D_2\nabla - \Sigma_2 \end{bmatrix} \begin{bmatrix} \phi_1 \\ \phi_2 \end{bmatrix} = 0\ . \tag{6.3.5}$$

The parameters, Σ_1, Σ_2, D_1, D_2, genf and p are constant within the fuel-coolant region, but the diffusion terms, the coupling of equation (6.3.5) to the moderator region and the boundary conditions give spatially dependent fluxes, ϕ_1 and ϕ_2. For the moderator region, equation (6.3.5) applies if we re-evaluate the parameters for the moderator as in chapter 4. The adjoint fluxes, ψ_1 and ψ_2 are given by

$$\underline{A}^T\ \underline{\psi} = 0\ , \tag{6.3.6}$$

or, for our model,

$$\begin{bmatrix} \nabla \cdot D_1\nabla - \Sigma_1 & p\ \Sigma_1 \\ \text{genf}\ \Sigma_2 & \nabla \cdot D_2\nabla - \Sigma_2 \end{bmatrix} \begin{bmatrix} \psi_1 \\ \psi_2 \end{bmatrix} = 0\ . \tag{6.3.7}$$

The solution to equation (6.3.7) is entirely analogous to equation (6.3.5).

Using the parametric values of section 4.1.6 given by the code, LATREP, we find the value of g necessary to give criticality under a given uniform void condition. Associated with the criticality conditions are the neutron fluxes, ϕ_1 and ϕ_2, and the adjoint fluxes, ψ_1 and ψ_2.

We are now in a position to impose the perturbation; $\bar{\alpha}$ is changed to $\alpha(z)$. The new parameters, functions of axial position since $\alpha = \alpha(z)$, can be obtained from the LATREP results. The perturbations, δD_1, $\delta \Sigma_1$, etc. are given by the differences of the new and old parameters. Equation (6.3.3) can now be integrated numerically to give Δg, the perturbation in the criticality parameter necessary to compensate for the direct component of the perturbation. We see, from equation (6.3.3), that the magnitude of the perturbation is weighted by the fluxes. Hence, a local perturbation, say $\delta \Sigma_1$, at one position within the reactor system will not necessarily cancel an opposing perturbation, $-\delta \Sigma_1$, at another spatial position unless the flux weightings are also equal. This has given rise to an alternate name for the adjoint flux, ψ: the importance function. Thus, although the average void fraction remains unchanged, a reactivity perturbation will result if the net effect of a void redistribution is to move voids into regions of higher or lower flux.

Application of equation (6.3.3) to the step void profile gives negligible reactivity difference from the flat profile of equal $\bar{\alpha}$. This arises naturally from the above discussion. The axial flux variation is symmetric about the axial midpoint. Hence the redistribution of α, where

void is uniformly removed from the lower half and is uniformly placed in the upper half, results in the same flux weighting. This, coupled with the linear void fraction-ρ relationship of figure 6.1, gives zero reactivity insertion.

However, for the more realistic profile, given by figure 6.6, considerable reactivity insertion results, as shown by the dashed line of figure 6.8. Using the total perturbation as given by figure 6.7, we find the indirect component, shown by the dotted area of figure 6.8. This is the amount which would have been neglected if the standard practice, using perturbation theory, had been employed. We see that the error is important since it is of the order of the prompt critical limitation ($\sim$7mk). It is clear, then, that full account of the effect of voiding on reactivity must be given if a proper design is to be established.

6.4 AXIAL FLUX AND VOID DISTRIBUTIONS

As an illustration of the magnitude of the flux and void perturbations due to non-uniform axial voiding, figures 6.9 to 6.12 show the redistribution of flux starting from nominal operating conditions of uniform void fraction (α = .7) and then introducing a void distribution as given by Hancox's model (maintaining $\bar{\alpha}$ = .7). Figure 6.13 shows the void distribution for the initial power distribution. The subsequent perturbed void distribution due to perturbations in the power, remains essentially unchanged from the initial distribution. Similar results were obtained for the full range of $\bar{\alpha}$. There exists, then, a one-way sensitivity between the neutron flux model and the void model. The flux model is sensitive to the axial void distribution, but the void model is insensitive to the details of the flux distribution. This insensitivity arises because of the effect of two

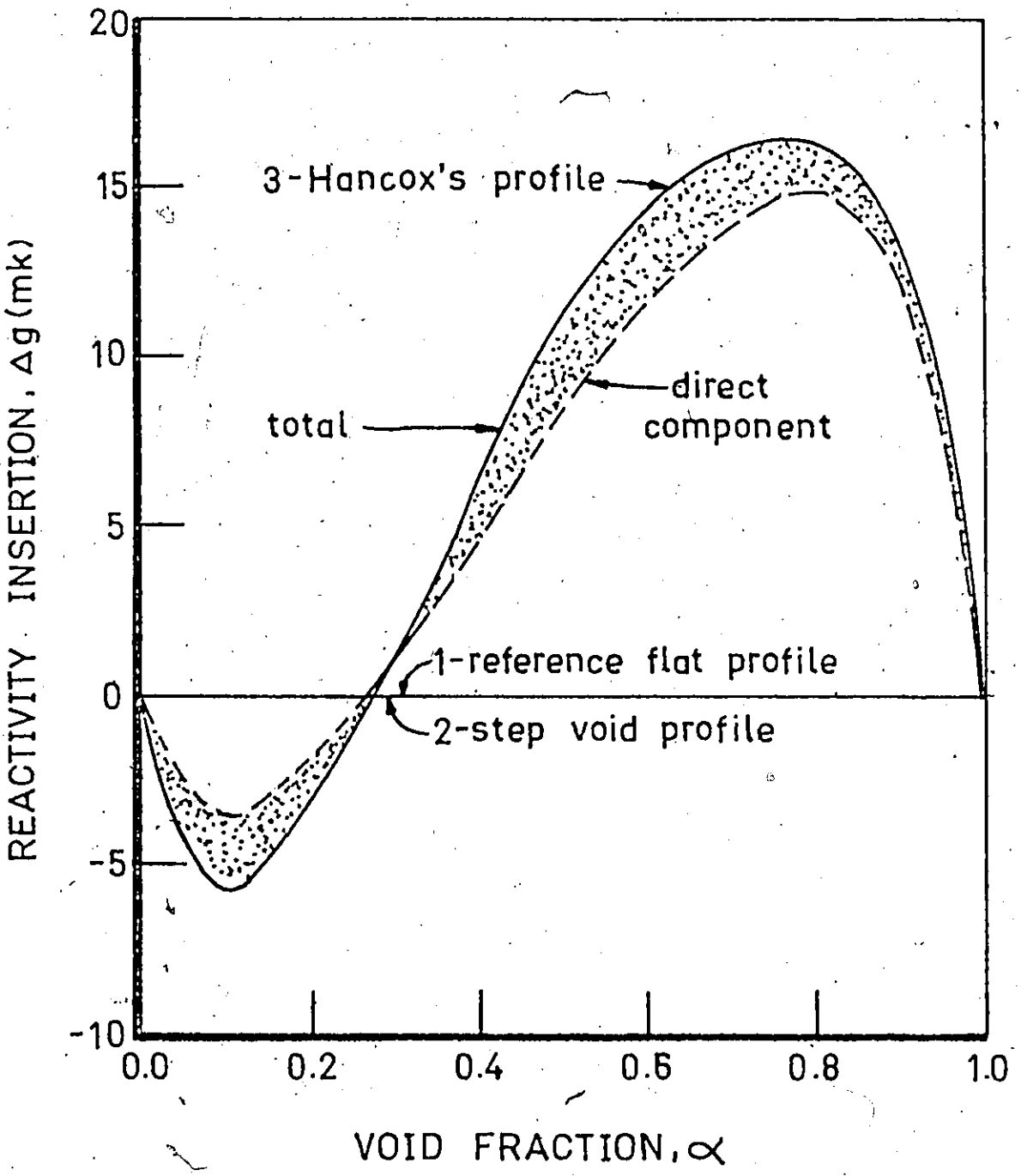

FIGURE 6.8: Reactivity insertions at various void fractions due to axially non-uniform voiding showing the direct and indirect components.

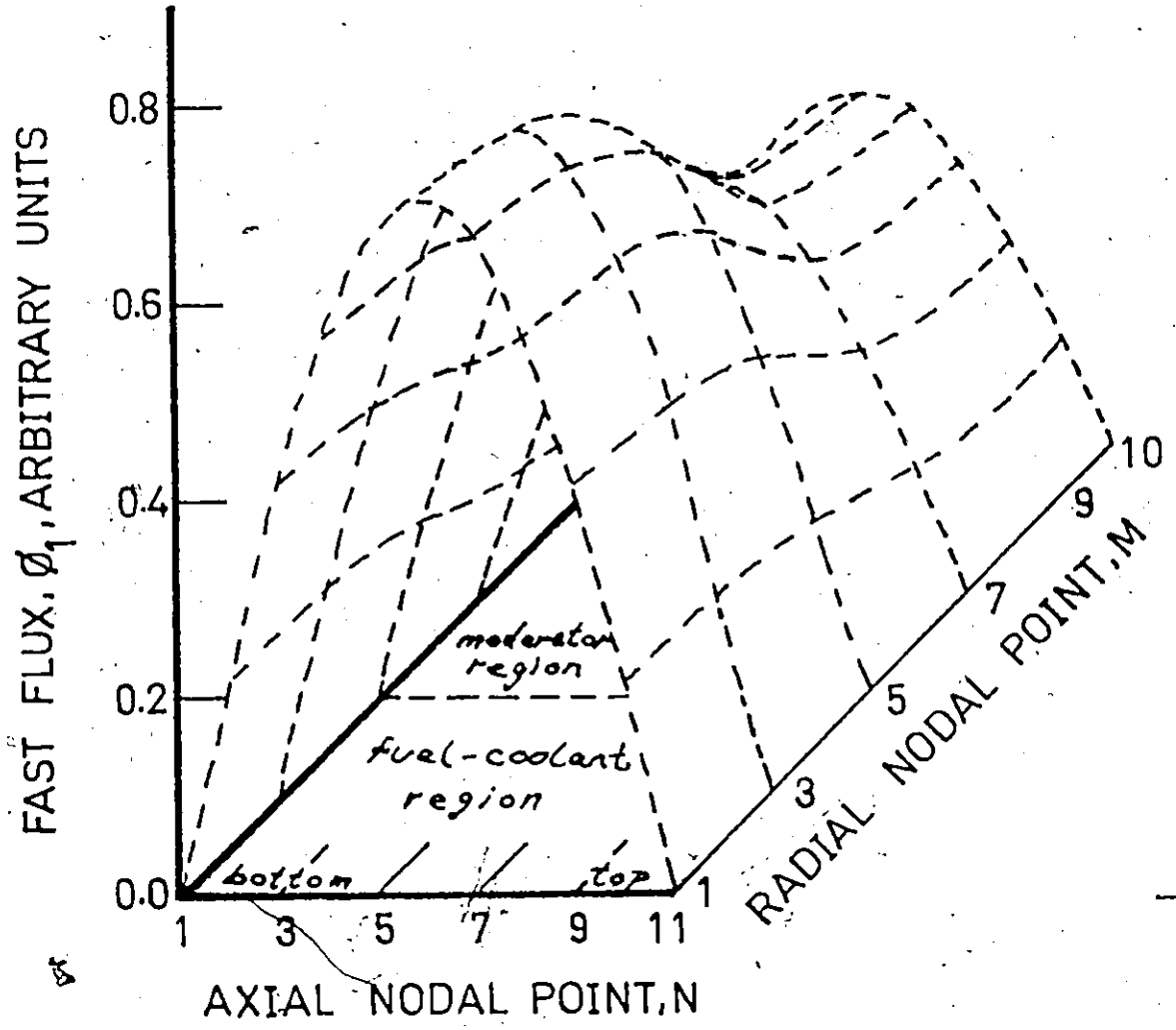

FIGURE 6.9: Nominal fast flux distribution for $\tilde{\alpha}$ = 0.7 (uniform)

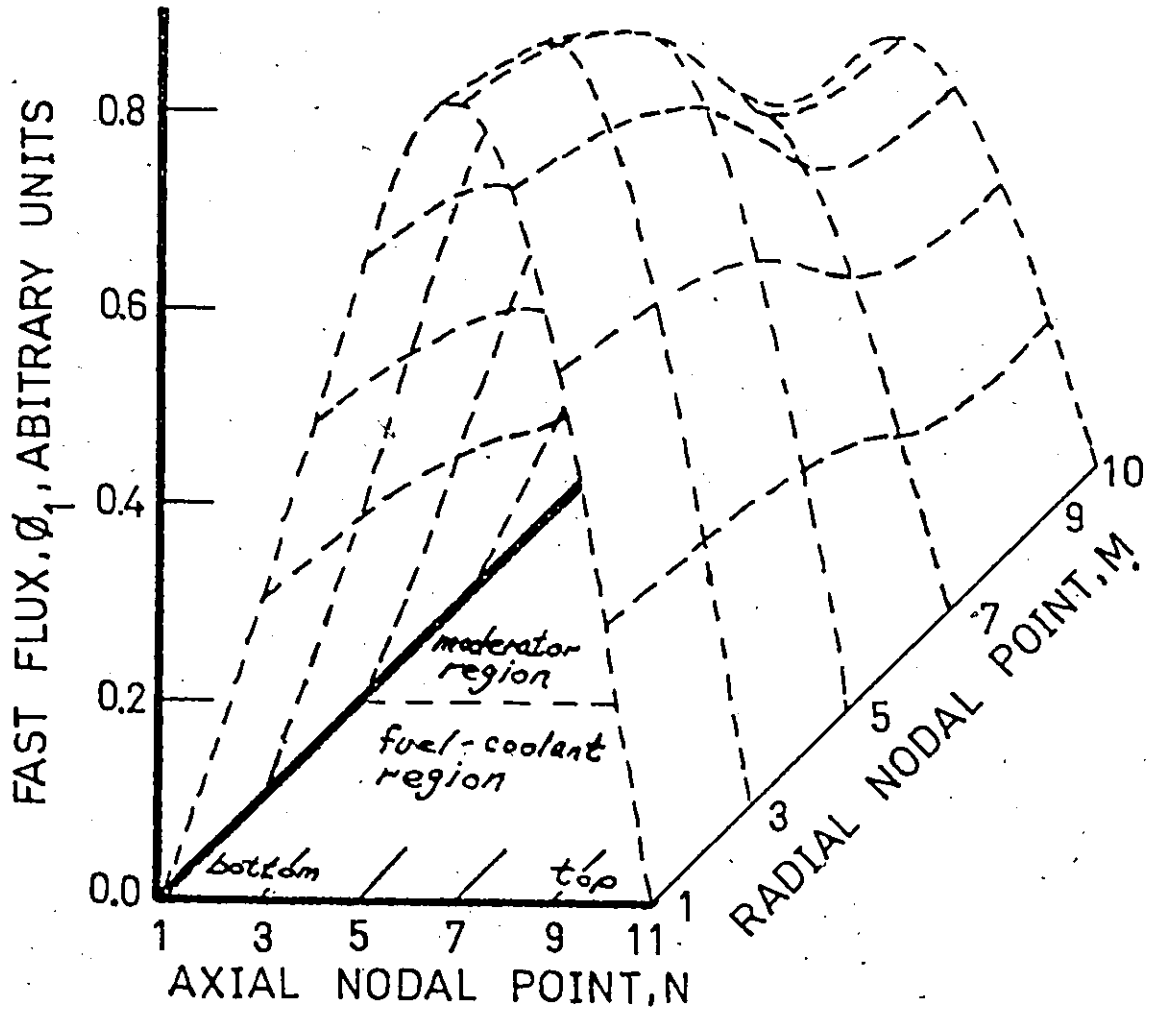

FIGURE 6.10: Perturbed fast flux distribution for $\bar{\alpha}$ = 0.7 (non-uniform).

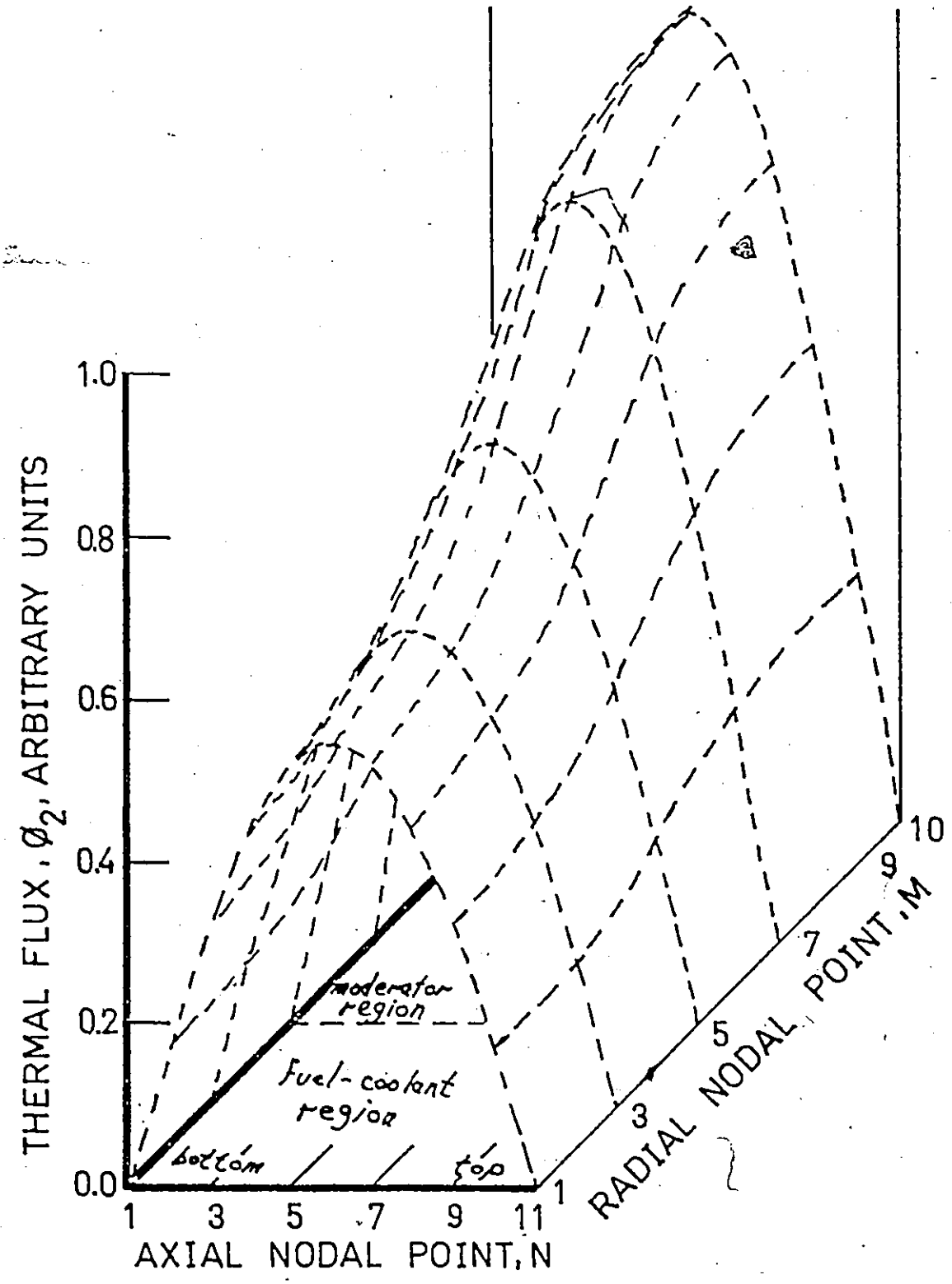

FIGURE 6.11: Nominal thermal flux distribution for $\bar{\alpha}$ = 0.7 (uniform).

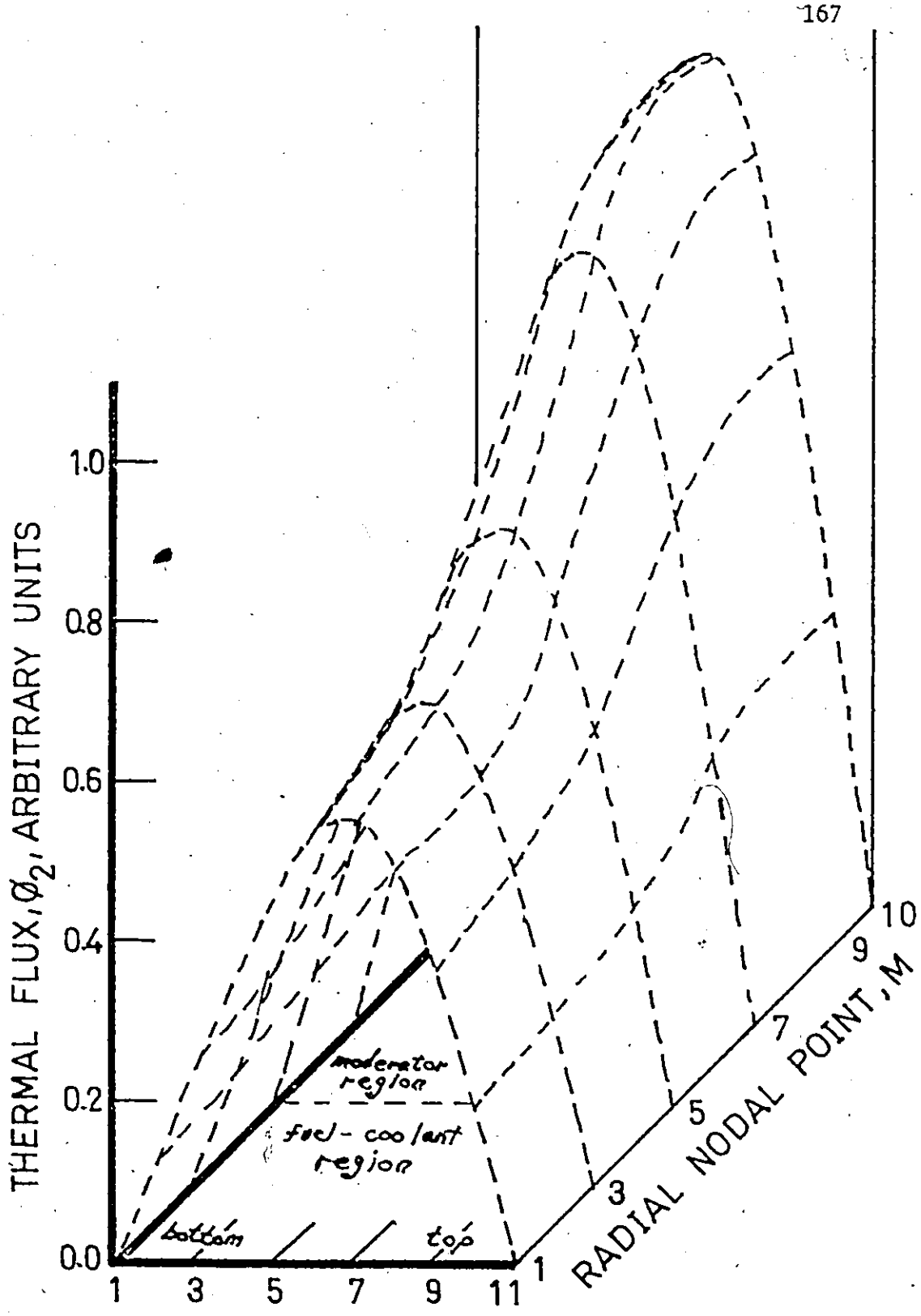

FIGURE 6.12: Perturbed thermal flux distribution for $\bar{\alpha}$ = 0.7 (non-uniform).

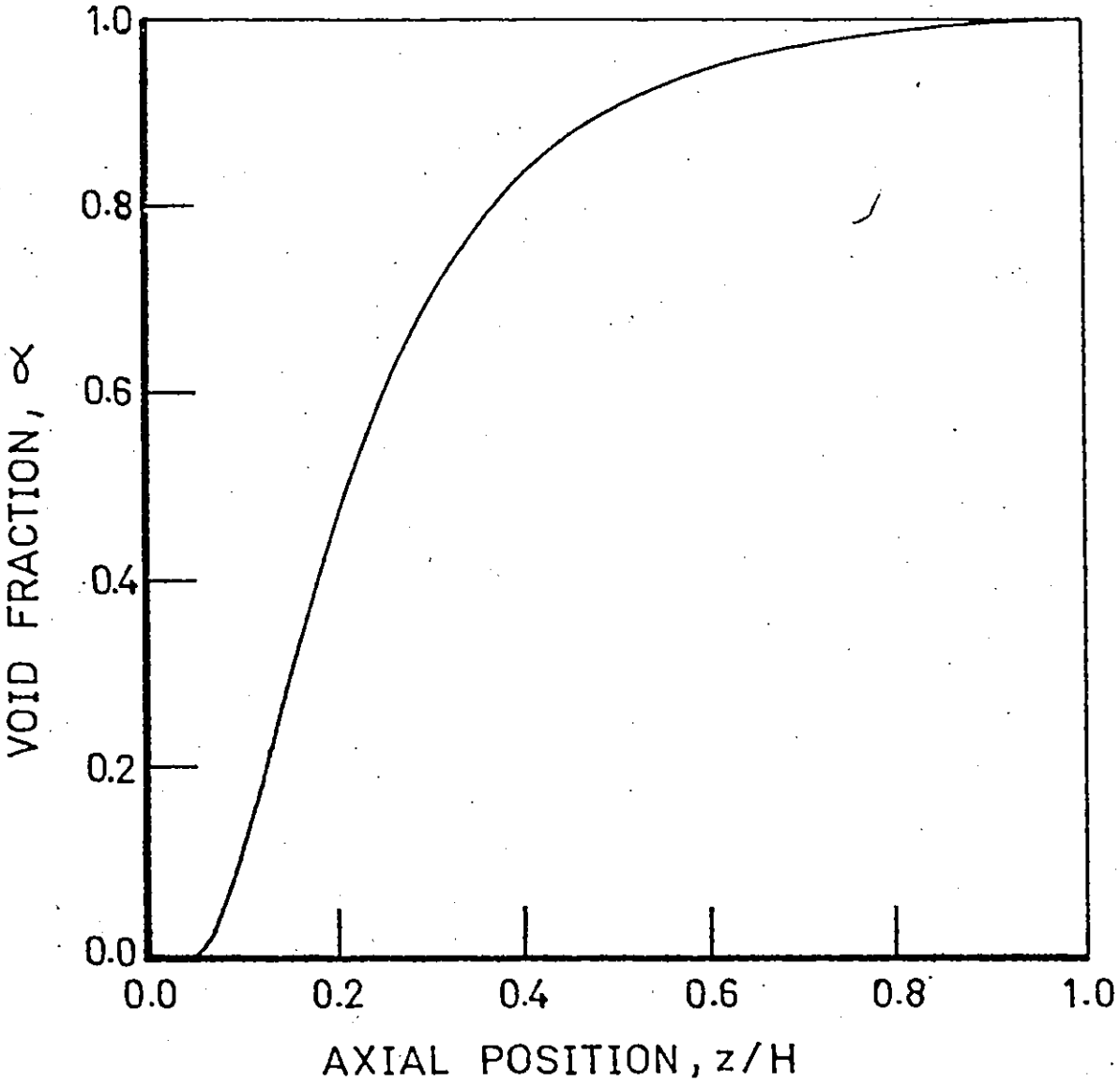

FIGURE 6.13: Void fraction vs. axial position; nominal distribution at $\bar{\alpha}$ = 0.7 (outlet qualtiy ≈ 90%).

compensating events. When the void fraction is increased the neutron flux distribution is radially flattened since the neutrons can diffuse more readily, that is, D is increased. In the case of overmoderated systems, as considered herein, reactivity is also inserted. Hence, for a void distribution as given by figure 6.13, the upper regions of the reactor experience a radial flux flattening and an axial flux peak due to the reactivity insertion in comparison to the case of uniform voiding. The integrated cross sectional power produced, proportional to the thermal flux, at a given axial position in the upper region, is, then, increased by the axial flux peaking and decreased by the radial flattening. The opposite effect happens at the lower end of the reactor where the void fraction is lower than average. The radially integrated thermal flux, for the cases of uniform and non-uniform voiding, is shown by figure 6.14. The near equality of the power generation for the two cases manifests itself in the one-way sensitivity effect.

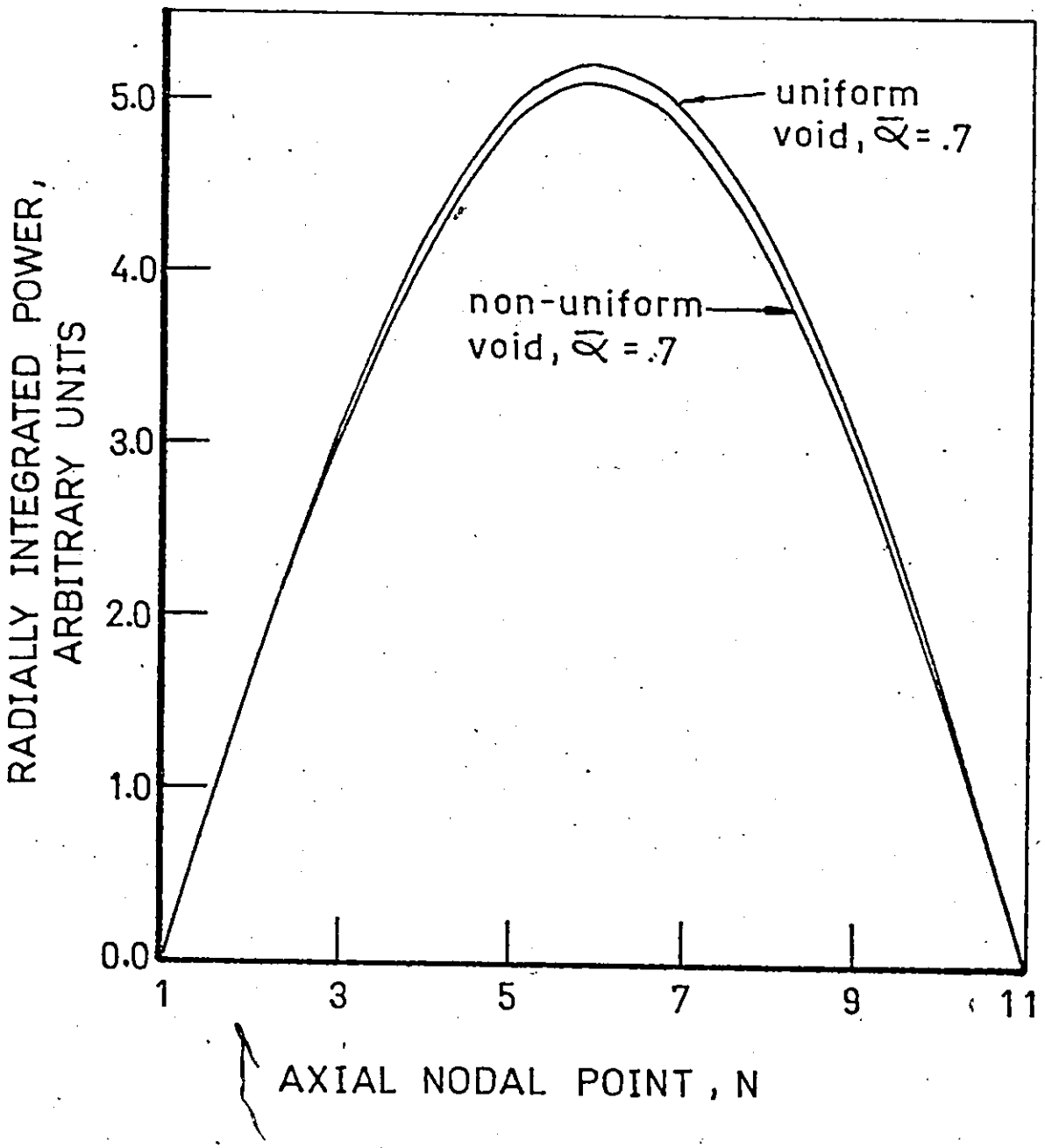

FIGURE 6.14: Radially integrated power, proportional to the thermal flux, vs. axial position for uniform and non-uniform voiding.

CHAPTER 7

CONCLUSIONS

DISCUSSION

To summarize, the developments as presented herein are discussed with the initial objective in mind: to present and evaluate models of the boiling-water nuclear reactor system in order to provide insight for future simulation studies and experimental design.

Based on the present experimental evidence, it was found that, for the neutron model, at least a two-group, two-region, two-dimensional model is necessary. For the fluid model, extension of the present models, proposed by Zuber and Hancox, is necessary to realistically simulate the boiling channel under reactor conditions. The principle uncertainties have been identified as the parameters, ϵ_{nf} and C_o. These, then, define the direction of experimental studies. It has also been found that the escape probability, p, is not as important as previous investigators considered it to be if the resonance phenomenon is correctly accounted for by a two-region cell. Finally, while discussing the individual models, it was found that numerical simulations of the neutron model are feasible and yield meaningful results. Numerical control presents no problem because of the long time constant for the diffusion process.

Coupling the two models has shown that perturbations introduced by void distributions, while considerably less important than that of

perturbations in the average void fraction, are sufficiently large to warrant consideration in reactor design. Errors in the predictions of reactivity insertions can approach the prompt critical limit when using the previously accepted perturbation technique. It was shown, also, that the radial void distribution is not likely to significantly affect the reactivity but, undoubtably, it is important in the determination of the axial void distribution and, consequently, is of sufficient concern to warrant experimental investigation. These studies have shown, too, that previous attempts(4-7) at coupled modelling are in error because of the lack of detail in either the neutron model or the fluid model or both. The most dominant characteristic of this work, then, is that it provides an investigation of the most comprehensive coupled model available in the open literature to date. It is only in this way that the shortcomings of the individual models used for determining the effect of coolant voiding on nuclear reactors can be ascertained.

Looking ahead to the future needs of transient analysis, a technique was developed to reduce the cost of extensive numerical simulations of nuclear kinetics. This technique, involving the use of an optimal temporal transformation of the neutron kinetics equations, is sufficiently general to constitute a significant development in the area of neutron space-time kinetics.

The problem areas of coolant void-reactivity effects have, then, been clearly delineated and several significant developments have been achieved.

CHAPTER 8

RECOMMENDATIONS

The previous chapters have foreshadowed the direction of future work. The most important shortcoming of the steady state models and experiments presented herein is their lack of independent parametric estimates. It is recommended that experiments, aimed at eliminating this shortcoming be carried out.

For the neutron model, an accurate independent estimate of $\epsilon\eta f$ is required. This could conceivably be carried out by extending the substitution experiments to partial channel substitutions in a manner analogous to small reactivity insertion techniques. This accurate estimate of $\epsilon\eta f$ will allow a rigorous testing of the applicability of the two-group model to the boiling-light-water reactor system.

For the fluid model, independent estimates of the parameter, C_o, and other distribution parameters are needed. The trend towards a complete phenomenological representation should continue on small scale prototypes and should be extended to include subchannel flow. This will enable a more reliable scale-up to the larger geometries of real CANDU-BLW's. This work should be complimented by full scale mockups whenever possible to guide the development of the fluid models. These mockups are hampered, however, mainly by cost and void detection capabilities. Bidirectional neutron diagnostics might provide the means of unfolding the void distributions of complex geometries.

The verification of the predictions of the coupled models is also recommended. By extending the air-injection experiments, as presented earlier, to non-uniform voiding, the reactivity and flux perturbations of non-uniform voiding can easily be measured.

Upon the successful completion of the steady state experiments suggested above, it is recommended that research take on a parallel development of transient analysis of single channels and steady state multichannel coupling. Both directions should encompass both the neutron flux modelling and fluid modelling as well as coupled modelling.

The introduction of an optimal transformation technique for the neutron kinetics equations has proven to be beneficial to the system investigated herein. It has been indicated that, when applied to systems of larger radial dimensions and to detailed transient analysis, even more gains can be realized. Thus, application of this technique, to the multichannel and transient investigations previously recommended, promises to be most beneficial. The utility of the technique might be extended by an investigation into global stability proofs for non-linear neutron space-time dynamics, which, to date, have eluded researchers.

The transformation technique offers additional gains when applied to multigroup analysis, which might be required for subsequent investigations when the neutron parametric uncertainties have been removed. The transformed multigroup neutron equations in matrix form are group-wise diagonal. Hence the order in which the energy (group) mesh is scanned, hitherto a problem in multigroup analysis, becomes unimportant. An additional unexplored area is the application of the transformation

technique to other systems which can be plagued by excessive computation times, such as the two-phase flow equations with a fixed pressure drop boundary condition.

The adoption of these recommendations will direct future research to those areas which will most significantly advance the knowledge of coolant-void effects in neutron multiplying media.

APPENDIX 1

DERIVATION OF THE BASIC NEUTRON EQUATIONS

A.1.1 THE GENERAL EQUATIONS

The general neutron transport equations (16,74) can be written as follows:

$$\frac{\partial n(\underline{r},E,\underline{\Omega},t)}{\partial t} = \int_{E'}\int_{\underline{\Omega}'} \nu(E')\, n(\underline{r},E',\underline{\Omega},t)\{\nu(\underline{r},E',\underline{\Omega}',t)$$

$$[1 - \beta(\underline{r},E',\underline{\Omega}',t)]\, \Sigma_f(\underline{r},E',\underline{\Omega}',t)\, \chi_p(\underline{r},E,\underline{\Omega},t)$$

$$+ \Sigma_s(\underline{r},E',\Omega',t)\, f_s(\underline{r};E',\underline{\Omega}' \rightarrow E,\underline{\Omega};t)\}\, d\underline{\Omega}'dE'$$

$$- v[n(\underline{r},E,\underline{\Omega},t)\ .\ \underline{v}(E)] + \sum_{i=1}^{N} \lambda_i\, \chi_i(E,\underline{\Omega})\, C_i(\underline{r},t)$$

$$+ s(\underline{r},E,\underline{\Omega},t) - [\Sigma_a(\underline{r},E,\underline{\Omega},t) + \Sigma_s(\underline{r},E,\underline{\Omega},t)]$$

$$v(E)\, n(\underline{r},E,\underline{\Omega},t) \qquad \text{(A1.1)}$$

and

$$\frac{\partial C_i(\underline{r},t)}{\partial t} = -\lambda_i\, C_i(\underline{r},t) + \int_{E'}\int_{\underline{\Omega}'} \beta_i(\underline{r},E',\underline{\Omega}'t)\, \nu(\underline{r},E',\underline{\Omega}',t)$$

$$\nu(E')\, \Sigma_f(\underline{r},E',\underline{\Omega}',t)\, n(\underline{r},E',\underline{\Omega}',t)\, d\underline{\Omega}'dE' \quad , \qquad \text{(A1.2)}$$

where

t = time [s] ,

E = energy [Mev] ,

$\underline{\Omega}$ = direction (vector) [radian] ,

$v(E)$ = velocity [cm/s] ,

$\underline{v}(E)$ = velocity (vector) = $v(E)\ \underline{\Omega}$ [cm/s] ,

$\underline{r}$ = space (vector) [cm] ,

$n(\underline{r},E,\underline{\Omega},t)$ = neutron density [neutrons/cm^3 radian Mev] ,

$\nu(\underline{r},E,\underline{\Omega},t)$ = total number of neutrons produced per fission in the fuel caused by a neutron of energy E and direction $\underline{\Omega}$ [dimensionless] ,

$\Sigma(\underline{r},E,\underline{\Omega},t)$ = macroscopic cross section [cm^{-1}] ,

$f_s(\underline{r};E',\underline{\Omega}' \rightarrow E,\underline{\Omega};t)$ = probability density function for a neutron at $(E',\underline{\Omega}')$ scattering to $(E,\underline{\Omega})$ [radian^{-1} Mev^{-1}] ,

$s(\underline{r},E,\underline{\Omega},t)$ = extraneous neutron sources [neutrons/cm^3 radian Mev s] ,

$C_i(\underline{r},t)$ = i^{th} delayed precursor concentration, $i = 1,2...N$ [number/cm^3] ,

λ_i = decay constant for i^{th} delayed precursor [s^{-1}] ,

β_i = fraction of total fission production from i^{th} delayed precursor [dimensionless] ,

$$\beta = \sum_{i=1}^{N} \beta_i \ ,$$

$\chi_p(\underline{r},E\ \underline{\Omega},t)$ = normalized fission spectrum [radian^{-1} Mev^{-1}] ,

$\chi_i(E,\underline{\Omega})$ = normalized spectrum for neutrons emitted by i^{th} delayed precursor [radian^{-1} Mev^{-1}] ,

with subscripts:

f = fission event,

s = elastic and inelastic scattering event,

a = absorption event.

Equation (A1.1) can be expressed in words as follows. The net rate of accumulation of neutrons, given by the left hand side of equation (A1.1), is composed of several sinks and sources. From left to right, the first term on the right hand side is the rate of gain in neutron population, at the space volume element about $(\underline{r},E,\underline{\Omega},t)$ from the element about $(\underline{r},E',\underline{\Omega}'t)$, by prompt fissioning and scattering. The second term represents the net rate of loss by neutron transport out of the volume element about $\underline{r}$. The third term is the delayed neutron source from the delayed precursors. The fourth is that due to extraneous sources, and the last is the rate of loss by absorption and scattering. The balance condition for the delayed precursors, equation (A1.2) is simpler in that there is no physical movement of the precursors and there is only one sink, radioactive decay, and one source, fission fragment production due to the fissioning process.

These equations hold in general except when there is material transport, as in a reactor disassembly or in aqueous solution reactors, or when the neutron population is so low as to have significant statistical fluctuations. These are rare cases, certainly not applicable for this study.

A1.2 SIMPLIFYING ASSUMPTIONS

A number of simplifying assumptions can be made to transform the general transport equations into a tractable formalism. We may set $s = 0$ since there are no extraneous sources in operating CANDU reactors. Also, for nuclear events below 2 Mev., typical of nuclear

reactors, the production, scattering and absorption events can be considered isotropic, that is, independent of direction. Thus,

$$\int_{\underline{\Omega}'} f(\underline{r};E',\underline{\Omega}' \rightarrow E,\underline{\Omega};t)\, d\underline{\Omega}' = f(\underline{r};E' \rightarrow E;t) \quad , \tag{A1.3}$$

$$\int_{\underline{\Omega}'} n(\underline{r},E',\underline{\Omega}',t)\, d\underline{\Omega}' = n(\underline{r},E',t) \quad , \tag{A1.4}$$

etc.

Hence,

$$\frac{\partial C_i(\underline{r},t)}{\partial t} = -\lambda_i C_i(\underline{r},t) + \int_{E'} \beta_i(\underline{r},E',t)\, \nu(\underline{r},E',t)\, v(E')$$

$$\Sigma_f(\underline{r},E',t)\, n(\underline{r},E',t)\, dE'$$

and

$$\frac{\partial n(\underline{r},E,t)}{\partial t} = \int_{E'} v(E')\, n(\underline{r},E't)\{\nu(\underline{r},E',t)[1 - \beta(\underline{r},E',t)]$$

$$\Sigma_f(\underline{r},E',t)\, \chi_p(\underline{r},E,t) + \Sigma_s(\underline{r},E',t)\, f_s(\underline{r};E' \rightarrow E;t)\}dE'$$

$$- \nabla[n(\underline{r},E,t)\, \underline{v}(E)] + \sum_{i=1}^{N} \lambda_i\, \chi_i(E)\, C_i(\underline{r},t)$$

$$- [\Sigma_a(\underline{r},E,t) + \Sigma_s(\underline{r},E,t)]\, v(E)\, n(\underline{r},E,t) \quad . \tag{A1.6}$$

Since the velocity vector is space independent

$$\nabla \cdot [n(\underline{r},E,t)\, \underline{v}(E)] = \nabla[n(\underline{r},E,t) \cdot \underline{v}(E)] \tag{A1.7}$$

and, by analogy to heat and mass diffusion,

$$\underline{n}(\underline{r},E,t)\,\underline{v}(E) = -D(\underline{r},E,t)\,\nabla[n(\underline{r},E,t)\,v(E)]$$

$$\equiv -D(\underline{r},E,t)\,\nabla\phi(\underline{r},E,t) \quad . \tag{A1.8}$$

Equation (A1.6) is, then,

$$\frac{\partial n(\underline{r},E,t)}{\partial t} = \int_{E'} v(E')\,n(\underline{r},E',t)\{\nu(\underline{r},E',t)[1-\beta(\underline{r},E',t)]$$

$$\Sigma_f(\underline{r},E',t)\,\chi_p(\underline{r},E,t) + \Sigma_s(\underline{r},E',t)\,f_s(\underline{r};E'\rightarrow E;t)\}dE'$$

$$+\nabla\cdot D(\underline{r},E,t)\,\nabla[n(\underline{r},E,t)\,v(E)] + \sum_{i=1}^{N}\lambda_i\,\chi_i(E)\,C_i(\underline{r},t)$$

$$-[\Sigma_a(\underline{r},E,t)+\Sigma_s(\underline{r},E,t)]\,v(E)\,n(\underline{r},E,t) \quad . \tag{A1.9}$$

The multigroup approximation is obtained by discretizing the energy continuum. Denoting the ℓ^{th} group by the subscript, ($\ell = 1,2,\ldots G$), and integrating equation (A1.9) over the energy interval, ΔE_ℓ, gives

$$\frac{\partial}{\partial t}\int_{\Delta E_\ell} n(\underline{r},E,t)dE = \int_{E'} v(E')\,n(\underline{r},E',t)\Big[\int_{\Delta E_\ell}\{\nu(\underline{r},E',t)$$

$$[1-\beta(\underline{r},E',t)]\,\Sigma_f(\underline{r},E',t)\,\chi_p(\underline{r},E,t)$$

$$+\Sigma_s(\underline{r},E',t)\,f_s(\underline{r};E'\rightarrow E;t)\}dE\Big]dE'$$

$$+\int_{\Delta E_\ell}\nabla\cdot D(\underline{r},E,t)\,\nabla[n(\underline{r},E,t)\,v(E)]dE$$

$$+\sum_{i=1}^{N}\lambda_i\,C_i(\underline{r},t)\int_{\Delta E_\ell}\chi_i(E)dE$$

$$-\int_{\Delta E_\ell}[\Sigma_a(\underline{r},E,t)+\Sigma_s(\underline{r},E,t)]\,v(E)\,n(\underline{r},E,t)dE \quad . \tag{A1.10}$$

We now introduce the following notation for conciseness and clarity:

$$\sum_{j=1}^{G} \int_{\Delta E_j} dE' \equiv \int_{E'} dE' \tag{A1.11}$$

and

$$T_\ell(\underline{r},\ldots) \equiv \int_{\Delta E_\ell} T(E,\underline{r},\ldots)dE \cdot , \tag{A1.12}$$

where T is a general function. Equation (A1.10) becomes

$$\frac{\partial n_\ell(\underline{r},t)}{\partial t} = \sum_{j=1}^{G} v_j \, n_j(\underline{r},t)\{\nu_j(\underline{r},t)[1 - \beta_j(\underline{r},t)] \, \Sigma_{fj}(\underline{r},t) \, \chi_{p\ell}(\underline{r},t)$$

$$+ \Sigma_{sj}(\underline{r},t) \, f_s(\underline{r};E_j \to E_\ell;t)\} + \nabla \cdot D_\ell(\underline{r},t) \, \nabla[n_\ell(\underline{r},t) \, v_\ell]$$

$$+ \sum_{i=1}^{N} \lambda_i \, C_i(\underline{r},t) \, \chi_{i\ell}$$

$$- [\Sigma_{a\ell}(\underline{r},t) + \Sigma_{s\ell}(\underline{r},t)] \, v_\ell \, n_\ell(\underline{r},t) \quad . \tag{A1.13}$$

The delayed precursor equation becomes, through a similar analysis,

$$\frac{\partial C_i(\underline{r},t)}{\partial t} = - \lambda_i \, C_i(\underline{r},t) + \sum_{j=1}^{G} \beta_{ij}(\underline{r},t) \, \nu_j(\underline{r},t) \, v_j \, \Sigma_{fj}(\underline{r},t)$$

$$n_j(\underline{r},t) \, . \tag{A1.14}$$

Since, for our study, we are interested in short time intervals compared to the time interval required for significant changes in the delayed precursor concentrations, we may write

$$\frac{\partial C_i(\underline{r},t)}{\partial t} = 0 \qquad \text{(A1.15)}$$

and hence

$$\lambda_i C_i(\underline{r},t) = \sum_{j=1}^{G} \beta_{ij}(\underline{r},t)\, \nu_j(\underline{r},t)\, \nu_j \Sigma_{fj}(\underline{r},t)\, n_j(\underline{r},t) \quad . \qquad \text{(A1.16)}$$

Equation (A1.13) now becomes

$$\frac{\partial n_\ell(\underline{r},t)}{\partial t} = \sum_{j=1}^{G} \nu_j\, n_j(\underline{r},t)\{\nu_j(\underline{r},t)\, \chi_{j\ell}(\underline{r},t)\, \Sigma_{fj}(\underline{r},t)$$

$$+ \Sigma_{sj}(\underline{r},t)\, f_s(\underline{r};E_j + E_\ell;t)\} + \nabla \cdot D_\ell(\underline{r},t)\, \nabla[n_\ell(\underline{r},t)\, \nu_\ell]$$

$$- [\Sigma_{a\ell}(\underline{r},t) + \Sigma_{s\ell}(\underline{r},t)]\, \nu_\ell\, n_\ell(\underline{r},t) \quad , \qquad \text{(A1.17)}$$

where

$$\chi_{j\ell}(\underline{r},t) \equiv [1 - \beta_j(\underline{r},t)]\, \chi_{p\ell}(\underline{r},t) + \sum_{i=1}^{N} \beta_{ij}(\underline{r},t)\, \chi_{i\ell} \quad . \qquad \text{(A1.18)}$$

Equation (A1.17) models the population density of neutrons in nuclear reactors. A typical energy spectrum, as given by figure A1.1, serves to guide the choice of energy groupings in the multigroup equations. The fission process gives a fission spectrum in the high energy range. A 1/E portion results from the moderation process and is perturbed by resonance absorption. Finally, a thermal (Maxwellian distribution) spectrum results from the attainment of equilibrium of the neutrons with the reactor media.

For practical computations a much used simplification of the multigroup equations is the two-group diffusion approximation with the

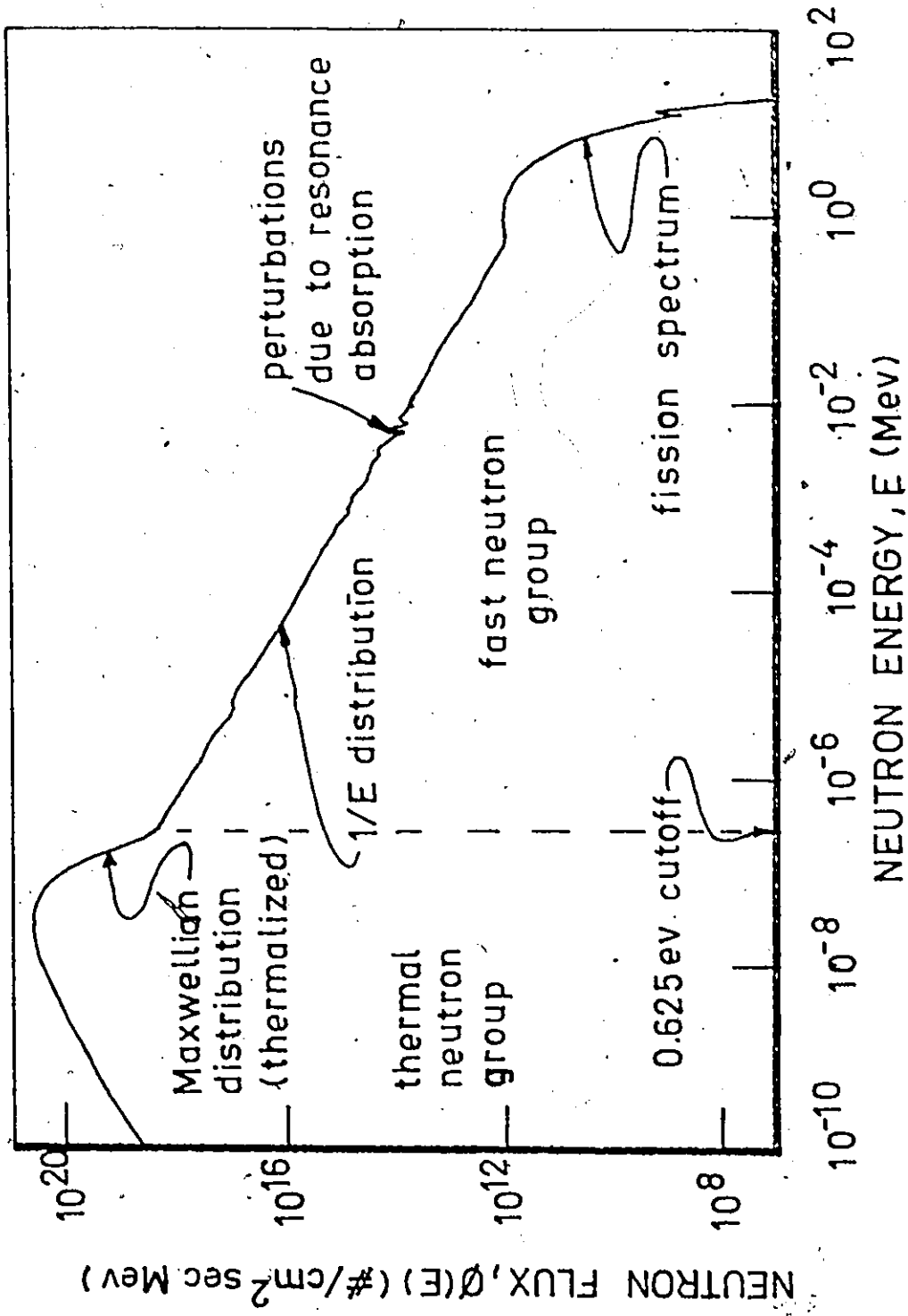

FIGURE A1.1: Typical energy spectrum for a nuclear reactor.

cutoff between groups chosen as 0.625 ev, separating the thermal portion from the epithermal and fast portions. This particular cutoff energy is experimentally convenient since, by using cadmium as a neutron filter, the relative intensities of the two neutron groups are easily measured.

A1.3 THE TWO-GROUP DIFFUSION APPROXIMATION

For the two-group diffusion approximation, ($\ell = 1,2$), we define:

$\ell = 1 \equiv$ fast group

and

$\ell = 2 \equiv$ thermal group.

The following assumptions are made:

(1) no fast fissioning: $\Sigma_{f1} = 0$;

(2) no upscatter: $f_s(E_2 \to E_1) = 0$;

(3) all fission neutrons are born in group 1: $\chi_{22} = 0$.

For convenience we drop the explicit notation of the space and time dependence and employ the above assumptions to find

$$\frac{\partial n_1}{\partial t} = n_1 v_1 \Sigma_{s1} f_s(E_1 \to E_1) + n_2 v_2 \nu_2 \Sigma_{f2} \chi_{21} + \nabla \cdot D_1 \nabla n_1 v_1 - (\Sigma_{a1} + \Sigma_{s1}) n_1 v_1$$

$$= \nabla \cdot D_1 \nabla n_1 v_1 + n_1 v_1 (\Sigma_{s1} f_s(E_1 \to E_1) - \Sigma_{s1} - \Sigma_{a1})$$

$$+ n_2 v_2 \Sigma_{f2} \chi_{21} \nu_2 \qquad \text{(A1.19)}$$

and

$$\frac{\partial n_2}{\partial t} = n_1 v_1 \Sigma_{s1} f_s(E_1 \to E_2) + n_2 v_2 \Sigma_{s2} f_s(E_2 \to E_2) + \nabla \cdot D_2 \nabla n_2 v_2$$

$$- (\Sigma_{a2} + \Sigma_{s2}) n_2 v_2 = n_1 v_1 \Sigma_{s1} f_s(E_1 \to E_2) - n_2 v_2 \Sigma_{a2}$$

$$+ \nabla \cdot D_2 \nabla n_2 v_2 \quad . \qquad \text{(A1.20)}$$

Equating coefficients with the traditional two-group equations as given in chapter 4 yields: (for the fuel-coolant region)

$$\Sigma_{1FC} = \Sigma_{a1} + \Sigma_{s1} [1 - f_s(E_1 \to E_1)] = \Sigma_{a1} + \Sigma_{s1} f_s(E_1 \to E_2) \quad ,$$

$$\epsilon\eta f \Sigma_{2FC} = \nu_2 \chi_{21} \Sigma_{f2} \quad ,$$

$$\Sigma_{2FC} = \Sigma_{a2} \quad ,$$

$$p\Sigma_{1FC} = \Sigma_{s1} f_s(E_1 \to E_2) \quad ,$$

(for the moderator region)

$$\Sigma_{1m} = \Sigma_{a1} + \Sigma_{s1} f_s(E_1 \to E_2) = \Sigma_{s1} f_s(E_1 \to E_2) \text{ for } D_2O \quad ,$$

$$\Sigma_{2m} = \Sigma_{a2} \quad .$$

Thus, given

$\nu(\underline{r},E,t)$,

$\Sigma_f(\underline{r},E,t)$,

$\Sigma_s(\underline{r},E,t)$,

$f_s(r;E' \to E;t)$,

$\chi_p(\underline{r},E,t)$,

$\chi_i(E)$,

$\beta_i(\underline{r},E,t)$,

$n(\underline{r},E,t)$

and

$\nu(E)$,

we can determine the two-group parameters as well as any other traditional grouping.

However, a problem arises when we try to determine the group parameters for use in determining the neutron flux distributions for a given case. We need to know the flux distribution in order to calculate the group parameters. In practice, an iterative procedure is used to give a consistent set of neutron flux distribution and group parameters. An alternate scheme is to determine the parameters experimentally; this technique has proved feasible in the past only in limited applications. The general present day practice is to theoretically determine the parameters on an iterative basis guided by what experiments can be done. The present state of the art gives errors of up to 10% in these parameters.

APPENDIX 2

SIMULATED BOILING EXPERIMENTS IN THE CANDU NUCLEAR REACTOR

A2.0 INTRODUCTION

In this appendix we summarize the major features of the simulated boiling experiments (26) used in the testing of the neutronic models in chapter 4.

Reference (26) describes the determination of nuclear reactor buckling, by the substitution technique for coolant densities in the range between 1.0 and 0.4 g cm^{-3}. The substitution technique is an experimental technique used to determine the properties of an unknown fuel bundle by measuring the response caused by the insertion of one or more of these unknown bundles into a lattice of known properties. In this case the known lattice is the air-cooled lattice and the unknown is a fuel bundle with a homogeneous air-water coolant.

A2.1 EXPERIMENTAL SETUP

The lattice was similar in fuel area and fuel/coolant/moderator ratio to that of the D_2O moderated, boiling H_2O-cooled Gentilly power reactor lattice. Experimental bucklings for the H_2O and air-cooled cases used in the analysis were taken from earlier Chalk River measurements in ZED-2.

Test fuel assemblies were of the 28-element type except that a maximum amount of material was removed from the Al bundle end plates to

permit free flow of air bubbles between the aligned bundles. Also, the bottom part of these assemblies was altered to facilitate introduction of air bubbles through a bank of hypodermic needles. The maximum number of air-water mixture cooled test assemblies substituted during the experiments was 7; the other 48 assemblies were air-cooled.

Although each element contains 47.73 cm of fuel, the zircaloy end cans and nuts plus Al end plates and boss increase the overall cluster length to 49.67 cm. The reference fuel assemblies consisted of five fuel bundles stacked end to end in a type 50S Al calandria tube, plus a sixth fuel bundle of the 7 element UO_2 type above them to ensure that the top extrapolation length, illustrated in figure A2.1, was independent of moderator level in the tank. Throughout the experimental program, the D_2O moderator level in the reactor was well below the top of the fifth bundle.

Since dry air was used, a water spray in a surge tank raised the humidity of the air for the air-water mixture and reduced the H_2O losses from the test assemblies.

Early experiments showed that direct inference of the density of the air-water mixture through measurement of air flow rate was not possible. This was considered to be due to effects of water temperature, impurities and dissolved gases on bubble formation. An indirect method of derivation of the density from the position of the air to air-water interface was worked out. This is based on the volumetric expansion of the water column upon introduction of air bubbles.

Variation of coolant density was mainly done by adjustment of air

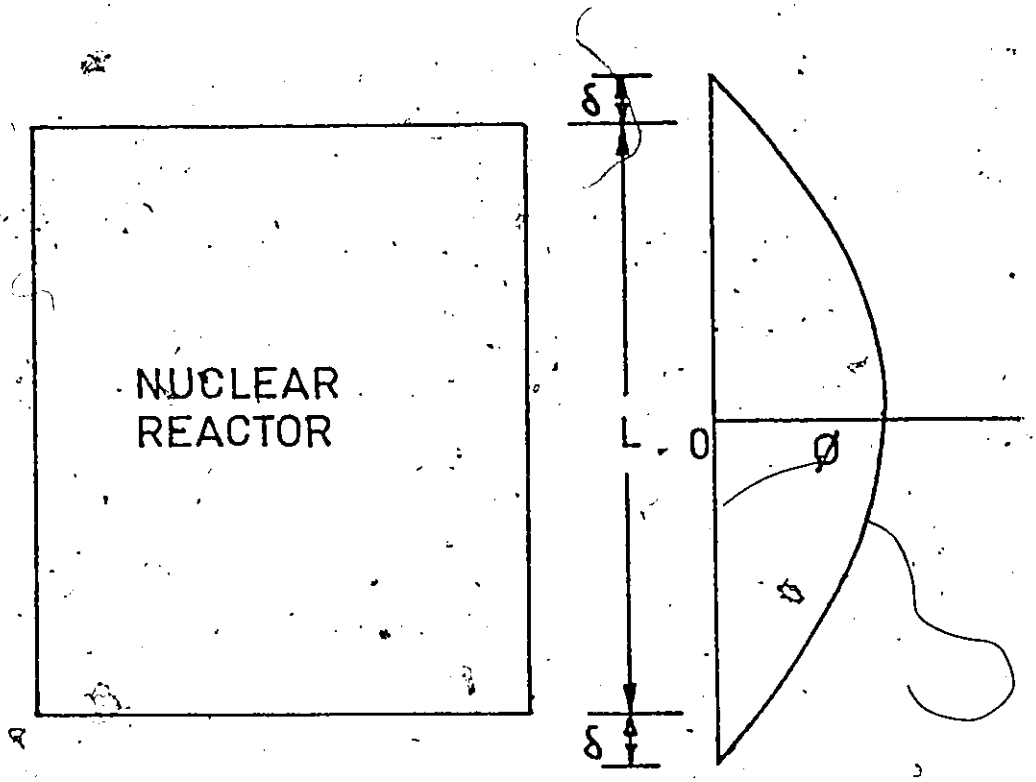

FIGURE A2.1: Illustration of the concept of extrapolation length, δ, the distance beyond the reactor core face at which the neutron flux vanishes.

flow rate. For lower density values, n-propanol (a surface tension reducing agent) was added to the H_2O to a maximum of 0.1% by volume to maintain smooth flow of air. This is not expected to alter the neutron parameters of the coolant since n-propanol has an effective chemical composition of the form $(CH_2)_n$.

To gain an insight into the nature of the vertical variation of coolant density that might exist, some out-of-pile measurements were carried out on a mockup of the fuel assembly. The variation of the coolant density with height within the active reactor region was found to give rise to relatively minor errors only. Error bars on the coolant density of $\pm$ 0.015 g cm^{-3} include estimates due to the possible contribution of vertical coolant density variation, axial cosine flux distribution and neutron importance variation effects.

A2.2 METHOD OF ANALYSIS

The code MICRETE3 employs an axially uniform two-group, line source-sink model developed at Chalk River by J.D. Stewart, et al (75,76). The fuel rods are represented by line sources of fast neutrons and line sinks of thermal neutrons. Slowing down and diffusion in the moderator are described by conventional diffusion theory. The analysis procedure, utilizing MICRETE3, is shown schematically in figure A2.2.

The only experimental information directly entering the analysis was the extrapolated critical heights of the reference and substituted cores. All other input quantities were calculated using the lattice recipe code LATREP, described briefly in chapter 4 and in more detail in

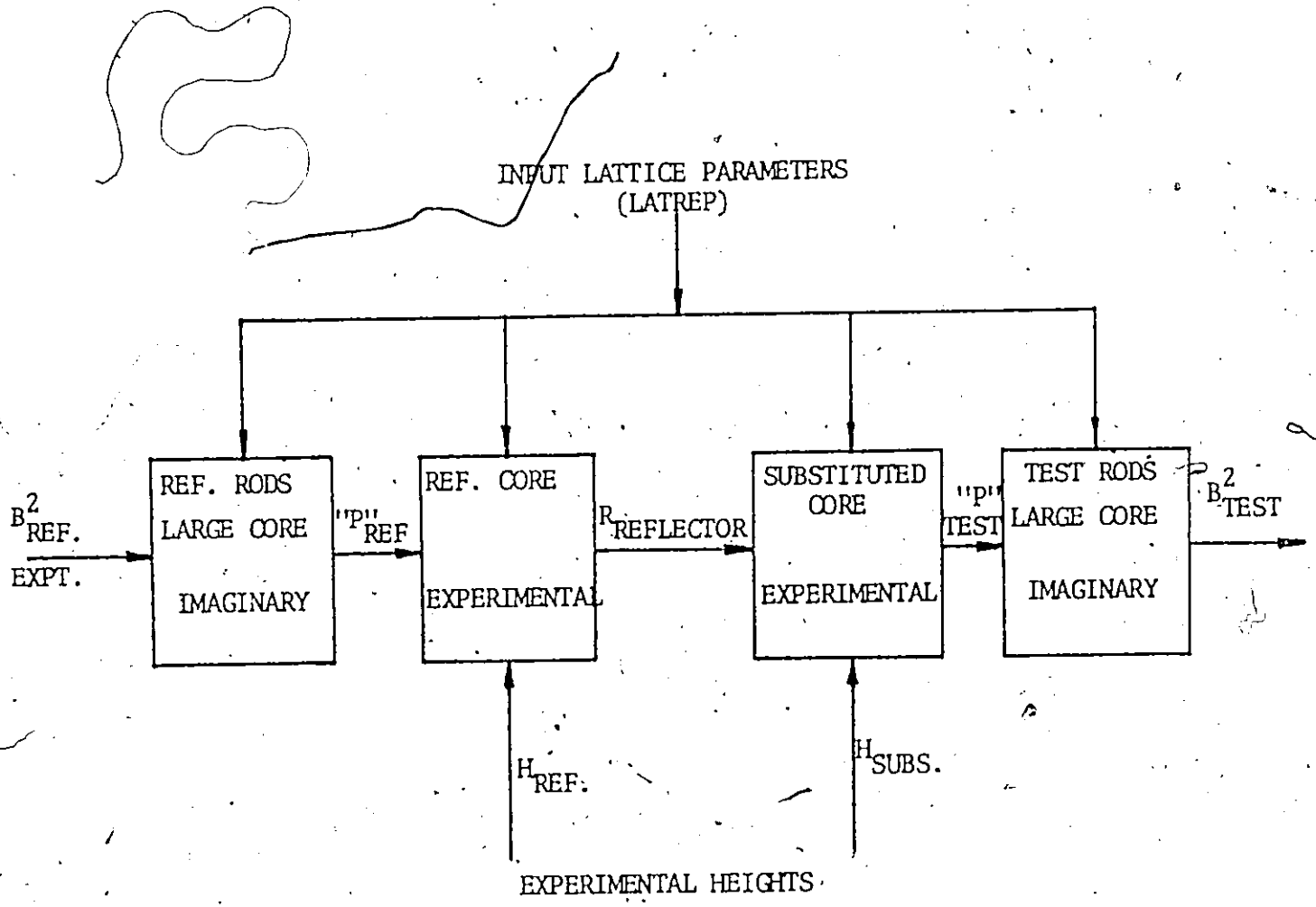

FIGURE A2.2: MICRETE3 analysis of the substitution experiments.

appendix 6; the data input to LATREP is composed of only fundamental data. The first and last blocks of figure A2.2 represent large, hypothetical cores mocked up for the purpose of deriving bucklings. Radial bucklings are obtained in a manner analogous to a flux mapping experiment, namely, by fitting an appropriate Bessel function to the radial distribution of MICRETE3 calculated fluxes. Axial buckling is taken as $(\pi/H)^2$, H being the extrapolated critical height of the mock-up. The total buckling is the sum of the axial and radial bucklings.

In the first block of figure A2.2 the resonance escape probability, p, of the reference air-cooled fuel is adjusted until the experimental buckling value is obtained.

In the second block, a mock-up of the reference core of the substitution experiments, this adjusted 'p_{ref}' is used and the radius, R, of the reflector outer boundary is altered until agreement is obtained between calculated and measured extrapolated critical heights of the reference core.

The third block mocks up the actual substituted core. Here 'p_{test}' of the fuel assembly is adjusted to give the observed critical height. Although any one of the calculated input parameters could have been adjusted the choice of p was dictated by the fact that its calculation by LATREP and representation in MICRETE3 are the least accurate of all the input parameters. In the last step, this adjusted 'p_{test}' is used along with other LATREP calculated inputs in a large, one region, hypothetical test core to obtain the buckling of the test lattice.

The outcome of the analytical procedure is a single number,

namely an adjusted 'p_{test}' value of the test fuel which satisfies the reactivity balance conditions of the substitution experiment. Errors in the LATREP calculated input parameters, approximations in the physical representation of the reactor by MICRETE3, uncertainties in the measured critical moderator levels, errors in the derivation of axial extrapolation lengths, etc. are all reflected as a reactivity discrepancy between experiment and MICRETE3. This is compensated for in the analytical procedure by adjusting p and R. The adjusted value of p may, therefore, not be in agreement with the true resonance escape probability of the lattice.

Apart from the critical moderator heights of the reference and substituted cores, the only input parameters obtained experimentally were the axial extrapolation lengths and the buckling of the air-cooled reference lattice. The former was obtained from an axial flux distribution measurement carried out during the substitution program. The derived total extrapolation length of 23 cm for the seven H_2O-cooled assembly plus 48 air-cooled assembly core was, within experimental errors, the same as that obtained for the 55 air-cooled assembly core. Therefore 23 cms was added to all measured critical moderator levels to yield extrapolated critical heights.

A2.3 RESULTS

In general, the buckling approaches the expected test lattice buckling value as N (the number of substituted test assemblies) increases. It was shown by Okazaki (77) that a plot of B against 1/N falls on a

reasonably straight line except for the one assembly substitute point. This line extrapolated to the flux map value of B of the test lattice at 1/N = 0. Figure A2.3 shows the results of the above analysis plotted against 1/N. For the case of coolant density of 1.0 g cm^{-3}, a line through 3, 5 and 7 assembly substitution points extrapolates to a test lattice buckling of 1.23 ± .10 m^{-2}. This compares well with the value of 1.17 ± .05 m^{-2} given as the experimental flux-map buckling value for the H_2O-cooled 28-element UO_2 lattice. An accuracy of ± 0.1 m^{-2} has been suggested (77) for bucklings derived by such an experimental technique. The difference is therefore well within the estimated errors. The close agreement gives confidence in the validity of the experimental technique, input parameters used, and method of analysis. Since the air-cooled reference assemblies and the H_2O-cooled test assemblies discussed above represent the extreme values of coolant density, it is reasonable to assume that the bucklings derived for intermediate coolant densities between 0.0 and 1.0 g cm^{-3} are also valid.

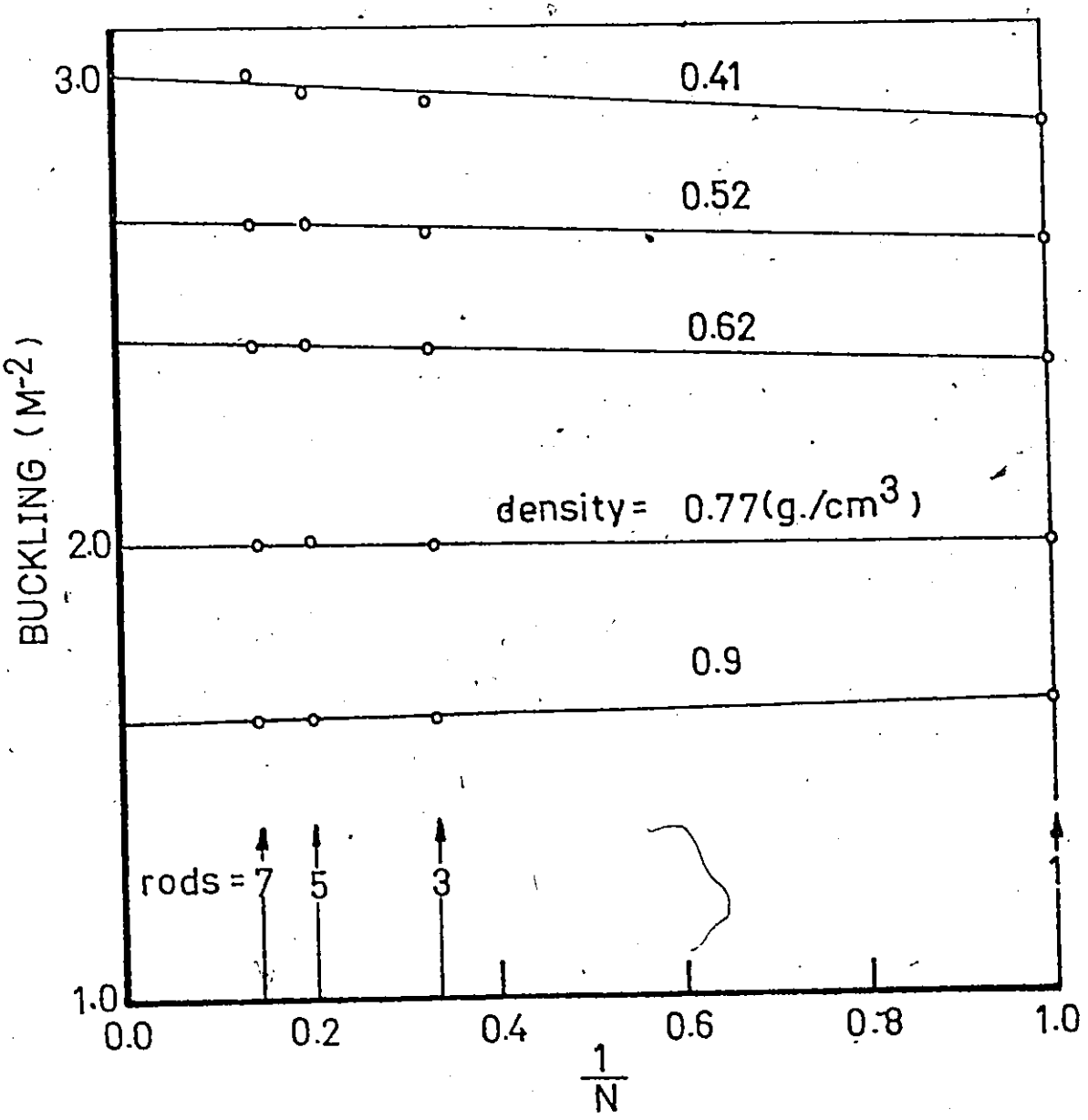

FIGURE A2.3: Buckling results.

APPENDIX 3

COMPUTER CODE FOR THE ONE-GROUP ANALYTICAL MODEL

The criticality expressions for the one-group, two-region model for uniform voiding described in section 4.1.2 are most easily evaluated by a computer code. The flow diagram of this code is given by figure A3.1. A program listing, with comments, is also given in the following.

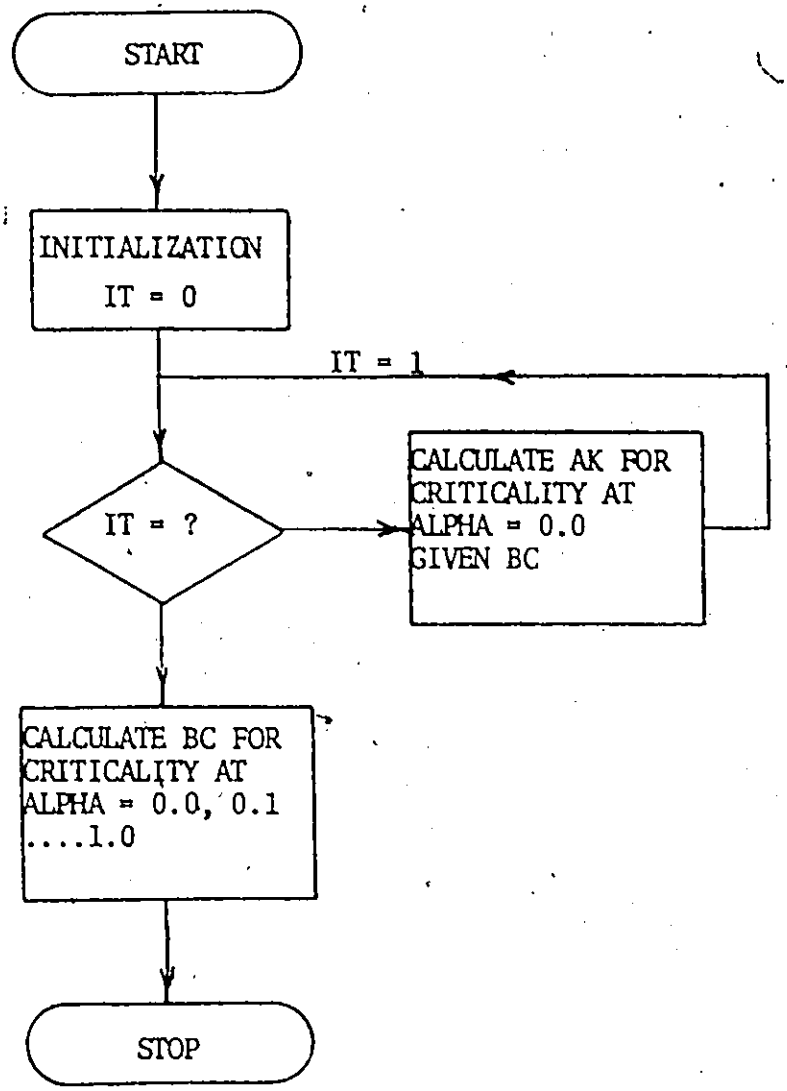

FIGURE A3.1: Flowchart for the one-group neutron diffusion model computer code.

```
      PROGRAM TST (INPUT,OUTPUT,TAPE5=INPUT,TAPE6=OUTPUT)
C   THIS CODE CALCULATES THE CRITICALITY DETERMINANT FOR THE ONE-GROUP
C   NEUTRON DIFFUSION MODEL FOR A TWO-REGION CYLINDRICAL REACTOR CELL
C   AS IN SECTION 4.1.2
C   C.G.S. SYSTEM OF UNITS USED THROUGHOUT
C   SYMBOLISM-
C   A      =FUEL-COOLANT RADIUS
C   B      =CELL RADIUS
C   SAM    =ABSORPTION CROSS SECTION OF MODERATOR
C   SAF    =ABSORPTION CROSS SECTION OF FUEL
C   SAFC   =ABSORPTION CROSS SECTION OF FUEL-COOLANT REGION
C   DFC    =DIFFUSION COEFFICIENT OF FUEL-COOLANT REGION
C   DM     =DIFFUSION COEFFICIENT OF MODERATOR
C   EF     =RADIAL PARAMETER FOR FUEL-COOLANT REGION (SEE EQUATION (4.1.5))
C   EM     =RADIAL PARAMETER FOR MODERATOR REGION (SEE EQUATION (4.1.6))
C   BC     =AXIAL BUCKLING=(3.14159/HEIGHT)**2
C   AK     =MULTIPLICATION FACTOR OF GROUP DIFFUSION THEORY
C   ALPHA  =VOID FRACTION
C   IT     =ITERATION CONTROL PARAMETER
      EXTERNAL FX
      COMMON A,Q1,Q2
C   INITIALIZATION
      A=6.37
      B=SQRT(779.43/3.14159)
      SAM=9.6E-05
      IT=0
      DM=.869
      ALPHA=0.
      BC=.000117
    9 IF(IT.NE.0)BC=.0001
   14 EM=SQRT(SAM/DM+BC)
      SAF=.07
    3 SAFC=(44.405*SAF+30.674*(1.-ALPHA)*.0197+(9.754+5.501)*.01416
     1 +5.897*.007724)/127.436
      DFC=127.436/((1.-ALPHA)*30.672/.16+44.405/.1)
      EFR=.1
      EFL=.01
      K=2
C   CALCULATION OF THE BESSEL FUNCTIONS FOR THE MODERATOR REGION
      CALL BESI(EM*A,0,AI0,IER)
      IF(IER.NE.0)WRITE(6,5)IER,K
    5 FORMAT(1H ,*   ERROR IN BESSEL ROUTINE*,2I3)
      K=3
      CALL BESI(EM*A,1,AI1,IER)
      IF(IER.NE.0)WRITE(6,5)IER,K
      K=4
      CALL BESI(EM*B,1,BI1,IER)
      IF(IER.NE.0)WRITE(6,5)IER,K
      K=5
      CALL BESK(EM*A,0,AK0,IER)
      IF(IER.NE.0)WRITE(6,5)IER,K
      K=6
      CALL BESK(EM*A,1,AK1,IER)
      IF(IER.NE.0)WRITE(6,5)IER,K
      K=7
      CALL BESK(EM*B,1,BK1,IER)
      IF(IER.NE.0)WRITE(6,5)IER,K
```

```
      Q1=(AI0*BK1+BI1*AK0)*DFC
      Q2=EM*(AI1*BK1-BI1*AK1)*DM
C   ON THE FIRST ITERATION , THE VALUE OF AK IS CALCULATED TO GIVE
C   CRITICALITY GIVEN BC. ON SUBSEQUENT ITERATIONS,BC IS VARIED TO PROVIDE
C   CRITICALITY.
      IF(IT.EQ.0)  GO TO 13
      EF=SQRT((SAF  *AK*44.405/127.436-SAFC)/DFC-BC)
      K=0
      CALL BESJ(EF*A,1,AJ1,.001 ,IER)
      IF(IER.NE.0)WRITE(6,5)IER,K
      K=1
      CALL BESJ(EF*A,0,AJ0,.001 ,IER)
      IF(IER.NE.0)WRITE(6,5)IER,K
      F =-AJ1*EF*Q1-AJ0*Q2
      WRITE(6,11)BC,F
   11 FORMAT(1H ,2E14.4)
C   STOP THE SEARCH IF BC CANNOT BE FOUND WITHIN REASONABLE LIMITS.
      IF(BC.GT..0005)  GO TO 12
      IF(IT.GT.1)  GO TO 13
      BCOLD=BC
      FXOLD=F
      IT=2
      BC=BC+.00001
      GO TO 14
   13 SIGN=F *FXOLD
      IF(SIGN.LT.0.)  GO TO 15
      BCOLD=BC
      FXOLD=F
      BC=BC+.00001
      GO TO 14
   15 IF(BC-BCOLD.LT.1.E-09)  GO TO 12
      BC=(BC+BCOLD)/2.
      GO TO 14
   12 WRITE(6,16)ALPHA,BC,EF
   16 FORMAT(1H ,3E14.4//)
      IF(ALPHA.GE.1.)  GO TO 2
      ALPHA=ALPHA+.1
      IT=1
      GO TO 9
C   RTMI IS A ROOT FINDING ROUTINE USED TO FIND THE VALUE OF EF NECESSARY
C   TO SATISFY EQUATION (4.1.9)
   10 CONTINUE
      CALL RTMI(EF,F,FX,EFL,EFR,.001,100,IER)
      IF(IER.NE.0)  GO TO 4
      FAKE=EF*EF+BC
C   AK IS CALCULATED DIRECTLY FROM THE CRITICAL VALUE OF EF ACCORDING TO
C   EQUATION (4.1.5)
      AK=(FAKE*DFC+SAFC)/SAF  *127.436/44.405
      REACT=AK
      WRITE(6,1)ALPHA,REACT,EF
    1 FORMAT(1H ,*   FOR ALPHA=*,E14.4,*  REACTIVITY=*,E14.4,*  WITH EF=
     1  *,E14.4,//)
      IT=1
C   HAVING FOUND THE FITTED VALUE OF AK AT ALPHA=0.0,RETURN TO THE START
C   AND PERMUTE THE VALUE OF BC TO PROVIDE CRITICALITY AT VARIOUS ALPHA
C   VALUES FROM 0.0 TO 1.0 IN STEPS OF 0.1
      GO TO 9
    4 WRITE(6,6) IER
    6 FORMAT(1H ,*  ERROR NUMBER*,I3,* IN ROUTINE RTMI*)
    2 STOP
      END
```

```
      FUNCTION FX(EF)
C  EVALUATION OF EQUATION (4.1.9), GIVEN THE VALUE OF EF
      COMMON A,Q1,Q2
      K=0
      CALL BESJ(EF*A,1,AJ1,.001 ,IER)
      IF(IER.NE.0)WRITE(6,1)IER,K
    1 FORMAT(1H ,*    ERROR IN BESSEL ROUTINE*,2I3)
      K=1
      CALL BESJ(EF*A,0,AJ0,.001 ,IER)
      IF(IER.NE.0)WRITE(6,1)IER,K
      FX=-AJ1*EF*Q1-AJ0*Q2
      RETURN
      END
```

APPENDIX 4

COMPUTER CODE FOR THE SEMI-TWO-GROUP ANALYTICAL MODEL

The criticality expressions for the semi-two-group, two-region model for uniform voiding in section 4.1.3 are most easily evaluated by a computer code. The flow diagram of this code is given by figure A4.1. A program listing, with comments, is also given in the following.

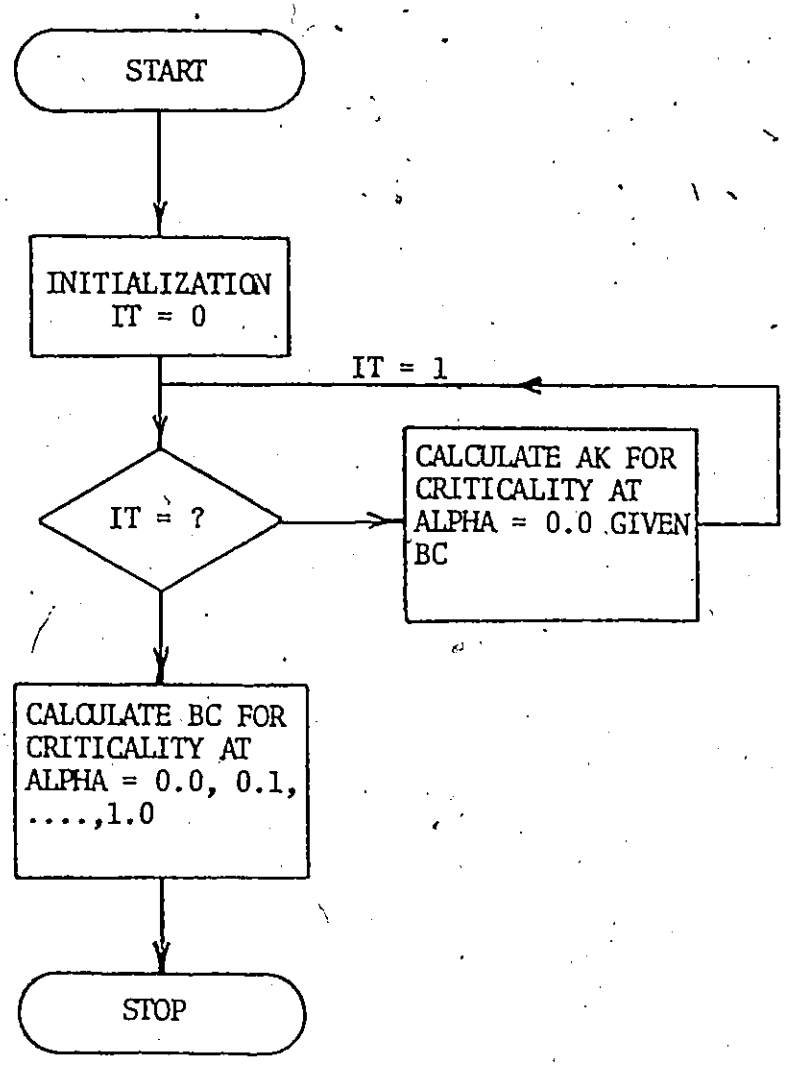

FIGURE A4.1: Flowchart for the semi-two-group neutron diffusion model computer code.

```
      PROGRAM TST (INPUT,OUTPUT,TAPE5=INPUT,TAPE6=OUTPUT)
C   THIS CODE CALCULATES THE CRITICALITY DETERMINANT FOR THE SEMI-TWO-GROUP
C   NEUTRON DIFFUSION MODEL FOR A TWO-REGION CYLINDRICAL REACTOR CELL
C   AS IN SECTION 4.1.3
C   C.G.S. SYSTEM OF UNITS USED THROUGHOUT
C   SYMBOLISM-
C   A      =FUEL-COOLANT RADIUS
C   B      =CELL RADIUS
C   SAM    =ABSORPTION CROSS SECTION OF MODERATOR
C   ET     =ABSORPTION CROSS SECTION OF FUEL
C   SAFC   =ABSORPTION CROSS SECTION OF FUEL-COOLANT REGION
C   DFC    =DIFFUSION COEFFICIENT OF FUEL-COOLANT REGION
C   DM     =DIFFUSION COEFFICIENT OF MODERATOR
C   EF     =RADIAL PARAMETER FOR FUEL-COOLANT REGION (SEE EQUATION (4.1.14))
C   EM     =RADIAL PARAMETER FOR MODERATOR (SEE EQUATION (4.1.15))
C   BC     =AXIAL BUCKLING=(3.14159/HEIGHT)**2
C   AK     =MULTIPLICATION FACTOR OF GROUP DIFFUSION THEORY
C   ALPHA  =VOID FRACTION
C   Q      =SLOWING DOWN DENSITY
C   IT     =ITERATION CONTROL PARAMETER
C   INITIALIZATION
      IT=0
      BC=.000117
      A=6.37
      B=SQRT(779.43/3.14159)
      SAM=9.6E-05
      DM=.869
      ALPHA=0.
      ET=.07
    6 IF(IT.EQ.1)BC=.0001
    3 SAFC=(44.405*ET    +30.674*(1.-ALPHA)*.0197+(9.754+5.501)*.01416
     1 +5.897*.007724)/127.436
      DFC=127.436/((1.-ALPHA)*30.672/.16+44.405/10.)
    4 EF=SQRT(SAFC/DFC+BC)
      EM=SQRT(SAM/DM+BC)
C   CALCULATION OF THE BESSEL FUNCTIONS FOR THE MODERATOR REGION
      IER=0
      K=0
      CALL BESI(EF*A,0,AI0F,IER)
      IF(IER.NE.0)WRITE(6,5)IER,K
    5 FORMAT(1H ,*   ERROR IN BESSEL ROUTINE*,2I3)
      K=1
      CALL BESI(EF*A,1,AI1F,IER)
      IF(IER.NE.0)WRITE(6,5)IER,K
      K=2
      CALL BESI(EM*A,0,AI0M,IER)
      IF(IER.NE.0)WRITE(6,5)IER,K
      K=3
      CALL BESI(EM*A,1,AI1M,IER)
      IF(IER.NE.0)WRITE(6,5)IER,K
      K=4
      CALL BESK(EM*A,0,AK0,IER)
      IF(IER.NE.0)WRITE(6,5)IER,K
      K=5
      CALL BESK(EM*A,1,AK1,IER)
      IF(IER.NE.0)WRITE(6,5)IER,K
      K=6
```

```
      CALL BESI(EM*B,1,BI1M,IER)
      IF(IER.NE.0)WRITE(6,5)IER,K
      K=7
      CALL BESK(EM*B,1,BK1,IER)
      IF(IER.NE.0)WRITE(6,5)IER,K
      Q=AIOF*     (1.-DFC*EF*AI1F/(AIOF*DM*EM)*(AIOM*BK1+AKO *BI1M)/
     1   (AI1M*BK1-AK1*BI1M))*(SAM+DM*BC)
      AK=Q*EF/(2.*3.14159*A*AI1F*ET  )*652.0*127.436/44.405
      WRITE(6,11)ALPHA,AK,BC
   11 FORMAT(1H ,3E14.4)
C   ON THE FIRST ITERATION, THE VALUE OF AK IS CALCULATED TO GIVE
C   CRITICALITY GIVEN BC. ON SUBSEQUENT ITERATIONS, BC IS VARIED TO
C   PROVIDE CRITICALITY.
      IF(IT.EQ.0)  GO TO 7
      IF(IT.GT.1)  GO TO 8
      IT=2
      BCOLD=BC
      BC=BC+.00001
      GO TO 6
    8 IF(BC.GT..0005) GO TO 9
      IF(ABS(AK-AKOLD).LT.1.E-09)  GO TO 9
      IF(AK.GT.AKOLD)BC=(BC+BCOLD)/2.
      IF(AK.LT.AKOLD)  BCOLD=BC
      IF(AK.LT.AKOLD)BC=BC+.00001
      GO TO 6
    9 WRITE(6,10)  ALPHA,BC,AK
   10 FORMAT(1H ,3E14.4)
      IF(ALPHA.GE.1.)  GO TO 2
      IT=1
      ALPHA=ALPHA+.1
      GO TO 6
    7 REACT=AK
      WRITE(6,1)ALPHA,REACT,EF
    1 FORMAT(1H ,*   FOR ALPHA=*,E14.4,*  REACTIVITY=*,E14.4,*  WITH EF=
     1  *,E14.4,//)
      AKOLD=AK
      IT=1
C   HAVING FOUND THE FITTED VALUE OF AK AT ALPHA=0.0,RETURN TO THE START
C   AND PERMUTE THE VALUE OF BC TO PROVIDE CRITICALITY AT VARIOUS ALPHA
C   VALUES FROM 0.0 TO 1.0 IN STEPS OF 0.1
      GO TO 6
    2 STOP
      END
```

APPENDIX 5

COMPUTER CODE FOR THE TWO-GROUP ANALYTICAL MODEL

The criticality expressions for the two-group, two-region model for uniform voiding in section 4.1.4 are most easily evaluated by a computer code. The flow diagram of this code is given by figures A5.1, A5.2 and A5.3. A program listing, with comments, is also given in the following.

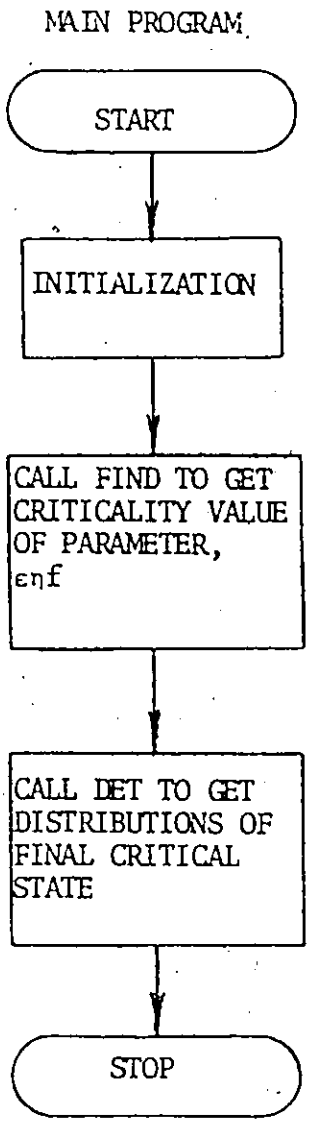

FIGURE A5.1: Flowchart for the two-group neutron diffusion model computer code: main progam.

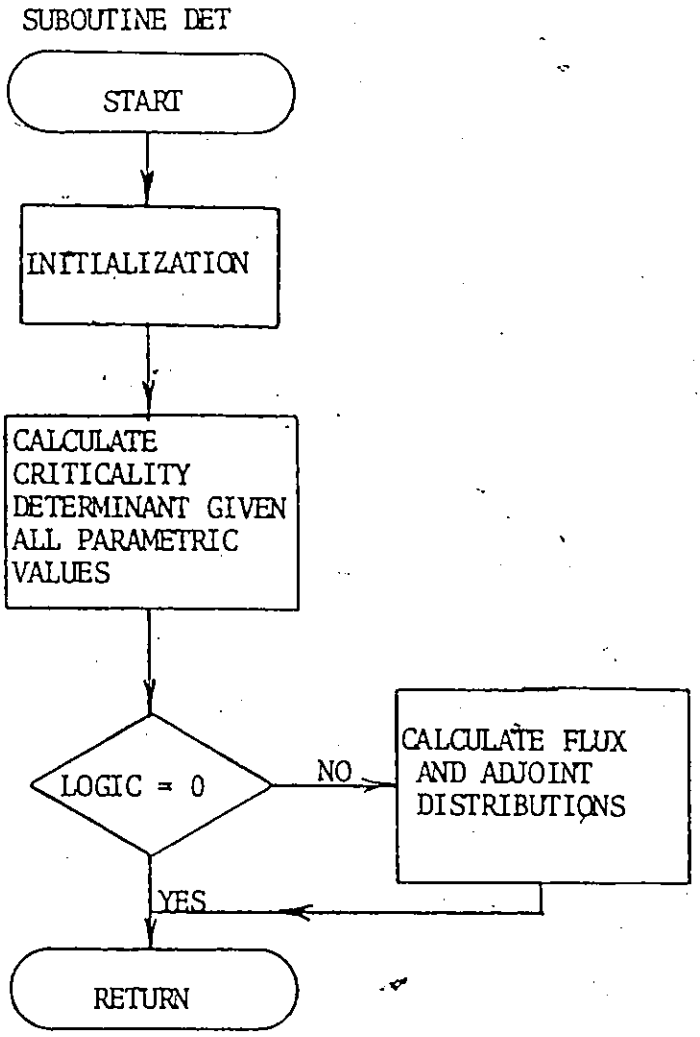

FIGURE A5.2: Flowchart for the two-group neutron diffusion model computer code: subroutine DET.

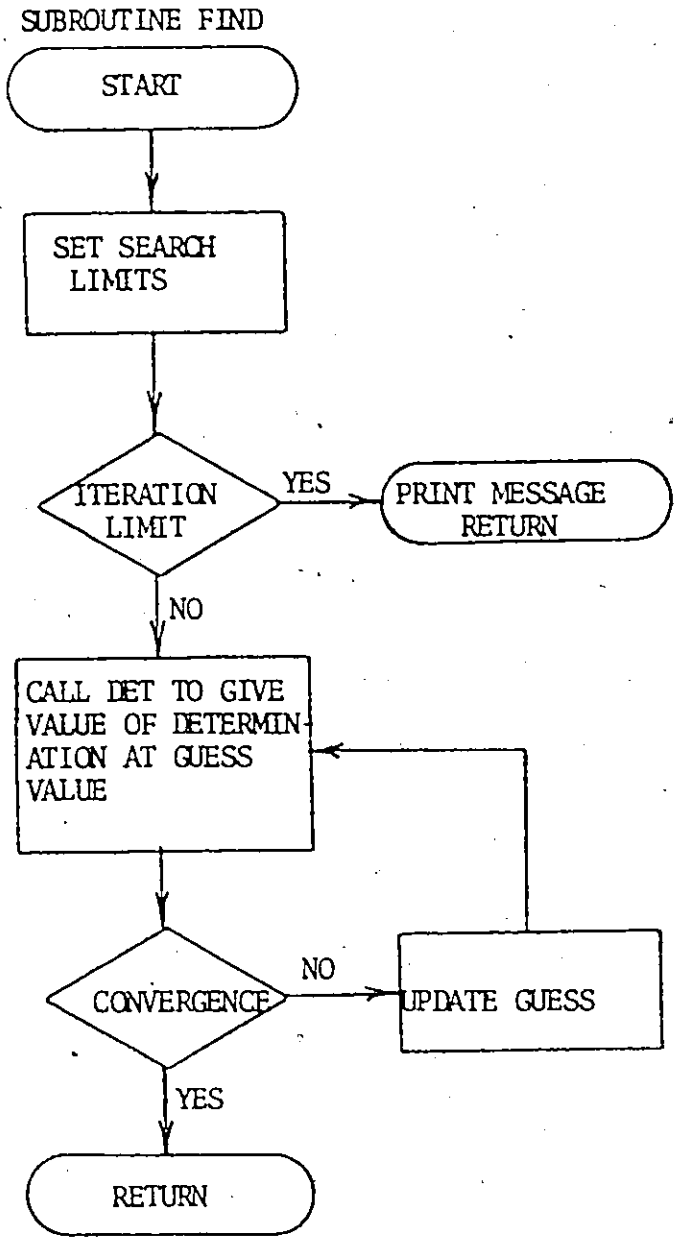

FIGURE A5.3: Flowchart for the two-group neutron diffusion model computer code: subroutine FIND.

```
      PROGRAM TS(INPUT,OUTPUT,PUNCH,TAPE5=INPUT,TAPE6=OUTPUT,TAPE7=PUNCH
     1)
C   THIS CODE CALCULATES THE CRITICALITY DETERMINANT FOR THE TWO-GROUP
C   NEUTRON DIFFUSION MODEL FOR A TWO-REGION CYLINDRICAL REACTOR CELL OF
C   SECTION 4.1.4
C   C.G.S.-SYSTEM OF UNITS USED THROUGHOUT
C   SYMBOLISM-
C   ETAF,EPSLON,PP=PARAMETERS OF THE FOUR FACTOR FORMULA
C   DTC    =THERMAL GROUP DIFFUSION COEFFICIENT FOR THE FUEL-COOLANT REGION
C   DFC    = FAST   GROUP DIFFUSION COEFFICIENT FOR THE FUEL-COOLANT REGION
C   DTR    =THERMAL GROUP DIFFUSION COEFFICIENT FOR THE MODERATOR(REFLECTOR)
C   DFR    = FAST   GROUP DIFFUSION COEFFICIENT FOR THE MODERATOR(REFLECTOR)
C   ETC    =THERMAL GROUP CROSS SECTION FOR FUEL-COOLANT REGION
C   EFC    = FAST   GROUP CROSS SECTION FOR FUEL-COOLANT REGION
C   ETR    =THERMAL GROUP CROSS SECTION FOR MODERATOR(REFLECTOR)
C   EFR    = FAST   GROUP CROSS SECTION FOR MODERATOR(REFLECTOR)
C   BC     =AXIAL BUCKLING=(3.14159/HEIGHT)**2
C   ALPHA  =VOID FRACTION
C   S(11)  =FUEL-COOLANT RADIUS
C   S(12)  =CELL CROSS SECTIONAL AREA
      DIMENSION S(13),T(13),U(13,13)
      COMMON DTC,ETC,DFC,EFC,ETAF,DTR,ETR,DFR,EFR,PP,EPSLON,ALPHA
      COMMON/SENSE/LOGIC
C   INITIALIZATION
C   DATA READIN
    1 CALL YREAD
      CALL READX(BC)
      LOGIC=0
      ETAF=ETAF*EPSLON
      S(1)=DTC
      S(2)=ETC
      S(3)=DFC
      S(4)=EFC
      S(5)=ETAF
      S(6)=DTR
      S(7)=ETR
      S(8)=DFR
      S(9)=EFR
      S(10)=PP
      S(11)=6.37
      S(12)=779.43
      S(13)=BC
C   CALCULATION OF ETAF NECESSARY TO GIVE CRITICALITY
      DO 4 I=1,13
    4 T(I)=S(I)
      CALL FIND(T,5)
      S(5)=T(5)
      LOGIC=1
C   CALCULATION OF FLUX AND ADJOINT DISTRIBUTIONS FOR CRITICALITY STATE
      CALL DET(T,5,F)
      FAKE=S(5)/EPSLON
      WRITE(6,5)S(5),FAKE,EPSLON
    5 FORMAT(1H ,3E14.7)
C   REPETITION FOR NEW DATA SET. UPON SUBSEQUENT ITERATIONS,SPECIFICATION
C   OF  ≠ CALL FIND(T,13) ≠ GIVES CRITICALITY BY VARING BC INSTEAD OF
C   ETAF,AS ABOVE.
      GO TO 1
      STOP
      END
```

```
      SUBROUTINE DET(TT,JOG,F)
C     THIS ROUTINE CALCULATES THE VALUE OF THE CRITICALITY DETERMINANT,
CC    EQUATION (4.1.21),GIVEN THE PARAMETRIC VALUES,TT. THE FLUX AND ADJOINT
CC    DISTRIBUTIONS ARE ALSO CALCULATED IF LOGIC IS SET TO 1 . SETTING
C     LOGIC=0 BYPASSES THIS CALCULATION .
      DIMENSION TT(13)
      COMMON DTC,ETC,DFC,EFC,ETAF,DTR,ETR,DFR,EFR,PP,EPSLON,ALPHA
      COMMON/SENSE/LOGIC
C     INITIALIZATION
      DTC=TT(1)
      ETC=TT(2)
      DFC=TT(3)
      EFC=TT(4)
      ETAF=TT(5)
      DTR=TT(6)
      ETR=TT(7)
      DFR=TT(8)
      EFR=TT(9)
      P=TT(10)
      A=TT(11)
      AREA=TT(12)
      BC=TT(13)
      IER=0
C     CALCULATION OF PARAMETRIC  AND FUNCTIONAL GROUPS,GIVEN BY SECTION 4.1.4
   18 AKFRSQ=EFR/DFR+BC
      B=SQRT(AREA  /3.14159)
      AKTRSQ=ETR/DTR+BC
      TC=DFC/EFC
      ACSQ=DTC/ETC
      A1=TC+ACSQ
      BKFRSQ=EFR/DFR
      BKTRSQ=ETR/DTR
      S3=EFR/DTR/(BKTRSQ-BKFRSQ)
      AKFR=SQRT(AKFRSQ)
      AKTR=SQRT(AKTRSQ)
      FB=AKFR*B
      FA=AKFR*A
      TB=AKTR*B
      TA=AKTR*A
      K=1
      CALL BESI(FA,0,FAI0,IER)
      IF(IER.NE.0)WRITE(6,4)IER,K
      K=K+1
      CALL BESI(TA,0,TAI0,IER)
      IF(IER.NE.0)WRITE(6,4)IER,K
      K=K+1
      CALL BESI(FA,1,FAI1,IER)
      IF(IER.NE.0)WRITE(6,4)IER,K
      K=K+1
      CALL BESI(TA,1,TAI1,IER)
      IF(IER.NE.0)WRITE(6,4)IER,K
      K=K+1
      CALL BESI(FB,1,FBI1,IER)
      IF(IER.NE.0)WRITE(6,4)IER,K
      K=K+1
      CALL BESI(TB,1,TBI1,IER)
      IF(IER.NE.0)WRITE(6,4)IER,K
```

```
      K=K+1
      CALL BESK(FB,1,FBK1,IER)
      IF(IER.NE.0)WRITE(6,4)IER,K
      K=K+1
      CALL BESK(TB,1,TBK1,IER)
      IF(IER.NE.0)WRITE(6,4)IER,K
      K=K+1
      CALL BESK(FA,1,FAK1,IER)
      IF(IER.NE.0)WRITE(6,4)IER,K
      K=K+1
      CALL BESK(TA,1,TAK1,IER)
      IF(IER.NE.0)WRITE(6,4)IER,K
      K=K+1
      CALL BESK(FA,0,FAK0,IER)
      IF(IER.NE.0)WRITE(6,4)IER,K
      K=K+1
      CALL BESK(TA,0,TAK0,IER)
      IF(IER.NE.0)WRITE(6,4)IER,K
    4 FORMAT(1H ,2I5)
      ZFP=AKFR*(FBK1*FAI1-FBI1*FAK1)
      ZF=FBK1*FAI0+FBI1*FAK0
      ZTP=AKTR*(TBK1*TAI1-TBI1*TAK1)
      ZT=TBK1*TAI0+TBI1*TAK0
      ZFR=ZFP/ZF
      ZTR=ZTP/ZT
    3 AK=ETAF*P
      S=P*EFC/ETC
      SQ=SQRT(A1*A1+4.*(AK-1.)*TC*ACSQ)
      ALSQ=(A1+SQ)/(2.*TC*ACSQ)
      AL=SQRT(ALSQ)
      USQ=(AK    -1.)/TC/ACSQ/ALSQ
      S1=S/(1.+USQ*ACSQ)
      S2=S/(1.-ALSQ*ACSQ)
      S1P=P/(1.+USQ*TC)
      S2P=P/(1.-ALSQ*TC)
      S3P=1./(1.-BKTRSQ/BKFRSQ)
      IC=0
      USE=USQ-BC
C   DEPENDING ON THE VALUE OF THE ARGUEMENT,USE,THE APPROPRIATE BESSEL
C   FUNCTION IS USED-GREATER THAN 0-USE J0 AND J1
C                   -LESS THAN 0-USE IC AND I1
C                   -EQUAL TO 0-IRRELEVANT
      IF(USE.GE.0.)  GO TO 12
      IC=1
   12 CONTINUE
      IF(IC.EQ.1)USE=ABS(USE)
      E=SQRT(USE)
      SIG=SQRT(ALSQ+BC)
      UA=E*A
      ALA=SIG*A
      IER=0
      K=K+1
      IF(IC.EQ.0)  GO TO 13
      CALL BESI(UA,0,AJ0,IER)
      IF(IER.NE.0)WRITE(6,4)IER,K
      K=K+1
      CALL BESI(UA,1,AJ1,IER)
```

```
      IF(IER.NE.0)WRITE(6,4)IER,K
      K=K+1
      GO TO 14
   13 CALL BESJ(UA,0,AJ0,1.E-09,IER)
      IF(IER.NE.0)WRITE(6,4)IER,K
      K=K+1
      CALL BESJ(UA,1,AJ1,1.E-09,IER)
      IF(IER.NE.0)WRITE(6,4)IER,K
      K=K+1
   14 CALL BESI(ALA,0,AI0,IER)
      IF(IER.NE.0)WRITE(6,4)IER,K
      K=K+1
      CALL BESI(ALA,1,AI1,IER)
      IF(IER.NE.0)WRITE(6,4)IER,K
C  FINALLY,THE EXPLICIT CALCULATION OF THE CRITICALITY DETERMINANT
      XP=-E*AJ1
      IF(IC.EQ.1)XP=E*AJ1
      X=AJ0
      YP=SIG*AI1
      Y=AI0
      XR=XP/X
      YR=YP/Y
      T1=DFC*DTR*(S3-S1)*YR*ZTR
      T2=(DFR*DTC*S2-DFC*DTR*S3)*YR*ZFR
      T3=DFR*DTR*(S1-S2)*ZFR*ZTR
      T=T1+T2+T3
      B1=DFC*DTC*(S2-S1)*YR
      B2=(DFR*DTC*S1-DFC*DTR*S3)*ZFR
      B3=DFC*DTR*(S3-S2)*ZTR
      Q=B1+B2+B3
      F=B*(T-XR*Q)
C  IF DISTRIBUTIONS ARE NOT REQUIRED,RETURN
      IF(LOGIC.EQ.0)RETURN
C  THE CALCULATION OF THE FLUX AND THE ADJOINT DISTRIBUTIONS FOLLOWS
C  LAMARSH(28) CHAPTER 15
      RTBC=SQRT(BC)
      H=3.14159/RTBC
      BETA=DFR*ZFR-DFC*YR
      C=X/Y/BETA*(DFC*XR-DFR*ZFR)
      F=X/ZF/BETA*(DFC*XR-DFC*YR)
      G=X/BETA/ZT*(DFC*(S2-S3)*XR+DFC*(S3-S1)*YR+DFR*(S1-S2)*ZFR)
      BETAP=DTR*ZTR-DTC*YR
      CP=X/Y/BETAP*(DTC*XR-DTR*ZTR)
      FP=X/BETAP/ZF *(DTC*(S2P-S3P)*XR+DTC*(S3P-S1P)*YR+DTR*(S1P-S2P)*
     1ZTR)
      GP=X/BETAP/ZT *(DTC*XR-DTC*YR)
C  SPECIFICATION OF MESH SIZE-N=NUMBER OF AXIAL MESH NODES
CC                           -M1=NUMBER OF RADIAL MESH NODES IN FUEL-
CC                               -COOLANT REGION
C                            -M2=NUMBER OF RADIAL MESH NODES IN MODERATOR
      N=11
      M1=5
      M2=11
      M=M2
      DR1=A/FLOAT(M1-1)
      DR2=(B-A)/FLOAT(M2-M1-1)
      DZ=H/FLOAT(N-1)
```

```
      DO 29 I=1,N
      ZH=FLOAT(I-1)*DZ
      FACT=COS((ZH*2.-H)*3.14159/2./H)
      FACT1=-3.14159/H/FACT*SIN((ZH*2.-H)*3.14159/2./H)
      DO 28 J=1,M
      IF(J.GT.M1)GO TO 29
      R=FLOAT(J-1)*DR1
      H1=1.
      IF(R.NE.0.)CALL BESJ(E*R,0,.001,H1,IER)
      IF(IC.EQ.1)CALL BESI(E*R,0,H1,IER)
      CALL BESI(SIG*R,0,H2,IER)
      P1=(H1+C*H2)*FACT
      P2=(S1*H1+S2*C*H2)*FACT
      PP1=(S1P*H1+CP*S2P*H2)*FACT
      PP2=(H1+CP*H2)*FACT
      DELH1=0.
      IF(R.NE.0.) CALL BESJ(E*R,1,.001,DELH1,IER)
      IF(IC.EQ.1) CALL BESI(E*R,1,DELH1,IER)
      CALL BESI(SIG*R,1,DELH2,IER)
      IF(IC.EQ.1)DELH1=-DELH1
      RP1=(-E*DELH1+C*SIG*DELH2)*FACT
      RP2=(-S1*E*DELH1+S2*C*SIG*DELH2)*FACT
      RPP1=(-S1P*E*DELH1+CP*S2P*SIG*DELH2)*FACT
      RPP2=(-E*DELH1+CP*SIG*DELH2)*FACT
      GO TO 31
   29 CONTINUE
      R=DR1*FLOAT(M1-1)+DR2*FLOAT(J-M1-1)
      CALL BESI(AKFR*R,0,H1,IER)
      CALL BESI(AKTR*R,0,H2,IER)
      CALL BESK(AKFR*R,0,H3,IER)
      CALL BESK(AKTR*R,0,H4,IER)
      CALL BESI(AKFR*R,1,DELH1,IER)
      CALL BESI(AKTR*R,1,DELH2,IER)
      CALL BESK(AKFR*R,1,DELH3,IER)
      CALL BESK(AKTR*R,1,DELH4,IER)
      P1=F*FACT*(H1*FBK1+H3*FBI1)
      P2=S3*P1+G*FACT*(H2*TBK1+H4*TBI1)
      PP1=FP*FACT*(H1*FBK1+H3*FBI1)+GP*S3P*FACT*(H2*TBK1+H4*TBI1)
      RPP1=FP*FACT*(AKFR*FBK1*DELH1-AKFR*FBI1*DELH3)+GP*S3P*FACT
     1*(AKTR*DELH2*TBK1-AKTR*DELH4*TBI1)
      PP2=GP*FACT*(H2*TBK1+H4*TBI1)
      RPP2=GP*FACT*(AKTR*DELH2*TBK1-AKTR*DELH4*TBI1)
      RP1=F*FACT*(AKFR*FBK1*DELH1-AKFR*DELH3*FBI1)
      RP2=S3*   RP1+G*FACT*(AKTR*DELH2*TBK1-AKTR*DELH4*TBI1)
   31 ZP1=P1*FACT1
      ZP2=P2*FACT1
      ZPP2=PP2*FACT1
      ZPP1=PP1*FACT1
      DEL1=RPP1*RP1+ZP1*ZPP1
      DEL2=RPP2*RP2+ZP2*ZPP2
      WRITE(6,30)ZH,R,P1,P2,PP1,PP2,DEL1,DEL2
   30 FORMAT(1H ,8E14.4)
      WRITE(7,32)P1,P2,PP1,PP2,DEL1,DEL2
   32 FORMAT(1H ,6E13.4)
   28 CONTINUE
      RETURN
      END
```

```
      SUBROUTINE YREAD
C DATA READIN ROUTINE UTILIZING THE FREE FORMAT READ OPTION
      COMMON DTC,ETC,DFC,EFC,ETAF,DTR,ETR,DFR,EFR,PP,EPSLON,ALPHA
      CALL READX(ALPHA)
      CALL READX(DTC)
      CALL READX(ETC)
      CALL READX(DFC)
      CALL READX(EFC)
      CALL READX(ETAF)
      CALL READX(DTR)
      CALL READX(ETR)
      CALL READX(DFR)
      CALL READX(EFR)
      CALL READX(PP)
      CALL READX(EPSLON)
      WRITE(6,1)ALPHA,DTC,ETC,DFC,EFC,ETAF,DTR,ETR,DFR,EFR,PP,EPSLON
    1 FORMAT(1H ,12E11.4)
      RETURN
      END
```

```
      SUBROUTINE FIND(T,J)
C  THIS IS THE SEARCH ROUTINE USED TO FIND THE ZERO OF THE DETERMINANT
C  GIVEN BY SUBROUTINE DET(T,J,F)
      DIMENSION T(13)
C  INITIALIZATION
      IT=0
C  INITIAL GUESS AT THE CRITICAL VALUE OF THE J-TH PARAMETER
      XL=T(J)
      XR=T(J)
C  LEFT AND RIGHT EXTREMES
    3 XL=XL/1.1
      XR=XR*1.1
      IT=IT+1
C  IF THE ROOT CANNOT BE FOUND TO WITHIN 1.E-06 IN 20 TRIES,THEN STOP
C  THE SEARCH
      IF(IT.EQ.20)GO TO 8
    2 T(J)=XL
      CALL DET(T,J,FL)
      T(J)=XR
      CALL DET(T,J,FR)
C  IF ROOT IS NOT BETWEEN THE LEFT AND RIGHT EXTREMES,READJUST THESE
C  EXTREMES AND START AGAIN
      IF(FR*FL.GT.0.)  GO TO 3
C  IF THE LEFT AND RIGHT EXTREMES ARE EQUAL TO WITHIN 1.E-06, STOP
C  THE SEARCH
      IF(XR-XL.LT.1.E-06)  GO TO 1
      X=(XL+XR)/2.
      T(J)=X
      CALL DET(T,J,F)
C  IF THE DETERMINANT IS EQUAL TO ZERO,STOP THE SEARCH
      IF(F.EQ.0.)GO TO 1
C  READJUST THE LEFT AND RIGHT EXTREMES ACCORDING TO THE RESULTS OF THE
C  LAST GUESS
      IF(F*FL.GT.0.)XL=X
      IF(F*FR.GT.0.)XR=X
      GO TO 2
    1 T(J)=X
      RETURN
    8 WRITE(6,9)J
    9 FORMAT(1H ,*  ERROR*,I5)
      T(J)=1.E+06
      RETURN
      END
```

APPENDIX 6

LATREP, A LATTICE REPRESENTATION CODE

A6.0 INTRODUCTION

In order to provide a basis for the discussion of LATREP proper, it is necessary to consider some general theory. A complete description can be found in references (30,32-33).

A6.1 COLLISION PROBABILITIES

Consider a series of concentric annular regions representing the cell under consideration. The inner region is designated 1, the next is designated 2, and so on to the N^{th} or outer annulus. Neutrons diffuse through these regions and interact with point nuclei within the regions. All interactions are called collisions. Between collisions, neutrons move without change of velocity or momentum and may freely cross the boundaries of the regions. Upon collision with a nucleus, a neutron is considered to have been born in the collision, though in an elastic process the same neutron may exist from before to after the collision. Emitted particles emerge isotropically. Collisons may decrease the number of neutrons (capture), increase the number (fission), or alter the velocity and momentum.

Consider now a single annular region, and the neutrons within it. One may distinguish three sources of neutrons; they enter across

the inner boundary, enter across the outer boundary, or are born in the above sense from collisions within the volume of the annulus. Similarly there are three distinct sinks of neutrons: they may leave across the inner boundary, across the outer boundary or die in a collision within the volume of the annulus. No other disposition of the neutrons is possible with the given assumptions.

We now define a series of probabilities relating these sources and sinks of neutrons, i.e., the probability that a neutron born in process, x, will die by process, y. In the n^{th} annulus, we express this collision probability as

$$p_n^{xy} \tag{A6.1}$$

where x and y may each have one of the three values:

v = collision within the volume of the annulus;

i = crossing the inner boundary;

o = crossing the outer boundary;

and we have a total of nine single collision probabilities for the n^{th} annulus. From reciprocity, conservation and geometric considerations, these nine probabilities can be expressed in terms of two, simple algebraic expressions.

Knowing these probabilities, the collision rates and neutron currents follow directly.

A6.2 CROSS SECTION CONVENTION

In the computer code, LATREP, the fixed cut-off convention is used, denoting the arbitrary but traditional cut-off of 0.625 ev dividing the Maxwellian thermal flux energy distribution from the epi-thermal or 1/E portion. The Maxwellian and 1/E distributions are used for averaging the fundamental parameters over the thermal and epi-thermal energy range as in appendix 1. In addition, the fast neutron energy distribution is taken as that of the fission spectrum, a realistic assumption, for purposes of cross sectional averaging. The distribution is, however, split into two energy regions at 1.4 Mev, the U-238 fast fission threshold.

The energy spectrum can thus be characterized by the effective neutron temperature of the Maxwellian distribution, the fraction of neutrons in the 1/E segment or equivalently the parameter, r, defined as a function of the fraction, and the relative fractions in the two fast neutron groups. Flux weighted cross sectional averaging, then, is accomplished by obtaining weighted averages using these 4 groups. Integral averages within these groups can be done a priori since the distributions within these groups are known functions.

For the special purpose of calculating the resonance escape probability, p, the 1/E spectrum is subdivided into 32 groups in order to pick up the detail in the resonance structure of the U-238 cross section and to account for the perturbations in the 1/E spectrum due to the absorption resonances.

A6.3 NEUTRON CYCLE AND LATTICE PARAMETERS

Governed by the collision probabilities, the neutrons undergo a cycle in the fission chain reaction. This neutron cycle is defined in figure A6.1. The reactivity of the lattice is defined in terms of reaction rates with the following notation:

Y = yield;

A = absorption;

and

L = leakage;

with subscripts,

f = fast neutrons,

r = resonance neutrons,

e = epi-cutoff neutrons,

s = sub-cutoff neutrons,

t = total.

From the definition of the infinite multiplication factor we have

$$k_\infty = \varepsilon\eta f p = Y_t/A_t \quad . \tag{A6.2}$$

Using figure A6.1, the above equations and the physical interpretations of the lattice parameters, ε, η, f, and p, we arrive at

$$\varepsilon = \frac{Y_t - A_f}{Y_s + Y_e} \quad , \tag{A6.3}$$

$$p = \frac{Y_t - A_f - A_r}{Y_t - A_f} \tag{A6.4}$$

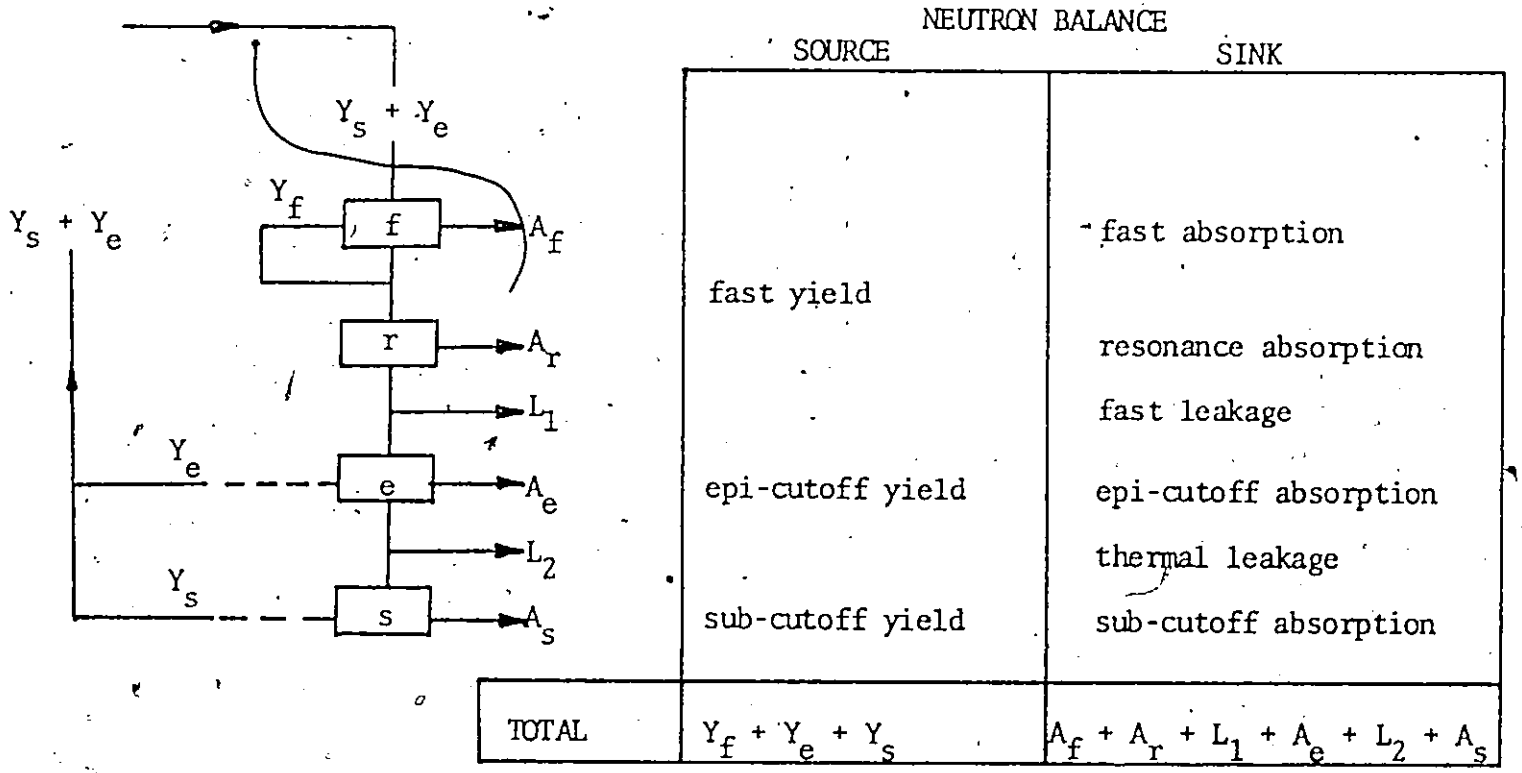

FIGURE A6.1: Neutron cycle.

and

$$\eta f = \frac{Y_s + Y_e}{A_s + A_e} \quad , \tag{A6.5}$$

all of which can be calculated utilizing the collision probabilities defined previously.

A6.4 CALCULATIONAL CYCLE

From this brief introduction into the calculational details, it is evident that an iterative process is necessary; the parameter values and the flux distributions depend on the energy spectrum description (r, etc.) while the energy spectrum depends on the parametric values and the fluxes.

The resonance escape calculation can be performed without iteration and is done first. An estimate of the value of r and the spatial distribution of flux is taken and the iterative loop is entered. The collision probabilities rates and currents are calculated using the library's fundamental cross sections and the estimated values of r and the fluxes. Next the fast spectrum and ϵ are calculated followed by the slowing down areas. The new value of r is then obtained from the fluxes and cross sections previously calculated. This new r is a function of space. The neutron temperature is updated using empirical correlations which are a function of the physical temperature, r and the fluxes. Finally the fine structure and hyperfine structure of the thermal flux is calculated to obtain an estimate of f and the thermal flux. This calculation loop is repeated until the value of r converges. After convergence, the lattice parameters

of the two-group approximation are readily calculated from the converged spectra and collision probabilities.

It has been estimated (30) that the lattice parameters thus calculated are accurate to within 4 - 10% provided the code is not used for the next generation fuels, thorium and plutonium.

APPENDIX 7

COMPUTER CODE FOR THE TWO-GROUP NUMERICAL MODEL

The neutron flux equations for the two-group, two-region model for space dependent void fraction and parameters are solved by the alternating direction implicit technique discussed in section 4.3.1. The flow diagram of this code is given by figures A7.1 and A7.2. A program listing, with comments, is also given in the following.

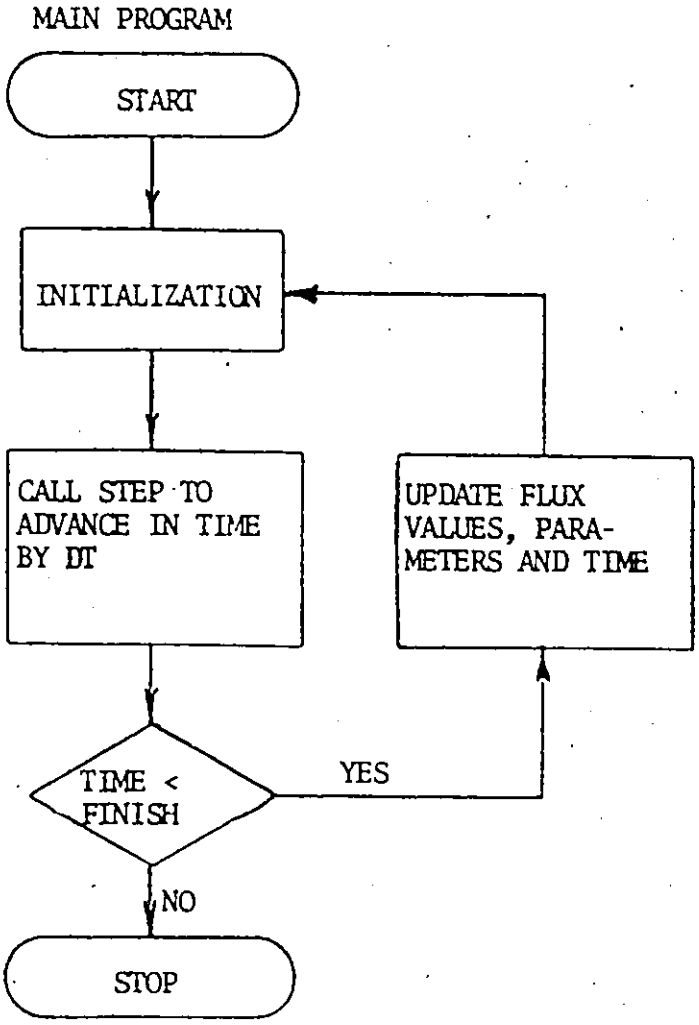

FIGURE A7.1: Flowchart for the numerical solution of the non-linear, transient two-group neutron diffusion equations by the ADI technique: main program.

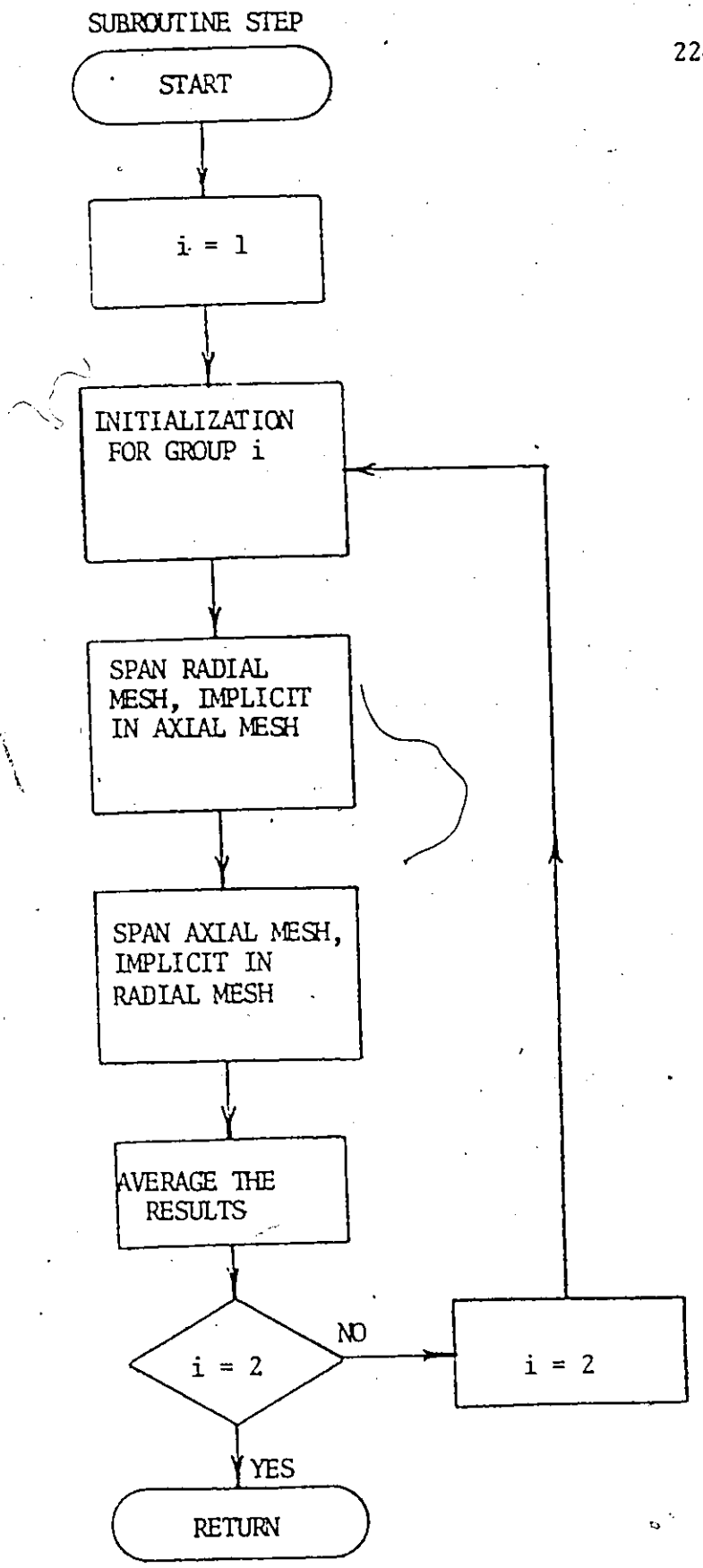

FIGURE A7.2: Flowchart for the numerical solution of the non-linear, transient, two-group neutron diffusion equations by the ADI technique: subroutine STEP.

```
      PROGRAM TST (INPUT,OUTPUT,TAPE5=INPUT,TAPE6=OUTPUT)
C   PROGRAM NAME-ADI
C   COMPUTER-CDC6400
C   LANGUAGE-FORTRAN IV
C   PROBLEM SOLVED- THIS COMPUTER CODE SOLVES THE TWO-GROUP NEUTRON
C   DIFFUSION EQUATIONS IN TWO DIMENSIONS AND TIME FOR A TWO-REGION CELL
C   OF A CANDU-BLW (SEE SECTION 4.2  ) USING THE ALTERNATING DIRECTION
C   IMPLICIT FINITE DIFFERENCE TECHNIQUE AS DESCRIBED IN SECTION 4.3.1.
C   TIME REQUIREMENTS- SEE SECTION 4.3.3
C   C.G.S. SYSTEM OF UNITS USED THROUGHOUT
C   SYMBOLISM-
C   V1     =FAST GROUP VELOCITY
C   V2     =SLOW GROUP VELOCITY
C   TRI    =GAIN FACTOR
C   D1C    =FAST GROUP DIFFUSION COEFFICIENT FOR THE FUEL-COOLANT REGION
C   D2C    =SLOW GROUP DIFFUSION COEFFICIENT FOR THE FUEL-COOLANT REGION
C   D1R    =FAST GROUP DIFFUSION COEFFICIENT FOR THE MODERATOR(REFLECTOR)
C   D2R    =SLOW GROUP DIFFUSION COEFFICIENT FOR THE MODERATOR(REFLECTOR)
C   E1C    =FAST GROUP CROSS SECTION FOR THE FUEL-COOLANT REGION
C   E2C    =SLOW GROUP CROSS SECTION FOR THE FUEL-COOLANT REGION
C   E1R    =FAST GROUP CROSS SECTION FOR THE MODERATOR(REFLECTOR)
C   E2R    =SLOW GROUP CROSS SECTION FOR THE MODERATOR(REFLECTOR)
C   TIME   =TIME
C   DT     =TIME STEP
C   REP    =RESONANCE ESCAPE PROBABILITY
C   ETAF,EPSLON=SEGMENTS OF THE FOUR FACTOR FORMULA
C   N      =NUMBER OF AXIAL NODES
C   M1     =NUMBER OF RADIAL NODES IN FUEL-COOLANT REGION
C   M2     =TOTAL NUMBER OF RADIAL NODES
C   DR1    =RADIAL GRID SIZE IN THE FUEL-COOLANT REGION
C   DR2    =RADIAL GRID SIZE IN THE MODERATOR
C   DZ     =AXIAL GRID SIZE
C   P1(I,J,K)=FAST FLUX AT TIME K,RADIAL NODE I,AXIAL NODE J
C   P2(I,J,K)=SLOW FLUX AT TIME K,RADIAL NODE I,AXIAL NODE J
      DIMENSION A1(11,11),A2(11,11),B1(11,11),B2(11,11),C1(11,11),C2(11,
     111)
      DIMENSION P1(11,11,2),P2(11,11,2),Z1(11,11),Z2(11,11),R1(11,11),
     1R2(11,11),A(11,11),B(11,11),C(11,11),T(3,11),S(11),P(11,11),PR(
     111,11)
C   INITIALIZATION
      DT=2.E-06
      V2=2.E+05
      V1=2.E+05
      TIME=0.
      D1C=1.899
      E1C=.002914
      TRI=1.
      EPSLON=1.0673
      ETAF=1.234
      E2C=.04031
      REP=.911814
      D1R=1.294
      E1R=.01136
      D2R=.8551
      D2C=1.578
      E2R=.0000953
      M1=5
```

```
      M2=11
      MP=M1+1
      N=11
      NM=N-1
C  SET MAXIMUM OF N AND M2 FOR FUTURE USE IN ARRAYS
      NN=N
      IF(M2.GT.N)NN=M2
      DR1=6.37/FLOAT(M1-1)
      DR2=(SQRT(779.-37/3.14159)-6.37)/FLOAT(M2-M1-1)
      DZ=3.14159/SQRT(.333117)/FLOAT(NM)
C  SET INITIAL FLUX DISTRIBUTIONS
      DO 3 J=1,N
      DO 3 I=1,M2
      P1(I,J,1)=1.
      P2(I,J,1)=1.
    3 CONTINUE
      DO 4 I=1,M2
      P1(I,1,1)=0.
      P2(I,1,1)=0.
      P2(I,N,1)=0.
    4 P1(I,N,1)=0.
      POWER1=P1(1,6,1)
C  SET COEFFICIENTS OF EQUATIONS,DEFINED FROM PARAMETERS
    9 DO 2 J=1,N
      DO 1 I=1,M1
      A1(I,J)=V1*D1C
      A2(I,J)=V2*D2C
      B1(I,J)=-V1*E1C
      B2(I,J)=-V2*E2C
      C1(I,J)=TRI*E2C*V1*ETAF*EPSLON
    1 C2(I,J)=  E1C*V2*REP
      DO 2 I=MP,M2
      A1(I,J)=V1*D1R
      A2(I,J)=V2*D2R
      B1(I,J)=-V1*E1R
      B2(I,J)=-V2*E2R
      C1(I,J)=0.
    2 C2(I,J)=E1R*V2
C  ADVANCE FLUXES ONE TIME STEP
      CALL        STEP(DT,DR1,DR2,DZ,P1,P2,A1,A2,B1,B2,C1,C2,M1,M2,N,NN,
     1P,PR,Z1,Z2,R1,R2,A,B,C,T,S)
C  UPDATE TIME
      TIME=TIME+DT
      WRITE(6,8)TIME,TRI
    8 FORMAT(1H ,*   TIME=*,2E14.4)
      WRITE(6,5)((P1(I,J,2),I=1,M2),J=1,N)
    5 FORMAT(1H ,11E12.5)
      WRITE(6,6)
    6 FORMAT(1H ,/)
      WRITE(6,5)((P2(I,J,2),I=1,M2),J=1,N)
      WRITE(6,7)
    7 FORMAT(1H ,///)
C  SETUP FOR THE NEXT ITERATION
      DO 10 I=1,M2
      DO 10 J=1,N
      P1(I,J,1)=P1(I,J,2)
      P2(I,J,1)=P2(I,J,2)
   10 CONTINUE
C  UPDATE THE GAIN ACCORDING TO THE CONTROLLER PRESCRIPTION
      TRI=1.-10.*(P1(1,6,1)-POWER1)
C  STOP IF THE SIMULATION TIME EQUALS THE TIME LIMIT. OTHERWISE,PROCEED
C  WITH THE NEXT ITERATION
      IF(TIME.LT.1.E-03)GO TO 9
      STOP
      END
```

```
      SUBROUTINE STEP(DT,DR1,DR2,DZ,P1,P2,A1,A2,B1,B2,C1,C2,M1,M2,N,NN,
     1P,PR,Z1,Z2,R1,R2,A,B,C,T,S)
C  THIS ROUTINE ADVANCES THE SIMULATION ONE TIME STEP,DT
      DIMENSION P1(M2,N,2),P2(M2,N,2),P(M2,N),PR(M2,N),Z1(M2,N),
     1Z2(M2,N),R1(M2,N),R2(M2,N),A1(M2,N),A2(M2,N),B1(M2,N),B2(M2,N),
     1C1(M2,N),C2(M2,N),T(3,NN),TERM(6),S(NN),A(M2,N),B(M2,N),C(M2,N)
C  INITIALIZATION
      MM1=M1-1
      MM2=M2-1
      NM=N-1
C  THE EQUATIONS CAN BE WRITTEN IN THE GENERAL FORM
C  DP/DT=DEL(A*GRAD P)+B*P+C*PR
      DO 3 I=1,M2
      DO 3 J=1,N
      A(I,J)=A1(I,J)
      B(I,J)=B1(I,J)
      C(I,J)=C1(I,J)
      P(I,J)=P1(I,J,1)
    3 PR(I,J)=P2(I,J,1)
C  DO TWICE,ONCE FOR EACH GROUP
      DO 4 K=1,2
      DO 1 I=1,M2
C  SPAN THE RADIAL SPATIAL MESH
      DR=DR1
      R=DR*FLOAT(I-1)
      IF(I.GT.M1)DR=DR2
      IF(I.GT.M1)R=DR1*FLOAT(M1-1)+DR*FLOAT(I-M1-1)
C  GENERATE THE TERMS TO SET UP THE TRIDIAGONAL MATRICES
C  SPAN THE AXIAL SPATIAL MESH
      DO 2 J=2,NM
      CALL GENRAT(I,J,TERM,DZ,DR,R,A,B,DT,M2,M1,N)
C  GENERATE THE MATRIX EQUATION ELEMENTS USING THE BOUNDARY CONDITIONS,
C  ZERO FLUX AT THE AXIAL END POINTS AND ZERO GRADIENTS AT THE RADIAL
C  END POINTS
      T(2,J)=-TERM(2)/2.+1.
      T(1,J)=-TERM(3)/2.
      T(3,J)=-TERM(1)/2.
      S(J)=(TERM(1)*P(I,J+1)+TERM(2)*P(I,J)+TERM(3)*P(I,J-1))/2.
     1  +P(I,J)+TERM(5)*P(I,J)+C(I,J)*PR(I,J)*DT
      IF(I.EQ.1.OR.I.EQ.M1+1)SAVE=2.*TERM(4)*P(I+1,J)
      IF(I.EQ.M2.OR.I.EQ.M1)SAVE=2.*TERM(6)*P(I-1,J)
      IF(I.NE.1.AND.I.NE.M2.AND.I.NE.M1+1.AND.I.NE.M1)SAVE=TERM(4)*P(
     1 I+1,J)+TERM(6)*P(I-1,J)
      S(J)=S(J)+SAVE
    2 CONTINUE
      T(3,1)=0.
      T(1,N)=0.
      T(2,1)=1.
      T(2,N)=1.
      S(1)=0.
      S(N)=0.
C  THIS TRIDIAGONAL MATRIX IS EXPLICIT IN THE RADIAL DIRECTION
      CALL DIAG3(T,S,N)
C  STORE RESULTS
      IF(K.EQ.2)  GO TO 5
      DO 6 J=1,N
    6 Z1(I,J)=S(J)
```

```
      GO TO 7
    5 DO 8 J=1,N
    8 Z2(I,J)=S(J)
    7 CONTINUE
    1 CONTINUE
C  REPEAT FOR EXPLICIT IN THE AXIAL DIRECTION
      DR=DR1
      RO=0.
      ML=1
      MR=M1
      DO 15 LL=1,2
      DO 9 J=2,NM
      R=RO
      DO 10 I=ML,MR
      L=I-ML+1
      R=RO+DR*FLOAT(L-1)
      CALL      GENRAT(I,J,TERM,DZ,DR,R,A,B,DT,M2,M1,N)
      T(2,L)=-TERM(5)/2.+1.
      T(1,L)=-TERM(6)/2.
      T(3,L)=-TERM(4)/2.
      S(L)=TERM(1)*P(I,J+1)+TERM(2)*P(I,J)+TERM(3)*P(I,J-1)+P(I,J)
     1 +TERM(5)*P(I,J)/2.+C(I,J)*PR(I,J)*DT
      IF(I.EQ.ML)SAVE=2.*TERM(4)*P(I+1,J)
      IF(I.EQ.MR)SAVE=2.*TERM(6)*P(I-1,J)
      IF(I.NE.ML.AND.I.NE.MR)SAVE=TERM(4)*P(I+1,J)+TERM(6)*P(I-1,J)
      S(L)=S(L)+SAVE/2.
   10 CONTINUE
      MA=MR-ML+1
      T(3,1)=T(3,1)+T(1,1)
      T(1,MA)=T(1,MA)+T(3,MA)
      IF(ML.NE.1)GO TO 25
      S(MA)=A(MA-1,J)*P(MA-1,J)/DR1+A(MA+2,J)*P(MA+2,J)/DR2
      T(1,MA)=0.
      T(2,MA)=A(MA-1,J)/DR1+A(MA+2,J)/DR2
      GO TO 26
   25 S(1)=A(ML-2,J)*P(ML-2,J)/DR1+A(ML+1,J)*P(ML+1,J)/DR2
      T(3,1)=0.
      T(2,1)=A(ML-2,J)/DR1+A(ML+1,J)/DR2
   26 CONTINUE
      CALL DIAG3(T,S,MA)
      IF(K.EQ.2)  GO TO 11
      DO 12 I=ML,MR
      L=I-ML+1
   12 R1(I,J)=S(L)
      GO TO 13
   11 DO 14 I=ML,MR
      L=I-ML+1
   14 R2(I,J)=S(L)
   13 CONTINUE
    9 CONTINUE
      DR=DR2
      RO=R
      ML=M1+1
   15 MR=M2
C  REPEAT FOR THE SECOND NEUTRON GROUP
      DO 18 I=1,M2
      DO 18 J=1,N
```

```
      A(I,J)=A2(I,J)
      B(I,J)=B2(I,J)
      C(I,J)=C2(I,J)
      P(I,J)=P2(I,J,1)
   18 PR(I,J)=P1(I,J,1)
    4 CONTINUE
C  AVERAGE THE RESULTS
      DO 16 I=1,M2
      DO 16 J=2,NM
      IF(I.EQ.M1.OR.I.EQ.M1+1)Z1(I,J)=R1(I,J)
      IF(I.EQ.M1.OR.I.EQ.M1+1)Z2(I,J)=R2(I,J)
      P1(I,J,2)=(Z1(I,J)+R1(I,J))/2.
   16 P2(I,J,2)=(Z2(I,J)+R2(I,J))/2.
      DO 17 I=1,M2
      P1(I,1,2)=0.
      P1(I,N,2)=0.
      P2(I,N,2)=0.
   17 P2(I,1,2)=0.
      RETURN
      END
```

```
      SUBROUTINE GENRAT(I,J,TERM,DZ,DR,R,A,B,DT,M2,M1,N)
C  THIS ROUTINE GENERATES THE TERMS FOR THE TRIDIAGONAL MATRIC GIVEN THE
C  COEFFICIENTS OF THE EQUATIONS. THESE TERMS ARISE AS COMMON GROUPS UPON
C  APPLICATION OF FINITE DIFFERENCING TO THE NEUTRON EQUATIONS
      DIMENSION TERM(6),A(M2,N),B(M2,N)
      S1=(A(I,J+1)-A(I,J-1))/4./DZ/DZ
      S2=A(I,J)/DZ/DZ
      TERM(1)=(S2+S1)*DT
      TERM(2)=(-2.*S2+B(I,J)/2.)*DT
      TERM(3)=(S2-S1)*DT
      IF(I.EQ.1)GO TO 1
      IF(I.EQ.M1)GO TO 1
      IF(I.EQ.M1+1)  GO TO 1
      IF( I.EQ.M2) GO TO 1
      S1=((A(I+1,J)-A(I-1,J))/2./DR    +A(I,J)/R)/2./DR
      GO TO 2
    1 S1=0.
    2 S2=A(I,J)/DR/DR
      IF(I.EQ.1)S2=S2*2.
      TERM(4)=(S2+S1)*DT
      TERM(5)=(-2.*S2+B(I,J)/2.)*DT
      TERM(6)=(S2-S1)*DT
      RETURN
      END
```

APPENDIX 8

COMPUTER CODE FOR THE TRANSFORMED TWO-GROUP NUMERICAL MODEL

The neutron flux equations for the two-group, two-region model, employing the transformation of section 4.2, for space dependent void fraction and parameters are solved by the alternating direction implicit technique discussed in section 4.3.1. The flow diagram of this code is given by figures A8.1 and A8.2. A program listing, with comments, is also given in the following.

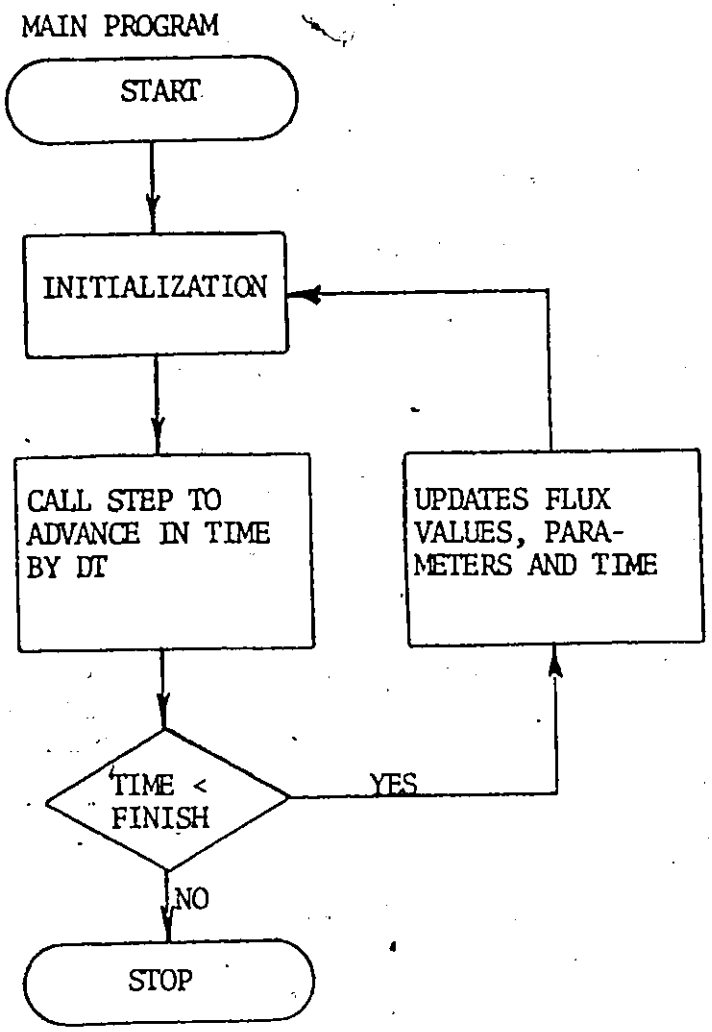

FIGURE A8.1: Flowchart for the numerical solution of the non-linear, transient, two-group neutron diffusion equations by the TADI technique: main program.

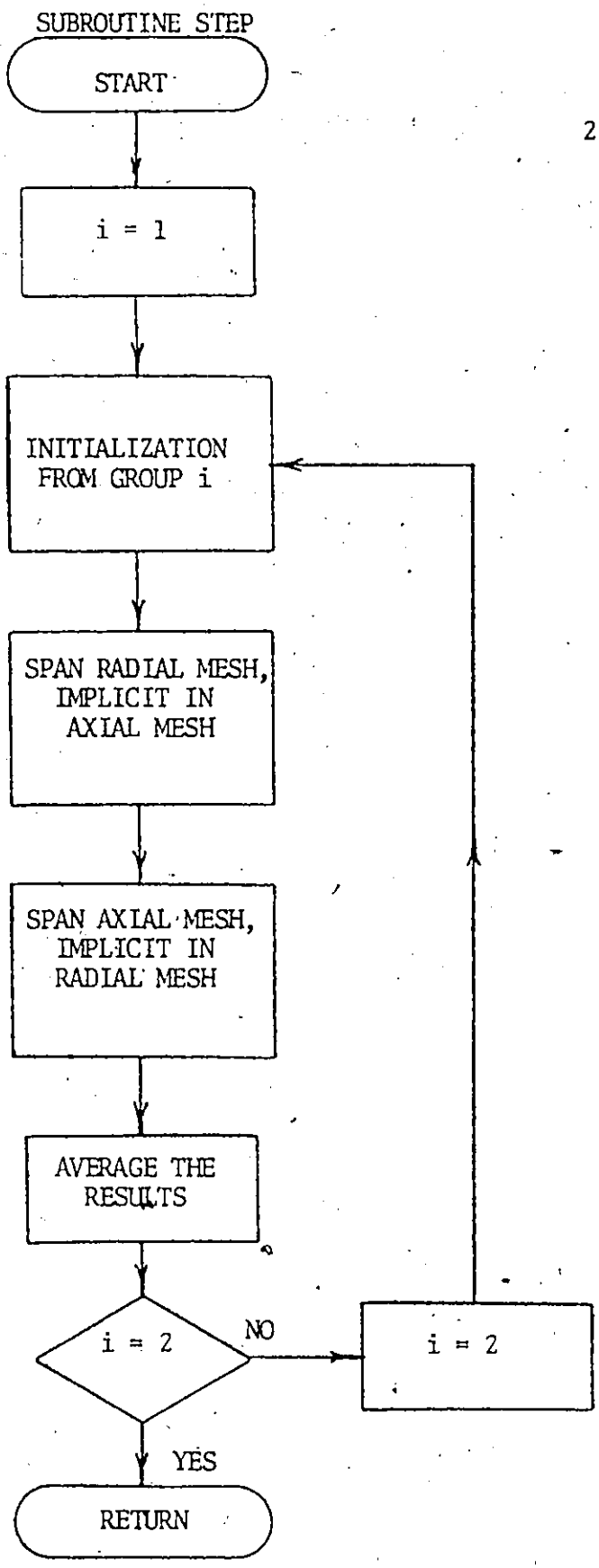

FIGURE A8.2: Flow chart for the numerical solution of the non-linear, transient, two-group neutron diffusion equations by the TADI technique: subroutine STEP.

```
      PROGRAM TS(INPUT,OUTPUT,PUNCH,TAPE5=INPUT,TAPE6=OUTPUT,TAPE7=PUNCH
     1)
C   PROGRAM NAME-TADI
CC  COMPUTER-CDC6400
CC  LANGUAGE-FORTRAN IV
C   PROBLEM SOLVED-THIS COMPUTER CODE SOLVES THE TRANSFORMED TWO-GROUP NEUTRO
C   DIFFUSION EQUATIONS IN TWO DIMENSIONS AND TIME FOR A TWO-REGION CELL
C   OF A CANDU-BLW (SEE SECTION 4.2  ) USING THE ALTERNATING DIRECTION
C   IMPLICIT FINITE DIFFERENCE TECHNIQUE AS DESCRIBED IN SECTION 4.3.1.
C   TIME REQUIREMENTS- SEE SECTION 4.3.3
C   C.G.S. SYSTEM OF UNITS USED THROUGHOUT
C   SYMBOLISM-
C   V1     =FAST GROUP VELOCITY
C   V2     =SLOW GROUP VELOCITY
C   TRI    =GAIN FACTOR
C   ST(1)  =SLOW GROUP DIFFUSION COEFFICIENT FOR THE FUEL-COOLANT REGION
C   ST(2)  =SLOW GROUP CROSS SECTION FOR THE FUEL-COOLANT REGION
C   ST(3)  =FAST GROUP DIFFUSION COEFFICIENT FOR THE FUEL-COOLANT REGION
C   ST(4)  =FAST GROUP CROSS SECTION FOR THE FUEL-COOLANT REGION
C   ST(5)*ST(11)=ETA*F*EPSLON OF THE FOUR FACTOR FORMULA
C   ST(6)  =SLOW GROUP DIFFUSION COEFFICIENT FOR THE MODERATOR(REFLECTOR)
C   ST(7)  =SLOW GROUP CROSS SECTION FOR THE MODERATOR(REFLECTOR)
C   ST(8)  =FAST GROUP DIFFUSION COEFFICIENT FOR THE MODERATOR(REFLECTOR)
C   ST(9)  =FAST GROUP CROSS SECTION FOR THE MODERATOR(REFLECTOR)
C   ST(10)=RESONANCE ESCAPE PROBABILITY
C   TIME   =TIME
C   DT     =TIME STEP
C   N      =NUMBER OF AXIAL NODES
C   M1     =NUMBER OF RADIAL NODES IN FUEL-COOLANT REGION
C   M2     =TOTAL NUMBER OF RADIAL NODES
C   DR1    =RADIAL GRID SIZE IN THE FUEL-COOLANT REGION
C   DR2    =RADIAL GRID SIZE IN THE MODERATOR
C   DZ     =AXIAL GRID SIZE
C   P1(I,J,K)=FAST FLUX AT TIME K,RADIAL NODE I,AXIAL NODE J
C   P2(I,J,K)=SLOW FLUX AT TIME K,RADIAL NODE I,AXIAL NODE J
C   VOID   =VOID FRACTION
C   GEN    =HEAT GENERATION
C   ITS    =ITERATION CONTROL PARAMETER REQUIRED FOR SUBROUTINE VOIDS
C   HR     =HEIGHT,REQUIRED FOR SUBROUTINE VOIDS
      DIMENSION A1(11,11),A2(11,11),B1(11,11),B2(11,11),C1(11,11),C2(11,
     111)
      DIMENSION P1(11,11,2),P2(11,11,2),Z1(11,11,1),Z2(11,11,1),
     1 R1(11,11,1),R2(11,11,1)  ,AA1(11,11),AA2(11,11)
     1          ,A(11,11),B(11,11),C(11,11),T(3,11),S(11),P(11,11),PR(
     111,11)  ,ALF(11,11,2),P11(11,11),P12(11,11),P21(11,11),P22(11,11)
     1,Q(11,11),Q11(11,11),Q12(11,11), Q21(11,11),Q22(11,11),BUC(11,11,2
     1),U(11,11,12)
      DIMENSION ST(11,11),VOID(11),GEN(11)
      DIMENSION TABLE(11,11)
      DIMENSION TERM(6)
C   INITIALIZATION
CC  READ IN PARAMETRIC DATA AS A FUNCTION OF VOID FRACTION,(J-1)/10.,
C.  AND STORE IN TABLE.
      DO 43 J=1,11
      CALL READX(DUM)
      DO 43 I=1,11
      CALL READX(TABLE(I,J))
```

```
      IF(I.EQ.5)TABLE(I,J)=TABLE(I,J)*1.029/1.124
   43 CONTINUE
      AR=.7
      ITE=0
      AIME=0.
      TIME=0.
      OPRINT=1.E-04
      PRINT=0.
      DT=2.E-06
      V1=2.E+05
      V2=2.E+05
      TRI=1.
      M2=11
      N=11
      M1=5
      MP=M1+1
      NM=N-1
      NN=N
C   SET MAXIMUM OF N AND M2 FOR FUTURE USE IN ARRAYS
      IF(M2.GT.N)NN=M2
      DR2=(SQRT(779.43/3.14159)-6.37)/FLOAT(M2-M1-1)
      DR1=6.37/FLOAT(M1-1)
      DZ=3.14159/SQRT(.000117)/FLOAT(NM)
      HR=DZ*FLOAT(NM)
      POWER1=0.
C   BYPASS OPTION- AT TIME=0,PUNCHED OUTPUT FROM THE TWO-GROUP ANALYTICAL
C   MODEL CODE IS USED TO GIVE THE STARTING FLUX VALUES AND POWER1,
C   AINT,TIME,TRI,AND DT NEED NOT BE SUPPLIED EXTERNALLY.AT THE END OF
C   THE SIMULATION,AS WELL AS AT INTERVALS OF .5E-03 SEC,PUNCHED OUTPUT
C   GIVES THE VALUES OF THE FLUXES,POWER1,AINT,TIME,TRI AND DT NEEDED TO
C   RESUME THE SIMULATION IF REQUIRED. THUS FOR SUBSEQUENT ITERATIONS,
C   SET IOPT=0
      IOPT=1
      IF(IOPT.EQ.1)GO TO 30
      CALL READX(POWER1)
      CALL READX(AINT)
      CALL READX(TIME)
      PRINT=TIME
      CALL READX(TRI)
      CALL READX(DT)
   30 CONTINUE
C   SET INITIAL FLUX DISTRIBUTIONS
      DO 3 J=1,N
      DO 3 I=1,M2
      BUC(I,J,1)=0.
      BUC(I,J,2)=0.
      CALL READX(P1(I,J,1))
      CALL READX(P2(I,J,1))
      IF(IOPT.EQ.1)GO TO 31
      CALL READX(BUC(I,J,1))
      CALL READX(BUC(I,J,2))
   31 CONTINUE
    3 CONTINUE
      DO 4 I=1,M2
      BUC(I,1,2)=0.
      BUC(I,N,2)=0.
      BUC(I,N,1)=0.
```

```
      BUC(I,1,1)=0.
      P1(I,1,2)=0.
      P1(I,N,2)=0.
      P2(I,N,2)=0.
      P2(I,1,2)=0.
      P1(I,1,1)=0.
      P2(I,1,1)=0.
      P2(I,N,1)=0.
 4    P1(I,N,1)=0.
      WRITE(6,5)((P1(I,J,1),I=1,M2),J=1,N)
 5    FORMAT(1H ,11E12.5)
      WRITE(6,6)
 6    FORMAT(1H ,/)
      WRITE(6,5)((P2(I,J,1),I=1,M2),J=1,N)
      WRITE(6,7)
 7    FORMAT(1H ,///)
      IF(IOPT.EQ.1)GO TO 47
      DO 48 I=1,N
      CALL READX(DUM)
 48   CONTINUE
 47   CONTINUE
      IF(IOPT.EQ.0)GO TO 100
      POWER1=P1(1,6,1)
      AINT=0.
100   CONTINUE
 45   CONTINUE
C  THE FOLLOWING ADJUSTS THE VALUE OF HEAT,THE PROPORTIONALITY CONSTANT
C  BETWEEN  HEAT GENERATION AND LOCAL THERMAL FLUX ,TO GIVE THE
C  REQUIRED AVERAGE VOID,AB. THIS SECTION CAN BE BYPASSED FOR GIVEN
C  VOID DISTRIBUTION INPUTS.
      ICC=0
      HEATL=1.E+04
      HEATU=5.E+05
      HEAT=HEATU
 302  CONTINUE
      DO 39 J=1,N
      SAVE=3.14159*DR1*DR1
      DO 40 I=1,M1
      CALC=FLOAT(I-1)*2.
      IF(I.EQ.1)CALC=1.
      IF(I.EQ.M1)CALC=CALC/2.
 40   CALC=CALC*P2(I,J,1)*SAVE
 39   GEN(J)=CALC*HEAT
C  SUBROUTINE VOIDS CALCULATES THE AXIAL VOID FRACTION DISTRIBUTION AS PER
C  APPENDIX 10
      CALL VOIDS(GEN,N,VOID,ITE,HR)
      VAVER=(VOID(1)+VOID(N))/2.
      DO 305 I=2,NM
305   VAVER=VAVER+VOID(I)
      VAVER=VAVER/10.
      WRITE(6,303)HEAT,VOID(N) ,VAVER
303   FORMAT(1H ,3E14.5)
      IF(ICC.EQ.0)GO TO 401
      IF(ICC.EQ.1)GO TO 402
      IF(ABS(VAVER-AB).LT.1.E-04)GO TO 400
      IF(ICC.GT.100)STOP
      IF(VAVER.LT.AB)HEATL=HEAT
```

```
      IF(VAVER.GT.AB)HEATU=HEAT
      IF(VAVER.GT.AB)VAVERU=VAVER
      IF(VAVER.LT.AB)VAVERL=VAVER
      HEAT=HEATL-(HEATU-HEATL)*(VAVERL-AB)/(VAVERU-VAVERL)
      ICC=ICC+1
      GO TO 302
  401 ICC=1
      HEAT=HEATL
      VAVERU=VAVER
      GO TO 302
  402 ICC=2
      VAVERL=VAVER
      HEAT=HEATL-(HEATU-HEATL)*(VAVERL-AB)/(VAVERU-VAVERL)
      GO TO 302
  400 CONTINUE
C   GENERATE COEFFICIENTS OF FLUX EQUATIONS FROM THE TABLE OF PARAMETRIC
C   VALUES AS A FUNCTION OF VOID FRACTION,GIVEN THE AXIAL VOID
C   DISTRIBUTION.
      CALL COEFF(ST,N,VOID,TABLE)
      IV=0
C   SET COEFFICIENTS OF EQUATIONS,DEFINED FROM PARAMETERS
C   FOR RADIAL VOID DISTRIBUTIONS,WE CAN GENERATE THE COEFFICIENTS IN A
C   SIMILAR FASHION
    9 DO 2 J=1,N
      DO 1 I=1,M1
      A1(I,J)=V1*ST(3,J)
      A2(I,J)=V2*ST(1,J)
      B1(I,J)=-V1*ST(4,J)
      B2(I,J)=-V2*ST(2,J)
      C1(I,J)=V1*ST(2,J)*ST(5,J)*ST(11,J)*TRI
    1 C2(I,J)=V2*ST(10,J)*ST(4,J)
      DO 2 I=MP,M2
      A1(I,J)=V1*ST(8,J)
      A2(I,J)=V2*ST(6,J)
      B1(I,J)=-V1*ST(9,J)
      B2(I,J)=-V2*ST(7,J)
      C1(I,J)=0.
    2 C2(I,J)=V2*ST(9,J)
C   ADVANCE FLUXES ONE TIME STEP
   33 CALL      STEP(DT,DR1,DR2,DZ,P1,P2,A1,A2,B1,B2,C1,C2,M1,M2,N,NN,
     1P,PR,Z1,Z2,R1,R2,A,B,C,T,S,ALF,P11,P12,P21,P22,AA1,AA2,Q,Q11,Q12,
     1Q21,Q22,BUC,U,IFLIP)
C   UPDATE TIME
      AIME=AIME+DT
      TIME=TIME+DT
C   TO SAVE PRINTING TIME, THE FLUX DISTRIBUTIONS ARE PRINTED ONLY EVERY
C   1.E-04 SEC.
      IF(TIME.LT.PRINT)GO TO 44
      PRINT=PRINT+DPRINT
      WRITE(6,8)TIME ,TRI,DT
    8 FORMAT(1H ,*   TIME=*,3E14.6)
      WRITE(6,5)((P1(I,J,2),I=1,M2),J=1,N)
      WRITE(6,6)
      WRITE(6,5)((P2(I,J,2),I=1,M2),J=1,N)
      WRITE(6,7)
   44 CONTINUE
C   SETUP FOR THE NEXT ITERATION
```

```
      DO 10 I=1,M2
      DO 10 J=1,N
      P2(I,J,1)=P2(I,J,2)
      P1(I,J,1)=P1(I,J,2)
   10 CONTINUE
C  UPDATE THE GAIN TO THE CONTROLLER PRESCRIPTION
      AINT=V1*DT*(P1(1,3,1)-POWER1)-AINT
      TRI=1.-10.*(P1(1,6,1)-POWER1) -AINT
C  THE VOID DISTRIBUTION IS UPDATED WHEN IV=1,IE,  EVERY .5E-03 SEC.
      IF(IV.GE.1)GO TO 45
C  THE RESULTS ARE PUNCHED ON CARDS AT REGULAR INTERVALS OF SIMULATION
C  TIME, .5E-03 SEC TO PROVIDE STARTING VALUES FOR SUBSEQUENT SIMULATIONS
      IF(AIME.LT. .5E-03)GO TO 9
      WRITE(6,8)TIME ,TRI,DT
      WRITE(6,5)((P1(I,J,2),I=1,M2),J=1,N)
      WRITE(6,6)
      WRITE(6,5)((P2(I,J,2),I=1,M2),J=1,N)
      WRITE(7,101)POWER1,AINT
  101 FORMAT(1H ,2E14.5)
      WRITE(7,12)TIME,TRI,DT,((P1(I,J,1),P2(I,J,1),BUC(I,J,1),BUC(I,J,2)
     1,I=1,M2),J=1,N)
   12 FORMAT(1H ,3E14.5,/,(4E14.5))
      WRITE(7,46)(VOID(I),I=1,N)
   46 FORMAT(1H ,(4E14.5))
      IV=1
C  STOP IF THE SIMULATION TIME EQUALS THE TIME LIMIT. OTHERWISE,PROCEED
C  WITH THE NEXT ITERATION
      IF(TIME.GT.2.5E-03)  GO TO 500
      AIME=0.
      GO TO 9
  500 CONTINUE
      STOP
      END
```

```
      SUBROUTINE COEFF(S,N,VOID,TABLE)
C  THIS SUBROUTINE PROVIDES THE PARAMETRIC DATA AS A FUNCTION OF VOID
C  FRACTION BY LINEAR INTERPOLATION BETWEEN THE GIVEN TABLE OF PARAMETRIC
C  VALUES AT 11 VOID FRACTIONS SPACED EQUALLY OVER THE RANGE,0 TO 1.
      DIMENSION S(11,N),VOID(N),TABLE(11,11)
      DO 1 J=1,N
      X=VOID(J)
      L=X*10.
      FRACT=X*10.-FLOAT(L)
      DO 2 I=1,11
      IF(L.EQ.10)GO TO 3
      S(I,J)=TABLE(I,L+1)+FRACT*(TABLE(I,L+2)-TABLE(I,L+1))
      GO TO 2
    3 S(I,J)=TABLE(I,L+1)
    2 CONTINUE
    1 CONTINUE
      WRITE(6,4)(VOID(J),(S(I,J),I=1,11),J=1,N)
    4 FORMAT(1H ,12E10.4)
      RETURN
      END
```

```
      SUBROUTINE STEP(DT,DR1,DR2,DZ,P1,P2,A1,A2,B1,B2,C1,C2,M1,M2,N,NN,
     1P,PR,Z1,Z2,R1,R2,A,B,C,T,S,ALF,P11,P12,P21,P22,AA1,AA2,Q,Q11,Q12,
     1Q21,Q22,BUC,U,IFLIP)
C   THIS ROUTINE ADVANCES THE SIMULATION ONE TIME STEP,DT
      DIMENSION P1(M2,N,2),P2(M2,N,2),P(M2,N),PR(M2,N),Z1(M2,N,1),
     1Z2(M2,N,1),R1(M2,N,1),R2(M2,N,1),AA1(M2,N),AA2(M2,N),
     1                              A1(M2,N),A2(M2,N),B1(M2,N),B2(M2,N),
     1C1(M2,N),C2(M2,N),T(3,NN),TERM(6),S(NN),A(M2,N),B(M2,N),C(M2,N)
     1 ,ALF(M2,N,2),P11(M2,N),P12(M2,N),P21(M2,N),P22(M2,N)     ,
     1Q(M2,N),Q12(M2,N),Q11(M2,N),Q21(M2,N),Q22(M2,N) ,BUC(M2,N,2)
     1,U(M2,N,12)
C   INITIALIZATION
      MM1=M1-1
      MM2=M2-1
      NM=N-1
C   THE EQUATIONS CAN BE WRITTEN IN THE GENERAL FORM
C   DP/DT=DEL(A*GRAD P)+B*P+C*PR
C   CALCULATION OF THE BUCKLING TERMS AS DEFINED IN SECTION 4.2
      DO 88 I=1,M2
      DO 88 J=1,N
      A(I,J)=A1(I,J)
      B(I,J)=B1(I,J)
      P(I,J)=P1(I,J,1)
      PR(I,J)=P2(I,J,1)
   88 CONTINUE
      DO 89 K=1,2
      DO 84 I=1,M2
      DR=DR1
      R=DR*FLOAT(I-1)
      IF(I.GT.M1)DR=DR2
      IF(I.GT.M1)R=DR1*FLOAT(M1-1)+DR*FLOAT(I-M1-1)
      DO 84 J=2,NM
      CALL       GENRAT(I,J,TERM,DZ,DR,R,A ,B ,DT,M2,M1,N)
      BU=TERM(1)*P(I,J+1)+TERM(2)*P(I,J)+TERM(3)*P(I,J-1)+TERM(5)*P(I,J)
      SAVE=TERM(4)*P(I+1,J)+TERM(6)*P(I-1,J)
      IF(I.EQ.1.OR.I.EQ.M1+1)SAVE=2.*TERM(4)*P(I+1,J)
      IF(I.EQ.M2.OR.I.EQ.M1)SAVE=2.*TERM(6)*P(I-1,J)
      BU=(BU+SAVE-B(I,J)*P(I,J)*DT)/DT
      BUC(I,J,K)=BU /P(I,J)
   84 CONTINUE
      DO 90 I=1,M2
      DO 90 J=1,N
      A(I,J)=A2(I,J)
      B(I,J)=B2(I,J)
      P(I,J)=P2(I,J,1)
      PR(I,J)=P1(I,J,1)
   90 CONTINUE
   89 CONTINUE
C   CALCULATION OF THE EIGENVALUES,ALF1 AND ALF2,AND THE EIGENVECTORS
C   P11,P12,P21,P22 AS PER SECTION 4.2
      DO 21 I=1,M2
      DO 21 J=1,N
      BB=-B1(I,J)-B2(I,J) -(BUC(I,J,1)+BUC(I,J,2))
      CC=(B1(I,J )+BUC(I,J,1))*(B2(I,J)+BUC(I,J,2))-C1(I,J)*C2(I,J)
      SQ=SQRT(BB*BB-4.*CC)
      ALF(I,J,1)=-BB+SQ
      ALF(I,J,2)=-BB-SQ
```

```
      ALF(I,J,1)=ALF(I,J,1)/2.
      ALF(I,J,2)=ALF(I,J,2)/2.
      AA1(I,J)=(ALF(I,J,1)-B2(I,J)-BUC(I,J,2))/C2(I,J)
      AA2(I,J)=(ALF(I,J,2)-B2(I,J)-BUC(I,J,2))/C2(I,J)
      P22(I,J)=(P1(I,J,1)-AA1(I,J)*P2(I,J,1))/(AA2(I,J)-AA1(I,J))
      P11(I,J)=AA1(I,J)*P2(I,J,1)-AA1(I,J)*P22(I,J)
      P21(I,J)=P2(I,J,1)-P22(I,J)
      P12(I,J)=P22(I,J)*AA2(I,J)
      IF(J.EQ.1.OR.J.EQ.N)GO TO 21
      P11(I,J)=P11(I,J)/P1(I,J,1)
      P12(I,J)=P12(I,J)/P1(I,J,1)
      P22(I,J)=P22(I,J)/P2(I,J,1)
      P21(I,J)=P21(I,J)/P2(I,J,1)
   21 CONTINUE
      DO 97 II=1,2
      I=M1+II-1
      DO 97 J=1,N
      ALF(I,J,1)=0.
      ALF(I,J,2)=0.
      P11(I,J)=1.
      P22(I,J)=1.
      P12(I,J)=0.
      P21(I,J)=0.
   97 CONTINUE
      IT=1
C  NEXT, THE TRANSFORMATION IS APPLIED TO THE COEFFICIENTS OF THE NEUTRON
C  EQUATIONS AS GIVEN BY EQUATIONS (4.2.50) AND (4.2.51)
      DO 3 I=1,M2
      DO 3 J=1,N
      Q11(I,J)=EXP(ALF(I,J,1)*DT)
      Q22(I,J)=EXP(ALF(I,J,2)*DT)
      FACT1=P11(I,J)*ALF(I,J,1)*Q11(I,J)          +P12(I,J)*ALF(I,J,2)*
     1Q22(I,J)
      FACT2=P11(I,J)*Q11(I,J)          +P12(I,J)*Q22(I,J)
      FACT3=P21(I,J)*Q11(I,J)          +P22(I,J)*Q22(I,J)
      IF(FACT2.EQ.0.)FACT2=1.
      FACT1=FACT1/FACT2
      FACT3=FACT3/FACT2
      A(I,J)=A1(I,J)
      B(I,J)=B1(I,J)       -FACT1
      C(I,J)=C1(I,J)*FACT3
      P(I,J)=P1(I,J,1)
      PR(I,J)=P2(I,J,1)
    3 CONTINUE
C  THE ANALYSIS THEN PROCEEDS AS FOR THE UNTRANSFORMED EQUATIONS
C  DO TWICE,ONCE FOR EACH GROUP
      DO 4 K=1,2
      KK=(K-1)*6
C  SPAN THE RADIAL SPATIAL MESH
      DO 1 I=1,M2
      DR=DR1
      R=DR*FLOAT(I-1)
      IF(I.GT.M1)DR=DR2
      IF(I.GT.M1)R=DR1*FLOAT(M1-1)+DR*FLOAT(I-M1-1)
C  GENERATE THE TERMS TO SET UP THE TRIDIAGONAL MATRICES
C  SPAN THE AXIAL SPATIAL MESH
      DO 2 J=2,NM
```

```
      CALL        GENRAT(I,J,TERM,DZ,DR,R,A,B,DT,M2,M1,N)
C   GENERATE THE MATRIX EQUATION ELEMENTS USING THE BOUNDARY CONDITIONS,
C   ZERO FLUX AT THE AXIAL END POINTS AND ZERO GRADIENTS AT THE RADIAL
C   END POINTS
      L=KK
      U(I,J,L+1)=TERM(1)
      U(I,J,L+2)=TERM(2)
      U(I,J,L+3)=TERM(3)
      U(I,J,L+4)=TERM(4)
      U(I,J,L+5)=TERM(5)
      U(I,J,L+6)=TERM(6)
      T(2,J)=-TERM(2)/2.+1.
      T(1,J)=-TERM(3)/2.
      T(3,J)=-TERM(1)/2.
      S(J)=(TERM(1)*P(I,J+1)+TERM(2)*P(I,J)+TERM(3)*P(I,J-1))/2.
     1+P(I,J)+TERM(5)*P(I,J)+C(I,J)*PR(I,J)*DT
      IF(I.EQ.1.OR.I.EQ.M1+1)SAVE=2.*TERM(4)*P(I+1,J)
      IF(I.EQ.M2.OR.I.EQ.M1)SAVE=2.*TERM(6)*P(I-1,J)
      IF(I.NE.1.AND.I.NE.M2.AND.I.NE.M1+1.AND.I.NE.M1)SAVE=TERM(4)*P(
     1 I+1,J)   +TERM(6)*P(I-1,J)
      S(J)=S(J)+SAVE
    2 CONTINUE
      T(3,1)=0.
      T(1,N)=0.
      T(2,1)=1.
      T(2,N)=1.
      S(1)=0.
      S(N)=0.
C   THIS TRIDIAGONAL MATRIX IS EXPLICIT IN THE RADIAL DIRECTION
      CALL DIAG3(T,S,N)
C   STORE RESULTS
      IF(K.EQ.2)GO TO 5
      DO 6 J=1,N
    6 Z1(I,J,IT)=S(J)
      GO TO 7
    5 DO 8 J=1,N
    8 Z2(I,J,IT)=S(J)
    7 CONTINUE
    1 CONTINUE
C   REPEAT FOR EXPLICIT IN THE AXIAL DIRECTION
      ML=1
      MR=M1
      DO 15 LL=1,2
      DO 9 J=2,NM
      DO 10 I=ML,MR
      L=I-ML+1
      TERM(1)=U(I,J,KK+1)
      TERM(2)=U(I,J,KK+2)
      TERM(3)=U(I,J,KK+3)
      TERM(4)=U(I,J,KK+4)
      TERM(5)=U(I,J,KK+5)
      TERM(6)=U(I,J,KK+6)
      T(2,L)=-TERM(5)/2.+1.
      T(1,L)=-TERM(6)/2.
      T(3,L)=-TERM(4)/2.
      S(L)=TERM(1)*P(I,J+1)   +TERM(2)*P(I,J)   +TERM(3)*P(I,J-1)   +P(I,J)
     1 +TERM(5)*P(I,J)/2.+C(I,J)*PR(I,J)*DT
```

```
      IF(I.EQ.ML)SAVE=2.*TERM(4)*P(I+1,J)
      IF(I.EQ.MR)SAVE=2.*TERM(6)*P(I-1,J)
      IF(I.NE.ML.AND.I.NE.MR)SAVE=TERM(4)*P(I+1,J)+TERM(6)*P(I-1,J)
      S(L)=S(L)+SAVE/2.
   10 CONTINUE
      MA=MR-ML+1
      T(3,1)=T(3,1)+T(1,1)
      T(1,MA)=T(1,MA)+T(3,MA)
C  THE INTERFACIAL BOUNDARY CONDITIONS REQUIRE THAT THE FLUX CURRENTS
C  BE EQUATED WHICH REQUIRES THAT THE TRANSFORMATION BE EVALUATED
C  AT THOSE SPATIAL POINTS.
      IF(ML.NE.1)GO TO 25
      IF(K.EQ.2)GO TO 93
      F1=P11(MA-1,J)*EXP(ALF(MA-1,J,1)*DT)+P12(MA-1,J)*EXP(ALF(MA-1,J,2)
     1   *DT)
      F2=P11(MA  ,J)*EXP(ALF(MA  ,J,1)*DT)+P12(MA  ,J)*EXP(ALF(MA  ,J,2)
     1   *DT)
      F3=P11(MA+1,J)*EXP(ALF(MA+1,J,1)*DT)+P12(MA+1,J)*EXP(ALF(MA+1,J,2)
     1   *DT)
      F4=P11(MA+2,J)*EXP(ALF(MA+2,J,1)*DT)+P12(MA+2,J)*EXP(ALF(MA+2,J,2)
     1   *DT)
      GO TO 94
   93 CONTINUE
      F1=P21(MA-1,J)*EXP(ALF(MA-1,J,1)*DT)+P22(MA-1,J)*EXP(ALF(MA-1,J,2)
     1   *DT)
      F2=P21(MA  ,J)*EXP(ALF(MA  ,J,1)*DT)+P22(MA  ,J)*EXP(ALF(MA  ,J,2)
     1   *DT)
      F3=P21(MA+1,J)*EXP(ALF(MA+1,J,1)*DT)+P22(MA+1,J)*EXP(ALF(MA+1,J,2)
     1   *DT)
      F4=P21(MA+2,J)*EXP(ALF(MA+2,J,1)*DT)+P22(MA+2,J)*EXP(ALF(MA+2,J,2)
     1   *DT)
   94 S(MA)=A(MA,J)*P(MA-1,J)*F1/DR1+A(MA+1,J)*P(MA+2,J)*F4/DR2
      T(2,MA)=A(MA,J)*F2/DR1+A(MA+1,J)*F3/DR2
      T(1,MA)=0.
      GO TO 26
   25 CONTINUE
      IF(K.EQ.2)GO TO 95
      F1=P11(ML-2,J)*EXP(ALF(ML-2,J,1)*DT)+P12(ML-2,J)*EXP(ALF(ML-2,J,2)
     1   *DT)
      F2=P11(ML-1,J)*EXP(ALF(ML-1,J,1)*DT)+P12(ML-1,J)*EXP(ALF(ML-1,J,2)
     1   *DT)
      F3=P11(ML  ,J)*EXP(ALF(ML  ,J,1)*DT)+P12(ML  ,J)*EXP(ALF(ML  ,J,2)
     1   *DT)
      F4=P11(ML+1,J)*EXP(ALF(ML+1,J,1)*DT)+P12(ML+1,J)*EXP(ALF(ML+1,J,2)
     1   *DT)
      GO TO 96
   95 CONTINUE
      F1=P21(ML-2,J)*EXP(ALF(ML-2,J,1)*DT)+P22(ML-2,J)*EXP(ALF(ML-2,J,2)
     1   *DT)
      F2=P21(ML-1,J)*EXP(ALF(ML-1,J,1)*DT)+P22(ML-1,J)*EXP(ALF(ML-1,J,2)
     1   *DT)
      F3=P21(ML  ,J)*EXP(ALF(ML  ,J,1)*DT)+P22(ML  ,J)*EXP(ALF(ML  ,J,2)
     1   *DT)
      F4=P21(ML+1,J)*EXP(ALF(ML+1,J,1)*DT)+P22(ML+1,J)*EXP(ALF(ML+1,J,2)
     1   *DT)
C  FINALLY,AFTER THE EVALUATION, THE B.C. CAN BE APPLIED
   96 S(1)=A(ML-1,J)*P(ML-2,J)*F1/DR1+A(ML,J)*P(ML+1,J)*F4/DR2
```

```
      T(2,1)=A(ML-1,J)*F2/DR1+A(ML,J)*F3/DR2
      T(3,1)=0.
   26 CONTINUE
      CALL DIAG3(T,S,MA)
      IF(K.EQ.2)  GO TO 11
      DO 12 I=ML,MR
      L=I-ML+1
   12 R1(I,J,IT)=S(L)
      GO TO 13
   11 DO 14 I=ML,MR
      L=I-ML+1
   14 R2(I,J,IT)=S(L)
   13 CONTINUE
    9 CONTINUE
C  REPEAT FOR THE SECOND NEUTRON GROUP
      ML=M1+1
   15 MR=M2
      DO 18 I=1,M2
      DO 18 J=1,N
      FACT1=P21(I,J)*ALF(I,J,1)*Q11(I,J)+P22(I,J)*ALF(I,J,2)*Q22(I,J)
      FACT2=P21(I,J)*Q11(I,J)           +P22(I,J)*Q22(I,J)
      FACT3=P11(I,J)*Q11(I,J)           +P12(I,J)*Q22(I,J)
      IF(FACT2.EQ.0.)FACT2=1.
      FACT1=FACT1/FACT2
      FACT3=FACT3/FACT2
      A(I,J)=A2(I,J)
      B(I,J)=B2(I,J)       -FACT1
      C(I,J)=C2(I,J)*FACT3
      P(I,J)=P2(I,J,1)
      PR(I,J)=P1(I,J,1)
   18 CONTINUE
    4 CONTINUE
   20 CONTINUE
C  AVERAGE THE RESULTS
      DO 16 J=2,NM
      Z1(M1,J,1)=R1(M1,J,1)
      Z2(M1,J,1)=R2(M1,J,1)
      Z1(M1+1,J,1)=R1(M1+1,J,1)
      Z2(M1+1,J,1)=R2(M1+1,J,1)
   16 CONTINUE
      DO 82 I=1,M2
      DO 82 J=2,NM
      FACT3=P21(I,J)*Q11(I,J)           +P22(I,J)*Q22(I,J)
      FACT2=P11(I,J)*Q11(I,J)           +P12(I,J)*Q22(I,J)
      P1(I,J,2)=(Z1(I,J,1)+R1(I,J,1))/2.
      P2(I,J,2)=(Z2(I,J,1)+R2(I,J,1))/2.
      P1(I,J,2)=P1(I,J,2)*FACT2
      P2(I,J,2)=P2(I,J,2)*FACT3
   82 CONTINUE
      DO 17 I=1,M2
      P1(I,1,2)=0.
      P1(I,N,2)=0.
      P2(I,N,2)=0.
   17 P2(I,1,2)=0.
      DO 19 J=1,N
      P1(M1,J,2)=(P1(M1,J,2)+P1(M1+1,J,2))/2.
      P2(M1,J,2)=(P2(M1,J,2)+P2(M1+1,J,2))/2.
      P1(M1+1,J,2)=P1(M1,J,2)
   19 P2(M1+1,J,2)=P2(M1,J,2)
      RETURN
      END
```

```
      SUBROUTINE GENRAT(I,J,TERM,DZ,DR,R,A,B,DT,M2,M1,N)
C     THIS ROUTINE GENERATES THE TERMS FOR THE TRIDIAGONAL MATRIC GIVEN THE
CC    COEFFICIENTS OF THE EQUATIONS. THESE TERMS ARISE AS COMMON GROUPS UPON
C     APPLICATION OF FINITE DIFFERENCING TO THE NEUTRON EQUATIONS
      DIMENSION TERM(6),A(M2,N),B(M2,N)
      S1=(A(I,J+1)-A(I,J-1))/4./DZ/DZ
      S2=A(I,J)/DZ/DZ
      TERM(1)=(S2+S1)*DT
      TERM(2)=(-2.*S2+B(I,J)/2.)*DT
      TERM(3)=(S2-S1)*DT
      IF(I.EQ.1)GO TO 1
      IF(I.EQ.M1)GO TO 1
      IF(I.EQ.M1+1)  GO TO 1
      IF( I.EQ.M2)  GO TO 1
      S1=((A(I+1,J)-A(I-1,J))/2./DR     +A(I,J)/R)/2./DR
      GO TO 2
    1 S1=0.
    2 S2=A(I,J)/DR/DR
      IF(I.EQ.1)S2=S2*2.
      TERM(4)=(S2+S1)*DT
      TERM(5)=(-2.*S2+B(I,J)/2.)*DT
      TERM(6)=(S2-S1)*DT
      RETURN
      END
```

APPENDIX 9

DERIVATION OF THE BASIC MASS, MOMENTUM AND ENERGY EQUATIONS

A9.0 - INTRODUCTION

Usually, the equations of motion are derived as differential equations based on an infinitesmal control volume of the system in question. To complete the description, boundary and initial conditions plus constitutive relationships are imposed. This approach is generally appropriate for continuous systems. Applying this differential description to forced convective boiling implies that each phase is treated separately with the appropriate interface boundary conditions applied at the phase discontinuities. Thus, a detailed knowledge of the phenomena at the phase interfaces is required. Such knowledge is presently not available and recourse to the more general integral approach has to be taken. Additionally, large computational expenses would accrue because of the fine structural detail of the system; this provides an extra incentive to find an alternative procedure.

It is possible, as in chapter 5, to reduce the integral form to pseudo-differential form by the appropriate definition of cross-sectional averages of the dependent variables. This is the concept employed by Zuber et al (11,12) and extended by Hancox et al (13,14).

A9.1 THE EQUATION OF CONTINUITY

A mass balance on the density, ρ, of a species within a fixed control volume, $\forall$ can be described in words:

$$\begin{pmatrix}\text{net rate of change}\\ \text{of density within}\\ \text{the volume}\end{pmatrix} = \begin{pmatrix}\text{flux of density}\\ \text{thru the volume}\\ \text{surface}\end{pmatrix} + \begin{pmatrix}\text{internal}\\ \text{sources}\end{pmatrix} \quad \text{(A9.1.1)}$$

or

$$\frac{\partial}{\partial t} \iiint_{\forall} \rho \, d\forall = - \iint_{S} \rho \, \underline{v}.d\underline{s} + \iiint_{\forall} r \, d\forall \quad , \qquad \text{(A9.1.2)}$$

where

t = time [s] ,

$\underline{s}$ = normal surface vector [cm^2] ,

$\underline{v}$ = velocity [cm/s] ,

r = internal sources [$gm/cm^3 s$] ,

and

$\forall$ = volume [cm^2] .

Gauss's theorem,

$$\iiint_{\forall} \nabla \cdot \underline{A} \, d\forall = \iint_{S} \underline{A}.d\underline{s} \quad , \qquad \text{(A9.1.3)}$$

where $\underline{A}$ is an arbitrary vector, enables equation (A9.1.2) to be rewritten as

$$\iiint_{\forall} \left(\frac{\partial \rho}{\partial t} + \nabla \cdot \rho \underline{v} - r\right) d\forall = 0 \quad , \qquad \text{(A9.1.4)}$$

which is the integral form of the continuity equation. From this we can directly get the differential form,

$$\frac{\partial \rho}{\partial t} + \nabla \cdot \rho \underline{v} = \Gamma \ . \qquad \text{(A9.1.5)}$$

Either form is perfectly valid for use in describing the system from a stationary observer or Eulerian point of view. The discussion of section A9.0 dictates that for our purposes, the integral form be adopted.

A9.2 THE MOMENTUM EQUATION

A balance of the forces acting upon the control volume gives, in words:

$$\begin{matrix}\text{response} \\ \text{(acceleration)}\end{matrix} = \text{body force} + \begin{matrix}\text{surface force} \\ \text{(stress)}\end{matrix} \qquad \text{(A9.2.1)}$$

or

$$\iiint_{\forall} \frac{\rho}{g_c} \frac{d\underline{v}}{dt} \, d\forall = \iiint_{\forall} \rho \, \underline{f} \, d\forall + \iint \underline{\underline{\sigma}} \cdot d\underline{s} \ , \qquad \text{(A9.2.2)}$$

where

$\underline{f}$ = body force vector [dynes/gm]

and

$\underline{\underline{\sigma}} = 2^{nd}$ order stress tensor [dynes/cm^2] .

Applying Gauss' theorem again and expanding the total derivative gives,

$$\iiint_{\forall} \left(\frac{\rho}{g_c} \frac{d\underline{v}}{dt} + \rho \, \underline{v} \cdot \nabla \underline{v} - \rho \underline{f} - \nabla \cdot \underline{\underline{\sigma}}\right) d\forall = 0 \ , \qquad \text{(A9.2.3)}$$

the integral form of the momentum equation. As with the continuity equation, dropping the integral yields the differential formulation commonly found in the literature.

A9.3 THE ENERGY EQUATION

As in the previous sections, a control volume balance leads to the conservation equation, this time for energy:

$$\begin{pmatrix}\text{net rate}\\ \text{of accumulation}\\ \text{of energy}\end{pmatrix} = \begin{pmatrix}\text{energy flux}\\ \text{into } \forall\end{pmatrix} + \begin{pmatrix}\text{energy gain from}\\ \text{body forces}\end{pmatrix} + \begin{pmatrix}\text{energy gain from}\\ \text{surface forces}\end{pmatrix} \tag{A9.3.1}$$

or

$$\frac{d}{dt}\iiint_{\forall} \rho\left(e + \frac{v^2}{2g_c}\right) d\forall = -\iint_S \underline{q} \cdot d\underline{s} + \iiint_{\forall} \rho \underline{f} \cdot \underline{v}\, d\forall + \iint_S \underline{v} \cdot \underline{\underline{\sigma}} \cdot d\underline{s} \quad , \tag{A9.3.2}$$

where

e = internal energy [ergs/gm] ,

g_c = proportionality constant [gm cm^2/ergs s^2] ,

and

q = energy flux [ergs/cm^2 s] .

Again manipulation gives the integral form,

$$\iiint_{\forall} \frac{d}{dt}\left(\rho e + \frac{\rho v^2}{2g_c} + \nabla\cdot\underline{q} - \rho\, \underline{f}\cdot\underline{v} - \nabla\cdot(\underline{v}\cdot\underline{\underline{\sigma}})\right) d\forall = 0 \quad , \tag{A9.3.3}$$

and leads to the differential form as before.

A9.4 DISCUSSION

In addition to these basic equations we have the boundary and initial conditions plus the constitutive relationships which provides the detailed phenomenological information of the system such as the structure of the stress tensor, state equation, base enthalpies, etc. Much of this information arrives in the form of empirical correlations derived from experimental observation. This, plus the numerous possible approximations of the basic conservation equations, accounts for the number and the diversity of models arising in the literature. The more successful model approximations are discussed in chapter 5.

APPENDIX 10

COMPUTER CODE FOR HANCOX'S VOID MODEL

The two-phase mass conservation equations and the mixture energy and momentum equations of Hancox's fluid model are solved by 4^{th} order Runge-Kutta integration. The flow diagram of this code is given by figures A10.1 and A10.2. A program listing with comments, is also given in the following.

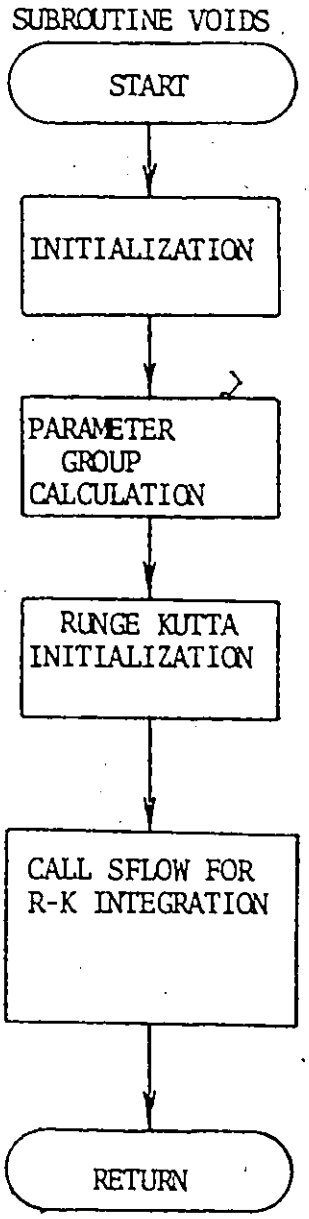

FIGURE A10.1: Flowchart for Hancox's void model using Runge-Kutta integration: subroutine VOIDS.

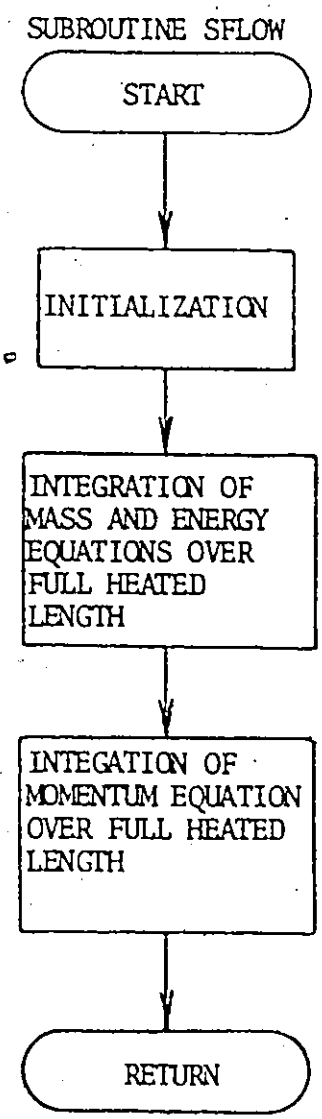

FIGURE A10.2: Flowchart for Hancox's void model using Runge-Kutta integration: subroutine SFLOW.

```
      SUBROUTINE VOIDS(GEN,N,VOID,ITE,HR)
C     THIS IS THE ROUTINE FOR THE AXIAL VOID DISTRIBUTION CALCULATION.
CCCCC THIS WAS OBTAINED FROM W.T.HANCOX (13,14)
CCCCC UNITS,LENGTH(M),MASS(KG),FORCE(N),TEMPERATURE(C),TIME(S),ENERGY(J)
CCCCC SYMBOLISM-
CCCCC AF     =FLOW AREA
CCCCC PH     =HEATED PERIMETER
CCCCC PW     =WETTED PERIMETER
CCCCC PS     =PRESSURE
CCCCC NTIMES=CONTROL PARAMETER FOR AXIAL MESH
CCCCC ZH     =HEATED LENGTH
CCCCC DZ     =AXIAL GRID SIZE
CCCCC DE     =EQUIVALENT WETTED DIAMETER
CCCCC DH     =HYDRAULIC DIAMETER
CCCCC DTIN   =INLET SUBCOOLING
CCCCC G      =MASS FLOW RATE
CCCCC ROF    =DENSITY OF FLUID
CCCCC ROG    =DENSITY OF GAS
CCCCC C01,C02,C31,C32,C0=DISTRIBUTION PARAMETERS AS PER SECTION 5.4
CCCCC F(J)   =VOID FRACTION AS A FUNCTION OF AXIAL POSITION ,J
CCCCC H(J)   =ENTHALPY AS A FUNCTION OF AXIAL POSITION,J
CCCCC V(J)   =VELOCITY AS A FUNCTION OF AXIAL POSITION,J
CCCCC GEN(J)=HEAT FLUX AS A FUNCTION OF AXIAL POSITION ,J
CCCCC N      =NUMBER OF AXIAL MESH POINTS OF THE CALLING PROGRAM
CCCCC ITE    =CONTROL PARAMETER FOR INITIALIZATION  BYPASS
CCCCC HR     =HEATED LENGTH IN CM.
C     VOID   =VOID FRACTION OUTPUTTED AT THE N INPUT AXIAL POSITIONS
      DIMENSION GEN(N),VOID(N)
      DIMENSION F(90),H(90),V(90),DP(90),Z(90),Q(90)  ,   X(90)
      COMMON M,  H,V,F,X,DP,      ROF,ROG,CP,CPM,HFG,PS,VISF,VISG,TK,DZ,
     *DH,DE,PR,BETA,DRO,C01,C02,C31,C32,ZH ,Q
C     INITIALIZATION
C     IF ROUTINE CALLED BEFORE,BYPASS INIALIZATION
      IF(ITE.EQ.1)GO TO 4
C     INITIALIZATION
      CALL READX(AF)
      CALL READX(PH)
      CALL READX(PW)
      CALL READX(PS)
      NTIMES=2
      M=NTIMES*(N-1)+1
      ZH=HR/100.
      DZ=ZH/FLOAT(M-1)
      DE=4.*AF/PW
      DH=4.*AF/PH
      CALL READX(DTIN)
      CALL READX(G)
C     GENERATE  PROPERTIES GIVEN PRESSURE AND  SUBSOOLING
      CALL PROP(PS,DTIN,DHIN,HFG,ROF,ROG,CP,CPM,VISF,VISG,TK,PR)
      WRITE(6,6)AF,PH,PW,PS,DTIN,G
    6 FORMAT(1H ,6E14.5)
    4 CONTINUE
C     CALCULATION OF PARAMETER GROUPS
      DRO=ROF-ROG
      BETA=1.-(ROF/ROG)*(VISG/VISF)**.2
      C01=19.
      C02=1.164-1.6534E-1*PS+.751E-2*PS**2
```

```
      C31=19.
      C32=2.86-4.6412E-1*PS+2.2929E-2*PS**2
C   INITIALIZATION OF RUNGE KUTTA ROUTINE
      Z(1)=0.
      DO 3 J=1,N
      IF(J.GT.1) Z(J)=Z(J-1)+DZ/ZH
    3 CONTINUE
      NL=4 *(N-1)+1
      DO 9 J=1,NL
      F(J)=.001
      H(J)=DHIN/HFG
    9 V(J)=G/ROF
      K=1
      NSUB=4*NTIMES
      DO 10 I=2,N
      DIFF=GEN(I)-GEN(I-1)
      Q(K)=GEN(I-1)
      FRACT=DIFF/FLOAT(NSUB)
      DO 11 J=2,NSUB
   11 Q(K+J-1)=Q(K)+FRACT*FLOAT(J-1)
      K=K+NSUB
   10 CONTINUE
      Q(NL)=GEN(N)
C   RUNGE KUTTA INTEGRATION
      CALL SFLOW
      WRITE(6,7)(GEN(I),I=1,N)
    7 FORMAT(1H ,11E12.4)
      WRITE(6,50)(F(J),X(J),H(J),V(J),DP(J),J=1,M)
   50 FORMAT(1H ,5E14.5)
C   EXTRACTION OF VOID FRACTION RESULTS AT NODAL POINTS CORRESPONDING
C   TO THE NEUTRON MODEL
      L=1
      DO 5 I=1,N
      VOID(I)=F(L)
    5 L=L+NTIMES
      ITE=1
      RETURN
      END
```

```
      SUBROUTINE SFLOW
C     SOLUTION OF THE STEADY STATE FORM OF THE CONSERVATION EQUATIONS
C     EMPLOYING A RUNGE-KUTTA NUMERICAL SCHEME.
      DIMENSION A(5),B(5),F(90),H(90),V(90),DP(90),X(90),DPDZ(90),U(90),
     *Q(90)
      COMMON M,  H,V,F,X,DP,     ROF,ROG,CP,CPM,HFG,PS,VISF,VISG,TK,DZ,
     *DH,DE,PR,BETA,DRO,C01,C02,C31,C32,ZH ,Q
C  INITIALIZATION ACCORDING TO REFERENCES (13,14)
      AG=9.80665
      N=4*(M-1)
      ROUGH=.001
      L=N+1
      S=DZ/4.
      G=ROF*V(1)
      RE=G*DE/VISF
      H0=0.40*TK/DE*PR*CPM/CP*RE**.662
      U(1)=ROF*V(1)**2
      X(1)=0.
      DP(1)=0.
      Z=S
      DO 3 J=2,L
      A(1)=0.
      B(1)=0.
      HSTAR=CP*Q(J)/(H0*HFG)
      WV    =4*Q(J)/(DH*HFG)
      DO 2 I=1,4
      C=2.
      IF(I.EQ.4)C=1.
      HN=H(J-1)+B(I)/C
      FN=F(J-1)+A(I)/C
      IF(FN.GE.1.)JS=J-1
      IF(FN.GE.1.) GO TO 8
      GAMMA=0.
      IF(HSTAR.GT.HN)GAMMA=WV-4.*H0*HN*(1.-FN)**.5/(CP*DH)
      C0=(1.+C02)/(1.-EXP(-C01))*(1.-EXP(-C01*FN))-C02*FN
      DC0=(1.+C02)/(1.-EXP(-C01))*C01*EXP(-C01*FN)-C02
      VN=V(1)/(1.-C0*FN*DRO/ROF)
      A(I+1)=0.
      IF(FN.EQ.0.) GO TO 1
      A(I+1)=S*(1.-C0*FN*DRO/ROF)*GAMMA/ROG/((C0+DC0*FN)*VN)
    1 B(I+1)=-S*(WV-GAMMA)/((1-C0*FN)*ROF*VN)
    2 CONTINUE
C  VOID FRACTION INTEGRATION(MASS BALANCE EQUATION)
      F(J)=F(J-1)+(A(2)+2.*(A(3)+A(4))+A(5))/6.
      IF(F(J).GE.1.)JS=J-1
      IF(F(J).GE.1.)GO TO 8
C  ENTHALPY INTEGRATION (ENERGY BALANCE EQUATION)
      H(J)=H(J-1)+(B(2)+2.*(B(3)+B(4))+B(5))/6.
      C0=(1.+C02)/(1.-EXP(-C01))*(1.-EXP(-C01*F(J)))-C02*F(J)
C  VELOCITY CALCULATION (FROM SECOND MASS BALANCE EQUATION)
      V(J)=V(1)/(1.-C0*F(J)*DRO/ROF)
C  QUALITY CALCULATION(FROM DEFINITION OF QUALITY)
      X(J)=C0*F(J)*V(J)*ROG/G
      C4=C0
      Z=Z+S
      C3=(1.-EXP(-C31*F(J)))*(1.+C32)/(1.-EXP(-C31))-C32*F(J)
      IF(C0.LT.1.)C4=1.05
```

```
    3 U(J)=(C4-C3*DRO*F(J)/ROF)*ROF*V(J)**2
      GO TO 10
    8 CONTINUE
      J1=JS+1
      DO 11 JJ=J1,L
      V(JJ)=V(JS)
      H(JJ)=H(JS)
      F(JJ)=1.
      X(JJ)=C0*F(JJ)*V(JJ)*ROG/G
      U(JJ)=U(JS)
   11 CONTINUE
   10 CONTINUE
C  PRESSURE DROP CALCULATION (FROM MOMENTUM BALANCE EQUATION)
      FF=.0055*(1.+(2.E+4*ROUGH+1.E+6/RE)**.3333)
      R=3.1*(1.-PS/22.106)*EXP(-5.55E-4*G)
      DO 4 J=1,L
      TSTAR=(1.-BETA*X(J))*(1.+R*X(J)**.5*(1.-X(J))**.25)
      TAU=TSTAR*FF*G**2/ROF/2.
      IF(J.EQ.1) DMDZ=(U(J+1)-U(J))/S
      IF(J.EQ.L) DMDZ=(U(J)-U(J-1))/S
      IF((J.GT.1).AND.(J.LT.L)) DMDZ=(U(J+1)-U(J-1))/(2.*S)
      RO=(1.-DRO*F(J)/ROF)*ROF
      DPDZ(J)=-(DMDZ+TAU/DE+AG*RO)
    4 CONTINUE
      DO 5 J=2,L
    5 DP(J)=DP(J-1)+(DPDZ(J)+DPDZ(J-1))*S/2.
      K=1
      DO 6 J=1,M
      F(J)=F(K)
      IF (F(J).LE.0.001)  F(J)=0
      X(J)=X(K)
      H(J)=H(K)
      V(J)=V(K)
      DP(J)=DP(K)
    6 K=K+4
      RETURN
      END
```

```
      SUBROUTINE PROP(PS,DTIN,DHIN,HFG,ROF,ROG,CP,CPM,VISF,VISG,TK,PR)
C   CALCULATION OF PROPERTIES
C   STATE PROPERTIES FOR SATURATED STEAM AND WATER
C   SI UNITS
      PS=PS/6.8948E-3
      DTIN=1.8*DTIN
      TS=EXP(0.22151*ALOG(PS)+4.77123)
      T=TS-DTIN
      HF=EXP(.26452*ALOG(PS)+4.46738)
      HI=-1.18E-3*PS-30.06+(.63E-4*PS+.98)*T-(2.719E-7*PS+.106E-4)*T**2
     1+(3.027E-10*PS+2.439E-7)*T**3
      DHIN=2327.8*(HF-HI)
      HFG=922.15-(0.40516-(1.717E-4-4.219E-8*PS)*PS)*PS
      ROF=63.8-(1.781E-2-(1.132E-5-6.786E-8*TS)*TS)*TS
      VFG=423.8/PS-.126
      IF(PS.GT.300.) VFG=524.0/PS-.10
      ROG=1./(VFG+1./ROF)
      CP=1.024+(2.18036E-4+(7.121E-9+4.1275E-11*PS)*PS)*PS
      VISF=1./(8.506E-3*TS-.3643)+4.1338E-4
      TC=(TS-32.)/1.8
      RO=.0160186*ROG
      V1=.407*TC+80.4
      V2=V1-RO*(1658.-5.9*TC)
      V3=V1+(353.+(676.5+102.1*RO)*RO)*RO
      IF(TC.LT.340.) V4=V2
      IF(TC.GT.365.) V4=V3
      IF(TC.GT.340..AND.TC.LT.365.) V4=((TC-340.)*V3+(365.-TC)*V2)/25.
      VISG=V4*1.E-7
      TT=1.+(TS-32.)/491.67
      TK=-922.47+(2839.5+(-1800.7+(525.77-73.44*TT)*TT)*TT)*TT
      TK=TK*1.E-4
      PS=6.8948E-3*PS
      DTIN=DTIN/1.8
      ROF=16.018*ROF
      ROG=16.018*ROG
      CP=CP*4190.05
      HFG=HFG*2327.8
      PR=CP*VISF/TK
      CPM=CP
      IF((DHIN.GT.0.).AND.(DTIN.GT.0.)) CPM=DHIN/DTIN
      RETURN
      END
```

REFERENCES

1. M.M. EL-WAKIL, Nuclear Energy Conversion, International Textbook Company, Scranton, Penn. (1971).
2. W.T. SHA and C.F. BONILLA, Nucl. App., 1, 69 (1965).
3. G.D. MCPHERSON, AECL-3691, Atomic Energy of Canada Limited (1970).
4. A. HÖLD, Nuc. Engin. and Design, 16, 103 (1971).
5. A.N. NAHAVANDI, Nucl. Sci. Eng., 14, 272 (1962).
6. A.N. NAHAVANDI and R.F. von HOLLEN, Nucl. Sci. Eng., 20, 392 (1964).
7. A.N. NAHAVANDI, Nucl. Sci. Eng., 36, 159 (1969).
8. G. KJAERHEIM, Nuc. Engin. and Design, 21, 279 (1972).
9. L.S. TONG, Nuc. Engin. and Design, 21, 1 (1972).
10. S.Y. AHMAD, J. Heat Transfer, 92, 595 (1970).
11. N. Zuber and F.W. STAUB, Int. J. Heat Transfer, 9, 871 (1966).
12. N. ZUBER and F.W. STAUB, Nuc. Sci. and Engin., 30, 296 (1967).
13. W.T. HANCOX and W.B. NICOLL, Int. J. Heat Mass Transfer, 14, 1377 (1971).
14. W.T. HANCOX and W.B. NICOLL, Int. Symposium on Two Phase Systems paper 1-6, Aug. 29 - Sept. 2, 1971, Technion City, Haifa, Israel.
15. M.Y. YOUNIS, Ph.D. dissertation, McMaster University, in preparation (1975).
16. G.I. BELL and S. GLASSTONE, Nuclear Reactor Theory, Van Nostrand Reinhold Company, New York (1970).
17. J.L. MEEM, Two Group Reactor Theory, Gordon and Breach Science Publishers, New York (1964).
18. J.H. TAIT, An Introduction to Neutron Transport Theory, Mathematical Physics Series, American Elsevier Publishing Co., Inc., New York (1965).
19. B. DAVISON, Neutron Transport Theory, Clarendon Press, Oxford (1958).

20. S. GLASSTONE and M.C. EDLUND, The Elements of Nuclear Reactor Theory, Van Nostrand, Princeton, N.J. (1957).

21. G.A. PON, AECL-2554, Atomic Energy of Canada Limited (1966).

22. B.M. TOWNES, D.B. PRIMEAU and M.F. DURET, AECL-2649, Atomic Energy of Canada Limited (1966).

23. R.E. GREEN, R.E. KAY and C.W. COLPITTS, AECL-2961, Atomic Energy of Canada Limited (1967).

24. G.A. PON, AECL-2942, Atomic Energy of Canada Limited (1968).

25. R.E. GREEN, AECL-3002, Atomic Energy of Canada Limited (1968).

26. M. SRINIVASAN and K.J. SERDULA, AECL-3513, Atomic Energy of Canada Limited (1969).

27. C.O. SMITH, Nuclear Reactor Materials, Addison-Wesley Publishing Company, Reading, Mass. (1967).

28. J.R. LAMARSH, Introduction to Nuclear Reactor Theory, Addison-Wesley Limited, Don Mills, Ontario (1966).

29. W.J. GARLAND and A.A. HARMS, J. of Nuc. Ener., 26, 461 (1972).

30. J. GRIFFITHS, AECL-3739, Atomic Energy of Canada Limited (1971).

31. REACTOR PHYSICS CONSTANTS, ANL-5800, 2nd ed., Argonne National Laboratory (1963).

32. I.H. GIBSON, AECL-2548, Atomic Energy of Canada Limited (1966).

33. G.J. PHILLIPS and J. GRIFFITHS, AECL-3857, Atomic Energy of Canada Limited (1971).

34. W.M. STACEY, JR., Nucl. Sci. Eng., 47, 449 (1972).

35. D.R. FERGUSON and K.F. HANSEN, Nucl. Sci. Eng., 51, 189 (1973).

36. W.M. STACEY, JR., Reactor Tech., 15, 210 (1972).

37. B. CARNAHAN, H.A. LUTHER, J.O. WILKES, Applied Numerical Methods, Wiley and Sons Inc., New York (1969).

38. W.M. REED and K.F. HANSEN, Nucl. Sci. Eng., 41, 431 (1970).

39. A.L. WIGHT, K.F. HANSEN, and D.R. FERGUSON, Nucl. Sci. Eng., 44, 239 (1971).

40. T.Y. NA and A.G. HANSEN, J. Franklin Inst., 292, 471 (1971).

41. W.M. STACEY, JR., Nucl. Sci. Eng., 45, 189 (1971).

42. O. ORBACH and C.M. CROWE, Canadian J. Chem. Eng., 49, 509 (1971).

43. W.J. GARLAND, A.A. HARMS and J. VLACHOPOULOS, Nucl. Sci. Eng., 55 119 (1974).

44. F.B. HILDEBRAND, Methods of Applied Mathematics, Prentice Hall, Englewood Cliffs, N.J. (1965).

45. W.H. McADAMS, W.K. WOODS, and L.C. HEROMAN, JR., Trans. ASME, 64, 193 (1942).

46. R.C. MARTINELLI and D.B. NELSON, Trans. ASME, 70, 695 (1948).

47. A.A. ARMAND, AERE translation 828, Atomic Energy Research Establishment Harwell, Berks. (1959).

48. S. LEVY, Second Midwestern Conf. on Fluid Mechanics, Proc. (1952).

49. P. GRIFFITH and G.B. WALLIS, J. Heat Transfer, 83, 307 (1961).

50. S.G. BANKOFF, J. Heat Transfer, 82, 265 (1960).

51. G.W. MAURER, Bettis Technical Review, WAPD-BT-19 (1960).

52. S. LEVY, J. Heat Transfer, 82, 113 (1960).

53. G.HOUGHTON, Nucl. Sci. Eng., 12, 390 (1962).

54. R.W. BOWRING, Institutt for Atomenergi, HPR 10, Halden, Norway (1962).

55. P.S. LARSEN and L.S. TONG, J. Heat Transfer, 91, 471 (1969).

56. S. LEVY, Int. J. Heat Mass Transfer, 10, 951 (1967).

57. S.Z. ROUHINI and E. AXELSSON, Int. J. Heat Mass Transfer, 13, 2, 383 (1970).

58. S. LEVY, J. Heat Transfer, 85, 137 (1963).

59. E.R. QUANDT, Chem. Eng. Prog. Symp. Series, 32, 111 (1961).

60. J.E. MEYER and R.P. ROSE, J. Heat Transfer, 85, 1 (1963).

61. J.L. HUDSON, K.M. ATIT and S.G. BANKOFF, Chem. Engin. Sci., 19, 387 (1964).

62. B.S. SHIRALKAR, L.E. SCHNEBLY and R.T. LAHEY, JR., Nucl. Engin. and Design, 25, 350 (1973).

63. K. SINGH and C.C. ST. PIERRE, Nucl. Sci. Eng., 50, 382 (1973).

64. J.M. GONZALEZ-SANTALO and P. GRIFFITH, American Society of Mechanical Engineers, ASME-72-WA/NE-19.

65. D.S. ROWE, American Society of Mechanical Engineers, ASME-72-WA/HT-49.

66. R.T. LAHEY, JR., B.S. SHIRALKAR and D.W. RADCLIFFE, J. Heat Transfer, Trans. A.S.M.E., 197 (1971).

67. H. CHELEMER, J. WEISMAN and L.S. TONG, Nucl. Eng. Design, 21, 35 (1972).

68. F.S. CASTELLANA and J.E. CASTERLINE, Nucl. Eng. Design, 22, 3 (1972).

69. TWO PHASE FLOW AND HEAT TRANSFER IN ROD BUNDLES, American Society of Mechanical Engineers, ASME, Nov. 18 (1969).

70. R.B. BIRD, W.E. STEWARD and E.N. LIGHTFOOT, Transport Phenomena, John Wiley and Sons, Inc., New York (1960).

71. G.B. WALLIS, One-Dimensional Two-Phase Flow, McGraw Hill, New York (1969).

72. J.A. BOURE, A.E. BERGLES and L.S. TONG, Nucl. Engin. and Design, 25, 165 (1973).

73. W. HARRISON, Atomic Energy of Canada Limited, private communication, May (1974).

74. A.A. HARMS and S.I. SCHREINER, Nucl. Tech., 11, 144 (1971).

75. J.D. STEWART, AECL-1470, Atomic Energy of Canada Limited (1962).

76. J.D. STEWART, J.M. KENNEDY and MRS. S.J. COWLEY, AECL-2547, Atomic Energy of Canada Limited (1966).

77. A. OKAZAKI and D.S. CRAIG, AECL-2593, Atomic Energy of Canada Limited (1967).